63-3-3

RADC-TDR-63-1, Vol. II

School of Electrical Engineering
CORNELL UNIVERSITY
Ithaca, New York

RESEARCH REPORT EE 556

THEORETICAL AND EXPERIMENTAL INVESTIGATION OF LINEAR BEAM MICROWAVE TUBES

Final Report, Vol. II

1 October 1961 to 30 September 1962

Approved by
G. Conrad Dalman
Lester F. Eastman
Paul R. McIsaac

Griffiss Air Force Base, New York
Rome Air Development Center, Air Research and Development Command
Prepared under Contract No. AF30(602)-2573

ASTIA Notice

Qualified requestors may obtain copies of this report from the ASTIA Document Service Center, Dayton 2, Ohio. ASTIA Services for the Department of Defense contractors are available through the "Field of Interest Register" on a "need-to-know" certified by the cognizant military agency of their project or contract.

RADC-TDR-63-1, Vol. II

School of Electrical Engineering
CORNELL UNIVERSITY
Ithaca, New York

RESEARCH REPORT EE 556

THEORETICAL AND EXPERIMENTAL INVESTIGATION OF LINEAR-BEAM MICROWAVE TUBES

Final Report, Vol. II 1 October 1961 to 30 September 1962

Approved by

G. Conrad Dalman
Lester F. Eastman
Paul R. McIsaac

Prepared under
Contract No. AF30(602)-2573, Project No. 5573, Task No. 557303
Rome Air Development Center, Air Research and Development Command
Griffiss Air Force Base, New York

CONTENTS OF FINAL REPORT

Page

GENERAL

ABSTRACT 1

INTRODUCTION 4

DISCUSSION 5

A. BEAM-CIRCUIT INTERACTION STUDIES 5

B. NANOSECOND PULSE STUDY 10

C. VELOCITY FILTERS 11

D. REDUCTION OF HARMONICALLY RELATED SPURIOUS OUTPUTS 12

CONCLUSIONS 15

A. BEAM-CIRCUIT INTERACTION 15

B. NANOSECOND PULSE STUDY 16

C. VELOCITY FILTERS 17

D. REDUCTION OF HARMONICALLY RELATED SPURIOUS OUTPUTS 17

TECHNICAL OR INTERIM REPORTS

THE CURRENT DISTRIBUTIONS IN A VELOCITY-MODULATED BRILLOUIN-FOCUSED ELECTRON BEAM
A. S. Gilmour, Jr. and L. F. Eastman

AN INVESTIGATION OF THE LAMINARITY OF FLOW IN A MAGNETICALLY CONFINED ELECTRON BEAM
D. D. Hallock

A RELATIVISTIC STUDY OF THE LLEWELLYN ELECTRONIC GAP AND ITS APPLICATIONS

C. Sun

School of Electrical Engineering
CORNELL UNIVERSITY
Ithaca, New York

RESEARCH REPORT EE 525

A RELATIVISTIC STUDY OF THE LLEWELLYN ELECTRONIC GAP AND ITS APPLICATIONS

Cheng Sun

LINEAR BEAM MICROWAVE TUBES

Technical Report No. 18 15 February 1962

Published under Contract No. AF30(602)-2573
Rome Air Development Center, Griffiss Air Force Base, New York

ACKNOWLEDGMENT

The author wishes to express his sincere thanks to Professor G. C. Dalman, Chairman of his Special Committee, for his encouragement and guidance. He is greatly indebted to Professor S. Olving for having suggested the problem originally and for much advice. He also wants to acknowledge the valuable suggestions of Professor P. R. McIsaac and L. F. Eastman in the course of the investigation and to thank Professor G. R. Liversay for serving on his committee.

The author is grateful to the Institute of International Education for the financial aid and the U. S. Air Force for supporting this research project and publishing this report.

CONTENTS

		Page
ABSTRACT		vii
I.	INTRODUCTION	1
II.	SUMMARY OF IMPORTANT FORMULAS	3
	A. Important A-C Relations	3
	B. Important D-C Relations	4
III.	EVALUATION OF WAVE POTENTIAL π AND LLEWELLYN'S RELATIVISTIC COEFFICIENTS	7
IV.	APPLICATIONS	16
	A. Space-Charge-Limited Diode	16
	B. Application of Klystron Gaps	27
V.	APPLICATIONS TO THE VERY HIGH-POWER KLYSTRON GAPS	40
VI.	CONCLUSIONS AND RECOMMENDATIONS	45
APPENDIX A:	DERIVATION OF BASIC EQUATIONS	47
APPENDIX B:	DERIVATION OF LLEWELLYN'S COEFFICIENTS BY THE USE OF WAVE THEORY IN THE NON-RELATIVISTIC CASE	56
APPENDIX C:	THE DERIVATION OF THE RELATIVISTIC EXPRESSION FOR THE CHILD-LANGMUIR LAW	62
APPENDIX D:	RELATIVISTIC BEAM-LOADING ADMITTANCE IN A KLYSTRON GAP BY THE BALLISTIC APPROACH	66

ABSTRACT

The Llewellyn relativistic coefficients have been solved in the range $v_o^2/2_c < \frac{1}{2}$, corresponding to 2.115×10^5 volts. These results are applied to high-frequency space-charge-limited diodes and to klystrons in which space-charge effects are not considered. In such klystrons, the range can be extended without limit.

The current and velocity modulation and the diode impedance are derived for high-frequency space-charge-limited diodes. Here the maximum diode resistance at 2.115×10^5 volts changes only 0.3 per cent in comparison to the nonrelativistic case.

For the klystron case, velocity modulation and beam-loading admittance are calculated at the first gap and are found to change from the nonrelativistic case by a large amount. The current and velocity behavior in the drift region are derived, and the transadmittance for the klystron is also given.

It is concluded that the relativistic effect is small for high-frequency space-charge-limited diodes, but significant for klystron tubes.

I. INTRODUCTION

Llewellyn[1,2] solved the parallel-plane problem by a continuous integration procedure and applied it to tubes. Rydbeck[3] got the same results later by the space-charge wave approach. Then Olving[4] modified it for the relativistic expressions for a-c quantities, such as the electronic field, the electronic velocity, and the conduction current density. He introduced the wave potential π to simplify the expressions. The details of Olving's work are given in Appendix A.

It is inevitable that modern microwave electronics will be directed toward high-power devices, thus requiring knowledge of their relativistic behavior. In the following analysis, it is assumed that the electron motion is in the axial direction only; in other words, the longitudinal magnetic field is so strong that transverse motion of the beam electronics may be considered negligible. Although this magnetic force is rather important at high velocity, we are not going to concern ourselves with it in this study. In addition, small-signal conditions are assumed to hold throughout.

The framework of this thesis is to solve for the wave potential π first under the assumption $v_o^2/c^2 < \frac{1}{2}$, then derive the Llewellyn relativistic coefficient sets by the various relativistic a-c expressions that formed the basis of "wave theory." Then in Chapter IV we apply these general expressions to the following special problems: (1) space-charge-limited diode with high voltage, and (2) the relativistic klystron gap, and then study the behavior of impedance, beam loading admittance, and velocity and current modulations. The evaluation of π in Chapter III is under the

assumption $v^2/c^2 << 0.5$, corresponding to 2.115×10^5 volts, but in the application of klystron gaps we can extend it without limit, as is done in Chapter V.

II. SUMMARY OF IMPORTANT FORMULAS

In this chapter, the important formulas are summarized. The details of the derivations will be given in Appendix A.

A. Important A-C Relations

Important a-c relations such as conduction current, electric field, velocity, and applied voltage between the gaps are expressed as follows:

$$i_1 = \frac{\beta_p^2}{\beta_e^2} \, e^{-j\theta} \, \pi \quad , \tag{1}$$

$$E_1 = \frac{1}{j\omega\epsilon_o} \, (i_c - i_1) = \frac{1}{j\omega\epsilon_o} \left\{ i_c - \frac{\beta_p^2}{\beta_e^2} \, e^{-j\theta} \, \pi \right\} \quad , \tag{2}$$

$$v_1 = \frac{1}{j\omega\epsilon_o} \, \frac{e}{m_o\omega} \, e^{-j\theta} \left(\frac{d\pi}{d\theta} - \pi \frac{1}{\frac{1}{\beta_e}} \, \frac{d\frac{1}{\beta_e}}{d\theta} \right) \quad , \tag{3}$$

$$\begin{aligned} \overline{V}_c &= \int_o^d E_1 \, dz = \int \frac{E_1}{\beta_e} \, d\theta = \frac{1}{j\omega\epsilon_o} \left\{ i_c \int_o^{\theta_o} \frac{d\theta}{\beta_e} - \frac{\beta_p^2}{\beta_e^2} \int_o^{\theta_o} e^{-j\theta} \, \pi \, d\theta \right\} \\ &= \frac{1}{j\omega\epsilon_o} \left\{ i_c d - \frac{\beta_p^2}{\beta_e^2} \int_o^{\theta_o} e^{-j\theta} \, \pi \, d\theta \right\} \quad , \end{aligned} \tag{4}$$

where d is the distance between the electrodes, and θ_o is the corresponding d-c transit angle $\int_o^d \beta_e \, dz$, and

$$\theta = \int \beta_e \, dz \qquad \therefore \int_{o}^{\theta_o} \frac{d\theta}{\beta_e} = \int_{o}^{d} dz = d \quad ,$$

where

$$\pi = \int (c_1 - j i_c \, e^{j\theta}) \left(1 - \frac{K_o^2}{\beta_e^2}\right)^{3/2} d\theta + c_2 \quad . \tag{5}$$

The integration constants c_1 and c_2 are to be determined from the a-c boundary conditions of the velocity and conduction current.

B. Important D-C Relations

In order to solve Equation (5), one has to express $\left(1 - \frac{K_o^2}{\beta_e^2}\right)^{3/2}$ as a function of θ from d-c relations. The energy relation in the relativistic region will be

$$c^2 \left[\frac{m_o}{\left(1 - \frac{K_o^2}{\beta_e^2}\right)^{1/2}} - m_o \right] = eV \quad ,$$

or

$$\left[\frac{1}{\left(1 - \frac{K_o^2}{\beta_e^2}\right)^{1/2}} - 1 \right] = \frac{V}{V_n} \quad , \tag{6}$$

where V is the potential difference and $V_n = m_o c^2/e = 5.11 \times 10^5$ volts. This can also be reduced to

$$\frac{\frac{1}{\beta_e}}{\left(1 - \frac{K_o^2}{\beta_e^2}\right)^{1/2}} = \frac{1}{K_o} \left[\frac{2V}{V_n} \left(1 + \frac{V}{2V_n}\right) \right]^{1/2} \quad . \tag{7}$$

Another important d-c relation in Equation (A. 22) is

$$\frac{d^2}{d\theta^2}\left[\frac{\frac{1}{\beta_e}}{\left(1-\frac{K_o^2}{\beta_e^2}\right)^{1/2}}\right] = \frac{\beta_p^2}{\beta_e^3} \quad .$$

Since

$$\frac{\beta_p^2}{\beta_e^3} = \frac{-e\zeta_o}{m_o \epsilon_o v_o^2} \quad ,$$

then

$$\frac{\omega^3}{v_o^3} = \frac{e J_o}{m_o \epsilon_o \omega^3}$$

is independent of v_o and z. After Equation (A. 22) is integrated twice, apply the boundary conditions of Equation (7), i.e., at $\theta = \theta_o$, $\nabla = \nabla_b$ and at $\theta = 0$, $\nabla = \nabla_a$:

$$\frac{\frac{1}{\beta_e}}{\left(1-\frac{K_o^2}{\beta_o^2}\right)^{1/2}} = \frac{\beta_p^2}{\beta_e^3}\frac{\theta}{2}(\theta - \theta_o) + \frac{1}{K_o}\left\{\left[\frac{2\nabla_b}{\nabla_n}\left(1+\frac{\nabla_b}{2\nabla_n}\right)\right]^{1/2} - \left[\frac{2\nabla_a}{\nabla_n}\left(1+\frac{\nabla_a}{2\nabla_n}\right)\right]^{1/2}\right\}\frac{\theta}{\theta_o} + \frac{1}{K_o}\left[\frac{2\nabla_a}{\nabla_n}\left(1+\frac{\nabla_a}{2\nabla_n}\right)\right]^{1/2} .$$

Denote the right side of above relation by $S(\theta)$, and then rearrange it:

$$\frac{\frac{1}{\beta_e}}{\left(1-\frac{K_o^2}{\beta_o^2}\right)^{1/2}} = S(\theta) = A\theta^2 + B\theta + D \quad . \qquad (8)$$

This relation will be used often in later chapters. In Equation (8)

$$A = \frac{1}{2} \frac{\beta_p^2}{\beta_e^3} , \tag{9}$$

$$B = \frac{\frac{1}{K_o}\left\{\left[\frac{2V_b}{V_n}\left(1 + \frac{V_b}{2V_n}\right)\right]^{1/2} - \left[\frac{2V_a}{V_n}\left(1 + \frac{V_a}{2V_n}\right)\right]^{1/2}\right\} - \frac{1}{2}\frac{\beta_p^2}{\beta_e^3}\theta_o^2}{\theta_o} , \tag{10}$$

$$D = \frac{1}{K_o}\left[\frac{2V_a}{V_n}\left(1 + \frac{V_a}{2V_n}\right)\right]^{1/2} . \tag{11}$$

From Equation (8), we can solve $1/\beta_e$ and $\left(1 - \frac{K_o^2}{\beta_e^2}\right)^{1/2}$ in terms of S:

$$\frac{1}{\beta_e} = \frac{S}{(1 + K_o^2 S^2)^{1/2}} , \tag{12}$$

$$\left(1 - \frac{K_o^2}{\beta_e^2}\right)^{1/2} = \frac{1}{(1 + K_o^2 S^2)^{1/2}} . \tag{13}$$

Since S is a known function of θ, it would now be possible to eliminate β_e and $\left(1 - \frac{K_o^2}{\beta_e^2}\right)^{1/2}$ from our a-c expressions by the use of Equations (12) and (13). And finally we have

$$d = \int_o^{\theta_o} \frac{d\theta}{\beta_e} = \int_o^{\theta_o} \frac{S}{\left(1 + K_o^2 S^2\right)^{1/2}} d\theta . \tag{14}$$

III. EVALUATION OF WAVE POTENTIAL π AND LLEWELLYN'S RELATIVISTIC COEFFICIENTS

In order to get the complete set of Llewellyn coefficients with the first-order relativistic correction, we have to solve for the wave potential π first, which is essentially a current dimension. The derivation of the nonrelativistic Llewellyn's coefficients using this wave potential π is given in Appendix B. For the relativistic case

$$\pi = \int (c_1 - ji_c e^{j\theta}) \left(1 - \frac{K_o^2}{\beta_e^2}\right)^{3/2} d\theta + c_2 \quad . \tag{5}$$

If

$$\frac{K_o^2}{\beta_e^2} \ll 1 \text{ or } \frac{v_o^2}{c^2} \ll 1 \quad ,$$

the integral will be reduced to

$$\pi = \int (c_1 - ji_c e^{j\theta}) \, d\theta + c_2$$

$$= c_1\theta - i_c e^{j\theta} + c_2 \quad . \tag{15}$$

This is the nonrelativistic wave potential as given in Appendix B.

But when the factor $\left(1 - \frac{K_o^2}{\beta_e^2}\right)^{3/2}$ is present in the integral, it is more difficult to integrate than the nonrelativistic case. Since by Equation (13)

$$\left(1 - \frac{K_o^2}{\beta_e^2}\right)^{1/2} = \frac{1}{\left(1 + K_o^2 S^2\right)^{1/2}} \quad ,$$

where S is given by Equation (8), then

$$\left(1 - \frac{K_o^2}{\beta_e^2}\right)^{1/2} = \frac{1}{\left(1 + K_o^2 S^2\right)^{1/2}} = \frac{1}{\left(1 + \dfrac{K_o^2 \dfrac{1}{\beta_e^2}}{1 - \dfrac{K_o^2}{\beta_e^2}}\right)^{1/2}} \quad .$$

If the condition $K_o^2/\beta_e^2 \leq 0.5$ is assumed, the preceding equation may be expanded by binomial theorem since $K_o^2 S^2 < 1$ as $K_o^2/\beta_e^2 < 0.5$. This limitation of velocity corresponds to 2.115×10^5 v. Now, we should bear in mind that the coefficients we are going to derive are valid up to 2.115×10^5 v, but that the correction factor of relativistic effect is only of first order:

$$\begin{aligned} \pi &= \int \left(c_1 - j i_c e^{j\theta}\right) \left(1 - \frac{K_o^2}{\beta_e^2}\right)^{3/2} d\theta + c_2 \\ &= \int \left(c_1 - j i_c e^{j\theta}\right) \left(1 + K_o^2 S^2\right)^{-3/2} d\theta + c_2 \\ &= \int \left(c_1 - j i_c e^{j\theta}\right) \left(1 - \frac{3}{2} K_o^2 S^2\right) d\theta + c_2 \quad . \end{aligned}$$

Substituting $S = A\theta^2 + B\theta + D$ in the previous equation gives

$$\begin{aligned} \pi &= c_1\theta - i_c e^{j\theta} - \frac{3}{2} K_o^2 c_1 \left[A^2 \frac{\theta^5}{5} + \frac{AB}{2}\theta^4 + (B^2 + 2AD)\frac{\theta^3}{3} + BD\theta^2 + D^2\theta\right] + c_2 \\ &\quad + j\frac{3}{2} K_o^2 i_c \left\{-jA^2\theta^4 e^{j\theta} + (4A^2 - j2AB)\theta^3 e^{j\theta} + \left[j12A^2 + 6AB - j(B^2 + 2AD)\right]\theta^2 e^{j\theta}\right. \\ &\quad + \left[-24A^2 + j12AB + 2(B^2 + 2AD) - j2BD\right]\theta\, e^{j\theta} \\ &\quad \left. + \left[-j24A^2 - 12AB + 2j(B^2 + 2AD) + 2BD - jD^2\right] e^{j\theta}\right\} \\ &= c_1\theta - i_c e^{j\theta} - \frac{3}{2} K_o^2 c_1 S_A + c_2 + j\frac{3}{2} K_o^2 i_c T \quad , \end{aligned} \tag{16}$$

where

$$S_A = A^2 \frac{\theta^5}{5} + \frac{AB}{2}\theta^4 + (B^2 + 2AD)\frac{\theta^3}{3} + BD\theta^2 + D^2\theta \quad , \tag{17}$$

$$T = \left\{ -jA^2\theta^4 e^{j\theta} + (4A^2 - j2AB)\theta^3 e^{j\theta} + \left[j12A^2 + 6AB - j(B^2 + 2AD)\right]\theta^2 e^{j\theta} \right.$$
$$+ \left[-24A^2 + j12AB + 2(B^2 + 2AD) - j2BD\right]\theta e^{j\theta}$$
$$\left. + \left[-j24A^2 - 12AB + 2j(B^2 + 2AD) + 2BD - jD^2\right] e^{j\theta} \right\} \tag{18}$$

Rewrite Equations (1) and (3) as

$$i_1 = \frac{\beta_p^2}{\beta_e^2} e^{-j\theta} \pi \tag{1}$$

and

$$v_1 = -\frac{1}{j\omega\epsilon_o} \frac{e}{m_o\omega} \left\{ \frac{d\pi}{d\theta} - \pi \frac{1}{\frac{1}{\beta_e}} \frac{d\left(\frac{1}{\beta_e}\right)}{d\theta} \right\}$$

$$= -\frac{1}{j\omega\epsilon_o} \frac{e}{m_o\omega} \left\{ \left(c_1 - j i_c e^{j\theta}\right)\left(1 + K_o^2 S^2\right)^{-3/2} - \pi \frac{1}{\frac{1}{\beta_e}} \frac{d\left(\frac{1}{\beta_e}\right)}{d\theta} \right\} , \tag{3}$$

where

$$\frac{1}{\beta_e} = \frac{S}{\left(1 + K_o^2 S^2\right)^{1/2}}$$

by Equation (12), and

$$\frac{d\left(\frac{1}{\beta_e}\right)}{d\theta} = \frac{\frac{dS}{d\theta}}{\left(1 + K_o^2 S^2\right)^{3/2}} \quad ,$$

with

$$\theta \to 0 \ , \quad i_1 = i_{1a} \ , \quad v_1 = v_{1a} \ , \quad \beta_e = \beta_{eo} \ , \quad \beta_p = \beta_{po} \quad ,$$

where i_{1a} is the initial a-c conduction current, and v_{1a} is the velocity. Then we solve for the constants c_1 and c_2:

$$c_2 = \frac{\beta_{eo}^2}{\beta_{po}^2} i_{1a} + i_c + \frac{3}{2} K_o^2 i_c \left[(2B^2 + 4AD - D^2 - 24A) + j(12AB - 2BD) \right]$$

$$= \frac{\beta_{eo}^2}{\beta_{po}^2} i_{1a} + i_c + \frac{3}{2} K_o^2 i_c \, Q \quad , \tag{19}$$

where

$$Q = (2B^2 + 4AD - D^2 - 24A^2) + j(12AB - 2BD) \quad , \tag{20}$$

and

$$c_1 = -j \frac{\omega \epsilon_o m_o \omega}{e} \left(1 + K_o^2 D^2\right)^{3/2} v_{1a} + j i_c + \frac{\beta_{eo}^2}{\beta_{po}^2} \frac{B}{D} \left(1 + K_o^2 D^2\right)^{1/2} i_{1a} \quad , \tag{21}$$

where

$$\frac{1}{\beta_{eo}} = \frac{1}{\beta_e}\Bigg]_{\theta \to 0} = \frac{S}{\left(1 + K_o^2 S^2\right)^{1/2}}\Bigg]_{\theta \to 0} = \frac{D}{\left(1 + K_o^2 D^2\right)^{1/2}} \quad ; \tag{22}$$

hence

$$\frac{\beta_{eo}^2}{\beta_{po}^2} = \frac{\beta_{eo}^3}{\beta_{po}^2} \cdot \frac{1}{\beta_{eo}} \frac{m_o \epsilon_o \omega^3}{e J_o} \cdot \frac{D}{\left(1 + K_o^2 D^2\right)^{1/2}} \quad . \tag{23}$$

Substitute c_1, c_2 into π, and rearrange Equations (1), and (3), then

$$i_1 = i_c \frac{e}{m_o \epsilon_o} \frac{J_o}{v_o} \frac{1}{(j\omega)^2} \left[1 - \left\{ 1 + \frac{3}{2} K_o^2 \left[Q + j(T - S_A) \right] \right\} e^{-j\theta} - j\theta \, e^{j\theta} \right]$$

$$+ i_{1a} \frac{\omega}{v_o} e^{-j\theta} \left[D(1 + K_o^2 D^2)^{-1/2} + B(\theta - \frac{3}{2} K_o^2 S_A) \right]$$

$$-jv_{1a}\frac{J_o}{v_o}\left(1+K_o^2D^2\right)^{3/2}\left(\theta-\frac{3}{2}K_o^2S_A\right)e^{-j\theta}\Bigg\} \qquad (24)$$

$$v_1 = -i_c\frac{e}{m_o\epsilon_o}\frac{1}{(j\omega)^2}\left(1+K_o^2S^2\right)^{-3/2}\left[(1-e^{-j\theta})-\frac{2A\theta+B}{js}\left(1+K_o^2S^2\right)^{1/2}\right.$$

$$\left.\left\{1-\left[1+\frac{3}{2}K_o^2\left(Q+j\overline{T-S_A}\right)\right]e^{-j\theta}-j\theta\ e^{-j\theta}\right\}\right]$$

$$-i_{1a}\frac{j\omega}{J_o}e^{-j\theta}\left(1+K_o^2S^2\right)^{-3/2}\left\{B-\frac{2A\theta+B}{S}\left(1+K_o^2S^2\right)^{1/2}\left[\frac{D}{\left(1+K_o^2D^2\right)^{1/2}}B\left(\theta-\frac{3}{2}K_o^2S_A\right)\right]\right\}$$

$$+v_{1a}e^{-j\theta}\left(1+K_o^2D^2\right)^{-3/2}\left(1+K_o^2S^2\right)^{-3/2}\left[1-\frac{2A\theta+B}{S}\left(1+K_o^2S^2\right)^{1/2}\left(\theta-\frac{3}{2}K_o^2S_A\right)\right] . \qquad (25)$$

The a-c voltage across the gap should be

$$V_c = \int_o^d E_1\,dz = \int_o^{\theta_o}\frac{E_1}{\beta_e}\,d\theta \quad .$$

Rewrite Equation (2) as

$$E_1 = \frac{1}{j\omega\epsilon_o}(i_c - i_1)\ \frac{1}{j\omega\epsilon_o}\left\{i_c-\frac{\beta_p^2}{\beta_e^2}\ e^{-j\theta}\ \pi\right\} \quad ; \qquad (2)$$

then integrate and arrange it:

$$V_c = i_c\frac{1}{\epsilon_o(j\omega)^4}\left\{(j\omega)^3 d+\frac{e\,J_o}{\epsilon_o m_o}\left[\left(2-2e^{-j\theta_o}-j\theta_o-j\theta_o e^{-j\theta_o}\right)\right.\right.$$

$$\left.\left.-\frac{3}{2}K_o^2\left(e^{-j\theta_o}-1\right)(Q-N+M)+j\frac{3}{2}K_o^2P\left(1+e^{-j\theta_o}\right)\right]\right\}$$

$$+ i_{1a} \frac{\omega^2}{\epsilon_o (j\omega)^3} \left(B \left\{ \left(j\theta_o e^{-j\theta_o} + e^{-j\theta_o} - 1 \right) + \frac{3}{2} K_o^2 \left[(M-N-jP) e^{-j\theta_o} - M \right] \right\} + j \frac{D\left(e^{-j\theta_o} - 1 \right)}{\left(1 + K_o^2 D^2 \right)^{1/2}} \right)$$

$$- v_{1a} \frac{J_o}{\epsilon_o} \frac{1}{(j\omega)^2} \left(1 + K_o^2 D^2 \right)^{3/2} \left[\left(j\theta_o e^{j\theta_o} + e^{-j\theta_o} - 1 \right) + \frac{3}{2} K_o^2 \left((M-N-jP) e^{-j\theta_o} - M \right) \right] , \tag{26}$$

where

$$M = \left[-24A^2 - j12AB + 2(B^2 + 2AD) + j2BD - D^2 \right] , \tag{27}$$

$$N = A^2\theta_o^4 + 2AB\theta_o^3 + \left[-12A^2 + (B^2 + 2AD) \right] \theta_o^2 + (-12AB + 2BD)\theta_o , \tag{28}$$

$$P = \frac{A^2}{5}\theta_o^5 + \frac{AB}{2}\theta_o^4 - \left[-4A^2 - \frac{(B^2 + 2AD)}{3} \right] \theta_o^3 - (6AB - BD)\theta_o^2 - \left[-24A^2 + 2(B^2 + 2AD) - D^2 \right] \theta_o , \tag{29}$$

$$Q = (2B^2 + 4AD - D^2 - 24A^2) + j(12AB - 2BD) . \tag{20}$$

Equations (24), (25), and (27) are analogous to the results of Llewellyn (with a slight relativistic correction) and express current density modulation, velocity modulation, and applied a-c voltage. Amplitudes and phases at any point in the gap are in terms of total current i_c, initial a-c conduction current and initial a-c velocity value.

If we write Equations (24), (25), and (27) in the following form;

$$\begin{aligned} \nabla_c &= A^* i_c + B^* i_{1a} + C^* v_{1a} , \\ v_1 &= D^* i_c + E^* i_{1a} + F^* v_{1a} , \\ i_1 &= G^* i_c + H^* i_{1a} + I^* v_{1a} , \end{aligned} \tag{30}$$

then A*, B*, C*, D*, E*, F*, G*, H*, I* are so-called relativistic Llewellyn's coefficients which have been explicitly expressed in Equations (24), (25), and (26).

Now, in order to compare Llewellyn's relativistic coefficients and nonrelativistic coefficients given in Appendix B, we have the following flow charts:

$$A^*_{rel} = \frac{1}{\epsilon_o (j\omega)^4} \left\{ (j\omega)^3 d + \frac{e J_o}{\epsilon_o m_o} \left[\left(2 - 2e^{-j\theta_o} - j\theta_o - j\theta_o e^{-j\theta_o} \right) - \frac{3}{2} K_o^2 \left(e^{-j\theta_o} - 1 \right) (Q - N + M) \right. \right.$$
$$\left. \left. + j \frac{3}{2} K_o^2 P \left(1 + e^{-j\theta_o} \right) \right] \right\} \quad , \tag{31}$$

$$A^*_{non} = \frac{1}{\epsilon_o (j\omega)^4} \left\{ (j\omega)^3 d + \frac{e J_o}{\epsilon_o m_o} \left[2 - 2e^{-j\theta_o} - j\theta_o - j\theta_o e^{-j\theta_o} \right] \right\} \quad , \tag{32}$$

$$B^*_{rel} = \frac{\omega^2}{\epsilon_o (j\omega)^3} \left\{ B \left[j\theta_o e^{-j\theta_o} + e^{-j\theta_o} - 1 \right] + \frac{3}{2} \left[(M - N - jP) e^{-j\theta_o} - M \right] \right.$$
$$\left. + j \frac{D \left(e^{-j\theta_o} - 1 \right)}{\left(1 + K_o^2 D^2 \right)^{1/2}} \right\} \quad , \tag{33}$$

$$B^*_{non} = \frac{1}{\epsilon_o (j\omega)^3} \left[a_a \left(j\theta_o e^{-j\theta_o} + e^{-j\theta_o} - 1 \right) + j\omega v_a \left(e^{-j\theta_o} - 1 \right) \right] \quad , \tag{34}$$

$$C^*_{rel} = - \frac{J_o}{\epsilon_o} \frac{1}{(j\omega)^2} \left(1 + K_o^2 D^2 \right)^{3/2} \left\{ \left[\left(j\theta_o e^{-j\theta_o} + e^{-j\theta_o} - 1 \right) + \frac{3}{2} K_o^2 (M - N - jP) e^{-j\theta_o} - M \right] \right\} \quad , \tag{35}$$

$$C^*_{non} = - \frac{J_o}{\epsilon_o (j\omega)^2} \left(j\theta_o e^{-j\theta_o} + e^{-j\theta_o} - 1 \right) \quad , \tag{36}$$

$$D^*_{rel} = -\frac{1}{(j\omega)^2}\,\frac{e}{m_o\epsilon_o}\left(1+K_o^2S^2\right)^{-3/2}\left[(1-e^{-j\theta})\right.$$

$$\left. -\frac{2A\theta+B}{jS}\left(1+K_o^2S^2\right)^{1/2}\left\{1-\left[1+\frac{3}{2}K_o^2(\Omega+j\overline{T-S}_A)\right]e^{-j\theta}-j\theta\,e^{-j\theta}\right\}\right] \quad , \quad (37)$$

$$D^*_{non} = -\frac{1}{(j\omega)^2}\,\frac{e}{m_o\epsilon_o}\left[(1-e^{-j\theta})-\frac{a_o}{j\omega v_o}(1-e^{-j\theta}-j\theta\,e^{-j\theta})\right] \quad , \quad (38)$$

$$E^*_{rel} = \frac{j\omega}{J_o}\,e^{-j\theta}\left(1+K_o^2S^2\right)^{-3/2}\left\{B-\frac{2A\theta+B}{S}\left(1+K_o^2S^2\right)^{1/2}\left[\frac{D}{\left(1+K_o^2D^2\right)^{1/2}}+\left(\theta-\frac{3}{2}K_o^2S_A\right)\right]\right\}, \quad (39)$$

$$E^*_{non} = \frac{e}{m_o\epsilon_o}\,\frac{1}{(j\omega)^2}\left[\frac{a_o\tau}{2v_o}-1\right]\,j\theta\,e^{-j\theta} \quad , \quad (40)$$

$$F^*_{rel} = e^{-j\theta}\left(1+K_o^2D^2\right)^{3/2}\left(1+K_o^2S^2\right)^{-1/2}\left[1-\frac{2A\theta+B}{S}\left(1+K_o^2S^2\right)^{1/2}\left(\theta-\frac{3}{2}K_o^2S_A\right)\right] \quad , \quad (41)$$

$$F^*_{non} = \left(1-\frac{a_o\tau}{v_o}\right)e^{-j\theta} \quad , \quad (42)$$

$$G^*_{rel} = \frac{e}{m_o\epsilon_o}\,\frac{J_o}{v_o}\,\frac{1}{(j\omega)^2}\left[1-\left\{1+\frac{3}{2}K_o^2\left[\Omega+j(T-S_A)\right]\right\}e^{-j\theta}-j\theta\,e^{-j\theta}\right] \quad , \quad (43)$$

$$G^*_{non} = \frac{e}{m_o\epsilon_o}\,\frac{J_o}{v_o}\,\frac{1}{(j\omega)^2}\,(1-e^{-j\theta}-j\theta\,e^{-j\theta}) \quad , \quad (44)$$

$$H^*_{rel} = \frac{\omega}{v_o}\,e^{-j\theta}\left[D\left(1+K_o^2D^2\right)^{-1/2}+B\left(\theta-\frac{3}{2}K_o^2\,S_A\right)\right] \quad , \quad (45)$$

$$H^*_{non} = \left[1-\frac{1}{2}\,\frac{e}{m_o\epsilon}\,\frac{J_o}{v_o}\,\tau^2\right]e^{-j\theta} \quad , \quad (46)$$

$$I^*_{rel} = -j \frac{J_o}{v_o} \left(1 + K_o^2 D^2\right)^{3/2} \left(\theta - \frac{3}{2} K_o^2 S_A\right) e^{-j\theta} \quad , \tag{47}$$

$$I^*_{non} = -j \frac{J_o}{v_o} \theta \, e^{-j\theta} \quad . \tag{48}$$

First, we should notice that these relativistic expressions could be reduced to nonrelativistic ones if $K_o^2/\beta_e^2 << 1$, corresponding to $K_o^2 S^2 << 1$, so that the integral,

$$\pi = \int (c_1 - j i_c e^{j\theta}) \left(1 + K_o^2 S^2\right)^{3/2} d\theta + c_2 \quad ,$$

is reduced to

$$\pi = \int (c_1 - j i_c e^{j\theta}) \, d\theta + c_2 \quad .$$

Therefore the terms containing K_o^2 would be missing. (The nonrelativistic results are given in Appendix B.)

Secondly, J_o and θ_o in the relativistic case are a little different from the nonrelativistic J_o and θ_o, since both of them may depend on the applied d-c voltage. However they will reduce to the same value when $K_o^2/\beta_e^2 << 1$.

Third, while it appears at first that some of the relativistic expressions cannot be reduced to the nonrelativistic case, even if K_o^2 terms are omitted, with realizing that $a_a \to \omega^2 B$, $v_a \to \omega_D$, $a_o \to \omega^2(2A\theta + B)$, $v_o \to \omega_s$, and $\theta = \omega\tau$, one can after a little manipulation reduce them to the nonrelativistic form.

IV. APPLICATIONS

A. Space-Charge-Limited Diode

The behavior of a space-charge-limited diode in the nonrelativistic case has been worked out by Llewellyn[1, 2]. Now we are going to investigate its pattern for the relativistic case by the results obtained in the last chapter.

Since the d-c potential at the cathode is zero, i.e., $V_a = 0$, then

$$D = \frac{1}{K_o}\left[\frac{2V_a}{V_n}\left(1 + \frac{V_a}{2V_n}\right)\right]^{1/2} = 0 \quad .$$

Also for a space-charge-limited diode, the electric field at the cathode has to be zero, from Equation (A-1):

$$\omega^2 \frac{d}{d\theta}\left[\frac{\frac{1}{\beta_e}}{\left(1 - \frac{K_o^2}{\beta^2}\right)^{1/2}}\right] = -\frac{e}{m_o} E_o \quad ,$$

where

$$\frac{\frac{1}{\beta_e}}{\left(1 - \frac{K_o^2}{\beta_e^2}\right)^{1/2}} = S = A\theta^2 + B\theta + D \quad ;$$

therefore

$$\omega^2 (2A\theta + B) = -\frac{e}{m_o} E_o \quad ,$$

where $E_o = 0$ at $\theta = 0$, hence $B = 0$. In a space-charge-limited diode we therefore have

$$B = 0, \quad D = 0 \quad . \tag{49}$$

By Equation (49), we find Equations (33), (39), and (45) equal to zero, i.e.,

$$B^* = E^* = H^* = 0 \quad . \tag{50}$$

Also, if we neglect the noise at the cathode, then $v_{1a} = 0$, so Equation (30) is left in the following form:

$$\bar{V}_c = A^* i_c \quad , \tag{51}$$

$$v_1 = D^* i_c \quad , \tag{52}$$

$$i_1 = G^* i_c \quad , \tag{53}$$

First, we study Equation (53) to see if the conduction current will be the total current when $\theta \to 0$, as in the nonrelativistic case. Equation (43) gives

$$G^* = \frac{e}{m_o \epsilon_o} \frac{J_o}{v_o} \frac{1}{(j\omega)^2} \left(1 - \left\{1 + \frac{3}{2} K_o^2 \left[Q + j(T - S_A)\right\}\right. e^{-j\theta} - j\theta\, e^{-j\theta}\right) \quad . \tag{54}$$

The quantities S_A, T, and Q are given in Equations (17), (18), and (20) respectively, but in the space-charge-limited case $B = 0$, $D = 0$; therefore,

$$S_A = A^2 \frac{\theta^5}{5} \quad ,$$

$$T = -jA^2\theta^4 e^{j\theta} + 4A^2\theta^3 e^{j\theta} + j12A^2\theta^2 e^{j\theta} - 24A^2\theta\, e^{j\theta} - j24A^2 e^{j\theta} \quad ,$$

$$Q = -24A^2 \quad , \tag{55}$$

and

$$\frac{1}{v_o} = \frac{\beta_e}{\omega} \quad .$$

By Equation (12), we have

$$\beta_e = \frac{\left(1 + K_o^2 S^2\right)^{1/2}}{S} = \frac{1 + \frac{1}{2} K_o^2 S^2}{S} \quad .$$

Since from Equation (17)

$$K_o^2 S^2 = \frac{2\nabla}{\nabla_n}\left(1 + \frac{\nabla}{2\nabla_n}\right) \quad ,$$

and since

$$S = \frac{\frac{1}{\beta_e}}{\left(1 - \frac{K_o^2}{\beta_e^2}\right)^{1/2}} \quad ;$$

therefore $S = A\theta^2$ in the space-charge-limited diode. From Equation (54), we get

$$\frac{e J_o}{m_o \epsilon_o} \frac{1}{v_o} \frac{1}{(j\omega)^2} = -\frac{e J_o}{m_o \epsilon_o} \frac{\beta_e}{\omega^3} = -\frac{e J_o}{m_o \epsilon_o \omega^3} \frac{1 + \frac{\nabla}{\nabla_n}\left(1 + \frac{\nabla}{2\nabla_n}\right)}{S}$$

$$= -\frac{e J_o}{m_o \epsilon_o \omega^3} \cdot \frac{1 + \frac{\nabla}{\nabla_n}}{A\theta^2} = -\frac{2}{\theta^2}\left(1 + \frac{\nabla}{\nabla_n}\right) \quad , \qquad (56)$$

where A is given in Equation (9) and where $(\nabla/\nabla_n)^2$ has been neglected since we are interested in the first-order effect only.

With Equation (55) and Equation (56) substituted into Equation (54)

$$G^* = \frac{2}{\theta^2}\left(1+\frac{V}{V_n}\right)\left\{1 - e^{-j\theta} - \frac{3}{2}K_o^2A^2\left[-24e^{-j\theta} + j(-j\theta^4+4\theta^3 - j12\theta^2 - 24\theta - j24) - \frac{\theta^5}{5}e^{-j\theta}\right] - j\theta\, e^{-j\theta}\right\} \quad . \qquad (57)$$

When $\theta \to 0$, expand $e^{-j\theta}$ into a series in Equation (57) to get

$$G^* = -\frac{2}{\theta^2}\left(1+\frac{V}{V_n}\right)\left(1 - \left(1 - j\theta - \frac{\theta^2}{2}\right) - \frac{3}{2}K_o^2A^2\left\{-24\left[1 - j\theta + \frac{(-j\theta)^2}{2!} + \frac{(-j\theta)^3}{3!} + \frac{(-j\theta)^4}{4!} + \frac{(-j\theta)^5}{5!} + \frac{(-j\theta)^6}{6!}\right] + (\theta^4 + j4\theta^3 - 12\theta^2 - j24\theta + 24) - j\frac{\theta^5}{5}(1-j\theta)\right\} - j\theta(1-j\theta)\right)$$

$$= -\frac{2}{\theta^2}\left(1+\frac{V}{V_n}\right)\left(\frac{3}{2}K_o^2A^2\,\frac{\theta^6}{6}\,\frac{\theta^2}{2}\right) = \left(1+\frac{V}{V_n}\right)\left(1 - \frac{K_o^2}{2}A^2\theta^4\right) \quad . \qquad (58)$$

But by Equation (7)

$$K_o^2S^2 = K_o^2A^2\theta^4 = \frac{2V}{V_n}\left(1+\frac{V}{2V_n}\right) \quad ,$$

and if we neglect the second-order effect, Equation (58) reduces to

$$G^* = \left(1+\frac{V}{V_n}\right)\left(1-\frac{V}{V_n}\right) = 1 \quad .$$

When $\theta \to 0$, this equation indicates that the conduction current is still the total current, as it is in the nonrelativistic case, which is as it should be. If we express Equation (52) and Equation (53) explicitly with the coefficients for D^* given in Equation (37) and G^* given in Equation (43) and setting $B = 0$ and $D = 0$, we get the velocity modulation

$$v_1 = D^* i_c = -i_c \frac{e}{\epsilon_o m_o} (1 + K_o^2 S^2)^{-3/2} \left[(1 - e^{-j\theta}) - \frac{2}{j\theta} (1 + K_o^2 S^2)^{1/2} \left\{ 1 - e^{-j\theta} - \frac{3}{2} K_o^2 A^2 \right.\right.$$

$$\left.\left. \left[(-24 - j\frac{\theta^5}{5}) e^{-j\theta} + (\theta^4 + j4\theta^3 - 12\theta^2 - j24\theta + 24) \right] - j\theta e^{j\theta} \right\} \right]$$

$$= -i_c \frac{e}{\epsilon_o m_o} \left(1 - \frac{3V}{V_n}\right) \left[1 - e^{-j\theta} - \frac{2\left(1 + \frac{V}{V_n}\right)}{j\theta} \left\{ 1 - e^{-j\theta} - \frac{3V}{\theta^4 V_n} \left[(-24 - j\frac{\theta^5}{5}) e^{-j\theta} \right.\right.\right.$$

$$\left.\left.\left. + (\theta^4 + j4\theta^3 - 12\theta^2 - j24\theta + 24) \right] - j\theta e^{-j\theta} \right\} \right] , \tag{59}$$

and the current modulation,

$$i_1 = G^* i_c = i_c \frac{e J_o}{m_o \epsilon_o} \frac{1}{v_o} \frac{1}{(j\omega)^2} \left\{ 1 - e^{-j\theta} - \frac{3}{2} K_o^2 A^2 \left[(-24 - j\frac{\theta^5}{5}) e^{-j\theta} + \theta^4 + j4\theta^3 - 12\theta^2 \right.\right.$$

$$\left.\left. - j24\theta + 24 \right] - j\theta e^{-j\theta} \right\}$$

$$= -i_c \frac{2}{\theta^2} \left\{ 1 - e^{-j\theta} - \frac{3V}{\theta^4 V_n} \left[(-24 - j\frac{\theta^5}{5}) e^{-j\theta} + \theta^4 + j4\theta^3 - 12\theta^2 - j24\theta + 24 \right] - j\theta e^{-j\theta} \right\} . \tag{60}$$

Next we consider the behavior of equivalent diode impedance. By Equations (51) and (31),

$$Z = \frac{V_c}{i_c} = A^* = \frac{1}{\epsilon_o (j\omega)^4} \left\{ (j\omega)^3 d + \frac{e J_o}{\epsilon_o m_o} \left[\left(2 - 2e^{-j\theta} - j\theta_o - j\theta_o e^{-j\theta_o} \right) - \frac{3}{2} K_o^2 A^2 (e^{-j\theta_o} - 1) \right.\right.$$

$$\left.\left. (-\theta_o^4 + 12\theta_o^2 - 48) + j\frac{3}{2} K_o^2 A^2 (1 + e^{-j\theta_o}) \left(\frac{\theta_o^5}{5} - 4\theta_o^3 + 24\theta \right) \right] \right\} \tag{61}$$

with $B = 0$ and $D = 0$. Separate Equation (60) into its real and imaginary parts:

$$Z = R + jX \tag{62}$$

where, from Equation (61)

$$R = \frac{e J_o}{\epsilon_o m_o \epsilon_o (j\omega)^4} \left[2(1-\cos\theta_o) - \theta_o \sin\theta_o - \frac{3}{2} K_o^2 A^2 (\cos\theta_o - 1)(-\theta_o^4 + 12\theta_o^2 - 48) \right.$$

$$\left. + \frac{3}{2} K_o^2 A^2 \sin\theta_o \left(\frac{\theta_o^5}{5} - 4\theta_o^3 + 24\theta_o \right) \right] \quad , \quad (63)$$

and

$$X = -\frac{d}{\omega\epsilon_o} - \frac{e J_o}{\epsilon_o m_o \epsilon_o (j\omega)^4} \left[\theta_o (1+\cos\theta_o) - 2\sin\theta_o - \frac{3}{2} K_o^2 A^2 \sin\theta_o \left(-\theta_o^4 + 12\theta_o^2 - 48 \right) \right.$$

$$\left. - \frac{3}{2} K_o^2 A^2 (1+\cos\theta_o) \left(\frac{\theta_o}{5} - 4\theta_o^3 + 24\theta_o \right) \right] \quad . \quad (64)$$

At very low frequencies, a diode with complete space charge in the nonrelativistic case acts like a pure resistance and not like a capacitance. In the relativistic case, expand Equation (64) in series. In the expansion, the term $d/\omega\epsilon_o$ may be written in terms of the current by the use of Equation (8):

$$d = \int_o^{\theta_o} \frac{S}{\left(1 + K_o^2 S^2\right)^{1/2}} \, d\theta = \int_o^{\theta_o} A\theta^2 \left(1 + K_o^2 A^2 \theta^4\right)^{-1/2} d\theta$$

$$\approx \int_o^{\theta_o} A\theta^2 \left(1 - \frac{1}{2} K_o^2 A^2 \theta^4\right) d\theta = A\left(\frac{1}{3}\theta_o^3 - \frac{1}{14} K_o^2 A^2 \theta_o^7\right)$$

$$= \frac{1}{2} \frac{\beta_p^2}{\beta_e^3} \left(\frac{1}{3}\theta_o^3 - \frac{1}{14} K_o^2 A^2 \theta_o^7\right) = \frac{1}{2} \frac{e J_o}{m_o \epsilon_o \omega^3} \left(\frac{1}{3}\theta_o^3 - \frac{1}{14} K_o^2 A^2 \theta_o^7\right) \quad . \quad (65)$$

Substituting Equation (65) into Equation (64) gives

$$X = -\frac{e J_o}{\epsilon_o (j\omega)^4 m_o \epsilon_o} \left\{ \left[\frac{1}{6}\theta_o^3 + \theta_o(1+\cos\theta_o) - 2\sin\theta_o \right] - \frac{3}{2} K_o^2 A^2 (1+\cos\theta_o) \right.$$

$$\left. \left(\frac{\theta_o^5}{5} - 4\theta_o^3 + 24\theta_o \right) - \frac{3}{2} K_o^2 A^2 \sin\theta_o \left(-\theta_o^4 + 12\theta_o^2 - 48 \right) - \frac{1}{28} K_o^2 A^2 \theta_o^7 \right\}$$

$$= -\frac{e J_o}{\epsilon_o (j\omega)^4 m_o \epsilon_o} \left[\frac{\theta_o^5}{40} - \frac{3}{2} K_o^2 A^2 \cdot \frac{11}{21 \times 144}\, \theta_o^9 \right] . \qquad (66)$$

Now the coefficient $e J_o / \epsilon_o (j\omega)^4 m_o \epsilon_o$ is present in both the resistance and reactance expressions given in Equations (63) and (64) respectively.

Since

$$S = A\theta_o^2 = \frac{1}{2}\left(\frac{\beta_p^2}{\beta_e^3}\right)\theta_o^2$$

by Equation (7), then

$$S^2 = \frac{1}{4}\left(\frac{\beta_p^2}{\beta_e^3}\right)^2 \theta_o^4 = \frac{1}{K_o^2} \cdot \left[\frac{2\nabla}{\nabla_n}\left(1 + \frac{1}{2}\frac{\nabla}{\nabla_n}\right) \right] ,$$

$$\frac{1}{4}\theta_o^4 = \frac{\frac{1}{K_o^2}\left[\frac{2\nabla}{\nabla_n}\left(1+\frac{\nabla}{2\nabla_n}\right)\right]}{\left(\frac{\beta_p^2}{\beta_e^3}\right)^2} = \frac{\frac{1}{K_o^2}\left[\frac{2\nabla}{\nabla_n}\left(1+\frac{\nabla}{2\nabla_n}\right)\right]}{\left(\frac{e J_o}{m_o \epsilon_o \omega^3}\right)^2} . \qquad (67)$$

If

$$\frac{e J_o}{\epsilon_o (j\omega)^4 m_o \epsilon_o} = \frac{e J_o}{\epsilon_o (j\omega)^4 m_o \epsilon_o} \cdot \frac{12}{\theta_o^4} \cdot \frac{\theta_o^4}{12} , \qquad (68)$$

substituting Equation (67) into Equation (68), we have

$$\frac{e J_o}{\epsilon_o (j\omega)^4 m_o \epsilon_o} = \frac{e J_o}{\epsilon_o (j\omega)^4 m_o \epsilon_o} \cdot \frac{12}{\theta_o^4} \frac{1}{3} \cdot \frac{\frac{2}{K_o^2} \frac{\overline{V}}{\overline{V}_n} \left(1 + \frac{\overline{V}}{2\overline{V}_n}\right)}{\left(\frac{e J_o}{m_o \epsilon_o \omega^3}\right)^2} = \frac{2}{3} \frac{v}{J_o} \cdot \frac{12}{\theta_o^4} \left(1 + \frac{1}{2} \frac{\overline{V}}{\overline{V}_n}\right), \tag{69}$$

where $\overline{V}_n = m_o c^2/e = 5.11 \times 10^5$ volts. Note that J_o here is the relativistic d-c current, a little different from the nonrelativistic case, the derivation of which is given in Appendix C. From Appendix C we have

$$J_o = K \overline{V}_o^{3/2} \left(1 - \frac{3}{28} \frac{\overline{V}}{\overline{V}_n}\right) = J_{o(non)} \left(1 - \frac{3}{28} \frac{\overline{V}}{\overline{V}_n}\right) , \tag{70}$$

where $J_{o(non)}$ is the nonrelativistic d-c current. Then Equation (69) will be

$$\frac{e J_o}{\epsilon_o (j\omega)^4 m_o \epsilon_o} = \frac{2}{3} \frac{\overline{V}}{J_{o(non)}} \frac{1}{\left(1 - \frac{3}{28} \frac{\overline{V}}{\overline{V}_n}\right)} \frac{12}{\theta_o^4} \left(1 + \frac{1}{2} \frac{\overline{V}}{\overline{V}_n}\right)$$

$$= r_{e(non)} \frac{12}{\theta_o^4} \left(1 + \frac{17}{28} \frac{\overline{V}}{\overline{V}_n}\right) , \tag{71}$$

and

$$K_o^2 A^2 = \frac{1}{\theta_o^4} \frac{2\overline{V}}{\overline{V}_n} \left(1 + \frac{1}{2} \frac{\overline{V}}{\overline{V}_n}\right) = \frac{1}{\theta_o^4} \frac{2\overline{V}}{\overline{V}_n}$$

written to first-order only.

Turning now to Equation (66) again, we have

$$X = -r_{c(non)} \frac{12}{\theta_o^4} \left(1 + \frac{17}{28} \frac{\overline{V}}{\overline{V}_n}\right) \left(\frac{\theta_o^5}{40} - \frac{3\overline{V}}{\overline{V}_n} \frac{1}{\theta_o^4} \frac{11}{21 \times 144} \theta_o^9\right)$$

$$= -r_{c(non)} \frac{3}{10} \theta \left(1 + \frac{43}{252} \frac{\overline{V}}{\overline{V}_n}\right) . \tag{72}$$

In Equation (72), as in the nonrelativistic case, $\theta \to 0$ and $X \to 0$.

The low-frequency resistance can also be found from Equation (63) by series expansion of trigonometric terms, giving

$$R = \frac{2}{3} \frac{V_o}{J_{o(non)}} \left(1 + \frac{17}{28} \frac{V}{V_n}\right) \left[1 - \frac{1}{15} \theta_o^2 - \frac{V}{V_n} \left(\frac{3}{7} - \frac{5}{168} \theta_o^2\right)\right] \quad . \quad (73)$$

When $\theta \to 0$,

$$R = r_{e(non)} \left(1 + \frac{17}{28} \frac{V}{V_n}\right) \left(1 - \frac{3}{7} \frac{V}{V_n}\right) = r_{e(non)} \left(1 + \frac{5}{28} \frac{V}{V_n}\right) \quad . \quad (74)$$

This value checks with the value calculated from Poisson's equation given in Appendix C, and this is recognized as the slope of the static relativistic characteristic. The physical interpretation is for any given voltage. The electron velocity is less than that calculated from nonrelativistic considerations. The charge density is therefore greater, and the current is thereby reduced, so that the resistance is increased. The form of the resistance and reactance as functions of transit angle is shown graphically in Figure 1, the data for which are presented in Table I. The curve shown in Figure 1 is for $V = 2.115 \times 10^5$ volts, the maximum limit of our analysis.

When using the figure, one should be careful about the transit angles. the relativistic transit angle is not equal to the nonrelativistic one.. By Equation (65), we have

$$d = \frac{1}{2} \frac{e J_o}{m_o \epsilon_o \omega^3} \left(\frac{1}{3} \theta_o^3 - \frac{1}{14} K_o^2 A^2 \theta_o^7\right) = \frac{1}{6} \frac{e J_o \theta_o^3}{m_o \epsilon_o \omega^3} \left(1 - \frac{3}{14} K_o^2 A^2 \theta_o^4\right)$$

$$= \frac{1}{6} \frac{e J_o \theta_o^3}{m_o \epsilon_o \omega^3} \left(1 - \frac{3}{7} \frac{V}{V_n}\right) \quad , \quad (75)$$

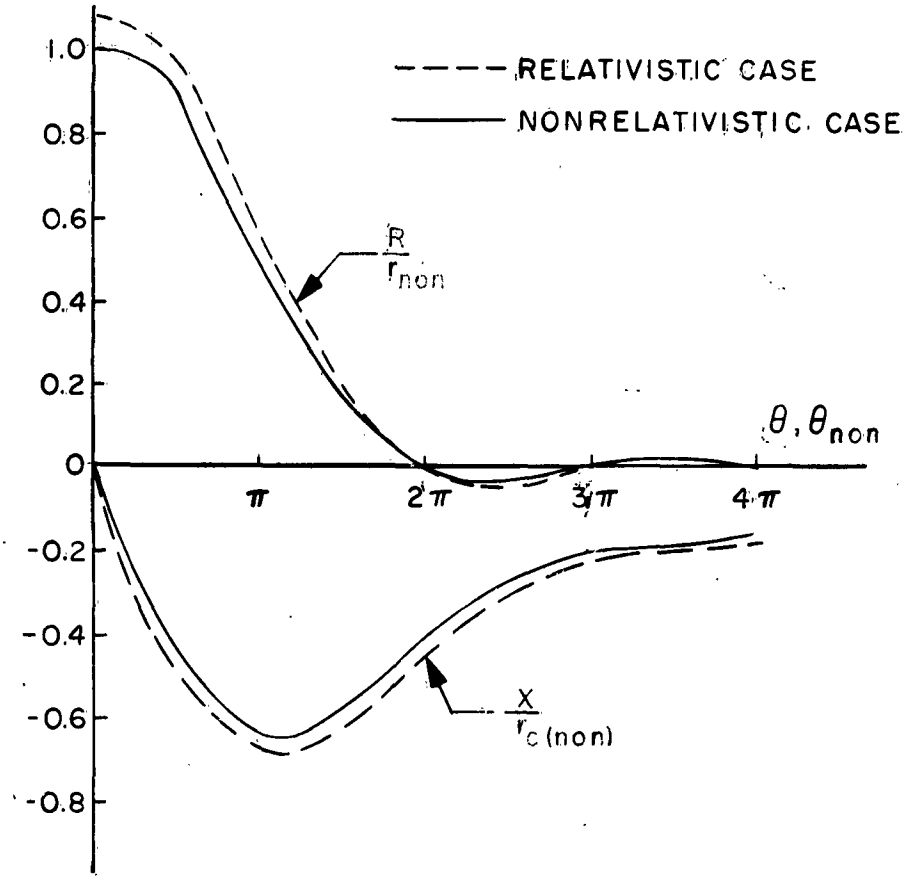

Figure 1. Internal Impedance of Diode as Function of Transit Angle θ.

In the nonrelativistic case,

$$d = \int_0^{\theta_{o(non)}} \frac{d\theta}{\beta_e} = \frac{1}{6} \frac{\beta_p^2}{\beta_e^3} \theta_{non}^3 = \frac{1}{6} \frac{e J_{o(non)}}{m_o \epsilon_o \omega^3} \theta_{o(non)}^3 \quad , \quad (76)$$

and equating Equations (75) and (76), and using Equation (70) gives

$$\theta_o^3 = \theta_{o(non)}^3 \left(1 + \frac{15}{28} \frac{V}{V_n}\right) \quad ,$$

Table I. Data for Internal Impedance of Diode as Function of Transit Angle θ.

Transit angle θ	Nonrelativistic value $r/r_{c(non)}$	Relativistic correction $\frac{r}{r_{c(non)}}\left(\frac{V}{V_n}\right)$	Nonrelativistic value $x/r_{c(non)}$	Relativistic core $\frac{x}{r_{c(non)}}\frac{V}{V_n}$
0	1.000000	0.178571	0.000000	0.000000
1.0	0.935093	0.113415	-0.288320	-0.146720
1.4	0.875997	0.135635	-0.388551	-0.119100
1.57096($1/2\pi$)	0.845991	0.153627	-0.427248	-0.073750
1.8	0.801872	0.146760	-0.474784	-0.095990
2.356195($3/4\pi$)	0.680630	0.126340	-0.566900	-0.133050
2.8	0.575244	0.110000	-0.615070	-0.110360
3.141593(π)	0.492768	0.094500	-0.636620	-0.113682
3.6	0.384844	0.079490	-0.645341	-0.119320
4.0	0.296930	0.061570	-0.635891	-0.117020
4.71239($3/2\pi$)	0.163340	0.034940	-0.587754	-0.110720
5.2	0.092785	0.010440	-0.538847	-0.103353
5.6	0.048612	0.011540	-0.493874	-0.096146
6.283186(2π)	0.000000	0.000000	-0.415605	-0.08120
6.8	-0.017391	-0.006500	-0.359815	-0.130135
7.2	-0.022019	-0.007400	-0.322399	-0.064610
7.853980($5/2\pi$)	-0.018462	-0.008430	-0.273109	-0.053910
8.4	-0.009979	-0.007020	-0.243708	-0.036473
9.0	-0.000206	-0.005920	-0.222267	-0.048130
9.424776(3π)	0.006084	-0.004260	-0.212207	-0.037894
10	0.010942	-0.003470	-0.203237	-0.033916
10.995592($7/2\pi$)	0.010669	-0.000312	-0.192560	-0.032164
12.566372(4π)	0.000000	0.000000	-0.017249	-0.029391

or, considering the first-order only,

$$\theta_o = \theta_{o(non)} \left(1 + \frac{5}{28} \frac{V}{V_n}\right) \quad . \tag{77}$$

Now, we want to know the change in its negative maximum resistance when θ is moderately large. Equation (63) could be written as

$$R \doteq - r_{c(non)} \frac{12}{\theta_o^4} \left(1 + \frac{17}{28} \frac{V}{V_n}\right) \left(\theta_o \sin\theta_o - \frac{3}{5} \frac{V}{V_n} \theta_o \sin\theta_o\right) \quad . \tag{78}$$

when

$$\theta_o = 2n\pi + \frac{1}{2}\pi, \quad R \to R_{max},$$

and

$$-R_{max} = r_{c(non)} \left(1 + \frac{1}{140} \frac{V}{V_n}\right) 12 \left[\frac{2}{(4n+1)\pi}\right]^3$$

$$= \frac{96}{\pi^3} r_{c(non)} \left(\frac{1}{4n+1}\right)^3 \left(1 + \frac{1}{140} \frac{V}{V_n}\right) \quad n = 1, 2, 3, \ldots \quad . \tag{79}$$

We can tell from Equation (79), that $-R_{max}$ is increased $\frac{1}{140} \frac{V}{V_n}$ compared with the nonrelativistic case, but this effect is very small, being approximately equal to 0.3 per cent when $V = 2.115 \times 10^5$ volts.

B. Application to Klystron Gaps:

The following analysis does not assume that the d-c space charge is sufficient to depress the space potential distribution, but is based on the fact that practical klystron tubes operate with grids at the same potential with relatively high d-c voltage so that the space charge is insufficient to

affect the space potential. The geometrical dimensions are given in Figure 2.

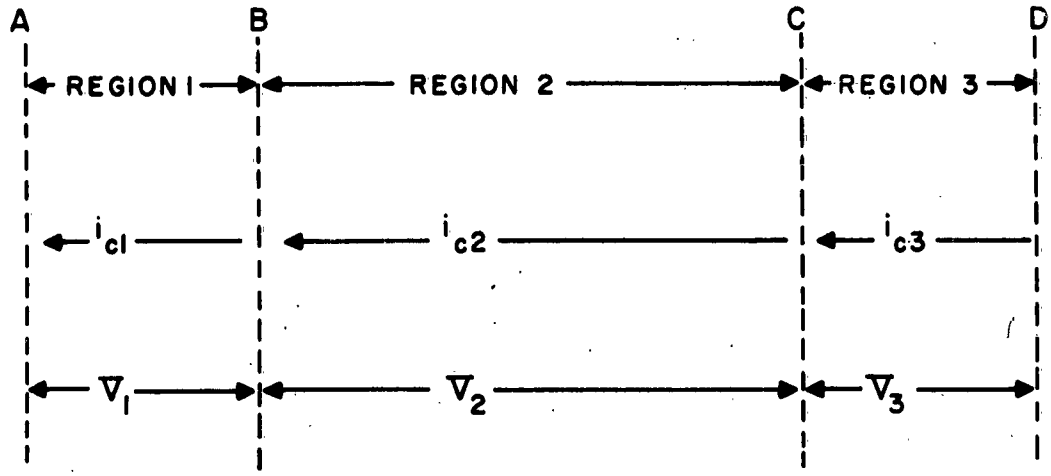

Figure 2. Sketch of Klystron Gaps Illustrating Nomenclature.

Region 1

$$v_A = v_B = v_C = v_D = \overline{V} \quad .$$

At plane A, $i_{1a} = 0$, $v_{1a} = 0$; that is, there is no initial velocity and current modulation. Thus Equation (30) is reduced to

$$\begin{aligned} V_1 &= A_1^* i_{c1} \quad , \\ v_1 &= D_1^* i_{c1} \quad , \\ i_1 &= G_1^* i_{c1} \quad . \end{aligned} \tag{80}$$

From Equation (80), we get

$$i_{c1} = \frac{V_1}{A_1^*} \quad ,$$

$$v_1 = \frac{D_1^*}{A_1^*} V_1 \quad , \tag{81}$$

$$i_1 = \frac{G_1^*}{A_1^*} V_1 \quad .$$

Now, we study the velocity modulation first, using D_1^* given in Equation (37), and A_1^* given in Equation (31):

$$D_1^* = -\frac{1}{(j\omega)^2} \frac{e}{m_o \epsilon_o} \left(1 + K_o^2 S^2\right)^{-3/2} \left[(1 - e^{-j\theta}) \right.$$

$$\left. - \frac{(2A\theta + B)\left(1 + K_o^2 S^2\right)^{-1/2}}{j\,S} \left\{ 1 - \left[1 + \frac{3}{2} K_o^2 (Q + j\overline{T - S_A}) \right] e^{-j\theta} - j\theta\, e^{-j\theta} \right\} \right] \quad ,$$

$$A_1^* = \frac{1}{\epsilon_o (j\omega)^4} \left\{ (j\omega)^3 \, d + \frac{e J_o}{\epsilon_o m} \left[\left(2 - 2e^{-j\theta_o} - j\theta_o - j\theta_o \, e^{-j\theta_o} \right) \right.\right.$$

$$\left.\left. - \frac{3}{2} K_o^2 \left(e^{-j\theta_o} - 1 \right) (Q - N + M) + j\frac{3}{2} K_o^2 P \left(1 + e^{-j\theta_o} \right) \right] \right\} \quad .$$

Since it is assumed $J_o \approx 0$ and $V_A = V_B$, therefore $A = 0$, $B = 0$; then

$$v_1 = \frac{D_1^*}{A_1^*} V_1 = \frac{-1}{(j\omega)^2} \frac{e}{m_o \epsilon_o} \left(1 + K_o^2 D^2\right)^{-3/2} \left(1 - e^{-j\theta_o}\right) V_1 - \frac{j\omega \epsilon_o}{d}$$

$$= \frac{-e}{m_o d} V_1 \left(1 + K_o^2 D^2\right)^{-\frac{3}{2}} e^{-j\frac{\theta_o}{2}} \frac{e^{+j\frac{\theta_o}{2}} - e^{-j\frac{\theta_o}{2}}}{j\omega\tau} \cdot \tau$$

$$= \frac{-e\tau}{m_o} \left(1 + K_o^2 D^2\right)^{-3/2} \frac{\sin\frac{\theta_o}{2}}{\frac{\theta_o}{2}} V_1 e^{-j\frac{\theta_o}{2}} \quad . \tag{82}$$

By Equation (14)

$$d = \int_o^{\theta_o} \frac{d\theta}{\beta_e} = \int_o^{\tau} \frac{\omega dt}{\beta_e} = v_o \tau \quad , \tag{83}$$

since $\omega/\beta_e = v_o$ and v_o is a constant. Then we can rewrite Equation (82) as

$$v_1 = \frac{e}{m_o} \frac{1}{v_o^2} \left(1 - \frac{3}{2} K_o^2 D^2\right) \frac{\sin\frac{\theta_o}{2}}{\frac{\theta_o}{2}} v_o v_1 e^{-j\frac{\theta_o}{2}} \quad . \tag{84}$$

From energy relation,

$$m_o c^2 \left[\frac{1}{\sqrt{1 - \frac{v_o^2}{c^2}}} - 1\right] = eV \quad ,$$

solve for v_o^2 :

$$v_o^2 = c^2 \left[1 - \frac{1}{\left(1 + \frac{V}{V_n}\right)^2}\right] = \frac{2eV}{m_o} \left(1 + \frac{V}{V_n}\right)\left(1 + \frac{V}{V_n}\right)^{-2} = \frac{2eV}{m_o} \left(1 - \frac{3}{2}\frac{V}{V_n}\right) \quad . \tag{84a}$$

And $K_o^2 D^2 = 2V/V_n$ by Equation (11), if we neglect the second-order effect.

Finally, Equation (84) will be in the following form:

$$v_1 = -\frac{e}{m_o}\frac{1}{\frac{2eV}{m_o}}\frac{\left(1-3\frac{V}{V_n}\right)}{\left(1-\frac{3}{2}\frac{V}{V_n}\right)}\frac{\sin\frac{\theta_o}{2}}{\frac{\theta_o}{2}}v_o V_1 e^{-j\frac{\theta_o}{2}} = -\frac{V_1}{2V}\left(1-\frac{3}{2}\frac{V}{V_n}\right)\frac{\sin\frac{\theta_o}{2}}{\frac{\theta_o}{2}}v_o e^{-j\frac{\theta_o}{2}}, \tag{85}$$

where the minus sign on the right-hand side of the equation indicates that the direction of the velocity is opposite to the direction of the total current i_c. It indicates that the operation of velocity modulation with high accelerating voltages is seriously affected by the relativistic increase in electron mass. In the nonrelativistic case, the change in velocity is only $V_1/2V$ as given by Hahn and Metcalf,[5] while in the relativistic case, it becomes

$$\frac{V_1}{2V}\left(1-\frac{3}{2}\frac{V}{V_n}\right) .$$

This factor, which measures the reduction of modulation from the nonrelativistic value amounts to 0.76 for 100 kv.

Furthermore, if one adds the factor $e^{j\omega t}$ in Equation (85) and takes the real part, one gets

$$R_e(v_1) = \frac{V_1}{2V}\left(1-\frac{3}{2}\frac{V}{V_n}\right)\frac{\sin\frac{\theta_o}{2}}{\frac{\theta_o}{2}}v_o\cos\left(\omega t-\frac{\theta_o}{2}\right) . \tag{86}$$

If one takes the center of the gap as the reference plane, and a reference point for time that will give a sine wave, then the total velocity is

$$v = v_o \left[1 + \frac{\bar{V}_1}{2\bar{V}} \left(1 - \frac{3}{2} \frac{\bar{V}}{\bar{V}_n} \right) M \sin \omega t_1 \right] \quad , \qquad (87)$$

where the beam-coupling coefficient $M = \sin \frac{\theta_o}{2} / \frac{\theta_o}{2}$.

Next, we want to know the current modulation. From Equation (81),

$$i_1 = \frac{G_1^*}{A_1^*} \bar{V}_1 \quad .$$

From Equation (31), A_1^* is reduced to $d/j\omega_o$, since $J_o \approx 0$. From Equation (43)

$$G_1^* = \frac{e}{m_o \epsilon_o} \frac{J_o}{v_o} \frac{1}{(j\omega)^2} \left\{ 1 - \left[1 + \frac{3}{2} K_o^2 (Q + j \overline{T - S_A}) \right] e^{-j\theta_o - j\theta_o} e^{-j\theta_o} \right\} \quad ,$$

where when $A = 0$, $B = 0$ and $d = v_o \tau$, Equation (17) reduces to $Q = -D^2$, Equation (18) to $T = -jD^2 e^{j\theta_o}$, and Equation (20) to $S_A = D^2 \theta_o$. Therefore

$$i_1 = \frac{e J_o}{m_o v_o^2} \frac{v_1}{(j\omega\tau)} \left(1 - \left\{ 1 + \frac{3}{2} K_o^2 \left[-D^2 + j\left(-jD^2 e^{j\theta_o} - D^2 \theta_o \right) \right] \right\} e^{-j\theta_o - j\theta_o} e^{-j\theta_o} \right)$$

$$= \frac{e J_o \bar{V}_1}{m_o v_o^2} \frac{1}{j\theta_o} \left\{ 1 - \left[1 + \frac{3}{2} K_o^2 D^2 \left(-1 + e^{j\theta_o} - j\theta_o \right) \right] e^{-j\theta_o - j\theta_o} e^{-j\theta_o} \right\} \quad .$$

Since the gap is very small, we can expand $e^{j\theta_o}$ and $e^{-j\theta_o}$ into the series,

$$i_1 = \frac{e J_o \bar{V}_1}{m_o v_o^2} \frac{1}{j\theta_o} \left\{ 1 - \left[1 + \frac{3}{2} K_o^2 D^2 \left(-1 + 1 + j\theta - \frac{\theta_o^2}{2} - j\theta_o \right) \right] e^{-j\theta_o - j\theta_o} e^{-j\theta_o} \right\}$$

$$= \frac{e J_o \bar{V}_1}{m_o v_o^2} \frac{1}{j\theta_o} \left\{ 1 - e^{-j\theta_o - j\theta_o} e^{-j\theta_o} + \frac{3}{4} K_o^2 D^2 \theta_o^2 e^{-j\theta_o} \right\}$$

$$= \frac{e J_o V_1}{m_o v_o^2} \frac{1}{j\theta_o} \left\{ 1 - (1 - j\theta_o) - j\theta_o (1 - j\theta_o) + \frac{3}{4} K_o^2 D^2 \theta_o^2 e^{-j\theta_o} \right\}$$

$$= 0 \quad \text{as} \quad \theta_o \to 0 \quad .$$

Therefore there is no current modulation as long as the gap is small, just as in the nonrelativistic case.

Now, the most interesting case left is the beam-loading conductance and susceptance. The admittance of the gap in Equation (81) is:

$$Y = \frac{i_c}{V_1} = \frac{1}{A_1^*} \quad ,$$

where from Equation (31),

$$A_1^* = \frac{(j\omega)^3 d}{\epsilon_o (j\omega)^4} \left\{ 1 + \frac{e J_o}{(j\omega)^3 d \epsilon_o m_o} \left[\left(2 - 2e^{-j\theta_o} - j\theta_o - j\theta_o e^{-j\theta_o} \right) \right. \right.$$

$$\left. \left. - \frac{3}{2} K_o^2 (Q - N + M) \left(e^{-j\theta_o} - 1 \right) + j \frac{3}{2} K_o^2 P \left(1 + e^{-j\theta_o} \right) \right] \right\} \quad .$$

Since $J_o \approx 0$, we can expand $1/A_1^*$ by binomial theorem to give

$$Y = \frac{1}{A_1^*} = \frac{(j\omega)\epsilon_o}{d} \left\{ 1 - \frac{e J_o}{(j\omega)^3 d \epsilon_o m_o} \left[\left(2 - 2e^{-j\theta_o} - j\theta_o - j\theta_o e^{-j\theta_o} \right) - \frac{3}{2} K_o^2 (Q - N + M) \left(e^{-j\theta_o} - 1 \right) \right. \right.$$

$$\left. \left. + j \frac{3}{2} K_o^2 P \left(1 + e^{-j\theta_o} \right) \right] \right\}$$

$$= \left\{ \frac{j\omega\epsilon_o}{d} - \frac{e J_o}{(j\omega)^2 d^2 m_o} \left[\left(2 - 2e^{-j\theta_o} - j\theta_o - j\theta_o e^{-j\theta_o} \right) - \frac{3}{2} K_o^2 (Q - N + M) \left(e^{-j\theta_o} - 1 \right) + j \frac{3}{2} K_o^2 P \right. \right.$$

$$\left. \left. \left(1 + e^{-j\theta_o} \right) \right] \right\} \quad ,$$

then divide this into the real and imaginary part. The real part will be

$$G = \frac{e J_o}{m_o \omega^2 d^2} \left[2(1 - \cos\theta_o) - \theta_o \sin\theta_o - \frac{3}{2} K_o^2 (\cos\theta_o - 1)(Q - N + M) \frac{3}{2} K_o^2 P \sin\theta_o \right] . \tag{88}$$

When $A = 0$, $B = 0$ and $d = V_o \tau$, Equation (20) reduced to $Q = -D^2$, Equation (27) to $N = 0$, Equation (28) to $M = -D^2$, and Equation (29) to $p = D^2\theta$. Substituting these values in Equation (88) gives

$$G = \frac{e J_o}{m_o v_o^2 \theta_o^2} \left(1 - \frac{3}{2} K_o^2 D^2 \right) \left[2(1 - \cos\theta_o) - \theta_o \sin\theta_o \right] . \tag{89}$$

In the nonrelativistic case, Equation (89) becomes

$$G_{non} = \frac{G_o}{2} \frac{1}{\theta_o^2} \left[2(1 - \cos\theta_o) - \theta_o \sin\theta_o \right] , \tag{90}$$

where use has been made of the fact that $G_o = J_o/V$ and $m_o v_o^2/2 = eV$. Equation (90) is the familiar form of beam-loading conductance of an ordinary gap as given by Beck.[6]

In the relativistic case, v_o^2 is given in Equation (84a) and $K_o^2 D^2$ is known to be $2V/V_n$, then Equation (89) will be

$$G = \frac{J_o}{V} \frac{1}{2\theta_o^2} \left(1 - \frac{3}{2} \frac{V}{V_n} \right) \left[2(1 - \cos\theta_o) - \theta_o \sin\theta_o \right]$$

$$= \frac{G_o}{2} \frac{\left(1 - \frac{3}{2} \frac{V}{V_n} \right)}{\theta_o^2} \left[2(1 - \cos\theta_o) - \theta_o \sin\theta_o \right] . \tag{91}$$

Note here that J_o is the relativistic current which may or may not be equal to the nonrelativistic value, but even for the space-charge-limited case, the current differs by only a small amount, hence we can still use $G_o = J_o/V$

without serious error. Furthermore what we are interested in is the ratio G/G_o. Equation (91) indicates that the relativistic effect is rather important since when $V = 2 \times 10^5$ volts, $G/G_o = 0.412$, which is a serious decrease in beam conductance.

For the susceptance, take the imaginary part,

$$B = \frac{(j\omega)\epsilon_o}{d} + j \frac{e J_o}{\omega^2 d^2 m_o} \left[2 \sin \theta_o - \theta_o(1+\cos\theta_o)\right]\left[1 - \frac{3}{2} K_o^2 D^2\right]$$

$$= \frac{(j\omega)\epsilon_o}{d} + j \frac{G_o\left(1 - \frac{3}{2}\frac{V}{V_n}\right)}{2\theta_o^2} \left[2\sin\theta_o - \theta_o(1+\cos\theta_o)\right] \quad . \qquad (92)$$

The first term in Equation (92) is the susceptance resulting from the gap itself, and the second is due to the beam, hence the beam-loading susceptance in the relativistic case is

$$B_1 = \frac{G_o}{2} \frac{1}{\theta_o^2}\left(1 - \frac{3}{2}\frac{V}{V_n}\right) \left[2\sin\theta_o - \theta_o(1+\cos\theta_o)\right] \quad , \qquad (93)$$

while in nonrelativistic case, it is reduced to

$$\frac{G_o}{2} \frac{1}{\theta_o} \left[2\sin\theta_o - \theta_o(1+\cos\theta_o)\right] \quad ,$$

as given by Beck.[6]

Region 2

In Region 2

$$V_2 = 0 = A_2^* i_{2c} + 0 + C_2^* v_b \quad , \qquad (94a)$$

$$v_2 = D_2^* i_{2c} + 0 + F_2^* v_b \quad , \tag{94b}$$

$$i_2 = G_2^* i_{2c} + 0 + I_2^* v_b \quad . \tag{94c}$$

The current modulation terms are missing, since there is no current modulation in the first gap.

From Equation (94a), we have $i_{2c} = C_2^*/A_2^* v_b$ and substituting this in Equation (94c) gives

$$i_2 = -\frac{G_2^* C_2^*}{A_2^*} v_b + I_2^* v_b = I_2^* \left(1 - \frac{G_2^* C_2^*}{A_2^* I_2^*}\right) v_b \quad ,$$

where G_2^*, C_2^*, A_2^*, I_2^* are given in Equations (43), (35), (31), and (47) respectively, and G_2^*, C_2^*, I_2^* all contain J_o in their expression, hence $G_2^* C_2^*/A_2^* I_2^*$ approaches the order of J_o. Since $J_o \approx 0$, $G_2^* C_2^*/A_2^* I_2^*$ approaches zero; therefore

$$i_2 = I_2^* v_b = -j \frac{J_o}{v_o} \left(1 + K_o^2 D^2\right)^{3/2} \left(\theta_2 - \frac{3}{2} K_o^2 S_A\right) e^{-j\theta_2} v_b \quad .$$

Now with $A = 0$, $B = 0$, Equation (17) gives $S_A = D^2\theta^2$, which if substituted in the preceding equation gives

$$i_2 = j \frac{J_o}{v_o} \left(1 + K_o^2 D^2\right)^{3/2} \theta_2 \left(1 - \frac{3}{2} K_o^2 D^2\right) e^{-j\theta_2} v_b$$

$$= -j \left(\frac{v_b}{v_o}\right) J_o \theta_2 e^{-j\theta_2} \quad . \tag{95}$$

The minus sign on the right-hand side of the equation indicates that i_2 is opposite to v_b in direction. This expression is the same as in the non-

relativistic case, except that here it is the relativistic expression. From this, it is apparent that the current in the drift region is not affected by the relativistic effect, since there is no relation between current and the mass of the electron, which accounts for the relativistic effect.

Similarly, we can solve for v_2 in Equation (94):

$$v_2 = D_2^* i_{2c} + F_2^* v_b = F_2^* \left(1 - \frac{D_2^* C_2^*}{A_2^* F_2^*}\right) v_b \quad .$$

Again

$$\frac{D_2^* C_2^*}{A_2^* F_2^*}$$

approaches the order of J_o; and since $J_o \approx 0$, therefore

$$\frac{D_2^* C_2^*}{A_2^* F_2^*} \approx 0$$

and

$$F_2^* = e^{-j\theta_2} \left(1 + K_o^2 D^2\right)^{3/2} \left(1 + K_o^2 D^2\right)^{-3/2} = e^{-j\theta_2} \quad ,$$

as in Equation (42) if $A = 0$, $B = 0$. Consequently

$$v_2 = e^{-j\theta_2} v_b \quad , \tag{96}$$

which indicates that as in the nonrelativistic case there is a phase shift only in the velocity at the drift region.

Region 3

In Region 3

$$v_3 = A_3^* i_{3c} + B_3^* i_2 + C_3^* v_c \quad .$$

Solve for i_{3c}

$$i_{3c} = \frac{\nabla_3}{A_3^*} - \frac{B_3^*}{A_3^*} i_2 - \frac{C_3^*}{A_3^*} v_c \quad . \tag{97}$$

The last term in Equation (97) is approximately equal to zero, since

$$C_3^* = -\frac{J_o}{\epsilon_o} \frac{1}{(j\omega)^2} \left(1 + K_o^2 D^2\right)^{3/2} \left\{\left(j\theta_o e^{-j\theta_o} + e^{-j\theta_o} - 1\right) + \frac{3}{2} K_o^2 \left[(M-N-jP)e^{-j\theta_o} - M\right]\right\} .$$

Since $J_o \approx 0$, then $C_3^* \approx 0$. We are not interested in the velocity modulation term. The first term in Equation (97) is observed to be the capacitive current; the second term is the induced current.

From Equation (33) and (21), if $A = 0$, $B = 0$, and $J_o \approx 0$, the relation between B_3^* and A_3^* is

$$\frac{B_3^*}{A_3^*} = \frac{j\omega^2}{\epsilon_o (j\omega)^3} D\left(+ K_o^2 D^2\right)^{-1/2} \left(e^{-j\theta_3} - 1\right) \frac{\epsilon_o (j\omega)^4}{(j\omega)^3 d} \quad . \tag{98}$$

Recognizing that $1/\beta_e = D/\left(1 + K_o^2 D^2\right)^{1/2}$ as given by Equation (12) when $A = 0$ and $B = 0$, one has

$$d = v_o \tau_3 = \frac{\omega}{\beta_e} \tau_3 = \frac{\omega D}{\left(1 + K_o^2 D^2\right)^{1/2}} \tau_3 \quad ;$$

hence Equation (98) will be

$$\frac{B_3^*}{A_3^*} = \frac{\left(e^{-j\theta_3} - 1\right)}{j\omega\tau_3} = -e^{-j\frac{\theta_3}{2}} \frac{\sin\frac{\theta_3}{2}}{\frac{\theta_3}{2}} = -e^{-j\frac{\theta_3}{2}} M_3 \quad .$$

The induced current is

$$J_i = -\frac{B_3^*}{A_3^*} i_2 = e^{-j\frac{\theta_3}{2}} M_3 i_2 \quad , \tag{99}$$

where i_2 is given in Equation (95).

$$J_i = -j\left(\frac{v_b}{v_o}\right) J_o M_3 \theta_2 e^{-j\frac{\theta_3}{2}} e^{-j\theta_2} \quad . \tag{100}$$

The transadmittance g_m is defined as $J_{i(out)}/V_{in}$, and v_b/v_o is given in Equation (85) with $\theta = \theta_1$, then

$$g_m = \frac{J_i}{V_1} = \left[-\frac{1}{2} M_1 M_3 \frac{J_o}{V}\left(1 - \frac{3}{2}\frac{V}{V_n}\right)(j\theta_2)\, e^{-j\left(\frac{\theta_1+\theta_3}{2}\right)} e^{-j\theta_2}\right] \quad , \tag{101}$$

where

$$M_1 = \frac{\sin\frac{\theta_1}{2}}{\frac{\theta_1}{2}} \quad , \quad M_3 = \frac{\sin\frac{\theta_3}{2}}{\frac{\theta_3}{2}} \quad .$$

The expression g_m is reduced to $1 - \frac{3}{2}\frac{V}{V_n}$ of the nonrelativistic case given by Hahn and Metcalf.[5] The factor,

$$e^{-j\left(\frac{\theta_1 + \theta_3}{2}\right)} \quad ,$$

is missing if the center of each gap is taken as a reference plane.

V. APPLICATIONS TO THE VERY HIGH-POWER KLYSTRON GAPS

The applications given in Chapter IV are limited to $K_o^2/\beta_e^2 < \frac{1}{2}$. The results obtained in Chapter III are applied in Chapter IV to space-charge-limited diodes and klystron gaps. We limited ourselves to $K_o^2/\beta_e^2 < \frac{1}{2}$ because of the difficulty in solving the wave potential integral π.

This difficulty is eliminated for klystron gaps, for if it is assumed that the space charge does not change the space-potential distribution in the gap, then the evaluation of the integral π is without any limitation; therefore we can extend this even for $K_o^2/\beta_e^2 \gg \frac{1}{2}$:

$$\pi = \int \left(C_1 - ji_c e^{j\theta}\right)\left(1 - \frac{K_o^2}{\beta_e^2}\right)^{3/2} d\theta + C_2$$

$$= \int \left(C_1 - ji_c e^{j\theta}\right)\left(1 + K_o^2 S^2\right)^{-3/2} d\theta + C_2$$

$$= \int \left(C_1 - ji_c e^{j\theta}\right)\left(1 + K_o^2 D^2\right)^{-3/2} d\theta + C_2$$

$$= \left(C_1\theta - i_c e^{j\theta}\right)\left(1 + K_o^2 D^2\right)^{-3/2} + C_2 \quad , \tag{102}$$

where $S = A\theta^2 + B\theta + D = D$, since $A = B = 0$.

For the first klystron gap, $i_{1a} = v_{1a} = 0$, and from Equation (1)

$$i_1 = \frac{\beta_p^2}{\beta_e^2} e^{-j\theta}\pi = \frac{\beta_p^2}{\beta_e^2} e^{-j\theta}\left[\left(1 + K_o^2 D^2\right)^{-3/2}\left(C_1\theta - i_c e^{j\theta}\right) + C_2\right] \quad ;$$

but as $\theta \to 0$ and $i_1 \to i_{1a} = 0$, we can solve for C_2 :

$$C_2 = i_c\left(1 + K_o^2 D^2\right)^{-3/2} \quad . \tag{103}$$

Similarly C_1 is obtained by substituting Equation (103) into Equation (3):

$$v_1 = -\frac{1}{j\omega\epsilon_o}\frac{e}{m_o\omega}\, e^{-j\theta}\left[\left(C_1 - ji_c e^{j\theta}\right)\left(1 - \frac{K_o^2}{\beta_e^2}\right)^{3/2} - \frac{1}{\frac{1}{\beta_e}}\frac{d\left(\frac{1}{\beta_e}\right)}{d\theta}\,\pi\right] .$$

With $\theta \to 0$, $v_1 \to v_{1a} = 0$, we get

$$(C_1 - ji_c)\left(1 + K_o^2 D^2\right)^{-3/2} - \frac{B}{D}\left(1 + K_o^2 D^2\right)^{-1}\left[-\left(1 + K_o^2 D^2\right)^{-3/2} i_c + C_2\right] = 0 \; ; \tag{104}$$

therefore $C_1 = ji_c$. Substituting C_1 and C_2 into i_1 and v_1 again, we have

$$i_1 = G^* i_c = \frac{e\, J_o}{m_o \epsilon_o v_o}\frac{1}{(j\omega)^2}\left(1 + K_o^2 D^2\right)^{-3/2}\left(1 - e^{j\theta} - j\theta\, e^{-j\theta}\right) i_c \quad , \tag{105}$$

$$v_1 = D^* i_c = \frac{e}{\epsilon_o m_o}\frac{1}{(j\omega)^2}\left(1 + K_o^2 D^2\right)^{-3/2}\left(1 - e^{-j\theta}\right) i_c \quad . \tag{106}$$

The applied voltage across the gaps is

$$V_1 = \int_o^d E_1\, dz = \int_o^{\theta_o} \frac{E_1}{\beta_e}\, d\theta \quad ,$$

where E_1 is given in Equation (2), resulting in

$$V_1 = \int_o^{\theta_o} \frac{E_1}{\beta_e} = \frac{1}{j\omega\epsilon_o}\left[i_c \int_o^{\theta_o} \frac{d\theta}{\beta_e} - \frac{\beta_p^2}{\beta_e^3}\int_o^{\theta_o} e^{-j\theta}\,\pi\, d\theta\right]$$

$$= A^* i_c \frac{1}{(j\omega)^4 \epsilon_o} \left[(j\omega)^3 d + \frac{e J_o}{m_o \epsilon_o} \left(1 + K_o^2 D^2\right)^{-3/2} \left(2 - 2e^{-j\theta_o} - j\theta_o - j\theta_o e^{-j\theta_o}\right) \right] . \tag{107}$$

Now, the velocity modulation given in Equation (81) becomes

$$v_1 = \frac{D^*}{A^*} \nabla_1 = \frac{j\omega\epsilon_o}{d} \frac{e}{\epsilon_o m_o} \frac{1}{(j\omega)^2} \left(1 + K_o^2 D^2\right)^{-3/2} \left(1 - e^{-j\theta}\right) \nabla_1$$

$$= \frac{e}{m_o v_o^2} \left(1 + K_o^2 D^2\right)^{-3/2} \frac{\sin \frac{\theta}{2}}{\frac{\theta}{2}} v_o \nabla_1 e^{-j\frac{\theta}{2}} , \tag{108}$$

where v_o^2 is as given in Equation (84a) and D is as given in Equation (11):

$$v_o^2 = \frac{2e\nabla}{m_o} \left(1 + \frac{1}{2} \frac{\nabla}{\nabla_n}\right) \left(1 + \frac{\nabla}{\nabla_n}\right)^{-2} \left(1 + K_o^2 D^2\right)^{-3/2} = \left[1 + \frac{2\nabla}{\nabla_n} \left(1 + \frac{1}{2} \frac{\nabla}{\nabla_n}\right)\right]^{-3/2}$$

$$= \left(1 + \frac{\nabla}{\nabla_n}\right)^{-3} .$$

Substituting the preceding two equations into Equation (108) gives

$$v_1 = \frac{\nabla_1}{2\nabla} \frac{1}{\left(1 + \frac{1}{2} \frac{\nabla}{\nabla_n}\right) \left(1 + \frac{\nabla}{\nabla_n}\right)} \frac{\sin \frac{\theta}{2}}{\frac{\theta}{2}} v_o e^{-j\frac{\theta}{2}} . \tag{109}$$

This expression is given by Beck,[7] and will reduce to

$$v_1 = \left(1 - \frac{3}{2} \frac{\nabla}{\nabla_n}\right) \frac{\nabla_1}{2\nabla} \frac{\sin \frac{\theta}{2}}{\frac{\theta}{2}} v_o e^{-j\frac{\theta}{2}} \qquad \text{for } \frac{K_o^2}{\beta_e^2} < \frac{1}{2} ,$$

as shown in Chapter IV. If V = 1000 kv,

$$\frac{1}{\left(1+\frac{1}{2}\frac{\nabla}{\nabla_n}\right)\left(1+\frac{\nabla}{\nabla_n}\right)} = 0.17 \quad ;$$

then the relativistic effect is seen to be very important in very high-power klystrons.

As for the current modulation,

$$i_1 = \frac{G^*}{A^*}\nabla_1 = \frac{j\omega\epsilon_o}{d}\frac{e J_o}{m_o\epsilon_o v_o}\frac{1}{(j\omega)^2}\left(1+K_o^2D^2\right)^{-3/2}(1-e^{-j\theta}-j\theta\, e^{-j\theta})\nabla_1$$

$$= \frac{e J_o \nabla_1}{m_o\epsilon_o v_o^2}\frac{1}{j\theta}\left(1+K_o^2D^2\right)^{-3/2}(1-e^{-j\theta}-j\theta\, e^{-j\theta}) \quad .$$

Since the klystron gap is very small, or $\theta \to 0$, then by series expansion;

$$i_1 = \frac{e J_o \nabla_1}{m_o\epsilon_o v_o^2}\frac{1}{j\theta}\left(1+K_o^2D^2\right)^{-3/2}\left[1-(1-j\theta)-j\theta(1-j\theta)\right] = 0 \quad .$$

Current modulation is still zero, as in the medium-power klystrons discussed in Chapter IV.

By Equation (107), the beam loading will be divided into real and imaginary components just as was done in Chapter IV, giving

$$G = \frac{G_o}{2}\frac{1}{\theta_o^2}\frac{1}{\left(1+\frac{1}{2}\frac{\nabla}{\nabla_n}\right)\left(1+\frac{\nabla}{\nabla_n}\right)}\left[2(1-\cos\theta_o)-\theta_o\sin\theta_o\right] , \tag{110}$$

$$B_1 = \frac{G_o}{2}\frac{1}{\theta_o^2}\frac{1}{\left(1+\frac{1}{2}\frac{\nabla}{\nabla_n}\right)\left(1+\frac{\nabla}{\nabla_n}\right)}\left[2\sin\theta_o-\theta_o(1+\cos\theta_o)\right] . \tag{111}$$

Equations (110) and (111) check with the results obtained by the ballistic approach given in Appendix D. The plot of both G and B_1 will be shown in Figure 3.

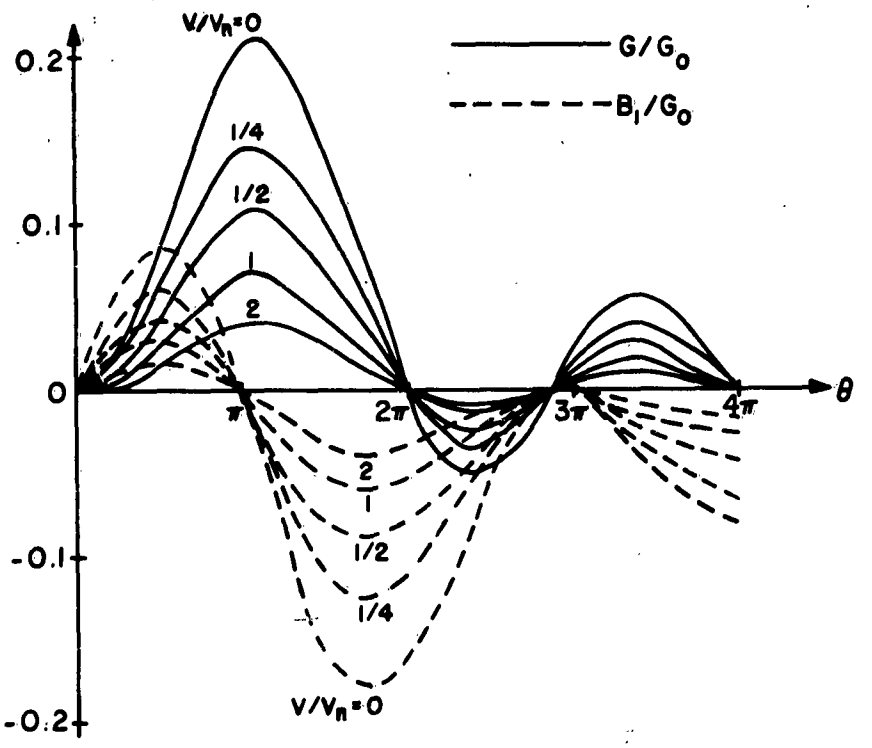

Figure 3. $\frac{G}{G_o}$, $\frac{B_1}{G_o}$, as a Function of D-C Transit Angle.

VI. CONCLUSIONS AND RECOMMENDATIONS

This study gives some idea of the importance of the relativistic effect in a space-charge-limited diode and in klystron gaps using Llewellyn's relativistic coefficients, which are derived from wave theory. We applied Llewellyn's coefficients to the space-charge-limited diode and klystron gaps under the restrictions that $K_o^2/\beta_e^2 < \frac{1}{2}$. Velocity and current modulations, and equivalent impedance and beam-loading admittance, were investigated in these two equations. For the diode impedance, the results obtained do not differ greatly from Llewellyn's and the negative maximum resistance which is related to the diode oscillation changes only 0.3 per cent of the nonrelativistic value at $K_o^2/\beta_e^2 = \frac{1}{2}$, the limit of our analysis. From this result we can predict that the maximum negative resistance cannot change too much even extending the analysis to the $K_o^2/\beta_e^2 > \frac{1}{2}$ region, or $V > 2.115 \times 10^5$ volts.

From the results obtained for klystron gaps, it is apparent that the relativistic effect is important. Since the assumption is made that the space charge does not affect the d-c space potential, exact integration without any approximation is feasible. We find that both the beam-loading admittance and the velocity modulation change appreciably, as shown in Figure 3.

Further work should be directed toward the following problems:

i) Find the exact solution of the wave potential integral π, given in Equation (5).

ii) Apply these results to high-frequency triodes and tetrodes.

iii) Study the power flow in the relativistic case.

iv) Study the noise phenomena.

v) Take account of the force resulting from the magnetic field.

APPENDIX A

DERIVATION OF BASIC EQUATIONS

The Basic A-C Equations

The analysis which follows is based on the following assumptions:

1) the motion is restricted to the z-direction only,

2) no Maxwellian velocity distribution,

3) no electron overtaking,

4) a small-signal analysis, and

5) positive ions are not present.

The relativistic equation of motion is

$$\frac{d}{dt}\left[\frac{v}{\left(1-\frac{v^2}{c^2}\right)^{1/2}}\right] = -\frac{e}{m_o}E \quad . \tag{A.1}$$

Since $dz/dt = v$, we can write

$$\frac{d}{dz}\left[\frac{c^2}{\left(1-\frac{v^2}{c^2}\right)^{1/2}}\right] = -\frac{e}{m_o}E \quad . \tag{A.2}$$

Now, if $|v_1| << c$, then expand the left side into the Taylor series about v_o:

$$\frac{c^2}{\left(1-\frac{v^2}{c^2}\right)^{1/2}} \simeq \frac{c^2}{\left(1-\frac{v_o^2}{c^2}\right)^{1/2}} + v_1 e^{j\omega t}\frac{d}{dv_o}\left[\frac{c^2}{\left(1-\frac{v_o^2}{c^2}\right)^{1/2}}\right]$$

$$= \frac{c^2}{\left(1-\frac{v_o^2}{c^2}\right)^{1/2}} + \frac{v_o v_1 e^{j\omega t}}{\left(1-\frac{v_o^2}{c^2}\right)^{3/2}} \quad . \tag{A.3}$$

From Equation (A. 3), we can separate Equation (A. 2) into its d-c part,

$$\frac{d}{dz}\left[\frac{c^2}{\left(1-\frac{v_o^2}{c^2}\right)^{1/2}}\right] = -\frac{e}{m_o} E_o \quad , \tag{A. 4}$$

and its a-c part,

$$\frac{d}{dz}\left[\frac{v_o v_1 e^{j\omega t}}{\left(1-\frac{v_o^2}{c^2}\right)^{3/2}}\right] = \frac{e}{m_o} E_1 e^{j\omega t} \quad . \tag{A. 5}$$

From Equation (A. 5), v_1 can be expressed as

$$v_1 e^{j\omega t} = -\frac{e\left(1-\frac{v_o^2}{c^2}\right)^{3/2}}{m_o v_o} \int E_1 e^{j\omega t}\, dz \quad . \tag{A. 6}$$

The equation of continuity is

$$\frac{\partial i_1 e^{j\omega t}}{\partial z} = -\frac{\partial \rho_1 e^{j\omega t}}{\partial t} \quad .$$

Since

$$\frac{d}{dz} = \frac{\partial}{\partial z} + \frac{dt}{dz}\frac{\partial}{\partial t} \simeq \frac{\partial}{\partial z} + \frac{1}{v_o}\frac{\partial}{\partial t} \quad ,$$

then

$$\frac{di_1 e^{j\omega t}}{dz} = \frac{\partial i_1 e^{j\omega t}}{\partial z} + \frac{1}{v_o}\frac{\partial i_1 e^{j\omega t}}{\partial t} \quad , \tag{A. 8}$$

and also

$$i_1 = -\rho_o v_1 + \rho_1 v_o \quad . \tag{A. 9}$$

Note that here $dz/dt = v_o + v_1$, but for small-signal analysis, v_1 should be neglected since $\partial/\partial t$ is another small a-c term.

From Equations (A. 7), (A. 8), and (A. 9), we have

$$\frac{di_1 e^{j\omega t}}{dz} = -j\omega \frac{|\rho_o|}{v_o} v_1 e^{j\omega t} \quad . \tag{A. 10}$$

The plasma phase constant is defined as

$$\beta_p^2 = \frac{e|\rho_o|}{m_o \epsilon_o v_o^2} = \frac{e J_o}{m_o \epsilon_o v_o^3} \quad .$$

Also define $\beta_e = \omega/v_o$ and $K_o = \omega/c$. Combine Equation (A. 6) and Equation (A. 10) to give

$$i_1 e^{j\omega t} = j\omega\epsilon_o \frac{\beta_p^2}{\beta_e^3} \int \left[\beta_e^3 \left(1 - \frac{K_o^2}{\beta_e^2} \right)^{3/2} \int E_1 e^{j\omega t} \, dz \right] dz \quad , \tag{A. 11}$$

where use has been made of the fact that β_p^2/β_e^3 is independent of z.

Define a wave potential $\pi(\theta)$ for convenience as

$$\pi = j\omega\epsilon_o \frac{1}{\beta_e} \int \left[\beta_e^2 \left(1 - \frac{K_o^2}{\beta_e^2} \right)^{3/2} \int E_1 e^{j\theta} \frac{1}{\beta_e} \, d\theta \right] d\theta \quad , \tag{A. 12}$$

where we have introduced the d-c transit angle $\theta = \int \beta_e dz$. Furthermore, one gets

$$\omega\tau = \int \omega dt \simeq \int \frac{\omega}{v_o} dz = \int \beta_e \, dz = \theta \quad ,$$

where τ is the d-c transit time. The field intensity E_1 can be expressed from Equation (A. 12) as

$$E_1 = \frac{1}{j\omega\epsilon_o} \beta_e e^{-j\theta} \frac{d}{d\theta} \left[\frac{1}{\beta_e^2 \left(1 - \frac{K_o^2}{\beta_e^2}\right)^{3/2}} \frac{d}{d\theta} (\beta_e \pi) \right] \quad ; \qquad (A. 13)$$

then by successive differentiation, we have

$$E_1 = \frac{1}{j\omega\epsilon_o} e^{-j\theta} \left\{ \frac{d}{d\theta} \left[\frac{1}{\left(1 - \frac{K_o^2}{\beta_e^2}\right)^{3/2}} \frac{d\pi}{d\theta} \right] - \pi\beta_e \frac{d^2}{d\theta^2} \left[\frac{\frac{1}{\beta_e}}{\left(1 - \frac{K_o^2}{\beta_e^2}\right)^{1/2}} \right] \right\} . \qquad (A. 14)$$

Equations (A. 6) and (A. 12) yield

$$v_1 = - \frac{1}{j\omega\epsilon_o} \frac{e}{m_o\omega} e^{-j\theta} \frac{1}{\beta_e} \frac{d}{d\theta} (\beta_e \pi) \quad . \qquad (A. 15)$$

Equations (A. 11) and (A. 12) yield

$$i_1 = \frac{\beta_p^2}{\beta_e^2} e^{-j\theta} \pi \quad . \qquad (A. 16)$$

Gauss' law for the electric field is

$$\frac{\partial E_1}{\partial z} = \frac{\zeta_1}{\epsilon_o} \quad . \qquad (A. 17)$$

From Equations (A. 17) and (A. 7), we obtain

$$\frac{\partial}{\partial z} (i_1 + j\omega_o E_1) = 0 \quad ,$$

or

$$i_1 + j\omega\epsilon_o E_1 = i_c \quad , \tag{A.18}$$

where i_c is called total current density. This must be zero for a truly one-dimensional problem, since an actual physical arrangement of infinite lateral extent obviously cannot exist in reality. A current flow of finite lateral extent must be considered, therefore i_c must be present in this case; in an external open circuit, however, i_c would have to be zero.

Upon the insertion of Equations (A.14) and (A.16) into Equation (A.18), we have the following wave equation for π :

$$\frac{d}{d\theta}\left[\frac{1}{\left(1 - \frac{K_o^2}{\beta_e^2}\right)^{3/2}} \frac{d\pi}{d\theta}\right] + \left\{\frac{\beta_p^2}{\beta_e^2} - \beta_e \frac{d^2}{d\theta^2}\left[\frac{\frac{1}{\beta_e}}{\left(1 - \frac{K_o^2}{\beta_e^2}\right)^{1/2}}\right]\right\} \pi = i_c e^{j\theta} \quad .$$

Since we assume that there are no positive ions, we have

$$\frac{\partial E_o}{\partial z} = \frac{\rho_o}{\epsilon_o}$$

or, since $J_o = -\rho_o v_o$,

$$\frac{dE_o}{d\theta} = \frac{-J_o}{\omega\epsilon_o} \quad . \tag{A.20}$$

Now, Equation (A.4) can be written in another form:

$$\omega^2 \frac{d}{d\theta}\left[\frac{\frac{1}{\beta_e}}{\left(1 - \frac{K_o^2}{\beta_e^2}\right)^{1/2}}\right] = -\frac{e}{m_o} E_o \quad . \tag{A.21}$$

Eliminating E_o between Equations (A. 20) and (A. 21), one obtains

$$\beta_e \frac{d^2}{d\theta^2} \left| \frac{\frac{1}{\beta_e}}{\left(1 - \frac{K_o^2}{\beta_e^2}\right)^{1/2}} \right| = \frac{\beta_p^2}{\beta_e^2} \quad . \tag{A. 22}$$

This reduces the wave Equation (A. 19) to the following simple form:

$$\frac{d}{d\theta} \left| \frac{1}{\left(1 - \frac{K_o^2}{\beta_e^2}\right)^{3/2}} \frac{d\pi}{d\theta} \right| = i_c e^{j\theta} \quad .$$

The general solution to this equation will be

$$\pi = \int \left(c_1 - j i_c e^{j\theta}\right) \left(1 - \frac{K_o^2}{\beta_e^2}\right)^{3/2} d\theta + c_2 \quad , \tag{A. 23}$$

where the integration constants c_1 and c_2 are to be determined from the a-c boundary conditions.

Now, we collect our expressions for the various a-c quantities:

$$i_1 = \frac{\beta_p^2}{\beta_e^2} e^{-j\theta} \pi \quad , \tag{A. 16}$$

$$E_1 = \frac{1}{j\omega\epsilon_o} (i_c - i_1) = \frac{1}{j\omega\epsilon_o} \left[i_c - \frac{\beta_p^2}{\beta_e^2} e^{-j\theta} \pi \right] \quad , \tag{A. 24}$$

$$v_1 = -\frac{1}{j\omega\epsilon_o}\frac{e}{m_o\omega}\, e^{j\theta_o}\left[\frac{d\pi}{d\theta} - \pi\,\frac{1}{\frac{1}{\beta_e}}\,\frac{d\left(\frac{1}{\beta_e}\right)}{d\theta}\right]$$

$$= -\frac{1}{j\omega\epsilon_o}\frac{e}{m_o\omega}\, e^{-j\theta_o}\left\{\left(c_1 - ji_c e^{j\theta_o}\right)\left(1 - \frac{K_o^2}{\beta_e^2\, 2}\right)^{3/2} - \frac{1}{\frac{1}{\beta_e}}\,\frac{d\left(\frac{1}{\beta_e}\right)}{d\theta}\right.$$

$$\left.\left[\int\left(c_1 - ji_c e^{j\theta}\right)\left(1 - \frac{K_o^2}{\beta_e^2}\right)^{3/2} d\theta + c_2\right]\right\} \quad . \qquad \text{(A. 25)}$$

The a-c applied voltage across the gap becomes

$$V_c = \int_o^d E_1\, dz = \int_o^{\theta_o} \frac{E_1}{\beta_e}\, d\theta = \frac{1}{j\omega\epsilon_o}\left\{i_c \int_o^{\theta_o} \frac{d\theta}{\beta_e} - \frac{\beta_p^2}{\beta_e^3}\int_o^{\theta_o} e^{-j\theta}\pi\, d\theta\right\}$$

$$= \frac{1}{j\omega\epsilon_o}\left\{i_c d - \frac{\beta_p^2}{\beta_e^3}\int_o^{\theta_o} e^{-j\theta}\pi\, d\theta\right\} \quad , \qquad \text{(A. 26)}$$

where d is the distance between the electrodes and θ_o is the corresponding d-c transit angle $\int_o^d \beta_e\, dz$.

The a-c gap impedance per unit area is expressed by $Z_c = V_c/i_c$. For a cold gap (i.e., $\beta_p = 0$ or $J_o = 0$, $Z_{co} = 1/j\omega c_o$, where $c_o = \epsilon_o/d$ is the cold-gap capacitance per unit area.

In order to solve the integrals appearing in the a-c equations, (A. 16), (A. 24), (A. 25), and (A. 26), one has to express $\left(1 - \frac{K_o^2}{\beta_e^2}\right)^{1/2}$ and β_e in

terms of θ. If V is the d-c potential difference between two planes, one gets from Equation (A. 4) the energy relation,

$$c^2 \left[\frac{1}{\left(1 - \frac{K_o^2}{\beta_e^2}\right)^{1/2}} - 1 \right] = \frac{e}{m_o} V \quad , \tag{A.27}$$

which can also be written

$$\frac{\frac{1}{\beta_e}}{\left(1 - \frac{K_o^2}{\beta_e^2}\right)^{1/2}} = \frac{1}{K_o} \left[\frac{2V}{V_n} \left(1 + \frac{V}{2V_n}\right) \right]^{1/2} \quad , \tag{A.28}$$

where $V_n = m_o c^2/e$ is the equivalent potential. Integrating Equation (A. 22) and using Equation (A. 26) as a boundary condition at $\theta = 0$, $V = V_a$, $\theta = \theta_o$, $V = V_b$, we have

$$\frac{\frac{1}{\beta_e}}{\left(1 - \frac{K_o^2}{\beta_e^2}\right)^{1/2}} = \frac{\beta_p^2}{\beta_e^3} \frac{\theta}{2} (\theta - \theta_o) + \frac{1}{K_o} \left\{ \left[\frac{2V_b}{V_n} \left(1 + \frac{V_b}{2V_n}\right) \right]^{1/2} \right.$$

$$\left. - \left[\frac{2V_a}{V_n} \left(1 + \frac{V_a}{2V_n}\right) \right]^{1/2} \right\} \frac{\theta}{\theta_o} + \frac{1}{K_o} \left[\frac{2V_a}{V_n} \left(1 + \frac{V_a}{2V_n}\right) \right]^{1/2} \quad . \tag{A.29}$$

Denote tha right-hand side of Equation (A. 29) by $S(\theta)$ and solve for $1/\beta_e$ and $\left(1 - \frac{K_o^2}{\beta_e^2}\right)^{1/2}$:

$$\frac{1}{\beta_e} = \frac{s}{\left(1 + K_o^2 S^2\right)^{1/2}} \tag{A. 30}$$

$$\left(1 - \frac{K_o^2}{\beta_e^2}\right)^{1/2} = \frac{1}{\left(1 + K_o^2 S^2\right)^{1/2}} \quad . \tag{A. 31}$$

Since S is a known function of θ, it would be possible to eliminate $1/\beta_e$ and $\left(1 - \frac{K_o^2}{\beta_o^2}\right)^{1/2}$ from our a-c expressions by Equations (A. 30) and (A. 31).

Finally, we express the distance as

$$d = \int_o^{\theta_o} \frac{d\theta}{\beta_e} = \int_o^{\theta_o} \frac{S}{\left(1 + K_o^2 S^2\right)^{1/2}} \, d\theta \quad . \tag{A. 32}$$

From this, we see that a d-c transit angle θ_o can be expressed in terms of J_o, V_a, V_b, d, and ω.

APPENDIX B

DERIVATION OF LLEWELLYN'S COEFFICIENTS BY THE USE OF WAVE THEORY IN THE NONRELATIVISTIC CASE

The wave potential π reduces to the following form in the nonrelativistic case:

$$\pi = \int \left(c_1 - ji_c e^{j\theta}\right) d\theta + c_2$$

$$= c_1\theta - i_c e^{j\theta} + c_2 \quad . \tag{B. 1}$$

The d-c relations will be

$$\frac{d^2\left(\frac{1}{\beta_e}\right)}{d\theta^2} = \frac{\beta_p^2}{\beta_e^3} \quad . \tag{B. 2}$$

Integrate Equation (B. 2) to give

$$\frac{a_o}{\omega^2} = \frac{d\left(\frac{1}{\beta_e}\right)}{d\theta} = \frac{\beta_p^2}{\beta_e^3}\theta + \frac{a_a}{\omega^2} \quad , \tag{B. 3}$$

where a_o is the acceleration at an arbitrary plane and a_a is the acceleration at plane a (the initial position); then integrate again to give

$$\frac{v_o}{\omega} = \frac{1}{\beta_e} = \frac{1}{2}\frac{\beta_p^2}{\beta_e^3}\theta^2 + \frac{a_a}{\omega^2}\theta + \frac{v_a}{\omega} \quad .$$

Here v_o, v_a are velocities of any arbitrary plane and initial plane respectively, where

$$\beta_p^2 = \frac{e J_o}{m_o \epsilon_o v_o^3} \quad ,$$

$$\beta_e^3 = \frac{\omega^3}{v_o^3} \quad ,$$

$$i_1 = \frac{\beta_p^2}{\beta_e^2} e^{-j\theta} \quad , \tag{B. 4}$$

$$E_1 = \frac{1}{j\omega\epsilon_o} (i_c - i_1) = \frac{1}{j\omega\epsilon_o} \left(i_c - \frac{\beta_p^2}{\beta_e^2} e^{-j\theta} \pi \right) \quad , \tag{B. 5}$$

$$v_1 = - \frac{1}{j\omega\epsilon_o} \frac{e}{m_o\omega} e^{-j\theta} \left\{ \left(c_1 - j i_c e^{j\theta} \right) - \frac{1}{\beta_e} \frac{d\left(\frac{1}{\beta_e}\right)}{d\theta} \left(c_2 + c_1\theta - i_c e^{j\theta} \right) \right\} \quad . \tag{B. 6}$$

Here $\theta \to 0$, $i_1 \to i_{1a}$, $v_1 \to v_{1a}$, $\beta_p \to \beta_{po}$, $\beta_e \to \beta_{eo}$, and from Equation (B. 4):

$$i_{1a} = \frac{\beta_{po}^2}{\beta_{eo}^2} (c_2 - i_c) \quad ,$$

therefore

$$c_2 = \frac{\beta_{eo}^2}{\beta_{po}^2} i_{1a} + i_c \quad . \tag{B. 7}$$

By Equation (B. 6)

$$v_{1a} = \frac{1}{j\omega\epsilon_o} \frac{e}{m_o\omega} \left\{ (c_1 - j i_c) - \frac{\omega}{v_a} \cdot \frac{a_a}{\omega^2} (c_2 - i_c) \right\}$$

$$= - \frac{1}{j\omega\epsilon_o} \frac{e}{m_o\omega} \left\{ (c_1 - j i_c) - \frac{a_a}{\omega v_a} \left(\frac{\beta_{eo}^2}{\beta_{po}^2} i_{1a} + i_c - i_c \right) \right\} \quad ;$$

therefore

$$c_1 = -j \frac{\omega \epsilon_o m_o \omega}{e} v_{1a} + j i_c + \frac{a_a}{\omega v_a} \frac{\beta_{eo}^2}{\beta_{po}^2} i_{1a} \quad . \qquad (B.8)$$

Substituting Equation (B. 7) and Equation (B. 8) into Equation (B. 4) gives

$$i_1 = \frac{\beta_p^2}{\beta_e^2} e^{-j\theta} \pi = \frac{\beta_p^2}{\beta_e^2} e^{-j\theta} \left(c_2 + c_1 \theta - i_c e^{j\theta} \right)$$

$$= i_c \frac{\beta_p^2}{\beta_e^2} e^{-j\theta} (1 + j\theta - e^{j\theta}) + i_{1a} \frac{\beta_p^2}{\beta_e^2} \frac{\beta_{eo}^2}{\beta_{po}^2} e^{-j\theta} \left(1 + \frac{a_a}{\omega v_a} \theta \right)$$

$$- v_{1a} j \frac{\beta_p^2}{\beta_e^2} \frac{\omega \epsilon_o m_o \omega}{e} \theta e^{-j\theta} \quad , \qquad (B.9)$$

where it should be remembered that

$$\beta_p^2 = \frac{e J_o}{m_o \epsilon_o v_o^3} \quad , \qquad \beta_{po}^2 = \frac{e J_o}{m_o \epsilon_o v_a^3} \quad ,$$

$$\beta_e^2 = \frac{\omega^2}{v_o^2} \quad , \qquad \beta_{eo}^2 = \frac{\omega^2}{v_a^2} \quad .$$

After a little manipulation, Equation (B. 9) reduces to

$$i_1 = i_c \frac{e}{m_o \epsilon_o} \frac{J_o}{v_o} \frac{1}{(j\omega)^2} (1 - e^{-j\theta} - j\theta e^{-j\theta}) + i_{1a} \left[1 - \frac{1}{2} \frac{e}{m_o \epsilon_o} \frac{J_o}{v_o} \tau^2 \right] e^{-j\theta}$$

$$- j v_{1a} \frac{J_o}{v_o} \theta e^{-j\theta} \quad . \qquad (B.10)$$

If written in Llewellyn's form, Equation (B. 10) becomes

$$i_1 = G^* i_c + H^* i_{1a} + I^* v_{1a} \quad . \tag{B. 11}$$

By comparing Equations (B. 10) and (B. 11), one obtains the following:

$$G^* = \frac{e}{m_o \epsilon_o} \frac{J_o}{v_o} \frac{1}{(j\omega)^2} \left[1 - e^{-j\theta} - j\theta\, e^{-j\theta}\right] \quad ,$$

$$H^* = \left[1 - \frac{1}{2} \frac{e}{m_o \epsilon_o} \frac{J_o}{v_o} \tau^2\right] e^{-j\theta} \quad , \tag{B. 12}$$

$$I^* = -j \frac{J_o}{v_o} \theta\, e^{-j\theta} \quad .$$

Substituting Equations (B. 7) and (B. 8) into Equation (B. 6) gives

$$v_1 = - \frac{1}{j\omega\epsilon_o} \frac{e}{m_o \omega} e^{-j\theta} \left\{ \left(c_1 - j i_c e^{j\theta}\right) - \frac{1}{\frac{1}{\beta_e}} \frac{d\left(\frac{1}{\beta_e}\right)}{d\theta} \left(c_2 + c_1 \theta - i_c e^{j\theta}\right) \right\}$$

$$= - \frac{1}{j\omega\epsilon_o} \frac{e}{m_o \omega} e^{-j\theta} \left\{ \left(c_1 - j i_c e^{j\theta}\right) - \frac{\omega}{v_o} \left(\frac{\beta_p^2}{\beta_e^2} + \frac{a_a}{\omega^2} \right) \left(c_2 + c_1 \theta - i_c e^{j\theta}\right) \right\}$$

$$= -i_c \frac{1}{(j\omega)^2} \frac{e}{m_o \epsilon_o} \left[(1 - e^{-j\theta}) - \frac{a_o}{j\omega v_o} (1 - e^{-j\theta} - j\theta\, e^{-j\theta}) \right]$$

$$- i_{1a} \frac{e}{m_o \epsilon_o} \frac{1}{(j\omega)^2} \left[\frac{a_o \tau}{2 v_o} - 1 \right] j\theta\, e^{-j\theta} + v_{1a} \left(1 - \frac{a_o \tau}{v_o} \right) e^{-j\theta} \quad . \tag{B. 13}$$

Compare Equation (B. 13) to Llewellyn's form,

$$v_1 = D^* i_c + E^* i_{1a} + F^* v_{1a} \quad . \tag{B. 14}$$

Then we have

$$D^* = -\frac{1}{(j\omega)^2}\frac{e}{m_o\epsilon_o}\left[(1-e^{-j\theta}) - \frac{a_o}{j\omega v_o}(1-e^{-j\theta} - j\theta\, e^{-j\theta})\right] ,$$

$$E^* = -\frac{e}{m_o\epsilon_o}\frac{1}{(j\omega)^2}\left[\frac{a_o\tau}{2v_o} - 1\right] j\theta\, e^{-j\theta} , \qquad \text{(B. 15)}$$

$$F^* = \left(1 - \frac{a_o\tau}{v_o}\right) e^{-j\theta} ,$$

where τ is the d-c transit time, and $\theta = \omega\tau$.

For applied a-c voltage across the gap,

$$V_c = \int_o^d E_1\, dz = \int_o^{\theta_o} \frac{E_1}{\beta_e}\, d\theta ,$$

where E_1 is given in Equation (B. 5). Substituting and integrating gives

$$V_c = \int_o^{\theta_o} \frac{E_1}{\beta_e}\, d\theta = \frac{1}{j\omega\epsilon_o}\left[i_c \int_o^{\theta_o} \frac{d\theta}{\beta_e} - \frac{\beta_p^2}{\beta_e^3}\int_o^{\theta_o} e^{-j\theta}\left(c_2 + c_1\theta - i_c e^{j\theta}\right)d\theta\right]$$

$$= \frac{1}{j\omega\epsilon_o}\left[i_c d + \frac{\beta_p^2}{\beta_e^3}\frac{c_2}{j}(e^{-j\theta}-1) - c_1\frac{\beta_p^2}{\beta_e^3}\left(j\theta_o e^{-j\theta_o} + e^{-j\theta_o} - 1\right) + \frac{\beta_p^2}{\beta_e^3} i_c\theta_o\right] .$$

(B. 16)

Substituting Equations (B. 7) and (B. 8) into Equation (B. 16) and rearranging gives

$$V_c = i_c \frac{1}{\epsilon_o (j\omega)^4} \left[(j\omega)^3 d + \frac{e J_o}{\epsilon_o m_o} \left(2 - 2e^{-j\theta_o} - j\theta_o - j\theta_o e^{-j\theta_o} \right) \right]$$

$$+ i_{1a} \frac{1}{\epsilon_o (j\omega)^3} \left[a_a \left(j\theta_o e^{-j\theta_o} + e^{-j\theta_o} - 1 \right) + j\omega v_a \left(e^{-j\theta_o} - 1 \right) \right]$$

$$- v_{1a} \frac{J_o}{\epsilon_o (j\omega)^2} \left(j\theta_o e^{-j\theta_o} + e^{-j\theta_o} - 1 \right) \quad . \qquad \text{(B. 17)}$$

Comparing this to Llewellyn's form,

$$V_c = A^* i_c + B^* i_{1a} + C^* v_{1a} \quad ,$$

we have

$$A^* = \frac{1}{\epsilon_o (j\omega)^4} \left[(j\omega)^3 d + \frac{e J_o}{m \epsilon_o} \left(2 - 2 e^{-j\theta_o} - j\theta_o - j\theta_o e^{-j\theta_o} \right) \right] \quad ,$$

$$B^* = \frac{1}{\epsilon_o (j\omega)^3} \left[a_a \left(j\theta_o e^{-j\theta_o} + e^{-j\theta_o} - 1 \right) + j\omega v_a \left(e^{-j\theta_o} - 1 \right) \right] \quad ,$$

$$C^* = - \frac{J_o}{\epsilon_o (j\omega)^2} \left(j\theta_o e^{-j\theta_o} + e^{-j\theta_o} - 1 \right) \quad . \qquad \text{(B, 18)}$$

APPENDIX C

THE DERIVATION OF THE RELATIVISTIC EXPRESSION FOR THE CHILD-LANGMUIR LAW

Poisson's equation is

$$\frac{d^2V}{dz^2} = -\frac{\rho}{\epsilon_o} = \frac{J_o}{\epsilon_o v_o} \quad . \tag{C. 1}$$

From the energy relation,

$$e\,V = m_o c^2 \left(\frac{1}{\sqrt{1 - \frac{v_o^2}{c^2}}} - 1 \right) \quad , \tag{C. 2}$$

solve for v_o :

$$v_o = \sqrt{\frac{2\,e\,V}{m_o}} \sqrt{\frac{1 + \frac{1}{2}\frac{V}{V_n}}{\left(1 + \frac{V}{V_n}\right)^2}} \quad , \tag{C. 3}$$

where

$$\frac{V}{V_n} = \frac{m_o c^2}{e} = 5.11 \times 10^5 \text{ volts} \quad . \tag{C. 4}$$

Substituting Equation (C. 3) into Equation (C. 1), and by binomial expansion to the first order, one gets

$$\frac{d^2V}{dz^2} = \frac{J_o}{\epsilon_o}\frac{1}{v_o} = \frac{J_o}{v_o}\sqrt{\frac{m_o}{2eV}} \left[\frac{\left(1 + \frac{V}{V_n}\right)^2}{\left(1 + \frac{1}{2}\frac{V}{V_n}\right)} \right]$$

$$= \frac{J_o}{\epsilon_o}\sqrt{\frac{m_o}{2eV}} \left(1 + \frac{3}{4}\frac{V}{V_n}\right) \quad . \tag{C. 5}$$

Multiply $2(dV/dz)$ on both sides, then integrate:

$$\left(\frac{dV}{dz}\right)^2 = 2\frac{J_o}{\epsilon_o}\sqrt{\frac{m_o}{2e}}\left[\int V^{-1/2}\,dV + \int \frac{3}{4V_n}\,V^{1/2}\,dV\right]$$

$$= 4\frac{J_o}{\epsilon_o}\sqrt{\frac{m_o}{2e}}\,V^{1/2}\left(1 + \frac{1}{4}\frac{V}{V_n}\right) + C \quad ,$$

where $\frac{dV}{dz} = 0$, when $V = 0$; therefore $C = 0$, and

$$\frac{dV}{dz} = \sqrt{\frac{4J_o}{\epsilon_o}\sqrt{\frac{m_o}{2e}}}\,V^{1/4}\left(1 + \frac{1}{8}\frac{V}{V_n}\right) \quad . \tag{C.6}$$

Integrate Equation (C. 6) again to get

$$\int \frac{dV}{V^{1/4}}\left(1 - \frac{1}{8}\frac{V}{V_n}\right) = \int \left(\frac{4J_o}{\epsilon_o}\sqrt{\frac{m_o}{2e}}\right)^{1/2} dz + c_1$$

or

$$\frac{V^{3/4}}{3/4} - \frac{V^{7/4}}{8V_n\frac{7}{4}} = \sqrt{\frac{4J_o}{\epsilon_o}\sqrt{\frac{m_o}{2e}}}\,z + c_1 \quad ,$$

where $V = 0$ at $z = 0$, therefore $c_1 = 0$. Therefore, we have

$$\frac{4}{3}\,V^{3/4}\left(1 - \frac{3}{56}\frac{V}{V_n}\right) = \sqrt{\frac{4J_o}{\epsilon_o}\sqrt{\frac{m_o}{2e}}}\,z \quad . \tag{C.7}$$

Square Equation (C. 7) to get the final expression for the relativistic case,

$$J_o = \frac{4\epsilon_o}{9}\sqrt{\frac{2e}{m_o}}\,\frac{V^{3/2}}{d^2}\left(1 - \frac{3}{28}\frac{V}{V_n}\right) \quad . \tag{C.8}$$

But in the nonrelativistic case,

$$J_{o(non)} = \frac{4\epsilon_o}{9}\sqrt{\frac{2e}{m_o}}\,\frac{V^{3/2}}{d^2} \quad ; \tag{C.9}$$

therefore Equation (C. 8) may be written in the following form;

$$J_o = J_{o(non)}\left(1 - \frac{3}{28}\,\frac{V}{V_n}\right) \quad . \tag{C.10}$$

To find the slope of the static characteristic, we can take the derivative of Equation (C, 8):

$$\frac{dJ_o}{dV} = K\left(\frac{3}{2}\,V^{-1/2} - \frac{3}{28}\,\frac{1}{V_n}\,\frac{5}{2}\,V^{-3/2}\right)$$

$$= \frac{3}{2}\,K\,V^{1/2}\left(1 - \frac{5}{28}\,\frac{V}{V_n}\right) \quad , \tag{C.11}$$

where

$$K = \frac{J_o}{V^{3/2}\left(1 - \frac{3}{28}\,\frac{V}{V_n}\right)} = \frac{4}{9}\,\epsilon_o\sqrt{\frac{2e}{m_o}}\,\frac{1}{d^2} \quad ; \tag{C.12}$$

then

$$R = \frac{dV}{dJ_o} = \frac{2}{3}\,\frac{1}{KV^{1/2}\left(1 - \frac{5}{28}\,\frac{V}{V_n}\right)} = \frac{2}{3}\,\frac{V^{3/2}}{J_o}\,\frac{\left(1 - \frac{3}{28}\,\frac{V}{V_n}\right)}{\left(1 - \frac{5}{28}\,\frac{V}{V_n}\right)}$$

$$= \frac{2}{3}\,\frac{V^{3/2}}{J_o}\left(1 - \frac{3}{28}\,\frac{V}{V_n}\right)\left(1 + \frac{5}{28}\,\frac{V}{V_n}\right) \quad . \tag{C.13}$$

Substituting Equation (C. 10) into Equation (C. 12), we obtain

$$R = \frac{2}{3}\,\frac{V^{3/2}}{J_{o(non)}}\left(1 + \frac{5}{28}\,\frac{V}{V_n}\right) = r_{c(non)}\left(1 + \frac{5}{28}\,\frac{V}{V_n}\right) \quad , \tag{C.14}$$

where

$$r_{c(non)} = \frac{2}{3} \frac{V^{3/2}}{J_{o(non)}}$$

is the slope of the static characteristic of nonrelativistic case.

APPENDIX D

RELATIVISTIC BEAM-LOADING ADMITTANCE IN A KLYSTRON GAP BY THE BALLISTIC APPROACH

The equation of motion is

$$\frac{d}{dt}\left[\frac{v}{\left(1-\frac{v^2}{c^2}\right)^{1/2}}\right] = -\frac{e}{m_o}E \quad . \tag{D. 1}$$

Expand

$$\frac{v}{\left(1-\frac{v^2}{c^2}\right)^{1/2}}$$

by Taylor series to the first-order; since $v_1 < v_o$, we get

$$\frac{v}{\left(1-\frac{v^2}{c^2}\right)^{1/2}} = \frac{v_o}{\left(1-\frac{v_o^2}{c^2}\right)^{1/2}} + v_1 \frac{d}{dv_o}\left[\frac{v_o}{\left(1-\frac{v_o^2}{c^2}\right)^{1/2}}\right]$$

$$= \frac{v_o}{\left(1-\frac{v_o^2}{c^2}\right)^{1/2}} + \frac{v_1}{\left(1-\frac{v_o^2}{c^2}\right)^{3/2}} \quad . \tag{D. 2}$$

Separate Equation (D. 1) into d-c and a-c parts and express the a-c part as

$$\frac{d}{dt}\left(v_1 \frac{1}{\left(1-\frac{v_o^2}{c^2}\right)^{3/2}}\right) = \frac{1}{\left(1-\frac{v_o^2}{c^2}\right)^{3/2}}\frac{dv_1}{dt} = \frac{e}{m_o}\frac{V_1}{d}\sin\omega t \tag{D. 3}$$

where v_o is a constant (since $E_o = 0$ for $V_A = V_B$ in the gap) and is $E_1 = -V_1 \sin \omega t/d$.

Integrate Equation (D. 3) once:

$$v_1 = \left(1 - \frac{v_o^2}{c^2}\right)^{3/2} \frac{e V_1}{m_o d\omega} (-\cos \omega t) + c_1 \quad ,$$

where $t = t_o$, $v_1 = 0$; therefore

$$c_1 = \frac{e V_1}{m_o d\omega} \left(1 - \frac{v_o^2}{c^2}\right)^{3/2} \cos \omega t \quad ,$$

and v_1 becomes

$$v_1 = \frac{e V_1}{m_o \omega d} \left(1 - \frac{v_o^2}{c^2}\right)^{3/2} (\cos \omega t_o - \cos \omega t) \quad . \qquad \text{(D. 4)}$$

The total velocity should be

$$v = \frac{dz}{dt} = v_o + v_1 = v_o + \frac{e V_1}{m_o \omega d} \left(1 - \frac{v_o^2}{c^2}\right)^{3/2} (\cos \omega t_o - \cos \omega t) \quad . \qquad \text{(D. 5)}$$

Integrate Equation (D. 5) again:

$$z = v_o t + \frac{e V_1}{m_o \omega d} \left(1 - \frac{v_o^2}{c^2}\right)^{3/2} \left(t \cos \omega t_o - \frac{1}{\omega} \sin \omega t\right) + c_2 \quad ,$$

where $t = t_o$, $z = 0$; therefore

$$c_2 = \frac{e V_1}{m_o \omega d} \left(1 - \frac{v_o^2}{c^2}\right)^{3/2} \left(\frac{1}{\omega} \sin \omega t_o - t_o \cos \omega t_o\right) - v_o t_o \quad ;$$

hence we have

$$z = v_o(t - t_o) + \frac{e V_1}{m_o \omega d} \left(1 - \frac{v_o^2}{c^2}\right)^{3/2} (t - t_o) \cos \omega t_o$$

$$+ \frac{e V_1}{m_o \omega^2 d} \left(1 - \frac{v_o^2}{c^2}\right)^{3/2} (\sin \omega t_o - \sin \omega t) \quad . \qquad \text{(D. 6)}$$

By the energy relation,

$$m_o c^2 \left[\frac{1}{\sqrt{1 - \frac{v_o^2}{c^2}}} - 1 \right] = eV \quad . \qquad \text{(D. 7)}$$

Solve for

$$\left(1 - \frac{v_o^2}{c^2}\right)^{3/2} = \frac{1}{\left(1 + \frac{V}{V_n}\right)^3} \quad , \qquad \text{(D. 8)}$$

and

$$v_o^2 = \frac{2eV}{m_o} \frac{\left(1 + \frac{1}{2} \frac{V}{V_n}\right)}{\left(1 + \frac{V}{V_n}\right)^2} \quad , \qquad \text{(D. 9)}$$

where $V_n = m_o c^2/e$.

If we let $V_1/V = a$, and d-c transit angle $\theta_o = \omega d/v_o$, then

$$\frac{e V_1}{m_o d\omega} = \frac{e V_1}{m_o v_o \frac{\omega d}{v_o}} = \frac{e V_1 v_o}{m_o v_o^2 \theta_o} \quad .$$

Substituting Equation (D. 9) in the preceding equation gives

$$\frac{e V_1}{m_o d\omega} = \frac{V_1}{2V} \frac{v_o}{\theta_o} \frac{\left(1 + \frac{V}{V_n}\right)^2}{\left(1 + \frac{1}{2}\frac{V}{V_n}\right)} = \frac{a v_o}{2\theta_o} \frac{\left(1 + \frac{V}{V_n}\right)^2}{\left(1 + \frac{1}{2}\frac{V}{V_n}\right)} \quad . \qquad (D. 10)$$

Then z in Equation (D. 6) with Equations (D. 8) and (D. 10) will be

$$z = v_o(t - t_o) + \frac{a v_o}{2\theta_o} \frac{1}{\left(1 + \frac{1}{2}\frac{V}{V_n}\right)\left(1 + \frac{V}{V_n}\right)} (t - t_o) \cos \omega t_o$$

$$+ \frac{a v_o}{2\theta_o \omega} \frac{1}{\left(1 + \frac{1}{2}\frac{V}{V_n}\right)\left(1 + \frac{V}{V_n}\right)} (\sin \omega t_o - \sin \omega t) \quad . \qquad (D. 11)$$

If τ is the transit time for the gap, $t - t_o = \tau$ and gives the relation,

$$\tau = \frac{d}{v_o} + \frac{\delta}{\omega} \quad . \qquad (D. 12)$$

The first term in Equation (D. 12) is the d-c transit time, and the second is the a-c transit time. Substituting $z = d$, at $t = t_o + \tau$ into Equation (D. 11), where τ is given in Equation (D. 12), gives

$$d = d + \frac{v_o \delta}{\omega} \frac{1}{\left(1 + \frac{1}{2}\frac{V}{V_n}\right)\left(1 + \frac{V}{V_n}\right)} \cos(\omega t - \theta_o)$$

$$+ \frac{a v_o}{2\theta_o \omega} \frac{1}{\left(1 + \frac{1}{2}\frac{V}{V_n}\right)\left(1 + \frac{V}{V_n}\right)} \left[\sin(\omega t - \theta_o) - \sin \omega t\right] \quad , \qquad (D. 13)$$

where we have neglected $a\delta$ terms, and approximated $\sin(\omega t - \theta_o - \delta)$ equal

to $\sin(\omega t - \theta_o)$ and $\cos(\omega t - \theta_o - \delta)$ equal to $\cos(\omega t - \theta_o)$, since we are basing our derivation on small-signal theory.

From Equation (D. 13), solved for δ:

$$\delta = \frac{1}{2\theta_o \left(1 + \frac{1}{2}\frac{V}{V_n}\right)\left(1 + \frac{V}{V_n}\right)} \left[\sin \omega t (1 - \cos\theta_o - \theta_o \sin\theta_o) + \cos \omega t (\sin\theta_o - \theta_o \cos\theta_o)\right] \quad . \quad \text{(D. 14)}$$

By Ramo's theorem, each electron induces a current pulse, ev/d, into the circuit across which a voltage $V_1 \sin \omega t$ is applied. Now our current at entry is J_o. The current induced at time $|t|$ as a result of the charge entering the gap in the interval $|dt_o|$ between times $|t_o|$ and $t_o + dt_o$ is

$$di = \frac{J_o}{d} v\, dt_o \quad ;$$

hence

$$i = \frac{J_o}{d} \int_{t-\tau}^{t} v\, dt_o \quad , \quad \text{(D. 15)}$$

and with v given in Equation (D. 5), we have

$$i = \frac{J_o}{d}\left[v_o t_o + \frac{\alpha v_o}{2\theta_o \left(1 + \frac{V}{V_n}\right)\left(1 + \frac{1}{2}\frac{V}{V_n}\right)}\left(\frac{\sin \omega t_o}{\omega} - t_o \operatorname{cis} \omega t\right)\right]$$

$$= \frac{J_o}{d}\left[v_o \tau + \frac{\alpha v_o}{2\theta_o} \frac{1}{\left(1 + \frac{V}{V_n}\right)\left(1 + \frac{1}{2}\frac{V}{V_n}\right)}\left(\frac{\sin \omega t - \sin \omega (t-\tau)}{\omega} - \tau \cos \omega t\right)\right] .$$

With the value of τ and δ given in Equations (D. 12) and (D. 14), we get

$$i = J_o \left[1 + \frac{a}{2\theta_o^2 \left(1 + \frac{V}{V_n}\right)\left(1 + \frac{1}{2}\frac{V}{V_n}\right)} \left[(2(1 - \cos\theta_o) - \theta_o \sin\theta_o) \sin \omega t \right.\right.$$

$$\left.\left. + (2 \sin\theta_o - \theta_o(1 + \cos\theta_o)) \cos \omega t\right]\right] .$$

(D. 16)

Compare this to the following form,

$$i = J_o + V_1 G \sin \omega t + V_1 B_1 \cos \omega t \quad ; \qquad \text{(D. 17)}$$

therefore

$$G = \frac{G_o}{2\theta_o^2} \frac{1}{\left(1 + \frac{V}{V_n}\right)\left(1 + \frac{1}{2}\frac{V}{V_n}\right)} \left[2(1 - \cos\theta_o) - \theta_o \sin\theta_o)\right] , \qquad \text{(D. 18)}$$

$$B_1 = \frac{G_o}{2\theta_o^2} \frac{1}{\left(1 + \frac{V}{V_n}\right)\left(1 + \frac{1}{2}\frac{V}{V_n}\right)} \left[2 \sin\theta_o - \theta_o(1 + \cos\theta_o)\right] , \qquad \text{(D. 19)}$$

where

$$G_o = \frac{J_o}{V} .$$

REFERENCES

1. F. B. Llewellyn, Electron Inertia Effects, London: Cambridge University Press, (1941).

2. F. B. Llewellyn and L. C. Peterson, "Vacuum Networks," Proc. I.R.E., 32 (March, 1944) pp. 144-166.

3. O. E. H. Rydbeck, "Electromagnetic and Space-Charge Waves in Inhomogeneous Structures," Research Report No. 8, Res. Lab. of Electronics, Chalmers University of Technology, Gothenburg, 1960.

4. S. Olving, "An Introductory Relativistic Study of the Llewellyn Electronic Gap," Research Report EE 498, Cornell University, 1961.

5. W. C. Hahn and G. F. Metcalf, "Velocity-modulated Tubes," Proc. I.R.E., 27 (February 1939), pp. 106-117.

6. A. H. W. Beck, Thermionic Valves, London: Cambridge University Press, (1953), ch. 7.

7. A. H. W. Beck, Space Charge Waves, London: Pergamon Press, (1958), pp. 155-158.

8. Rudolf G. E. Hutter, Beam and Wave Electronics in Microwave Tubes, Princeton, N. J.: D. Van Nostrand (1960), ch. 8.

9. Willis W. Harman, Fundamentals of Electronic Motion, New York: McGraw-Hill (1953).

RESPONSE OF KLYSTRONS TO NANOSECOND PULSES

N. Bose

School of Electrical Engineering
CORNELL UNIVERSITY
Ithaca, New York

RESEARCH REPORT EE 542

RESPONSE OF KLYSTRONS TO NANOSECOND PULSES

N. Bose

LINEAR BEAM MICROWAVE TUBES

Technical Report No. 21 30 September 1962

Published under Contract No. AF30(602)-2573
Rome Air Development Center, Griffiss Air Force Base, New York

ACKNOWLEDGMENTS

The author takes great pleasure in thanking Prof. P. R. McIsaac for stimulating discussions and guidance throughout the course of his research; Prof. G. C. Dalman, whose class lectures were very valuable; Prof. L. F. Eastman for his encouragement; and Prof. J. J. Price for serving as a member of his Special Committee.

This research was carried out under Air Force Contract No. AF 30(602)-2573, whose support was indispensable.

CONTENTS

	Page
LIST OF SYMBOLS USED	vii
ABSTRACT	ix
I. INTRODUCTION	1
A. OBJECTIVE	1
B. MODEL	3
II. RESPONSE OF KLYSTRON TO DOUBLE-FREQUENCY INPUT	4
A. FIRST GAP	4
B. DRIFT REGION	8
III. BALLISTIC ANALYSIS	19
A. FIRST-ORDER BUNCHING THEORY	19
B. KLYSTRON RESPONSE WITH VARIABLE GAP LENGTH	25
C. RESPONSE WITH FIXED ENVELOPE AND VARYING FREQUENCY	30
IV. LARGE SIGNALS AND FINITE GAPS	31
A. FIRST GAP REGION	
1. Induced R-F Current	31
2. Velocity Modulation	39
B. DRIFT SPACE REGION	41
C. SECOND GAP REGION	43

	Page
V. NONLINEAR SPACE-CHARGE WAVE ANALYSIS	48
VI. CONCLUSIONS AND RECOMMENDATIONS	57
APPENDIX A. A NOTE ON THE GAUSSIAN SPECTRUM	58
APPENDIX B. FOURIER COEFFICIENTS	63
APPENDIX C. EVALUATION OF erf(a - jb)	66
REFERENCES	69

LIST OF SYMBOLS USED

a_n = $\dfrac{\text{magnitude of applied voltage}}{\text{d-c beam voltage}} = \dfrac{V_n}{V_o}$

δ_n = transit time correction factor for n^{th} gap

ω_n = angular frequency of applied voltages, V_n

ϕ''_m = d-c gap-transit angle for m^{th} gap and angular frequency ω_2

β''_m = gap-coupling coefficient for m^{th} gap and ω_2

k''_m = bunching parameter = $\dfrac{\omega_2 S_m}{u_o}\, a_m \beta_m$

Γ_n = the n^{th} gap transit time

$\begin{bmatrix} A_0, A_1, \\ A_2, A_3, \end{bmatrix}$ = the four planes of reference in a two-cavity klystron

$\begin{bmatrix} a_o, a_r \\ b_r \end{bmatrix}$ = the Fourier coefficients

C = velocity of light

d_n = the length of n^{th} gridded gap

$e_{erf(x)}$ = error function(x) = $\dfrac{2}{\sqrt{\pi}} \int_o^x e^{-t^2}\, dt$

I_o = d-c beam current

i_n = total conduction current at plane A_n

J_p = Bessel function of first kind and p^{th} order

m = electronic mass

m_o = electronic mass at rest

R_e = real part

t = time that an electron arrives at an arbitrary plane Z within the gap

s_n = the n^{th} drift distance

S''_m = the normalized drift angle for the m^{th} drift space and angular frequency ω_2

t_n = time at which an electron passes plane A_n

u_o = d-c electron beam velocity

u_n = velocity of electron at an arbitrary plane Z in the n^{th} gap region

u = velocity of electron at an arbitrary plane Z in the first gap

v_1 = total electron velocity at exit from plane A

V_o = d-c electron beam velocity

V_n = amplitude of signal

z = arbitrary position co-ordinate of an electron within the gap

ABSTRACT

This investigation uses ballistic theory in the analysis of the behavior of an electron beam passing through alternate gap and drift regions, with the gap regions having excitation fields. The analysis develops the response to a complicated frequency spectrum of the drive signal. First the double frequency case is analyzed. Relativistic effects are taken into account and their influence on the current response studied. Then the theory is extended to the more complicated case of a Gaussian spectrum. The first-order bunching theory is used to plot current response curves. An estimate of the pulse distortion resulting from nonlinear electron beam dynamics is obtained from the curves. It is also of interest that the envelope shape of the exit current is almost completely independent of the r-f frequency. The large-signal, finite-gap analysis is carried out, and the results extended to the multiple-cavity klystron.

I. INTRODUCTION

A. OBJECTIVE

Many stages of development followed the invention of the klystron by the Varian brothers in 1939. Until now, most of the analysis and discussion has been limited to the case of a continuous-wave drive signal. The purpose here is to open the door to investigation of the numerous problems associated with the use of pulsed microwave amplifiers for amplification of nanosecond pulses whose pulse lengths are of the order of several cycles of the r-f carrier frequency. The main concern is with high-power amplifiers with average power capabilities comparable to conventional pulsed amplifiers; thus for comparable repetition rates, the peak power would be higher by the inverse ratio of the pulse lengths.

Several factors may be important in determining the pulse response capability of high-power amplifiers such as the klystron. It follows, from Fourier analysis, that a long pulse of constant carrier frequency includes a narrow bandwidth, while a pulse that is short in terms of cycles of the r-f carrier has a broad frequency spectrum. The spectrum of the long signal can, however, be significantly broadened by introducing modulation. Klauder[3] showed that to utilize the transmitting tubes efficiently, this modulation must take the form of frequency modulation. By this method one can introduce the frequency-spread characteristic of a short pulse within the envelope of a long-duration signal. Klauder[4] also showed certain advantages of short constant-frequency r-f signals over the long signals with linear frequency modulation. This emphasizes the importance of nanosecond pulse studies. One of the problems that arises is that the broad frequency spec-

trum associated with the short pulses might be affected by the bandwidth of the circuits associated with the amplifier, which will limit the response and therefore cause distortion of the pulse. Operation of the amplifier at maximum efficiency entails nonlinear behavior in the electron beam dynamics. This will cause the frequency spectrum of the output pulse to be altered from that of the input pulse and produce distortion. Ballistic theory will be utilized to determine the response of klystrons to the complicated frequency spectrum and lead to an estimate of the pulse distortion.

Studies in this direction will provide a solution for the conflicting requirements of long range and high resolution in radar systems. Resolution depends on the transmitted pulse bandwidth, and nanosecond pulses will, no doubt, satisfy the conditions for high resolution. For long-range capabilities, large power requirements are necessary; hence, high-power nanosecond pulses are expected to solve the two conflicting radar requirements. Radar systems that yield simultaneous information about the range and velocity of a target would be useful in certain applications. Klauder[4] showed an inherent ambiguity in a simultaneous determination of both the range and velocity of a moving target, when using the so-called "chirp" scheme. If the transmitted signal with an ambiguity function that is highly peaked only at about $t = 0$ exists, then high resolution is expected in both range and velocity. Using analogs from quantum mechanics, Klauder showed that the sequence of signals, f(t), that satisfy these conditions are:

$$f(t) = \frac{\gamma^{1/4}}{\sqrt{\pi^{1/2} n!\, 2^n}} H_n(\sqrt{\gamma}t)\, e^{-\frac{\gamma t^2}{2}} ,$$

where $H_n(z)$ represents the n^{th} Hermite polynomial defined by

$$H_n(z) = (-1)^n \, e^{z^2} \, \frac{d^n}{dz^n} \, e^{-z^2} \quad .$$

When n is taken equal to zero, the Gaussian envelope, on which this analysis is chiefly based, results. Further details on the Gaussian spectrum are given in Appendix A.

B. MODEL

Since a one-dimensional model of the electron beam is used, a univelocity electron beam is incident at the entrance plane $z = 0$, moving in the $+z$ direction in confined flow. This assumption of a very strong longitudinal magnetic field will depress the potential at the center of the beam so that peripheral electrons travel faster than axial ones, introducing a phase difference between the radio-frequency current carried by different beam segments. This difficulty is overcome by assuming the existence of a thread of positive ions along the axis of the beam, just sufficient to neutralize the charge density of electrons; thus, the effects of depressing the potential across the beam caused by space charge are neglected, and so also are variations in electron velocities caused by thermal noise. Electron velocities are assumed small compared to the velocity of light, permitting a nonrelativistic treatment of the problem. In the analysis of a double-frequency signal, however, the change in response caused by relativistic effects is studied. The electric field is assumed constant throughout the cross section of the klystron beam.

II. RESPONSE OF KLYSTRON TO DOUBLE-FREQUENCY INPUT

In this section, the response of a klystron to a double-frequency input will be treated. The signal is $V = V_1 \sin\omega_1 t + V_2 \sin\omega_2 t$. The

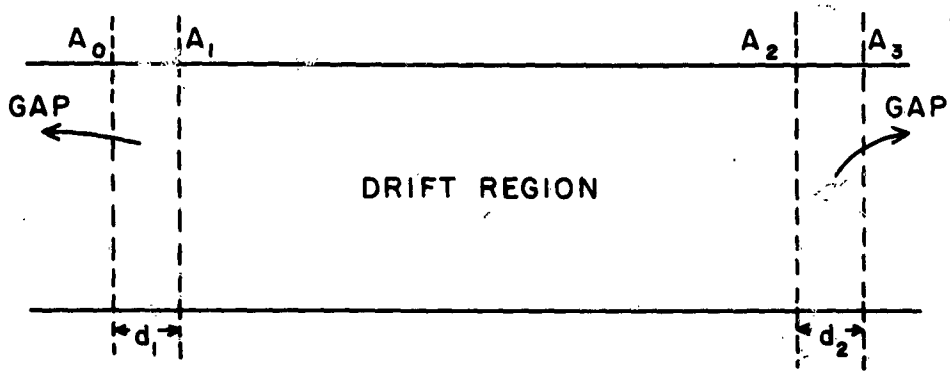

four planes of reference in a two-cavity klystron are represented by A_o, A_1, A_2, A_3, and the subscripts o, 1, 2, 3, respectively will be used to identify quantities in the respective planes.

A. FIRST GAP

Applying Newton's second law of motion, we have

$$\frac{d^2z}{dt^2} = \frac{eV_1}{md_1} \sin\omega_1 t + \frac{eV_2}{md_1} \sin\omega_2 t \quad ;$$

therefore

$$\frac{dz}{dt} = \frac{-eV_1}{md_1\omega_1} \cos\omega_1 t - \frac{eV_2}{md_1\omega_2} \cos\omega_2 t + k_1 \quad ,$$

where k_1 is a constant to be determined from the initial condition; at $t = t_o$, the velocity $dz/dt = u_o$; therefore

$$\frac{dz}{dt} = u_o + \frac{eV_1}{md_1}\left[\frac{\cos\omega_1 t_o}{\omega_1} - \frac{\cos\omega_1 t}{\omega_1}\right] + \frac{eV_2}{md_1}\left[\frac{\cos\omega_2 t_o}{\omega_2} - \frac{\cos\omega_2 t}{\omega_2}\right] . \tag{2.1}$$

Integrating again gives

$$z = u_o t + \left[\frac{eV_1}{md_1}\frac{\cos\omega_1 t_o}{\omega_1} + \frac{eV_2}{md_1}\frac{\cos\omega_2 t_o}{\omega_2}\right] t - \left[\frac{eV_1}{md_1\omega_1^2}\sin\omega_1 t + \frac{eV_2}{md_1\omega_2^2}\sin\omega_2 t\right] + k_2 ,$$

where k_2 is a constant, evaluated by inserting the initial condition: at $t = t_o$, the distance $z = 0$; therefore

$$z = \left[u_o + \frac{eV_1}{md_1}\frac{\cos\omega_1 t_o}{\omega_1} + \frac{eV_2}{md_1\omega_2}\cos\omega_2 t_o\right](t - t_o) - \frac{eV_1}{md_1\omega_1^2}(\sin\omega_1 t - \sin\omega_1 t_o) - \frac{eV_2}{md_1\omega_2^2}(\sin\omega_2 t - \sin\omega_2 t_o) .$$

Putting

$$\frac{V_1}{V_o} = a_1 , \quad \frac{V_2}{V_o} = a_2 , \quad \frac{\omega_1 d_1}{u_o} = \phi_1' , \quad \frac{\omega_2 d_1}{u_o} = \phi_1'' ,$$

gives

$$z = \left[u_o + \frac{a_1 u_o}{2\phi_1'}\cos\omega_1 t_o + \frac{a_2 u_o}{2\phi_1''}\cos\omega_2 t_o\right](t - t_o) +$$

$$+ \frac{a_1 u_o}{2\phi_1' \omega_1} (\sin\omega_1 t_o - \sin\omega_1 t) + \frac{a_2 u_o}{2\phi_1'' \omega_2} (\sin\omega_2 t_o - \sin\omega_2 t) \quad . \quad (2.2)$$

The distance is $z = d$ at $t = t_1$, where

$$t_1 = t_o + \Gamma_1 ,$$

$$\Gamma_1 = \text{transit time in first gap} = \frac{d_1}{u_o} + \frac{\delta_1}{\omega_o} ,$$

$$\delta_1 = \text{correction factor,}$$

$$\omega_o = \frac{\omega_1 + \omega_2}{m + n} , \quad m \text{ and } n \text{ being two numbers defined by } -\omega_1 = m\omega_o \text{ and } \omega_2 = n\omega_o .$$

Substitution of this condition in Equation (2.2) gives,

$$d = u_o \left(1 + \frac{a_1}{2\phi_1'} \cos\omega_1 t_o + \frac{a_2}{2\phi_1''} \cos\omega_2 t_o\right) \Gamma_1$$

$$+ \frac{a_1 u_o}{2\phi_1' \omega_1} (\sin\omega_1 t_o - \sin\omega_1 t) + \frac{a_2 u_o}{2\phi_1'' \omega_2} (\sin\omega_2 t_o - \sin\omega_2 t) \quad . \quad (2.3)$$

The following assumptions are made:

$$\begin{matrix}\sin \\ \cos\end{matrix} \left(\omega_1 t - \phi_1' - \frac{\omega_1}{\omega_o} \delta_1\right) = \begin{matrix}\sin \\ \cos\end{matrix} \left(\omega_1 t - \phi_1'\right)$$

$$\begin{matrix}\sin \\ \cos\end{matrix} \left(\omega_2 t - \phi_1'' - \frac{\omega_2}{\omega_o} \delta_1\right) = \begin{matrix}\sin \\ \cos\end{matrix} \left(\omega_2 t - \phi_1''\right) \quad .$$

The products $a_1\delta_1$ and $a_2\delta_1$ are negligible, and Equation (2.3) reduces to,

$$-\frac{u_o\delta_1}{\omega_o} = \frac{a_1 d_1}{2\phi_1'}\cos(\omega_1 t - \phi_1') + \frac{a_2 d_1}{2\phi_1''}\cos(\omega_2 t - \phi_1'') + \frac{a_1 u_o}{2\phi_1'\omega_1}\left[\sin(\omega_1 t - \phi_1') - \sin\omega_1 t\right]$$

$$+ \frac{a_2 u_o}{2\phi_1''\omega_2}\left[\sin(\omega_2 t - \phi_1'') - \sin\omega_2 t\right]$$

$$= \frac{a_1 d_1}{2\phi_1'}(\cos\omega_1 t\cos\phi_1' + \sin\omega_1 t\sin\phi_1') + \frac{a_2 d_1}{2\phi_1''}(\cos\omega_2 t\cos\phi_1'' + \sin\omega_2 t\sin\phi_1'')$$

$$+ \frac{a_1 u_o}{2\phi_1'\omega_1}\left[\sin\omega_1 t\cos\phi_1' - \cos\omega_1 t\sin\phi_1' - \sin\omega_1 t\right]$$

$$+ \frac{a_2 u_o}{2\phi_1''\omega_2}\left[\sin\omega_2 t\cos\phi_1'' - \cos\omega_2 t\sin\phi_1'' - \sin\omega_2 t\right] ,$$

therefore

$$\delta_1 = \frac{a_1}{2\phi_1' m}\left[(1 - \cos\phi_1' - \phi_1\sin\phi_1')\sin\omega_1 t + (\sin\phi_1' - \phi_1'\cos\phi_1')\cos\omega_1 t\right]$$

$$+ \frac{a_2}{2\phi_1'' n}\left[(1 - \cos\phi_1'' - \phi_1''\sin\phi_1'')\sin\omega_2 t + (\sin\phi_1'' - \phi_1''\cos\phi_1'')\cos\omega_2 t\right] . \tag{2.4}$$

Thus, the expression for the correction factor as given by Equation (2.4) is a superposition for each frequency, considered separately. The induced current is calculated by Ramo's theorem; i.e.

$$i_1 = \frac{I_o}{d_1}\int_{t-\Gamma_1}^{t}\left(\frac{dz}{dt}\right)dt_o = \frac{I_o}{d_1}\int_{t-J_1}^{t}\left\{u_o + \frac{eV_1}{md_1}\left(\frac{\cos\omega_1 t_o}{\omega_1} - \frac{\cos\omega_1 t}{\omega_1}\right)\right.$$

$$+ \frac{eV_2}{md_1}\left(\frac{\cos\omega_2 t_o}{\omega_2} - \frac{\cos\omega_2 t}{\omega_2}\right)\Bigg\} dt_o$$

$$= \frac{I_o}{d_1}\left\{u_o\Gamma_1 + \frac{1u_o}{2\phi_1'}\left[\frac{\sin\omega_1 t - \sin\omega_1(t-\Gamma_1)}{\omega_1} - \Gamma_1\cos\omega_1 t\right]\right.$$

$$\left. + \frac{2u_o}{2\phi_1''}\left[\frac{\sin\omega_2 t - \sin\omega_2(t-\Gamma_1)}{\omega_2} - \Gamma_1\cos\omega_2 t\right]\right\}$$

After simplifying, and in the process neglecting $m\delta_1 \cos\omega_2 t$ and $n\delta_1 \cos\omega_1 t$, we have

$$i_1 = I_o + I_o a_1\left[\left(\frac{1-\cos\phi_1'}{2\phi_1'^2} - \frac{\sin\phi_1'}{2\phi_1'}\right)\sin\omega_1 t + \left(\frac{\sin\phi_1''}{\phi_1'^2} - \frac{1+\cos\phi_1'}{2\phi_1'}\right)\cos\omega_1 t\right]$$

$$+ I_o a_2\left[\left(\frac{1-\cos\phi_1''}{2\phi_1''^2} - \frac{\sin\phi_1''}{2\phi_1''}\right)\sin\omega_2 t + \left(\frac{\sin\phi_1''}{\phi_1''^2} - \frac{1+\cos\phi_1''}{2\phi_1''}\right)\cos\omega_2 t\right] . \tag{2.5}$$

From Equation (2.5), it is evident that the effects of the different frequency components of excitation on the induced current are mutually independent. The double-frequency case can therefore be extended to the multiple-frequency input, and it can be concluded that the different frequency effects are independent of each other, subject to the approximations made in this section.

B. DRIFT REGION

Thus the electrons enter the drift space with both velocity and current modulation. From Equation (2.1),

$$u_1 = u_o + \frac{e V_1}{m d_1 \omega_1}\left[\cos\omega\left(t_1 - \frac{d_1}{u_o} - \frac{\delta_1}{\omega_o}\right) - \cos\omega_1 t_1\right] + \frac{e V_2}{m d_1 \omega_2}\left[\cos\omega_2\left(t_1 - \frac{d_1}{u_o} - \frac{\delta_1}{\omega_o}\right) - \cos\omega_2 t_1\right] .$$

Resorting to approximation made in Section A gives

$$u_1 = u_o + \frac{1}{2}\, u_o a_1 \frac{\frac{\sin\phi_1'}{2}}{\frac{\phi_1'}{2}} \sin\left(\omega_1 t_1 - \frac{\phi_1'}{2}\right) + \frac{1}{2}\, u_o a_2 \frac{\frac{\sin\phi_1''}{2}}{\frac{\phi_1''}{2}} \sin\left(\omega_2 t_1 - \frac{\phi_1''}{2}\right) . \qquad (2.6)$$

Putting

$$\frac{\frac{\sin\phi_1'}{2}}{\frac{\phi_1'}{2}} = \beta_1' , \qquad \frac{\frac{\sin\phi_1''}{2}}{\frac{\phi_1''}{2}} = \beta_1'' ,$$

where β_1' and β_1'' are defined as the gap-coupling coefficients for the respective frequency components of excitation, gives the time of arrival at plane A_2 as

$$t_2 = t_1 + \frac{S_1}{u_o\left[1 + \frac{1}{2}\, a_1\beta_1' \sin\left(\omega_1 t_1 - \frac{\phi_1'}{2}\right) + \frac{1}{2}\, a_2\beta_1'' \sin\left(\omega_2 t_1 - \frac{\phi_1''}{2}\right)\right]} .$$

For small excitations, we get

$$t_2 = t_1 + \frac{S_1}{u_o}\left[1 - \frac{1}{2}\, a_1\beta_1' \sin\left(\omega_1 t_1 - \frac{\phi_1'}{2}\right) - \frac{1}{2}\, a_2\beta_1'' \sin\left(\omega_2 t_1 - \frac{\phi_1''}{2}\right)\right]$$

$$\frac{dt_2}{dt_1} = 1 + \frac{S_1}{u_o}\left[-\frac{\omega_1 a_1 \beta_1'}{2}\cos\left(\omega_1 t_1 - \frac{\phi_1'}{2}\right) - \frac{\omega_1 a_2 \beta_1''}{2}\cos\left(\omega_2 t_1 - \frac{\phi_1''}{2}\right)\right] .$$

The equation for conservation of charge gives,

$$i_2 = \frac{i_1}{\frac{dt_2}{dt_1}} = \frac{1}{\frac{dt_2}{dt_1}}\,\frac{I_o}{\frac{dt_1}{dt_o}} \qquad (2.7)$$

Again $t_1 = t_o + \Gamma_1 = t_o + \frac{d_1}{u_o} + \frac{\delta_1}{\omega_o}$; therefore

$$\frac{dt_1}{dt_o} = 1 + \frac{d}{dt_o}\left(\frac{\delta_1}{\omega_o}\right) ,$$

as d_1 is independent of t_o, and

$$\frac{dt_1}{dt_o} = 1 + \frac{a_1}{2\phi_1'}\left[\left(1 - \phi_1' \sin\phi_1' - \cos\phi_1'\right)\cos\left(\omega_1 t_o + \phi_1'\right) - \left(\sin\phi_1' - \phi_1'\cos\phi_1'\right)\sin\left(\omega_1 t_o + \phi_1'\right)\right]$$

$$+ \frac{a_2}{2\phi_1''}\left[\left(1 - \phi_1'' \sin\phi_1'' - \cos\phi_1''\right)\cos\left(\omega_2 t_o + \phi_1''\right) - \left(\sin\phi_1'' - \phi_1''\cos\phi_1''\right)\sin\left(\omega_2 t_o + \phi_1''\right)\right] .$$

As a result,

$$i_2 = I_o\left(\left[1 - \frac{S_1' a_1 \beta_1'}{2}\cos\left(\omega_1 t_1 - \frac{\phi_1'}{2}\right) - \frac{S_1'' a_2 \beta_1''}{2}\cos\left(\omega_2 t_1 - \frac{\phi_1''}{2}\right)\right]\right.$$

$$\left\{1 + \frac{a_1}{2\phi_1'}\left[\left(1 - \phi_1' \sin\phi_1' - \cos\phi_1'\right)\cos\left(\omega_1 t_o + \phi_1'\right) - \left(\sin\phi_1' - \phi_1'\cos\phi_1'\right)\sin\left(\omega_1 t_o + \phi\right.\right.\right.$$

$$+ \frac{a_2}{2\phi_1''}\left[\left(1 - \phi_1'' \sin\phi_1'' - \cos\phi_1''\right)\cos\left(\omega_2 t_o + \phi_1''\right) - \left(\sin\phi_1'' - \phi_1'' \cos\phi_1''\right)\sin\left(\omega_2 t_o + \phi_1''\right)\right]\Bigg)\Bigg)^{-1} \tag{2.8}$$

where

$$S_1' = \frac{\omega_1 S_1}{u_o} \quad , \qquad S_1'' = \frac{\omega_2 S_1}{u_o} \quad .$$

With

$$\begin{matrix}\sin \\ \cos\end{matrix}\left(\omega_1 t_o + \phi_1'\right) = \begin{matrix}\sin \\ \cos\end{matrix}\left(\omega_1 t_1\right) \quad ,$$

and with approximations similar to those made previously, the current i_2 can be expressed as a function of t_1, and hence t_2.

The periodicity of i_2 is obvious, and therefore i_2 can be expanded in Fourier series as follows. First, t_2 will be related to t_o, as follows:

$$t_2 = t_o + \frac{d_1}{u_o} + \frac{S_1'}{u_o}\left[1 - \frac{1}{2}\alpha_1\beta_1' \sin\left(\omega_1 t_o + \frac{\phi_1''}{2}\right) - \frac{1}{2}\alpha_2\beta_1'' \sin\left(\omega_2 t_o + \frac{\phi_1''}{2}\right)\right] ,$$

i.e., the term δ_1/ω_o is neglected, while the approximations with regard to the sinusoidal terms are justified; then

$$i_2 = \frac{1}{2} a_o + \sum_{r=1}^{\infty} a_r \cos n\left(\omega t_2 - S_1 - \phi_1\right) + \sum_{r=1}^{\infty} b_r \cos n\left(\omega t_2 - S_1 - \phi_1\right) ,$$

where

$$S_1 = \frac{\omega_o S_1}{u_o} , \qquad \phi_1 = \frac{\omega_o d_1}{u_o} , \qquad a_o = 2I_o ,$$

and

$$a_r = \frac{1}{\pi} \int_{-\pi}^{\pi} \frac{I_o}{\frac{dt_2}{dt_o}} \cos r(\omega t_2 - S_1 - \phi_1) \quad d(\omega t_2)$$

$$= \frac{1}{\pi} \int_{-\pi}^{\pi} I_o \cos r\left[\omega_o t_o - k_1' \sin\left(m\omega_o t_o + \frac{\phi_1'}{2}\right) - k_1'' \sin\left(n\omega_o t_o + \frac{\phi_1''}{2}\right)\right] d(\omega_o t_o),$$

$$b_r = \frac{1}{\pi} \int_{-\pi}^{\pi} I_o \sin r\left[\omega_o t_o - k_1' \sin\left(m\omega_o t_o + \frac{\phi_1'}{2}\right) - k_1'' \sin\left(n\omega_o t_o + \frac{\phi_1''}{2}\right)\right] d(\omega_o t_o), \tag{2.9}$$

where

$$k_1' = \frac{S_1 \alpha_1 \beta_1'}{2} \quad , \qquad k_1'' = \frac{S_1 \alpha_1 \beta_1''}{2} \quad .$$

The coefficients a_r and b_r are simplified by a method indicated in Appendix B.

The general equation of motion has to be formulated for the calculation of the induced current in plane A_3, and the method adopted is similar to that used in the first gap, with only the initial conditions different. This is done later for the more complicated Gaussian spectrum and will be omitted here. The main purpose of this section is to show the absence of intermodulation of the different frequency components at the output, subject, of course, to the approximations made. It must be stated that the preceding analysis was based upon frequencies ω_1 and ω_2 not being very far from the central frequency ω_o in the frequency spectrum, i.e., the numbers m and n should not be much greater than 1. As the main purpose of this study is the extension of this analysis to the response of a klystron to short pulses

with a narrow bandwidth of frequencies, the assumptions made are compatible with the condition desired.

No account has been taken of the relativistic variation of mass with velocities. This problem becomes especially serious when the beam voltage is large in high-power klystrons and where the very hard X-rays produced present an additional hazard to the operating personnel. A simple treatment will be given of the relativistic effects on the response, using the same model as before.

According to Einstein, nothing can move with a speed greater than the speed of light. Newtonian mechanics combined with this postulate demands that a mass subjected to a constant force must be accelerated till the speed of light is attained; but, as the force is still present, the speed must still increase, which is impossible. This ambiguity is solved by accepting the increase of mass with velocity, and assuming that mass is a manifestation of energy, the two related to each other by the famous equation $w = c^2 m$, where c is the velocity of light.

An increase in mass, dm, when accelerated, results in $c^2\, dm = d\omega = F\, ds$, where F is the applied force over a distance ds. Newton's second law gives

$$F = \frac{d}{dt}\,(mv) \quad ;$$

therefore

$$c^2 \int dm = \int \frac{d}{dt}\,(mv)\; ds = \int v\, d\,(mv) \quad .$$

Equating the integrands and separating variables, we have

$$\frac{dm}{m} = \frac{v\, dv}{(c^2 - v^2)} \quad .$$

Assuming that rest mass equals m_o gives, by integration,

$$m = \frac{m_o}{\sqrt{1 - \frac{v^2}{c^2}}} \quad , \tag{2.10}$$

the equation that demonstrates the variation of mass with velocity. In this case, Newton's force equation gives

$$\frac{d}{dt}\left[\frac{m_o u}{\sqrt{1 - \frac{u^2}{c^2}}}\right] = eE \quad .$$

With $u(z, t) = u_o(z) + v(z)\, e^{j\omega t}$, where

$u(z, t)$ = total electron velocity,

$u_o(z)$ = d-c beam velocity,

$v(z)$ = amplitude of a-c velocity.

The basic assumption will be that $v << c$, which is justified, since the signal voltage is not sufficiently high in practice to make the a-c velocity appreciable in comparison to the speed of light. Using the Taylor series expansion, we have

$$\frac{u}{\left(1 - \frac{u^2}{c^2}\right)} = \frac{u_o}{\left(1 - \frac{u_o^2}{c^2}\right)^{1/2}} + ve^{j\omega t}\, \frac{d}{du_o}\left[\frac{u_o}{\left(1 - \frac{u_o^2}{c^2}\right)^{1/2}}\right] = \frac{u_o}{\left(1 - \frac{u_o^2}{c^2}\right)^{1/2}} + \frac{ve^{j\omega t}}{\left(1 - \frac{u_o^2}{c^2}\right)^{3/2}} \quad ;$$

therefore

$$\frac{d}{dt}\left[\frac{u_o}{\left(1-\frac{u_o^2}{c^2}\right)^{1/2}}+\frac{ve^{j\omega t}}{\left(1-\frac{u_o^2}{c^2}\right)^{3/2}}\right]=-\frac{e}{m_o}E \quad . \qquad (2.11)$$

As the excitation is variational, separating Equation (2.11) into the d-c and a-c parts gives,

$$\frac{d}{dt}\left[\frac{u_o}{\left(1-\frac{u_o^2}{c^2}\right)^{1/2}}\right]=0 \quad ,$$

$$\frac{d}{dt}\left[\frac{ve^{j\omega t}}{\left(1-\frac{u_o^2}{c^2}\right)^{3/2}}\right]=\frac{e}{m_o d_1}\left[V_1 \sin\omega_1 t+V_2 \sin\omega_2 t\right] \quad ; \qquad (2.12a)$$

therefore

$$v_{1a\text{-}c}=-\left(1-\frac{u_o^2}{c^2}\right)^{3/2}\frac{e}{m_o d_1}\left[\frac{V_1\cos\omega_1 t}{\omega_1}+\frac{V_2\cos\omega_2 t}{\omega_2}\right]+k_3 \quad ,$$

where k_3 is a constant evaluated from the initial condition that at $t=t_o$, $v_{1\,a\text{-}c}=0$. Finally

$$v_{1\,a\text{-}c}=-\left(1-\frac{u_o^2}{c^2}\right)^{3/2}\frac{e}{m_o d_1}\left[V_1\left(\frac{\cos\omega_1 t_o}{\omega_1}-\frac{\cos\omega_1 t}{\omega_1}\right)+V_2\left(\frac{\cos\omega_2 t_o}{\omega_2}-\frac{\cos\omega_2 t}{\omega_2}\right)\right] \quad .$$

The total velocity at any instant in the gap is

$$\frac{dz}{dt} = u_o + v_{1\,a\text{-}c} \quad .$$

Integrating again and using the initial condition that $z = 0$ at $t = t_o$, we have

$$z = \left[u_o + \left(1 - \frac{u_o^2}{c^2}\right)^{3/2} \frac{e}{m_o d_1}\left(\frac{V_1 \cos\omega_1 t_o}{\omega_1} + \frac{V_2 \cos\omega_2 t_o}{\omega_2}\right)\right](t - t_o)$$

$$+ \left(1 - \frac{u_o^2}{c^2}\right)^{3/2} \frac{e}{m_o d_1}\left(\frac{V_1 \sin\omega_1 t_o}{\omega_1^2} - \frac{V_1 \sin\omega_1 t_o}{\omega_1^2} + \frac{V_2 \sin\omega_2 t_o}{\omega_2^2} - \frac{V_2 \sin\omega_2 t_o}{\omega_2^2}\right) .$$

Now $z = d$ at $t = t_1 = t_o + \Gamma_1$. Following the procedure of Section A of this chapter, and making similar approximations, we obtain the expression for the correction factor in this equation:

$$\delta_1 = \frac{a_1\omega_1}{2\phi_1'\omega_1}\left\{\left[\left(1 - \cos\phi_1' - \phi_1' \sin\phi_1'\right)\sin\omega_1 t + \left(\sin\phi_1' - \phi_1' \cos\phi_1'\right)\cos\omega_1 t\right]\right.$$

$$\left. + \frac{a_2\omega_o}{2\phi_1''\omega_2}\left[1 - \cos\phi_1'' - \phi_1'' \sin\phi_1'' \sin\omega_1 t + \left(\sin\phi_1'' - \phi_1'' \cos\phi_1''\right)\cos\omega_1 t\right]\right\}$$

$$\left(1 - \frac{u_o^2}{c^2}\right)^{3/2} . \qquad (2.12b)$$

Equation (2.12b) is very similar to Equation (2.4) and shows that the correction factor is only multiplied by a constant $\left(1 - u_o^2\right)^{3/2} \Big/ c^2$ when relativistic effects are included. Again, the total current induced as a result of

the passage of electrons in the interval $t_o = t - \Gamma_1$, and $t_o = t$ is

$$i_1 = \frac{I_o}{d} \int_{t-\Gamma_1}^{t} u \, dt_o \quad .$$

Carrying out this integration as in the nonrelativistic case, we have

$$i_1 = I_o + \left(1 - \frac{u_o^2}{c^2}\right)^{3/2} I_o \left(a_1 \left\{ \left(1 - \frac{\cos\phi_1'}{2\phi_1'^2} - \frac{\sin\phi_1'}{2\phi_1'} \right) \sin\omega_1 t + \left[\frac{\sin\phi_1'}{2\phi_1'^2} - \frac{(1+\cos\phi_1')}{2\phi_1'} \right] \cos\omega_1 t \right\} \right.$$
$$\left. + a_2 \left\{ \left(1 - \frac{\cos\phi_1'}{2\phi_1''^2} - \frac{\sin\phi_1''}{2\phi_1''} \right) \sin\omega_2 t + \left(\frac{\sin\phi_1''}{2\phi_1''^2} - \frac{1+\cos\phi_1''}{2\phi_1''} \right) \cos\omega_2 t \right\} \right) \quad . \tag{2.13}$$

From Equation (2.13) the relativistic effects on the induced current in the first gap are very clearly observed. The explicit effect on the r-f current resulting from electrons at high beam voltages subject to the simple approximations made should be noted. For a particular beam voltage, the r-f induced current is lower by the factor $\left(1 - u_o^2/c^2\right)^{3/2}$ when the relativistic variation of mass with velocity is taken into account. A curve has been plotted to show this effect (Figure 2).

For low voltages and hence low values of u_o, the factor $\left(1 - u_o^2/c^2\right)^{3/2}$ is equal to unity, and the result becomes similar to that derived for the nonrelativistic case. For $u_o/c = \frac{1}{10}$,

$$\left(1 - \frac{u_o^2}{c^2}\right)^{3/2} = 0.999 \quad .$$

At a beam voltage of 10^4 volts,

$$\left(1 - \frac{u_o^2}{c^2}\right)^{3/2} = \left(1 - \frac{1}{25}\right)^{3/2} = 0.94 \quad .$$

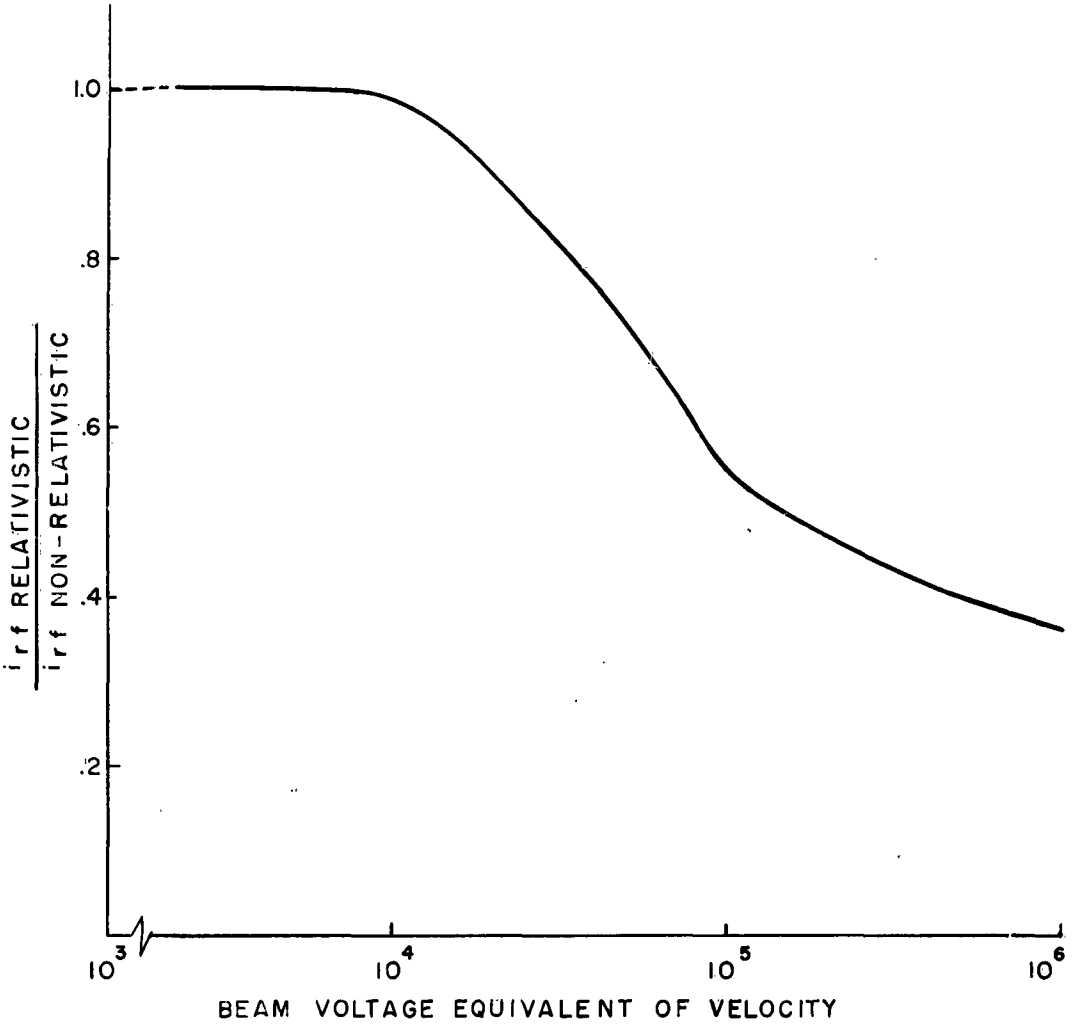

Figure 2. Graph Showing Relativistic Effects on Current Response.

III. BALLISTIC ANALYSIS

A. FIRST-ORDER BUNCHING THEORY

The problem under consideration is formulated as follows: A beam of parallel electrons which have been accelerated through a potential of V_o volts is passed through the grids of a resonator across which there appears a voltage $V_1 e^{-at^2} \sin\omega t$. The resultant electric field is assumed parallel to the electron motion. Since the velocity of an electron is proportional to the square root of the voltage through which it has been accelerated, the velocity with which an electron emerges from the first, or bunching, resonator of a two-resonator klystron will be[1]

$$V_a = u_o \sqrt{1 + \frac{\beta_1 V_1}{V_o} e^{-at^2} \sin\omega t} = v_o \sqrt{1 + \alpha_1 \beta_1 e^{-at^2} \sin\omega t} \quad .$$

where $u_o = \sqrt{\frac{2e}{m} V_o}$ is the d-c beam velocity, β_1 is the gap-coupling coefficient (taking into account the effect of the gap transit angle), and $\alpha_1 = V_1/V_o$. Here β_1 may not be related to the gap transit angle in the same way as for the sinusoidal case, but it obeys the general definition of the ratio of the velocity gained in the real gap with V_1 across it to the velocity gained in an infinitely narrow gap with V_1 across it and, as such, is always less than 1. The time taken by an electron to move a certain distance along the beam depends upon the point on the cycle at which it passed through the resonator gap as well as upon the magnitude of the gap voltage. If S_1 is the drift length, t_o, the time at which the electron leaves the first resonator, and t_2 the time of arrival at the catcher; then

$$t_2 = t_o + \frac{S_1}{u_o \left(1 + a_1 \beta_1 e^{-at_o^2} \sin \omega t_o\right)^{1/2}} \quad .$$

Now, if the modulation factor a_1 is small compared to unity; then the following approximation is reasonably valid:

$$t_2 = t_o + \frac{S_1}{u_o} \left(1 - \frac{a_1 \beta_1}{2} e^{-at_o^2} \sin \omega t_o\right) \quad .$$

To find the current associated with the electron bunches, one must remember that the principle of conservation of charge applies to electron bunches for an interval with corresponding departure and arrival times. The electron stream is subject to the conservation of charge, so that

$$\left| I_o dt_o \right| = \left| i_2 dt_2 \right| \quad ,$$

where i_2 is the catcher current; hence

$$i_2 = \frac{I_o}{\left| \frac{dt_2}{dt_o} \right|}$$

$$= \frac{I_o}{1 + \frac{S_1}{u_o} \frac{a_1 \beta_1}{2} \left[- \left(-2at_o e^{-at_o^2} \sin \omega t_o + \omega e^{-at_o^2} \cos \omega t_o \right) \right]}$$

$$= \frac{I_o}{1 - k \left(e^{-a\theta_o^2/\omega^2} \cos \theta_o - 2 \frac{a\theta_o}{\omega^2} e^{-a\theta_o^2/\omega^2} \sin \theta_o \right)} \quad ,$$

where the bunching parameter, $\frac{\omega S_1}{u_o} \frac{\alpha_1 \beta_1}{2} = S_1 \frac{\alpha_1 \beta_1}{2}$. As this expression is aperiodic, it cannot be represented by Fourier series, contrary to the analysis carried out by Beck[2] for the pure sine wave. Since the catcher response is desired, it has been found convenient to plot the output current versus t_2 for different bunching parameters, similar to the treatment given by Spangenburg[1] for the sinusoidal excitation. Since $i_2 = f(\theta_o) = f(-\theta_o)$ the curves are expected to be symmetrical. If the Gaussian spectrum is represented by $V e^{-at^2} \cos \omega t$, then

$$i_2 = \frac{I_o}{1 + k\left[e^{-a\theta_o^2/\omega^2} \sin \theta_o + 2\frac{a\theta_o}{\omega^2} e^{-a\theta_o^2/\omega^2} \cos \theta_o\right]} \quad .$$

In this case $i_2 = f(\theta_o) \neq f(-\theta_o)$. For negative values of θ_o, we have

$$i_2 = \frac{I_o}{1 - k\left[e^{-a\theta_o^2/\omega^2} \sin \theta_o + 2\frac{a\theta_o}{\omega^2} e^{a\theta_o^2/\omega^2} \cos \theta_o\right]} \quad .$$

The choice of a/ω^2 is governed by the following consideration. The envelope has its maximum value at $t = 0$ (since the envelope is $V e^{-at^2} \cos \omega t$) and is supposed to fall to $1/e$ of its maximum when $\omega t = 10\pi$, so that 10 r-f cycles are enclosed between the points where the amplitude is $1/e$ of the maximum value; therefore

$$\frac{a}{\omega^2} (10\pi)^2 = 1 \qquad \frac{a}{\omega^2} = \frac{1}{(10\pi)^2} \quad .$$

Graphs have been drawn for the output current versus exit time for different values of bunching parameter for the envelopes $V_1 e^{-at^2} \sin\omega t$, and $V_1 e^{-at^2} \cos\omega t$. In the first case the infinite peaks occur for values of θ_o satisfying the transcendental equation,

$$\left(\cos\theta_o - 2\,\frac{a\theta_o}{2}\,\sin\theta_o\right) = \frac{1}{k}\, e^{a\theta_o^2} \quad .$$

The values of θ_o at which infinite peaks occur are found graphically: For $k < 1$, there are no infinite peaks, as is evident from the equations also (Figure 3); for $k = 1$, one infinite peak occurs (Figure 4); for $k = 1.5$, there are 14 infinite peaks (Figure 5); for $k=2$, there are 18 infinite peaks.*

This can be justified as follows. In the pure sine-wave case, two infinite peaks occur for $k > 1$; hence, for simplicity, we associate two infinite peaks with two peaks of the excitation signal. In the Gaussian envelope, the seventh peak occurs on either side of $t_o = 0$, when $\omega t_o = \pm 6.5\pi$. When $\omega t_o = 10\pi$, then $e^{-at_o^2} = 1/e$; therefore when $\omega t_o = 6.5\pi$, then

$$e^{-at_o^2} = \frac{1}{e^{0.425}} \quad .$$

*The response for $k = 2$ has not been actually plotted, for it is not expected to be very dissimilar from the $k = 1.5$ response plot. The number of infinite peaks, however, were determined by finding the points of intersection of the curves:

$$\left(\cos\theta_o - 2\,\frac{a\theta_o}{\omega^2}\,\sin\theta_o\right) \quad \text{and} \quad \frac{1}{2}\, e^{a\theta_o^2} \quad .$$

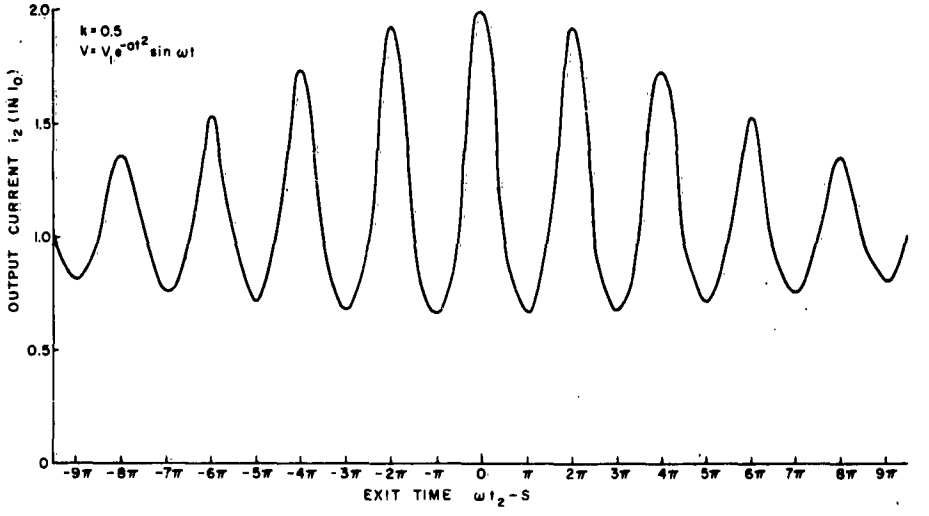

Figure 3. Output Current i_2 versus Exit Time $\omega t_2 - S$.

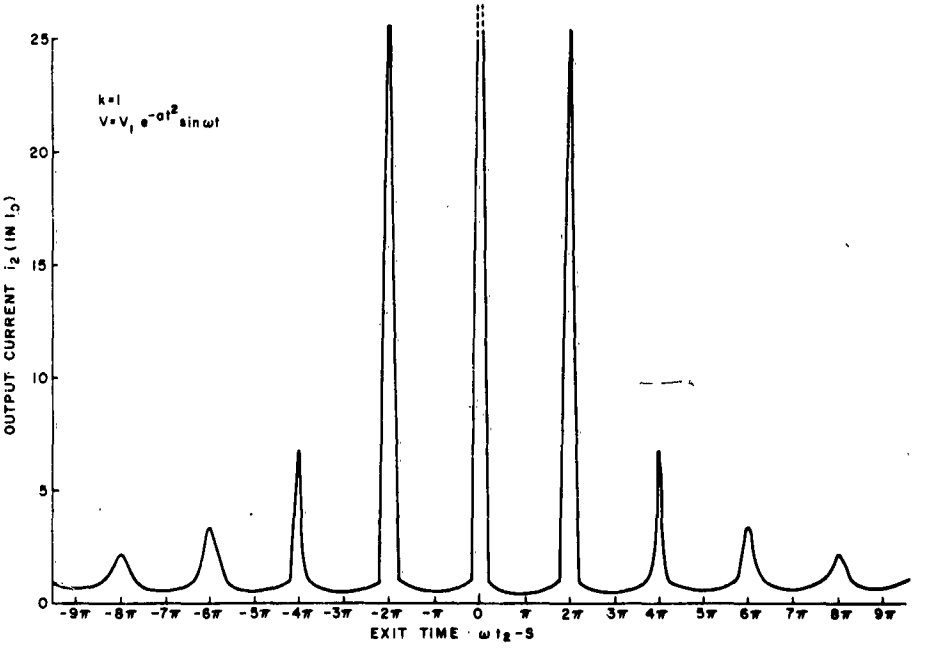

Figure 4. Output Current i_2 versus Exit Time $\omega t_2 - S$.

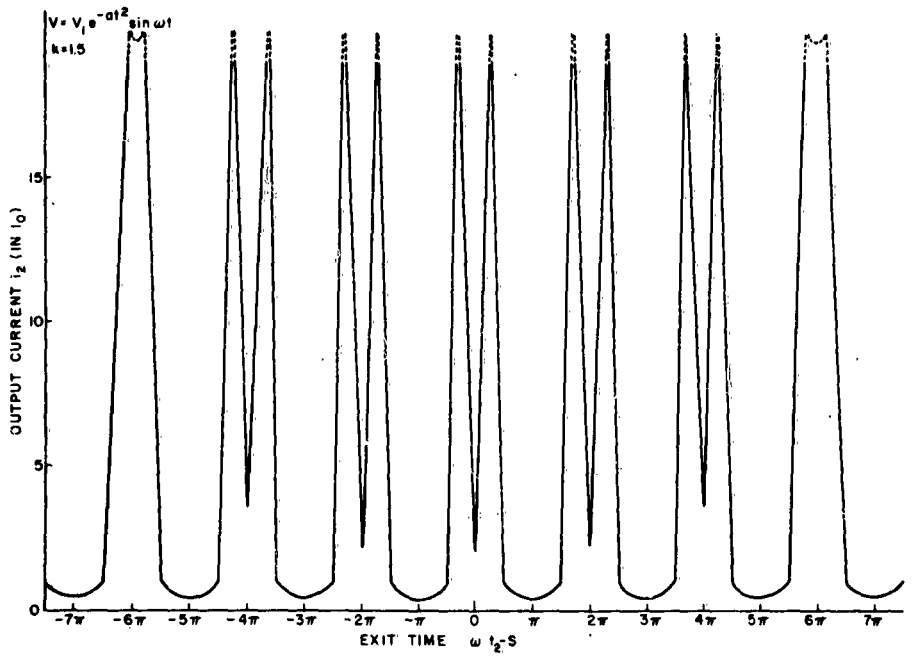

Figure 5. Output Current i_2 versus Exit Time $\omega t_2 - S$.

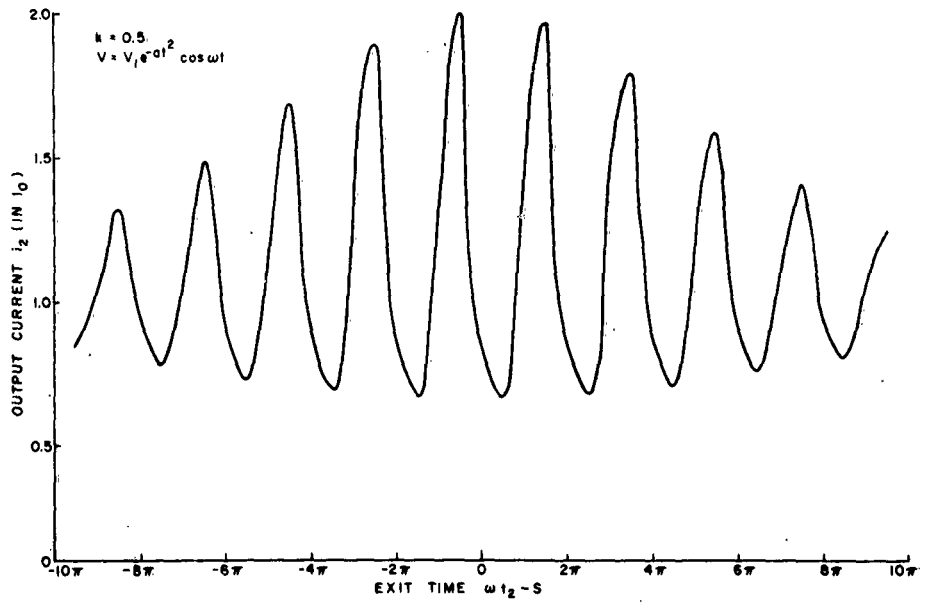

Figure 6. Output Current i_2 versus Exit Time $\omega t_2 - S$.

The value of k when $\omega t_o = 6.5\pi$ (if $k_o = 1.5$, when $t_o = 0$) is

$$k_{6.5} = \frac{1.5}{e^{0.425}} = \frac{1.5}{1.5} = 1 \quad .$$

Hence, 14 peaks are enclosed in the region for which $k > 1$.

Again, the ninth peak occurs on either side of $t_o = 0$, when $\omega t_o = 8.5\pi$, so that this region encloses 18 peaks. The value of k at $\omega t_o = 8.5\pi$ (if $k_o = 2$, at $t_o = 0$) is

$$k_{8.5} = \frac{2}{e^{0.725}} = \frac{2}{2.02} \simeq 1 \quad .$$

Thus, the occurrence of 18 infinite peaks for $k = 2$ is justified.

If the envelope is $V_1 e^{-at^2} \cos \omega t$, no infinite peaks occur for $k \leq 1$ (Figures 6 and 7). For $k = 1.5$, there are 12 infinite peaks (Figure8). This has also been justified by a process similar to the $V_1 e^{-at^2} \sin \omega t$ case.

B. KLYSTRON RESPONSE WITH VARIABLE GAP LENGTH

From Newton's equation of motion,

$$m \frac{d^2 z}{dt} = \frac{e V_1}{d} e^{-at^2} \cos \omega t \quad ;$$

hence

$$\frac{dz}{dt} = \int^{t} \frac{e V_1}{md} e^{-at^2} \cos \omega t \, dt + C \quad ,$$

where C is a constant. When $t = t_o$, then $dz/dt = u_o$. Thus,

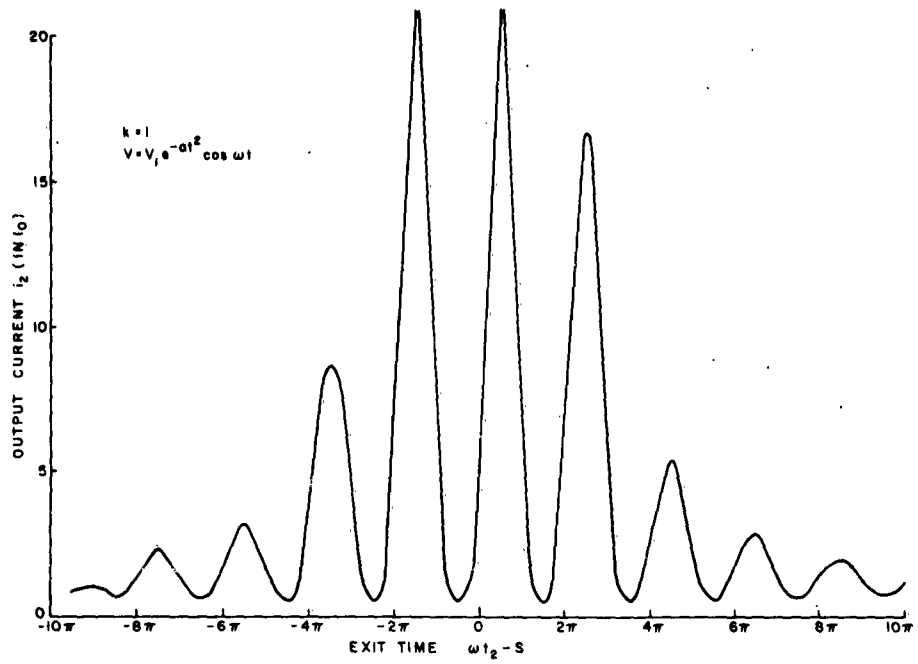

Figure 7. Output Current i_2 versus Exit Time $\omega t_2 - S$.

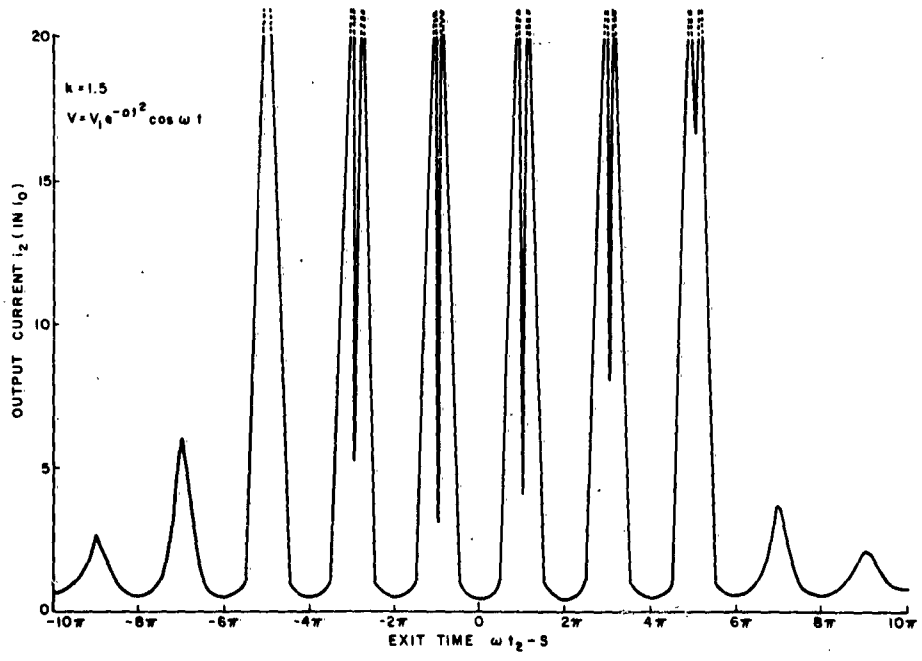

Figure 8. Output Current i_2 versus Exit Time $\omega t_2 - S$.

$$u_o - \int^{t_o} \frac{e V_1}{md} e^{-at^2} \cos \omega t \, dt = C \quad ,$$

from which

$$\frac{dz}{dt} = u_o + \int_{t_o}^{t} \frac{e V_1}{md} e^{-at^2} \cos \omega t \, dt \quad ;$$

hence the exit velocity u_1 from the first gap at $t = t_1$ is

$$u_1 = u_o + \int_{t_o}^{t_1} \frac{e V_1}{md} e^{-at^2} \cos \omega t \, dt \quad .$$

The time of arrival at the catcher, if S_1 is the drift distance, is

$$t_2 = t_o + \frac{S_1}{u_o + \frac{e V_1}{md} \int_{t_o}^{t_1} e^{-at^2} \cos \omega t \, dt} \quad ;$$

therefore

$$t_2 = t_o + \frac{S_1}{u_o} \left(1 + \frac{e V_1}{md u_o} \int_{t_o}^{t_1} e^{-at^2} \cos \omega t \, dt \right)^{-1} \quad .$$

Here an approximation will be made to permit analytical computation: $t_1 = t_o + r$, where the transit angle r is $(d/u_o) + (\delta/\omega)$.

We assume here that $\delta = 0$, so that $r = d/u_o$. Again for small modulation, the following expansion is permissible, at least for a first approximation:

$$t_2 = t_o + \frac{S_1}{u_o}\left(1 - \frac{e V_1}{m d u_o}\int_{t_o}^{t_o+r} e^{-at^2}\cos\omega t\ dt\right)$$

$$\frac{dt_2}{dt_o} = 1 + \frac{S_1}{u_o^2}\frac{e V_1}{md}\left[-e^{-a(t_o+r)^2}\cos\omega(t_o+r) + e^{-at_o^2}\cos\omega t_o\right] .$$

$$\frac{S_1}{u_o^2}\frac{e V_1}{md} = \frac{k'}{\phi_o} ,$$

where $\phi_o = \omega d/u_o$, and $k' = S_1 a_1/2$, hence,

$$\frac{dt_2}{dt_o} = 1 - \frac{k'}{\phi_o}\left[e^{-\frac{a}{\omega^2}(\theta_o+\phi_o)^2}\cos(\theta_o+\phi_o) - e^{-\frac{a}{\omega^2}\theta_o^2}\cos\theta_o\right] ;$$

thus

$$i_2 = \frac{I_o}{\frac{dt_2}{dt_o}} = \frac{I_o}{1 - \frac{k'}{\phi_o}\left[e^{-\frac{a}{\omega^2}(\theta_o+\phi_o)^2}\cos(\theta_o+\phi_o - e^{-\frac{a}{\omega^2}\theta_o^2}\cos\theta_o\right]} .$$

The above expression for i_2, though approximate, does give an idea of the catcher response at least for small signals.*

* The expression for i_2 becomes a poor approximation for large gap angles also. The graph of i_2 versus θ_o with $\phi_o = \pi/2$ has been plotted (Figure 10), taking $k = 0.5$, and 1.0; and the difference between this and the first-order bunching theory is obvious. It has been found convenient to plot i_2 versus θ_o, in this case, rather than i_2 versus θ_2, as we are only interested in an approximate estimate of the response curve.

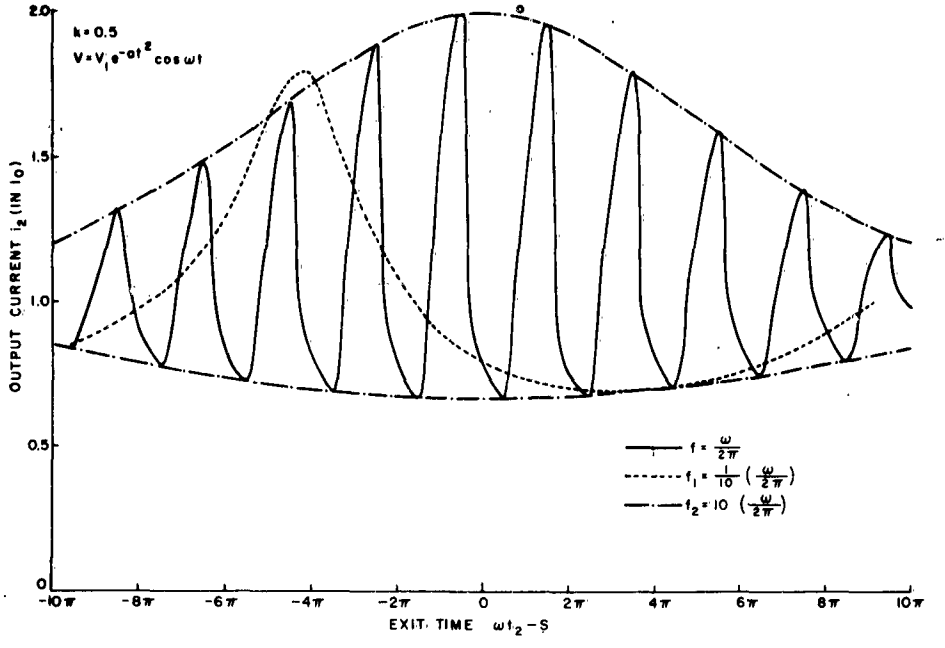

Figure 9. Output Current i_2 versus Exit Time $\omega t_2 - S$.

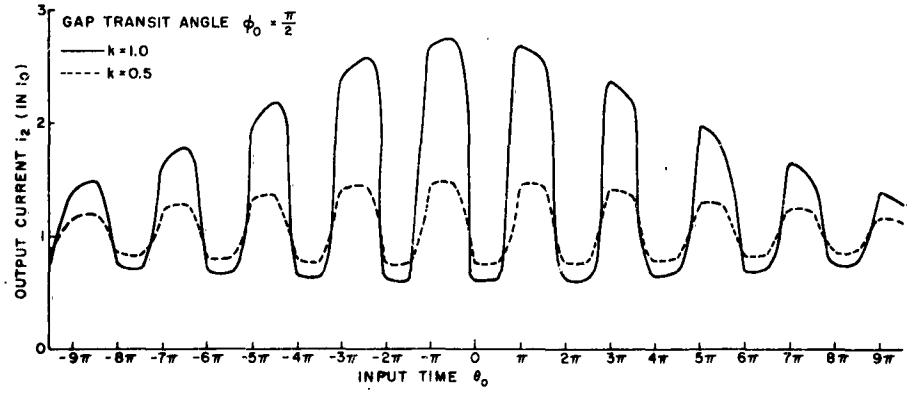

Figure 10. Output Current i_2 versus θ_0.

C. RESPONSE WITH FIXED ENVELOPE AND VARYING FREQUENCY

Using the first-order bunching theory, and taking $k = 0.5$, we have plotted the catcher current response for a fixed envelope for three different r-f frequencies (Figure 9). It has been found that the shape of the response envelope is almost independent of the change in frequency, especially at high values of $\omega/\sqrt{a}$.

IV. LARGE SIGNALS AND FINITE GAPS

The ballistic analysis for large signals with finite gaps is carried out as follows. Analysis is based on a two-cavity klystron (Figure 11).

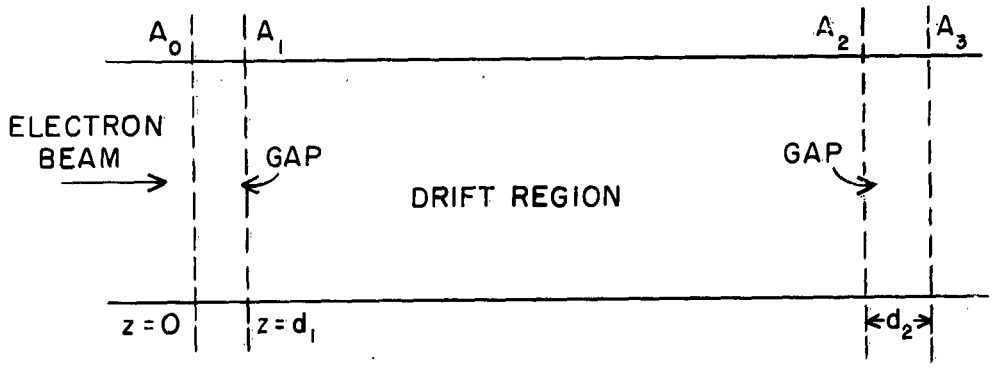

Figure 11. Schematic of Model for Velocity-modulated Tube.

In the diagram, A_0, A_1, A_2, A_3 represent the four planes under consideration. The numbers 0, 1, 2, 3 will be used to identify quantities in the respective planes.

A. FIRST GAP REGION

1. Induced R-F Current

Confining our attention first to the motion of an electron in the first gap, excited by a Gaussian pulse $V_1 e^{-at^2} \cos\omega t$, and applying Newton's second law of motion, we get

$$\frac{d^2z}{dt^2} = \frac{eV_1}{md} e^{-at^2} \cos\omega t \quad ;$$

therefore

$$\frac{dz}{dt} = K_1 \, \mathrm{Re} \int e^{-at^2 + j\omega t} \, dt + C_1$$

$$= K_1 \, e^{-\frac{\omega^2}{4a}} \, \mathrm{Re} \int e^{-a\left(t - \frac{j\omega}{2a}\right)^2} \, dt + C_1 \quad ,$$

where $K_1 = eV_1/md_1$ and C_1 is a constant. Now at $t = t_o$, $dz/dt = u_o$, from which C_1 is evaluated; thus

$$\frac{dz}{dt} = K_1 \, e^{-\frac{\omega^2}{4a}} \, \mathrm{Re} \int_{t_o}^{t} e^{-a\left(t - \frac{j\omega}{2a}\right)^2} \, dt + u_o$$

$$= u_o + \frac{K_1 \, e^{-\omega^2/4a}\sqrt{\pi}}{\sqrt{a}\ 2} \, \mathrm{Re}\left[\mathrm{erf}\sqrt{a}\left(t - \frac{j\omega}{2a}\right) - \mathrm{erf}\sqrt{a}\left(t_o - \frac{j\omega}{2a}\right)\right] \quad . \tag{4.1a}$$

$$\frac{dz}{dt} = u_o + \frac{K_1 e^{-\omega^2/4a}\sqrt{\pi}}{2\sqrt{a}} \left\{ \mathrm{erf}\sqrt{a}\, t - \mathrm{erf}\sqrt{a}\, t_o + \frac{2}{\sqrt{\pi}} \int_0^{\frac{\omega}{2\sqrt{a}}} \left[e^{-(at^2 - y^2)} \sin\sqrt{a}\, ty \right. \right.$$

$$\left. \left. - e^{-(at_o^2 - y^2)} \sin\sqrt{a}\, ty \ dy \right] \right\} \quad . \tag{4.1b}$$

Integrating again, we get

$$z = u_o t + \frac{K_1}{2}\sqrt{\frac{\pi}{a}}\, e^{-\omega^2/4a} \left\{ \mathrm{erf}\sqrt{a}\, t - \mathrm{erf}\sqrt{a}\, t_o + \frac{2}{\sqrt{\pi}} \int_0^{\frac{\omega}{2\sqrt{a}}} \left[e^{-(at^2 - y^2)} \sin\sqrt{a}\, ty \right. \right.$$

$$\left. \left. - e^{-(at_o^2 - y^2)} \sin\sqrt{a}\, t_o y \right] dy \right\} dt + C_2 \quad ,$$

where C_2 = constant. This constant is evaluated by using the condition that at $z = 0$, $t = t_o$; therefore

$$z = u_o(t-t_o) + \frac{K_1}{2}\sqrt{\frac{\pi}{a}}\, e^{-\omega^2/4a}\left[\int_{t_o}^{t} \operatorname{erf}\sqrt{a}\, t\, dt + \frac{2}{\sqrt{\pi}}\int_{t_o}^{t}\int_{o}^{\frac{\omega}{2\sqrt{a}}} e^{-(at^2 - y^2)}\sin\sqrt{a}\, ty\, dy\, dt\right]$$

$$- \frac{K_1}{2}\sqrt{\frac{\pi}{a}}\, e^{-\omega^2/4a}\left[(t-t_o)\left\{\operatorname{erf}\sqrt{a}\, t + \frac{2}{\sqrt{\pi}}\int_{o}^{\frac{\omega}{2\sqrt{a}}} e^{-(at_o^2 - y^2)}\sin\sqrt{a}\, t_o y\, dy\right\}\right] . \qquad (4.2)$$

When $t = t_1$, $z = d_1$. Also the transit time is $\Gamma_1 = t_1 - t_o$; therefore

$$d_1 = u_o\Gamma_1 + \frac{K_1}{2}\sqrt{\frac{\pi}{a}}\, e^{-\omega^2/4a}\left[\int_{t_o}^{t_1} \operatorname{erf}\sqrt{a}\, t\, dt + \frac{2}{\sqrt{\pi}}\int_{t_o}^{t_1}\int_{o}^{\frac{\omega}{2\sqrt{a}}} e^{-(at^2 - y^2)}\sin\sqrt{a}\, ty\, dy\, dt\right]$$

$$- \frac{K_1}{2}\sqrt{\frac{\pi}{a}}\, e^{-\omega^2/4a}\,\Gamma_1\left[\operatorname{erf}\sqrt{a}\, t_o + \frac{2}{\sqrt{\pi}}\int_{o}^{\frac{\omega}{2\sqrt{a}}} e^{-(at_o^2 - y^2)}\sin\sqrt{a}\, t_o y\, dy\, dt\right] . \qquad (4.3)$$

Suppose $\Gamma_1 = \frac{d_1}{u_o} + \frac{\delta_1}{\omega}$, where δ_1 is the correction factor; then $\omega d_1/u_o = \phi_1$ is the d-c transit angle. From Equation (4.3),

$$\phi_1 = \phi_1 + \delta_1 + \frac{K_1\omega}{2u_o}\sqrt{\frac{\pi}{a}}\, e^{-\omega^2/4a}\left[\int_{t_o}^{t_1} \operatorname{erf}\sqrt{a}\, t\, dt + \frac{2}{\sqrt{\pi}}\int_{t_o}^{t_1}\int_{o}^{\frac{\omega}{2\sqrt{a}}} e^{-(at^2 - y^2)}\sin\sqrt{a}\, ty\, dy\, dt\right]$$

$$- \frac{K_1\sqrt{\pi}}{2\sqrt{a}} \frac{e^{-\omega^2/4a}}{u_o} (\phi_1 + \delta_1) \left[\operatorname{erf}\sqrt{a}\, t_o + \frac{2}{\sqrt{\pi}} \int_o^{\frac{\omega}{2\sqrt{a}}} e^{-(at_o^2 - y^2)} \sin\sqrt{a}\, t_o y \, dy \right] .$$

Writing t_1 as t and replacing t_o by $t_1 - \Gamma_1 = t_1 - \frac{d_1}{u_o} - \frac{\delta_1}{\omega}$, we get

$$\delta_1 = \left(\frac{K_1\omega}{2u_o} \sqrt{\frac{\pi}{a}}\, e^{-\omega^2/4a} \left[\int_{t - \frac{d_1}{u_o} - \frac{\delta_1}{\omega}}^{t} \operatorname{erf}\sqrt{a}\, t \, dt + \frac{2}{\sqrt{\pi}} \int_{t - \frac{d_1}{u_o} - \frac{\delta_1}{\omega}}^{t} \int_o^{\frac{\omega}{2\sqrt{a}}} e^{-(at^2 - y^2)} \sin\sqrt{a}\, t y \, dy \right] \right.$$

$$- \frac{K_1}{2} \sqrt{\frac{\pi}{a}}\, e^{-\omega^2/4a} \frac{\phi_1}{u_o} \left\{ \operatorname{erf}\sqrt{a} \left(t - \frac{d_1}{u_o} - \frac{\delta_1}{\omega} \right) \right.$$

$$\left. \left. + \frac{2}{\sqrt{\pi}} \int_o^{\frac{\omega}{2\sqrt{a}}} e^{-\left[a\left(t_1 - \frac{d_1}{u_o} - \frac{\delta_1}{\omega} \right)^2 - y^2 \right]} \sin\sqrt{a} \left(t_1 - \frac{d_1}{u_o} - \frac{\delta_1}{\omega} \right) dy \right\} \right) .$$

$$\left(1 - \frac{K_1 e^{-\omega^2/4a}}{2u_o} \sqrt{\frac{\pi}{a}} \left\{ \operatorname{erf}\sqrt{a} \left(t - \frac{d_1}{u_o} - \frac{\delta_1}{\omega} \right) \right. \right.$$

$$\left. \left. + \frac{2}{\sqrt{\pi}} \int_o^{\frac{\omega}{2\sqrt{a}}} e^{-\left[a\left(t - \frac{d_1}{u_o} - \frac{\delta_1}{\omega} \right)^2 - y^2 \right]} \sin\sqrt{a} \left(t - \frac{d_1}{\omega} - \frac{\delta_1}{\omega} \right) dy \right\} \right)^{-1} . \quad (4.4)$$

In Equation (4.4), δ_1 is implicit, and approximation must be made to obtain an explicit expression for it.

We shall assume that δ_1 is small so that

$$\text{Re erf}\left[\sqrt{a}\left(t - \frac{d_1}{u_o} - \frac{\delta_1}{\omega}\right) - \frac{j\omega}{2\sqrt{a}}\right] = \text{Re}\left\{\left[\sqrt{a}\left(t - \frac{d_1}{u_o}\right) - \frac{j\omega}{2\sqrt{a}}\right] - \frac{\sqrt{a}\,\delta_1}{\omega}\,\text{erf}^1\left[\sqrt{a}\left(t - \frac{d_1}{u_o}\right) - \frac{j\omega}{2\sqrt{a}}\right]\right\},$$

where

$$\text{erf}^1\left[\sqrt{a}\left(t - \frac{d_1}{u_o}\right) - \frac{j\omega}{2\sqrt{a}}\right] = e^{-\left[\sqrt{a}\left(t - \frac{d_1}{u_o}\right) - \frac{j\omega}{2\sqrt{a}}\right]^2}.$$

Now as Γ_1 is small compared to t, the following approximation is justified:

$$\int_{t - \frac{d_1}{u_o} - \frac{\delta_1}{\omega}}^{t} \text{erf}\sqrt{a}\,t\,dt = \left(\frac{d_1}{u_o} + \frac{\delta_1}{\omega}\right)\text{erf}\sqrt{a}\,t$$

$$\int_{t - \frac{d_1}{u_o} - \frac{\delta_1}{\omega}}^{t}\int_{o}^{\frac{\omega}{2\sqrt{a}}} e^{-(at^2 - y^2)}\sin\sqrt{a}ty\,dy\,dt = \left(\frac{d_1}{u_o} + \frac{\delta_1}{\omega}\right)\int_{o}^{\frac{\omega}{2\sqrt{a}}} e^{-(at^2 - y^2)}\sin\sqrt{a}ty\,dy.$$

Substituting these in Equation (4.4), we have

$$\delta_1 = -\left(\frac{K_1\omega}{2u_o}\sqrt{\pi/a}\,e^{-\frac{\omega^2}{4a}}\left(\frac{d_1}{u_o} + \frac{\delta_1}{\omega}\right)\text{Re}\left[\text{erf}\left(\sqrt{a}\,t - \frac{j\omega}{2\sqrt{a}}\right)\right] -$$

$$-\frac{K_1}{2}\sqrt{\frac{\pi}{a}}\, e^{-\frac{\omega^2}{4a}}\, \frac{\phi_1}{u_o}\, \mathrm{Re}\left\{\mathrm{erf}\left[\sqrt{a}\left(t-\frac{d_1}{u_o}\right)-\frac{j\omega}{2\sqrt{a}}\right]-\sqrt{a}\,\frac{\delta_1}{\omega}\left[\mathrm{erf}^1\sqrt{a}\left(t-\frac{d_1}{u_o}\right)-\frac{j\omega}{2\sqrt{a}}\right]\right\}$$

$$\left(1-\frac{K}{2}\sqrt{\frac{\pi}{a}}\,\frac{e^{-\frac{\omega^2}{4a}}}{u_o}\,\mathrm{Re}\left\{\mathrm{erf}\left[\sqrt{a}\left(t-\frac{d_1}{u_o}\right)-\frac{j\omega}{2\sqrt{a}}\right]-\sqrt{a}\,\frac{\delta_1}{\omega}\,\mathrm{erf}^1\left[\sqrt{a}\left(t-\frac{d_1}{u_o}\right)-\frac{j\omega}{2\sqrt{a}}\right]\right\}\right)^{-1}.$$

This equation obviously gives a quadratic in δ_1, which might be complicated to solve. For a simpler solution, we will neglect the δ_1^2 term; therefore

$$\delta_1 = -\left[\frac{K_1}{2}\sqrt{\frac{\pi}{a}}\, e^{-\frac{\omega^2}{4a}}\, \frac{\phi_1}{u_o}\left(\mathrm{Re}\left\{\mathrm{erf}\left(\sqrt{a}\,t-\frac{j\omega}{2\sqrt{a}}\right)-\mathrm{erf}\left[\sqrt{a}\left(t-\frac{d_1}{u_o}\right)-\frac{j\omega}{2\sqrt{a}}\right]\right\}\right)\right]$$

$$\left[1+\frac{K_1}{2}\sqrt{\frac{\pi}{a}}\,\frac{e^{-\frac{\omega^2}{4a}}}{u_o}\left(\mathrm{Re}\left\{\mathrm{erf}\left(\sqrt{a}\,t-\frac{j\omega}{2\sqrt{a}}\right)\right.\right.\right.$$

$$\left.\left.\left.-\mathrm{erf}\left[\sqrt{a}\left(t-\frac{d_1}{u_o}\right)-\frac{j\omega}{2\sqrt{a}}\right]+\left[\frac{d_1\sqrt{a}}{u_o}\,\mathrm{erf}^1\sqrt{a}\left(t-\frac{d_1}{u_o}\right)-\frac{j\omega}{2\sqrt{a}}\right]\right\}\right)\right]^{-1}. \tag{4.5}$$

Thus Equation (4.5) gives an explicit expression for δ_1. Denoting

$$F(t) = \frac{K_1}{2}\sqrt{\frac{\pi}{a}}\, e^{-\frac{\omega^2}{4a}}\, \frac{\phi_1}{u_o}\left(\mathrm{Re}\left\{\mathrm{erf}\left(\sqrt{a}\,t-\frac{j\omega}{2\sqrt{a}}\right)-\mathrm{erf}\left[\sqrt{a}\left(t-\frac{d_1}{u_o}\right)-\frac{j\omega}{2\sqrt{a}}\right]\right\}\right),$$

$$G(t) = \frac{K_1}{2}\sqrt{\frac{\pi}{a}}\, e^{-\frac{\omega^2}{4a}}\, \frac{d_1\sqrt{a}}{u_o^2}\,\mathrm{Re}\,\mathrm{erf}^1\left[\sqrt{a}\left(t-\frac{d_1}{u_o}\right)-\frac{j\omega}{2\sqrt{a}}\right],$$

gives

$$\delta_1 = -\frac{F(t)}{1+\frac{1}{\phi_1}F(t)+G(t)}. \tag{4.6}$$

According to Ramo's theorem, the current at time t resulting from the charge entering the gap in the interval dt_o between time t_o and $t_o + dt_o$ is

$$di_1 = \frac{I_o}{d_1} \, u \, dt_o \quad ,$$

where u = velocity at time t. The total current induced is

$$i_1 = I_o/d_1 \int_{t-\Gamma_1}^{t} u \, dt_o \quad .$$

Substituting Equation (4. 1b) in the preceding integral, we have

$$i_1 = \frac{I_o}{d_1} \int_{t-\Gamma_1}^{t} \left(u_o + \frac{K_1}{2} \sqrt{\frac{\pi}{a}} \, e^{-\frac{\omega^2}{4a}} \left[\operatorname{erf}\sqrt{a}\, t - \operatorname{erf}\sqrt{a}\, t_o + \frac{2}{\sqrt{\pi}} \int_0^{\frac{\omega}{2\sqrt{a}}} e^{-(at^2 - y^2)} \sin \sqrt{a}\, ty \right. \right.$$

$$\left. \left. - e^{-(at_o^2 - y^2)} \sin \sqrt{a}\, t_o y \, dy \right] \right)$$

$$= \frac{I_o}{d_1} \left\{ u_o \Gamma + \frac{K_1}{2} \sqrt{\frac{\pi}{a}} \, e^{-\frac{\omega^2}{4a}} \, \Gamma \left[\operatorname{erf}\sqrt{a}\, t + \frac{2}{\sqrt{\pi}} \int_0^{\frac{\omega}{2\sqrt{a}}} e^{-(at^2 - y^2)} \sin \sqrt{a}\, ty \quad dy \right] \right.$$

$$\left. - \frac{K_1}{2} \sqrt{\frac{\pi}{a}} \, e^{-\frac{\omega^2}{4a}} \left[\int_{t-\Gamma_1}^{t} \operatorname{erf}\sqrt{a}\, t_o \, dt_o + \frac{2}{\sqrt{\pi}} \int_{t-\Gamma_1}^{t} \int e^{-(at_o^2 - y^2)} \sin \sqrt{a}\, t_o y \quad dy \, dt_o \right] \right\} ;$$

therefore

$$i_1 = I_o + \frac{I_o}{d_1} \left\{ u_o \frac{\delta_1}{\omega} + \frac{K_1 \sqrt{\pi}}{2\sqrt{a}} \left(\frac{d_1}{u_o} + \frac{\delta_1}{\omega} \right) e^{-\frac{\omega^2}{4a}} \left[\operatorname{erf}\sqrt{a}\, t + \frac{2}{\sqrt{\pi}} \int_0^{\frac{\omega}{2\sqrt{a}}} e^{-(at^2 - y^2)} \sin \sqrt{a}\, ty \, dy \right] \right.$$

$$- \frac{K_1}{2} \sqrt{\frac{\pi}{a}}\, e^{-\frac{\omega^2}{4a}} \left[\int_{t-\Gamma_1}^{t} \operatorname{erf}\sqrt{a}\, t_o\, dt + \frac{2}{\sqrt{\pi}} \int_{t-\Gamma_1}^{t} \int e^{-(at_o^2 - y^2)} \sin\sqrt{a}\, t_o y\, dy\, dt_o \right] \Bigg\} \quad . \tag{4.7}$$

The above expression is considerably simplified if the following approximations are accepted as valid:

$$\int_{t-\Gamma_1}^{t} \operatorname{erf}\sqrt{a}\, t_o\, dt_o = \Gamma_1 \operatorname{erf}\sqrt{a}\, t \quad ,$$

$$\frac{2}{\sqrt{\pi}} \int_{t-\Gamma_1}^{t} \int_{0}^{\frac{\omega}{2\sqrt{a}}} e^{-(at_o^2 - y^2)} \sin\sqrt{a}\, t_o y\, dy dt_o = \frac{2}{\sqrt{\pi}}\, \Gamma_1 \int_{0}^{\frac{\omega}{2\sqrt{a}}} e^{-(at^2 - y^2)} \sin\sqrt{a}\, ty\, dy \quad .$$

This is very nearly true, especially for small gaps; then, Equation (4.7) reduces to

$$\begin{aligned} i_1 &= I_o \left(1 + \frac{\delta_1}{\phi_1} \right) \\ &= I_o \left\{ 1 + \frac{\left[-F(t) \right]}{1 + \frac{F(t)}{\phi_1} + G(t)} \quad \frac{1}{\phi_1} \right\} \quad . \end{aligned} \tag{4.8}$$

It is interesting to note in this case that the time-dependent component of current i_1 is directly proportional to the correction factor δ_1.

A more accurate simplification of Equation (4.7) than that given by Equation (4.8) is obtained if

$$\int_{t-\Gamma_1}^{t} \operatorname{erf}\sqrt{a}\, t_o\, dt = \Gamma_1 \operatorname{erf}\sqrt{a} \left(t - \frac{\Gamma_1}{2} \right)$$

$$\simeq \Gamma_1 \operatorname{erf}\sqrt{a}\left(t - \frac{d_1}{2u_o} - \frac{\delta_1}{2\omega}\right) \quad .$$

Putting this in Equation (4.7), we have

$$i_1 = I_o + \frac{I_o}{d_1}\left[\frac{u_o\delta_1}{\omega} + \frac{K_1}{2}\sqrt{\frac{\pi}{a}}\, e^{-\frac{\omega^2}{4a}}\left(\frac{d_1}{u_o} + \frac{\delta_1}{\omega}\right)\left(\mathrm{Re}\left\{\operatorname{erf}\left(\sqrt{a}\,t - \frac{j\omega}{2\sqrt{a}}\right) - \operatorname{erf}\left[\sqrt{a}\left(t - \frac{d_1}{2u_o} - \frac{\delta_1}{2\omega}\right) - \frac{j\omega}{2\sqrt{a}}\right]\right\}\right)\right] .$$

After expansion in a Taylor series, we get

$$i_1 = I_o + \frac{I_o}{d_1}\left[\frac{u_o\delta_1}{\omega} + \mathrm{Re}\,\frac{K_1}{2}\,\frac{\sqrt{\pi}}{\sqrt{\pi}}\, e^{-\frac{\omega^2}{4a}}\left(\frac{d_1}{u_o} + \frac{\delta_1}{\omega_1}\right)^2 e^{-\left(\sqrt{a}\,t - \frac{j\omega}{2\sqrt{a}}\right)^2}\right]$$

$$= I_o + \frac{I_o}{d_1}\left[u_o\frac{\delta_1}{\omega} + \frac{K_1}{2}\,\frac{\sqrt{\pi}}{\sqrt{\pi}}\left(\frac{d_1}{u_o} + \frac{\delta_1}{\omega}\right)^2 e^{-at^2}\cos\omega t\right] \quad .$$

If the δ_1^2 term is neglected,

$$i_1 = I_o + \frac{I_o}{d_1}\left(\frac{\delta_1}{\omega}u_o + \frac{V_1}{2V_o}\,\frac{u_o}{\omega}\,\delta_1 e^{-at^2}\cos\omega t + \frac{V_1}{4V_o}\,d_1\, e^{-at^2}\cos\omega t\right) , \tag{4.9}$$

where V_o = d-c beam voltage = $\frac{m}{2e}u_o^2$.

2. Velocity Modulation

From Equation (4.1a), we have

$$v_1 = u_o + \frac{K_1}{2}\sqrt{\frac{\pi}{a}}\, e^{-\frac{\omega^2}{4a}}\,\mathrm{Re}\left[\operatorname{erf}\sqrt{a}\left(t_1 - \frac{j\omega}{2a}\right) - \operatorname{erf}\sqrt{a}\left(t_o - \frac{j\omega}{2a}\right)\right] \quad .$$

Making suitable approximations to simplify solution gives

$$\frac{2}{\sqrt{\pi}} \int_{\sqrt{a}\, t_o - \frac{j\omega}{2\sqrt{a}}}^{\sqrt{a}\, t_1 - \frac{j\omega}{2\sqrt{a}}} e^{-t^2}\, dt = \frac{2\sqrt{a}}{\sqrt{\pi}} \left(\frac{d_1}{u_o} + \frac{\delta_1}{\omega} \right) e^{-\left(\sqrt{a}\, t_1 - \frac{j\omega}{2\sqrt{a}} \right)^2} \quad ;$$

from which

$$\frac{v_1}{u_o} = 1 + \frac{K_1}{2} \frac{\sqrt{\pi}}{u_o} \left(\frac{d_1}{u_o} + \frac{\delta_1}{\omega} \right) e^{-at_1^2} \cos \omega t_1 \quad . \tag{4.10}$$

This is justified if the gaps are very short and the transit time small. For larger gaps, a better approximation would be

$$\int_{\sqrt{a}\, t_o - \frac{j\omega}{2\sqrt{a}}}^{\sqrt{a}\, t_1 - \frac{j\omega}{2\sqrt{a}}} e^{-t^2}\, dt = \sqrt{a} \left(\frac{d_1}{u_o} + \frac{\delta_1}{\omega} \right) e^{-\left[\sqrt{a} \left(t_1 - \frac{d}{2u_o} \right) - \frac{j\omega}{2\sqrt{a}} \right]} \quad ;$$

then

$$\frac{v_1}{u_o} = 1 + \frac{K_1}{2u_o} \left(\frac{d_1}{u_o} + \frac{\delta_1}{\omega} \right) \sqrt{\pi}\, e^{-a\left(t_1 - \frac{d}{2u_o} \right)^2} \cos \left(\omega t_1 - \frac{\phi_1}{2} \right) \quad . \tag{4.11}$$

The neglect of δ_1 in the exponential is reasonable when the resulting simplification in computation is taken into consideration. Note that when $\delta_1 = 0$, Equation (4.10) reduces to

$$\frac{v_1}{u_o} = 1 + \frac{V_1}{2V_o} e^{-at_1^2} \cos \omega t_1 \quad ,$$

an expression similar to the velocity modulation in the sinusoidal excitation case.

B. DRIFT SPACE REGION

The electron beam enters the drift space with both velocity and current modulation, as shown above, and it drifts in a field-free space resulting in further increase in the harmonic content of the beam current.

Neglecting space-charge debunching, we have $t_2 = t_1 + (S_1/v_1)$, where S_1 is the drift length; therefore

$$t_2 = t_1 + \frac{S_1}{u_o \left\{ 1 + \frac{K_1}{2} e^{-\frac{\omega^2}{4a}} \sqrt{\frac{\pi}{a}} \left[\operatorname{erf}\left(\sqrt{a}\, t_1 - \frac{j\omega}{2\sqrt{a}} \right) - \operatorname{erf}\left(\sqrt{a}\, t_o - \frac{j\omega}{2\sqrt{a}} \right) \right] \right\}} \quad .$$

Using the simplified expression in Equation (4.10) gives

$$t_2 = t_1 + \frac{S_1}{u_o \left[1 + \frac{K_1}{2u_o} \left(\frac{d_1}{u_o} + \frac{\delta_1}{\omega} \right) \sqrt{\pi}\, e^{-at_1^2} \cos \omega t_1 \right]} \quad . \qquad (4.12)$$

Using Equation (4.11) results in a slight modification:

$$t_2 = t_1 + \frac{S_1}{u_o \left[1 + \frac{\sqrt{\pi}}{2} \frac{K_1}{u_o} \left(\frac{d_1}{u_o} + \frac{\delta_1}{\omega} \right) e^{-a\left(t_1 - \frac{d_1}{u_o} \right)^2} \cos \left(\omega t_1 - \frac{\phi_1}{2} \right) \right]} \quad . \qquad (4.13)$$

This expression for small modulation becomes

$$t_2 = t_1 + \frac{S_1}{u_o}\left[1 - \frac{K_1}{u_o}\left(\frac{d_1}{u_o} + \frac{\delta_1}{\omega}\right) e^{-a\left(t_1 - \frac{d_1}{u_o}\right)^2} \cos\left(\omega t_1 - \frac{\phi_1}{2}\right)\right] .$$

It is difficult to differentiate this function because of the presence of δ_1. It is better to keep the integral in the expression for dz/dt rather than divided into error functions; thus

$$t_2 = t_1 + \frac{S_1}{u_o\left[1 + \frac{K_1}{u_o} e^{-\frac{\omega^2}{4a}} \mathrm{Re} \int_{t_o}^{t_1} e^{-a\left(t - \frac{j\omega}{2a}\right)^2} dt\right]}$$

$$\simeq t_1 + \frac{S_1}{u_o}\left[1 - \frac{K_1}{u_o} e^{-\frac{\omega^2}{4a}} \mathrm{Re} \int_{t_o}^{t_1} e^{-a\left(t - \frac{j\omega}{2a}\right)^2} dt\right] ,$$

$$\frac{dt_2}{dt_1} = 1 - \frac{S_1 K_1}{u_o^2} \mathrm{Re}\left\{e^{-a\left(t_1 - \frac{j\omega}{2a}\right)^2} - e^{-\left[\sqrt{a}\,(t_1 - \Gamma_1) - \frac{j\omega}{2\sqrt{a}}\right]^2}\right\} e^{-\frac{\omega^2}{4a}}$$

$$\simeq 1 - \frac{S_1}{u_o^2} K_1\left[e^{-at_1^2} \cos \omega t_1 - e^{-a\left(t_1 - \frac{d_1}{u_o}\right)^2} \cos(\omega t_1 - \phi_1)\right] ,$$

assuming that

$$e^{-a\left(t_1 - \frac{d_1}{u_o} - \frac{\delta_1}{\omega}\right)^2} \cos(\omega t_1 - \phi_1 - \delta_1) = e^{-a\left(t_1 - \frac{d_1}{u_o}\right)^2} \cos(\omega t_1 - \phi_1) , \qquad (4.14)$$

therefore

$$i_2 = \frac{i_1}{\frac{dt_2}{dt_1}} = \frac{i_1}{1 - \frac{S_1}{2d}\frac{V_1}{V_o}\left[e^{-at_1^2}\cos \omega t_1 - e^{-a\left(t_1 - \frac{d_1}{u_o}\right)^2}\cos\left(\omega t_1 - \phi_1\right)\right]} \quad .$$

But by Equation (4. 7), i_1 is related to I_o; therefore theoretically, it is possible to express

$$i_2 = I_o \; f(t_1) \quad , \tag{4. 15}$$

where $f(t_1)$ denotes a function in t_1. Again as t_2 is related to t_1, as shown above, it is possible to express i_2 as a function of t_2, i.e.,

$$i_2 = I_o \; g(t_2) \quad . \tag{4. 16}$$

Although Equation (4. 16) is expected to be very complicated, and rigid mathematical analysis seems highly improbable in practice, a theoretical formulation is not ruled out. It is desirable to expand i_2 in a series in such a way that the various frequency components become distinguishable, but the obvious aperiodicity of i_2 rules out the possibility of expanding in a Fourier series, as in the sinusoidal case analyzed by Beck.

C. SECOND GAP REGION

At this stage, attention will be directed to the motion of electrons in the second gap. The beam induces a voltage on the grids, and because the voltage produces a change in beam current and velocity, we can consider this behavior as a reciprocal relationship, so that knowing the effect of the

voltage on the beam is equivalent to knowing the effect of the changing beam upon the induced voltage. With this in mind, let us assume the voltage induced in the second gap to have a spectrum given by the equation $V_2 e^{-b(t+\rho)^2} \cos \omega(t+\rho)$, where ρ is a constant introduced to take into account the possible change of phase with respect to the original envelope $V_1 e^{-at^2} \cos \omega t$. Although this assumption might differ from the actual physical conditions, it is acceptable as a first approximation. The equation of motion in the gap can therefore be written as

$$\frac{d^2 z}{dt^2} = K_2 \, e^{-b(t+\rho)^2} \cos \omega(t+\rho) \quad ;$$

therefore

$$\frac{dz}{dt} = K_2 \int e^{-b(t+\rho)^2} \cos \omega(t+\rho) \, dt + C_3 \quad ,$$

where C_3 = constant. Now at $t = t_2$,

$$\frac{dz}{dt} = u_o + \frac{K_1}{2} \sqrt{\frac{\pi}{a}} \, e^{-\frac{\omega^2}{4a}} \, \mathrm{Re} \left[\mathrm{erf} \left(\sqrt{a} \, t_1 - \frac{j\omega}{2\sqrt{a}} \right) - \mathrm{erf} \left(\sqrt{a} \, t_o - \frac{j\omega}{2\sqrt{a}} \right) \right] \quad .$$

Using this condition to calculate C_3, we have

$$\frac{dz}{dt} = K_2 \int_{t_2}^{t} e^{-b(t+\rho)^2} \cos \omega(t+\rho) \, dt + V_2 \quad , \qquad (4.17)$$

where

$$V_2 = u_o + \frac{K_1}{2} \sqrt{\frac{\pi}{a}} \, e^{-\frac{\omega^2}{4a}} \, \mathrm{Re} \left[\mathrm{erf} \left(\sqrt{a} \, t_1 - \frac{j\omega}{2a} \right) - \mathrm{erf} \left(\sqrt{a} \, t_o - \frac{j\omega}{2\sqrt{a}} \right) \right] \quad .$$

Integrating again, we have

$$z = K_2 \int_{t_2}^{t} e^{-b(t+\rho)^2} \cos\ \omega(t+\rho)\ dt + V_2 t + C_4 \quad , \tag{4.18}$$

where C_4 = constant. At $t = t_2$, $z = d_1 + S_1$; therefore

$$z = K_2 \int_{t_2}^{t} \int_{t_2}^{t} e^{-b(t+\rho)^2} \cos\ \omega(t+\rho)\ dt\ dt + V_2(t - t_2) + d_1 + S_1 \quad .$$

Now at $z = d_2 + S_1 + d_1$, we have $t = t_3$. Also $t_3 - t_2 = \Gamma_2$ is the transit time in the second gap; therefore

$$d_2 = K_2 \int_{t-\Gamma_2}^{t_3} \frac{e^{-\frac{\omega^2}{4b}}}{2} \sqrt{\frac{\pi}{b}}\ \mathrm{Re}\left\{\mathrm{erf}\left[\sqrt{b}\,(t+\rho) - \frac{j\omega}{2\sqrt{b}}\right] - \mathrm{erf}\left[\sqrt{b}\,(t_2+\rho) - \frac{j\omega}{2\sqrt{b}}\right]\right\} dt + V_2\Gamma_2 \ .$$

Suppose

$$\Gamma_2 = \frac{d_2}{u_2} + \frac{\delta_2}{\omega} \quad , \quad \text{and} \quad \frac{\omega d_2}{V_2} = \phi_2 \quad ,$$

where δ_2 is a correction factor for second gap. Then, by a process similar to that used for the first gap, and with similar approximations, we have

$$\delta_2 = -\left[\frac{K_2 e^{-\frac{\omega^2}{4b}}}{2 V_2} \sqrt{\frac{\pi}{b}}\ \phi_2\ \mathrm{Re}\left\{\mathrm{erf}\left[\sqrt{b}\,(t+\rho) - \frac{j\omega}{2\sqrt{b}}\right] - \mathrm{erf}\sqrt{b}\,(t_2+\rho) - \frac{j\omega}{2\sqrt{b}}\right\}\right]$$

$$\left[1 + \frac{K_2}{2}\sqrt{\frac{\pi}{b}}\,\frac{e^{-\frac{\omega^2}{4b}}}{v_2}\left(\mathrm{Re}\left\{\mathrm{erf}\left[\sqrt{b}\,(t+\rho) - \frac{j\omega}{2\sqrt{b}}\right]\right.\right.\right.$$

$$\left.\left.\left. - \mathrm{erf}\left[\sqrt{b}\,(t_2+\rho) - \frac{j\omega}{2\sqrt{b}}\right] + \frac{d_2\sqrt{b}}{u_2}\,\mathrm{erf}^1\left[\sqrt{b}\,t_2+\rho) - \frac{j\omega}{2\sqrt{b}}\right]\right\}\right)\right]^{-1}$$

$$\delta_2 = -\frac{F_2(t)}{1 + \frac{F_2(t)}{\phi_2} + G_2(t)} \quad , \tag{4.19}$$

where

$$F_2(t) = \frac{K_2 e^{-\frac{\omega^2}{4b}}}{2v_2}\sqrt{\frac{\pi}{b}}\,\phi_2\,\mathrm{Re}\left\{\mathrm{erf}\left[\sqrt{b}\,(t+\rho) - \frac{j\omega}{2\sqrt{b}}\right] - \mathrm{erf}\left[\sqrt{b}\,(t_2+\rho) - \frac{j\omega}{2\sqrt{b}}\right]\right\}$$

$$G_2(t) = \frac{K_2}{2v_2}\sqrt{\frac{\pi}{b}}\,e^{-\frac{\omega^2}{4b}}\,\frac{d_2\sqrt{b}}{v_2}\,\mathrm{erf}^1\left[\sqrt{b}\,(t_2+\rho) - \frac{j\omega}{2\sqrt{b}}\right] \quad .$$

Thus, the expression for δ_2 is very similar to that for δ_1.

As before, the total current induced as a result of the passage of charge in the interval Γ_2 is

$$i_3 = \int_{t-\Gamma_2}^{t} \frac{i_2}{d_2}\,u_2\,dt_2 \quad ,$$

where u_2 is the velocity at any instant t in gap 2; therefore

$$i_3 = \frac{1}{d_2}\int_{t-\Gamma_2}^{t} u_2 dt_2 \left(\frac{i_1}{\frac{dt_2}{dt_1}}\right)$$

$$= \frac{I_o}{d_1 d_2} \int_{t-\Gamma_2}^{t} u_2 dt_2 \int_{t-\Gamma_1}^{t} \frac{u\, dt_o}{\frac{dt_2}{dt_1}} \quad ,$$

where u is, as usual, the velocity at any instant t in the first gap. As we have seen in the above analysis dt_2/dt_1 can be expressed as a function of t_1; therefore

$$i_3 = \frac{I_o}{d_1 d_2} \frac{dt_1}{dt_2} \int_{t-\Gamma_2}^{t} u_2 dt_2 \int_{t-\Gamma_1}^{t} u\, dt_o \quad .$$

This analysis can be extended to n gaps, and n-1 drift spaces; under these conditions

$$i_{2n-1} = \frac{I_o \left(\frac{dt_1}{dt_2} \cdot \frac{dt_3}{dt_4} \cdots \right)}{d_1 d_2 \cdots d_n} \int_{t-\Gamma_n}^{t} u_{2(n-1)}\, dt_{2(n-1)} \int_{t-\Gamma_{n-1}}^{t} u_{2(n-2)} dt_{2(n-2)} \int_{t-\Gamma_1}^{t} u\, dt_o \quad . \tag{4.20}$$

Expression (4.20) is of theoretical interest since it indicates the dependence of the final current in the output gap upon the excitation imposed upon all other gaps.

V. NONLINEAR SPACE-CHARGE WAVE ANALYSIS

Here also attention will be directed to the Gaussian excitation, since the behavior of an electron passing through alternate gaps and drift regions with sinusoidal excitation in the gap has already been determined. McIsaac[5] has derived a general expression for polarization in the drift region. Using his symbols for the input gap and the drift case, the polarization $Z_1(T_1, T_o)$ in the drift region is:

$$Z_1(T_1, T_o) = -\frac{1}{2D} \int_0^{\Gamma} \theta(\Gamma + T_o) \sin(T_1 - \Gamma)\, d\Gamma \quad .$$

For the Gaussian case, $\theta(T) = Ae^{-\gamma T^2} \cos \sigma T$,

$$Z_1(T_1, T_o) = -\frac{1}{2D} \int_0^{\Gamma} Ae^{-\gamma(r + T_o)^2} \cos \sigma(r + T_o) \sin(T_1 - r)\, dr \quad .$$

Replacing the sine and cosine terms by exponentials and defining

$$\operatorname{erf} x = \frac{2}{\sqrt{\pi}} \int_0^{x} e^{-t^2}\, dt \quad ,$$

we have

$$Z(T, T_o) = \frac{A}{16} \sqrt{\frac{\pi}{\gamma}} \left(je^{\frac{(\sigma-1)^2}{4\gamma}} e^{jT} \left\{ \operatorname{erf}\left[\sqrt{\gamma}(r+T_o) - j\frac{(\sigma-1)}{2\sqrt{\gamma}}\right] - \operatorname{erf}\left[\sqrt{\gamma}\, T_o - j\frac{(\sigma-1)}{2\sqrt{\gamma}}\right] \right\} \right.$$

$$-je^{\frac{(\sigma+1)^2}{4\gamma}} e^{-jT} \left\{ \operatorname{erf}\left[\sqrt{\gamma}(r+T_o) - j\frac{(\sigma+1)}{2\sqrt{\gamma}}\right] - \operatorname{erf}\left[\sqrt{\gamma}\, T_o - j\frac{(\sigma+1)}{2\sqrt{\gamma}}\right] \right\}$$

$$\left. + \text{complex conjugate} \right) \quad . \qquad (5.1)$$

For the input gap region,

$$Z_1(T_1 T_o) = -\frac{1}{2D}\int_0^{T_1} \theta(r + T_o)\sin(T_1 - r)\, dr \quad ;$$

therefore, for the case under consideration:

$$Z_1(T_1, T_o) = \frac{A}{16}\sqrt{\frac{\pi}{\gamma}}\left(je^{-\frac{(\sigma-1)^2}{4\gamma}} e^{jT}\left\{\operatorname{erf}\left[\sqrt{\gamma}\,T - j\frac{(\sigma-1)}{2\sqrt{\gamma}}\right] - \operatorname{erf}\left[\sqrt{\gamma}\,T_o - j\frac{(\sigma-1)}{2\sqrt{\gamma}}\right]\right\}\right.$$
$$-je^{-\frac{(\sigma+1)^2}{4\gamma}} e^{-jT}\left\{\operatorname{erf}\left[\sqrt{\gamma}\,T - \frac{(\sigma+1)}{2\sqrt{\gamma}}\right] - \operatorname{erf}\left[\sqrt{\gamma}\,T_o - j\frac{(\sigma+1)}{2\sqrt{\gamma}}\right]\right\}$$
$$\left. + \text{complex conjugate}\right) \quad . \qquad (5.2)$$

A method will be indicated to express the complex error function in terms of real integrals. Consider the expression,

$$\operatorname{erf}(a-jb) = \frac{2}{\sqrt{\pi}}\int_0^{a-jb} e^{-z^2}\, dz \quad ,$$

in the complex plane with $z = x + jy$. As e^{-z^2} is an analytic function, $\oint f(z) = 0$ around a closed path of integration. Hence integrating along the path shown by the arrows gives

$$\int_0^a e^{-x^2} dx - j\int_0^b e^{-(a-jy)^2} dy = \int_0^{a-jb} e^{-z^2} dz \quad ,$$

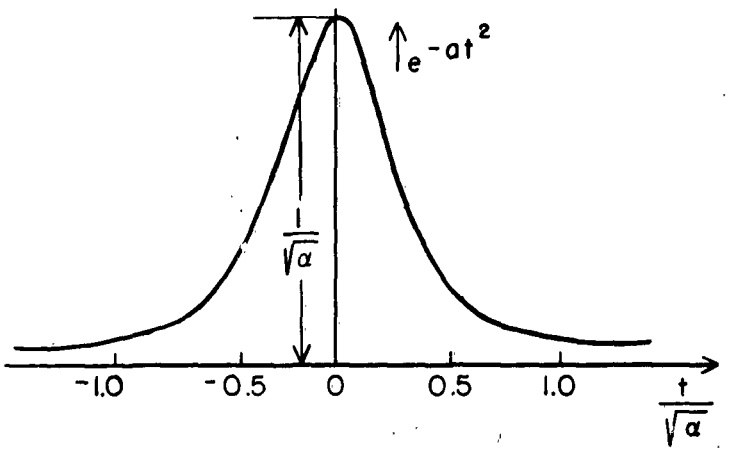

Figure 12. Gaussian Envelope.

from which

$$\operatorname{erf}(a-jb) = \frac{2}{\sqrt{\pi}}\int_0^{\infty} e^{-x^2}dx - \frac{2}{\sqrt{\pi}}j\int_0^{b} e^{-(a^2-y^2)+2jay}\,dy$$

$$= \operatorname{erf}(x) + \frac{2}{\sqrt{\pi}}\int_0^{b} e^{-(a^2-y^2)}\sin 2aydy - j\frac{2}{\sqrt{\pi}}\int_0^{b} e^{-(a^2-y^2)}\cos 2aydy \qquad (5.3)$$

As the polarization has to be a real quantity, and noting that $T_o = T - T_1 = T - Z_o = T - Z + Z_1$, we have Equation (5.3) written in the Z, T coordinate system as follows:

$$Z_1(Z,T) = 2\mathrm{Re}\,\frac{A}{16}\sqrt{\frac{\pi}{\gamma}}\left(je^{-\frac{(\sigma-1)^2}{4\gamma}}e^{jT}\left\{\operatorname{erf}\left[\sqrt{\gamma}(r+T-Z+Z_1) - j\frac{(\sigma-1)}{2\sqrt{\gamma}}\right]\right.\right.$$

$$\left.\left. - \operatorname{erf}\left[\sqrt{\gamma}(T-Z+Z_1) - j\frac{(\sigma-1)}{2\sqrt{\gamma}}\right]\right\}\right.$$

$$\left. - je^{-\frac{(\sigma+r)^2}{4\gamma}}e^{-jT}\left\{\operatorname{erf}\left[\sqrt{\gamma}(r+T-Z+Z_1) - j\frac{(\sigma+1)}{2\sqrt{\gamma}}\right]\right.\right.$$

$$-\operatorname{erf}\left[\sqrt{\gamma}\,(T-Z+Z_1) - j\,\frac{(\sigma+1)}{2\sqrt{\gamma}}\right]\Bigg\}\Bigg) \quad , \tag{5.4}$$

where Re represents the real part. Equation (5.4) is obviously implicit in Z_1 and hence cannot be evaluated easily.

Assuming Z_1 to be small, a series expansion of the complex functions will be made, and only the first-order term in Z_1 will be taken into account. A typical term is expanded as follows:

$$\operatorname{erf}\left[\sqrt{\gamma}\,(r+T-Z+Z_1) - j\,\frac{(\sigma-1)}{2\sqrt{\gamma}}\right]$$

$$= \operatorname{erf}\left[\sqrt{\gamma}\,(r+T-Z) - j\,\frac{(\sigma-1)}{2\sqrt{\gamma}}\right] + \sqrt{\gamma}\,Z_1 \operatorname{erf}^1\left[\sqrt{\gamma}\,(r+T-Z) - j\,\frac{(\sigma-1)}{2\sqrt{\gamma}}\right] \quad ,$$

where

$$\operatorname{erf}^1 = e^{-\left[\sqrt{\gamma}\,(r+T-Z) - j\,\frac{(\sigma-1)}{2\sqrt{\gamma}}\right]^2} \quad .$$

Substituting in Equation (5.4), we have

$$Z_1(Z,T) = \frac{A}{8}\sqrt{\frac{\pi}{\gamma}}\,\mathrm{Re}\Bigg[je^{-\frac{(\sigma-1)^2}{4\gamma}}e^{jT}\Bigg(\Bigg\{\operatorname{erf}\left[\sqrt{\gamma}(r+T-Z) - j\,\frac{(\sigma-1)}{2\sqrt{\gamma}}\right]$$

$$+ \sqrt{\gamma}\,Z_1\, e^{-\left[\sqrt{\gamma}\,(r+T-Z) - j\,\frac{(\sigma-1)}{2\sqrt{\gamma}}\right]^2}\Bigg\} - \Bigg\{\operatorname{erf}\left[\sqrt{\gamma}\,(T-Z) - j\,\frac{(\sigma-1)}{2\sqrt{\gamma}}\right]$$

$$+ \sqrt{\gamma}\,Z_1 e^{-\left[\sqrt{\gamma}\,(T-Z) - j\,\frac{(\sigma-1)}{2\sqrt{\gamma}}\right]^2}\Bigg\}\Bigg) - je^{-\frac{(\sigma+1)^2}{4\gamma}}e^{-jT}\Bigg(\Bigg\{\operatorname{erf}\left[\sqrt{\gamma}\,(r+T-Z)\right.$$

$$-j\frac{(\sigma+1)}{2\sqrt{\gamma}}\Big] + \sqrt{\gamma}\, Z_1 e^{-\left[\sqrt{\gamma}(r+T-Z)-j\frac{(\sigma+1)}{2\sqrt{\gamma}}\right]^2}\Bigg\} - \Bigg\{\operatorname{erf}\Big[\sqrt{\gamma}(T-Z)$$

$$-j\frac{(\sigma+1)}{2\sqrt{\gamma}}\Big] + \sqrt{\gamma}\, Z_1 e^{-\left[\sqrt{\gamma}(T-Z)-j\frac{(\sigma+1)}{2\sqrt{\gamma}}\right]^2}\Bigg\}\Bigg)\Bigg] \quad . \qquad (5.5)$$

Now, putting

$$\sqrt{\gamma}(r+T-Z) = a_1 \quad , \qquad \sqrt{\gamma}(T-Z) = a_2$$

$$\frac{(\sigma-1)}{2\sqrt{\gamma}} = b_1 \quad , \qquad \frac{\sigma+1}{2\sqrt{\gamma}} = b_2 \quad ,$$

in Equation (5.5), taking the real parts, and transferring Z_1 to the left-hand side, one derives an explicit expression for Z_1 as follows:

$$Z_1(Z,T) = \frac{A}{8}\sqrt{\frac{\pi}{\gamma}}\Bigg[e^{-\frac{(\sigma-1)^2}{4\gamma}}\Bigg(\Bigg\{\operatorname{erf}(a_2)-\operatorname{erf}(a_1) + \frac{2}{\sqrt{\pi}}\int_0^{b_1}\Big[e^{-\left(a_2^2-y^2\right)}\sin 2a_2y$$

$$-e^{-\left(a_1^2y^2\right)}\sin 2a_1y\Big]dy\Bigg\}\sin T + \Bigg\{\frac{2}{\sqrt{\pi}}\int_0^{b_1}\Big[e^{-\left(a_1^2-y^2\right)}\cos 2a_1y$$

$$-e^{-\left(a_2^2-y^2\right)}\cos 2a_2y\Big]dy\Bigg\}\cos T\Bigg) + e^{-\frac{(\sigma+1)^2}{4\gamma}}\Bigg(\Bigg\{\operatorname{erf}(a_2)-\operatorname{erf}(a_1)$$

$$+\frac{2}{\sqrt{\pi}}\int_0^{b_2}\Big[e^{-\left(a_2^2-y^2\right)}\sin 2a_2y - e^{-\left(a_1^2-y^2\right)}\sin 2a_1y\Big]dy\Bigg\}\sin T$$

$$+\left[\frac{2}{\sqrt{\pi}}\int_0^{b_2} e^{-\left(a_2^2-y^2\right)}\cos 2a_2y\ dy - e^{-\left(a_1^2-y^2\right)}\cos 2a_1y\ dy\right]\cos T\Bigg)\Bigg]$$

$$\left(1+\frac{A}{8}\sqrt{\pi}\left\{\left[e^{-\left(a_1^2-b_1^2\right)}\cos 2a_1b_1 - e^{-\left(a_2^2-b_1^2\right)}\cos 2a_2b_1\right]\sin T\right.$$

$$\left.+\left[e^{-\left(a_1^2-b_1^2\right)}\sin 2a_1b_1 - e^{-\left(a_2^2-b_1^2\right)}\sin 2a_2b_1\right]\cos T\right\} e^{-\frac{(\sigma-1)^2}{4\gamma}}$$

$$+\frac{A}{8}\sqrt{\pi}\left\{\left[e^{-\left(a_1^2-b_2^2\right)}\cos 2a_1b_2 - e^{-\left(a_2^2-b_2^2\right)}\cos 2a_2b_2\right]\sin T\right.$$

$$\left.-\left[e^{-\left(a_1^2-b_2^2\right)}\sin 2a_1b_2 - e^{-\left(a_2^2-b_2^2\right)}\sin 2a_2b_2\right]\cos T\right\} e^{-\frac{(\sigma+1)^2}{4\gamma}}\Bigg)^{-1}.$$

If

$$\frac{2}{\sqrt{\pi}}\int_0^{b_n} e^{-\left(a_m^2-y^2\right)}\sin 2a_my\ dy = F(a_m, b_n)$$

$$\frac{2}{\sqrt{\pi}}\int_0^{b_n} e^{-\left(a_m^2-y^2\right)}\cos 2a_my\ dy = f(a_m, b_n) \quad ;$$

then

$$Z_1(Z, T) = \frac{A}{8}\sqrt{\frac{\pi}{\gamma}}\left(e^{-\frac{(\sigma-1)^2}{4\gamma}}\left\{\left[\operatorname{erf}(a_2)-\operatorname{erf}(a_1)+F(a_2, b_1)-F(a_1, b_1)\right]\sin T\right.\right.$$

$$\left.+\left[f(a_1, b_1) - f(a_2b_1)\right]\cos T\right\}$$

$$+ e^{-\frac{(\sigma+1)^2}{4\gamma}}\left\{\left[\operatorname{erf}(a_2)-\operatorname{erf}(a_1)+F(a_2, b_2)-F(a_1, b_2)\right]\sin T\right.$$

$$+ \left[f(a_2, b_2) - f(a_1, b_2)\right] \cos T\Big\}\Big)$$

$$\left(1 + \frac{A}{8}\sqrt{\pi}\left\{\left[e^{-\left(a_1^2-b_1^2\right)}\cos 2a_1b_1 - e^{-\left(a_2^2-b_1^2\right)}\cos 2a_2b_1\right] \sin T\right.$$

$$\left. + \left[e^{-\left(a_1^2-b_1^2\right)}\sin 2a_1b_1 - e^{-\left(a_2^2-b_2^2\right)}\sin 2a_2b_2\right] \cos T\right\} e^{-\frac{(\sigma-1)^2}{4\gamma}}$$

$$+ \frac{A}{8}\sqrt{\pi}\left\{\left[e^{-\left(a_1^2-b_2^2\right)}\cos 2a_1b_2 - e^{-\left(a_2^2-b_2^2\right)}\cos 2a_2b_2\right] \sin T\right.$$

$$\left. - \left[e^{-\left(a_1^2b_2^2\right)}\sin 2a_1b_2 - e^{-\left(a_2^2-b_2^2\right)}\sin 2a_2b_2\right] \cos T\right\} e^{-\frac{(\sigma+1)^2}{4\gamma}}\Bigg)^{-1} \quad . \tag{5.6}$$

Now putting

$$\sqrt{\gamma}\,(r + T - Z + Z_1) = a_3$$

$$\sqrt{\gamma}\,(T - Z + Z_1) = a_4$$

$$e^{-\left(a_m^2-b_n^2\right)}\sin 2a_mb_n = G(a_m, b_n)$$

$$e^{-\left(a_m^2-b_n^2\right)}\cos 2a_mb_n = g(a_m, b_n)$$

$$\operatorname{erf}(a_m) - \operatorname{erf} a_n = E(a_m - a_n) \quad ,$$

we obtain

$$\frac{\partial Z_1}{\partial T}(Z, T) = \frac{A}{8}\sqrt{\frac{\pi}{\gamma}}\left[e^{-b^2}1\left(\left\{\sqrt{\gamma}\left[g(a_4, b_1) - g(a_3, b_1)\right] + f(a_3, b_1) - f(a_4, b_1)\right\} \sin T\right.\right.$$

$$\left. + \left\{\sqrt{\gamma}\left[G(a_4, b_1) - G(a_3, b_1)\right] - E(a_3 - a_4) + F(a_4, b_1) - F(a_3, b_1)\right\} \cos T\right)$$

$$- e^{-b_2^2}\left(\left\{\sqrt{\gamma}\left[g(a_3, b_2) - g(a_4, b_2)\right] + f(a_4, b_2) - f(a_3, b_2)\right\} \sin T\right.$$

$$+ \left\{\sqrt{\gamma}\left[G(a_4, b_2) - G(a_3, b_2)\right] + E(a_3 - a_4) + F(a_3, b_2) - F(a_4, b_2)\right\} \cos T\Bigg)\Bigg]$$

$$1 + \frac{A}{8}\sqrt{\pi}\left(e^{-b_1^2}\left\{\left[g(a_3, b_1) - g(a_4, b_1)\right] \sin T + \left[G(a_3, b_1) - G(a_4, b_1)\right] \cos T\right\}\right.$$

$$\left. + e^{-b_2^2}\left\{\left[g(a_3, b_2) - g(a_4, b_2)\right] \sin T + \left[G(a_4, b_2) - G(a_3, b_2)\right] \cos T\right\}\right)^{-1} . \tag{5.7}$$

In Equation (5.7), the term Z_1 occurs on the right-hand side. To obtain $\partial Z_1/\partial T$ at a particular Z and T, therefore, the value of Z_1 has to be obtained from Equation (5.6) for the given Z, T, and then has to be substituted in Equation (5.7). Thus, the ratio J_{a-c}/J_o can be calculated. Now, from Equation (5.5)

$$\frac{\partial Z_1}{\partial Z} = \frac{A}{8}\sqrt{\frac{\pi}{\gamma}}\left(e^{-b_1^2}\left\{\left[g(a_3, b_1) - g(a_4, b_1)\right] \sin T + \left[-G(a_4, b_1) + G(a_3, b_1)\right] \cos T\right\}\sqrt{\gamma}\right.$$

$$\left. e^{-b_2^2}\left\{\left[g(a_4, b_2) - g(a_3, b_2)\right] \sin T + \left[G(a_3, b_2) - G(a_4, b_2)\right] \cos T\right\}\sqrt{\gamma}\right)$$

$$\left[1 + \frac{A}{8}\sqrt{\frac{\pi}{\gamma}}\left(e^{-b_1^2}\left\{\left[g(a_3, b_1) - g(a_4, b_1)\right] \sin T + \left[G(a_4, b_1) - G(a_3, b_1)\right] \cos T\right\}\sqrt{\gamma}\right.\right.$$

$$\left.\left. + e^{-b_2^2}\left\{\left[-g(a_4, b_2) + g(a_3, b_2)\right] \sin T + \left[-G(a_3, b_2) + G(a_4, b_2)\right] \cos T\right\}\sqrt{\gamma}\right)\right]^{-1} . \tag{5.8}$$

Since

$$\frac{dZ_1}{dT} = \frac{\dfrac{\partial Z_1}{\partial Z} + \dfrac{\partial Z_1}{\partial T}}{1 - \dfrac{\partial Z_1}{\partial Z}} \quad ;$$

then

$$\frac{dZ_1}{dT} = \frac{A}{8}\sqrt{\frac{\pi}{\gamma}}\left(e^{-b_1^2}\left\{\left[f(a_3,b_1)-f(a_4,b_1)\right]\sin T+\left[-E(a_3-a_4)+F(a_4,b_1)-F(a_3,b_1)\right]\cos T\right\}\right.$$
$$\left.-e^{-b_2^2}\left\{\left[f(a_4,b_2)-f(a_3,b_2)\right]\sin T+\left[E(a_3-a_4)+F(a_3,b_2)-F(a_4,b_2)\right]\cos T\right\}\right) \tag{5.9}$$

The relative simplicity in the expression for

$$\frac{u}{u_o} = \frac{\partial Z_1}{\partial T}$$

is observed.

VI. CONCLUSIONS AND RECOMMENDATIONS

The ballistic theory of an electron beam has been developed, for multiple signals, subject to approximations made to simpfly solution. Some work, using nonlinear space-charge wave analysis, has also been done and a comparison of the ballistic and space-charge wave analysis should be attempted to throw more light on the problem. The graphic plot obtained (Figure 9) which gives a value of 0.5 for the bunching parameter indicates that there is pulse distortion. The saturation of the lower half of the envelope indicates that the exit current is rich in harmonics, even for low depths of modulation.

The theoretical study indicates that experiments can provide solutions where theoretical formulation would be cumbersome. An experimental verification of the theory should therefore be undertaken, using a set of parameters designed to approximate closely the assumption of an infinite beam and no space-charge effects.

Attention is now being directed to the generation of high peak-power radar using nanosecond pulses of the Gaussian type. Once such pulses are generated, the response of the klystron to them can be observed. Good microwave amplification of these pulses would lead to their use in radars.

APPENDIX A: A NOTE ON THE GAUSSIAN SPECTRUM

As this report deals with the klystron response to a Gaussian envelope, a short note on the Gaussian spectrum is useful. The analysis presented has been mostly based on the envelope $g(t) = Ve^{-at^2} \cos\omega t$:

$$g(\omega_o) = \text{Re}\ \frac{1}{2\pi} \int_{-a}^{a} Ve^{-at^2} e^{-j\omega_o t} e^{+j\omega t}\, dt$$

$$= \text{Re}\ \frac{1}{2\pi} \int_{-a}^{a} Ve^{-a\left(t^2 + j\ \frac{(\omega_o - \omega)}{a}\right)}\, dt$$

$$= Ve^{-\frac{(\omega_o - \omega)^2}{4a}}\ \frac{1}{2\pi} \int_{-a}^{a} e^{-a\left(t + j\ \frac{(\omega_o - \omega)}{2a}\right)^2}\, dt$$

$$= \frac{1}{2\pi} \sqrt{\frac{\pi}{a}}\ Ve^{-\frac{(\omega_o - \omega)^2}{4a}} .$$

Thus, in the frequency plane the envelope is also Gaussian. The Gaussian envelope is evidently economical in bandwidth for a given pulse length, the majority of the energy being confined to a finite range of the frequency spectrum centered on the carrier frequency. These factors together with the fact that a Gaussian pulse is easier to generate, are the criterion determining its selection for analysis. It might be interesting to note to what extent the envelope shape depends on the parameter a. Consider just the envelope given by the equation,

$$f(t) = e^{-at^2} \quad ;$$

then

$$g(\omega_o) = \frac{1}{2} \frac{e^{-\frac{\omega_o^2}{4a}}}{\sqrt{\pi a}}$$

Select $a = \pi/\alpha$, and multiply both $f(t)$ and $f(\omega_o)$ by $1/\sqrt{\alpha}$; then

$$f_1(t) = \frac{e^{-\frac{\pi t^2}{\alpha}}}{\sqrt{\alpha}} ,$$

$$g_1(\omega_o) = \frac{e^{-\frac{\alpha\omega_o^2}{4\pi}}}{2\pi} .$$

The area under the curve $f_1(t) = e^{-at^2}/\sqrt{\alpha}$ is given by

$$A = 2\pi\, g_1(\omega_o)\Big|_{\omega_o = 0}$$

$$= \frac{2\pi}{2\pi} = 1 .$$

Therefore as α becomes smaller and smaller, the curve $f_1(t)$ becomes taller and narrower and approaches a unit impulse as α approaches zero. Since a is inversely proportional to α, one must have a high value of a to obtain short pulses. If the frequency is increased, the value of a has to be increased also, if the pulse is to decay to a fixed fraction of its amplitude after a fixed number of r-f cycles. Actually for this purpose the ratio a/ω^2, where $\omega = 2\pi x$ frequency, has to be maintained constant.

The transition from a frequency spectrum consisting of a series of

discrete frequencies to one consisting of a continuous band of frequencies can be made by treating the nonperiodic function as a periodic function in which the period approaches α . The unit Gaussian envelope $e^{-at^2}\cos\omega t$ will be considered. The amplitude of the spectrum at ω_o, is

$$g(\omega_o) = \frac{1}{2\pi} \operatorname{Re} \int_{-\alpha}^{\alpha} e^{-at^2 + j\omega t} \; e^{-j\omega_o t} \; dt \quad .$$

For a single pulse, where $f(t) = 0$ for all values of t except $-L < t < L$, we have

$$g(\omega_o) = \frac{1}{2\pi} \; e^{-\frac{(\omega - \omega_o)^2}{4a}} \; \operatorname{Re} \int_{-L}^{L} e^{-a\left[t - j \frac{(\omega - \omega_o)}{2a}\right]^2} \; dt$$

$$= \frac{1}{2\pi\sqrt{a}} \; e^{-\frac{(\omega - \omega_o)^2}{4a}} \; \operatorname{Re} \left[\operatorname{erf}\sqrt{a} \left(L - j \frac{(\omega - \omega_o)}{2a} \right) + \operatorname{erf}\sqrt{a} \left(L + j \frac{(\omega - \omega_o)}{2a} \right) \right] ,$$

where use has been made of the identity,

$$\operatorname{erf}(-x) = -\operatorname{erf}(x) \quad .$$

With the expansion for the complex error function and then taking the real part, one obtains

$$g(\omega_o) = \frac{1}{2\pi\sqrt{a}} \; e^{-\frac{(\omega - \omega_o)^2}{4a}} \; (2 \operatorname{erf}\sqrt{a}\, L)$$

$$= \left(\frac{\operatorname{erf}\sqrt{a}\, L}{\pi\sqrt{a}} \right) \; e^{-\frac{(\omega - \omega_o)^2}{4a}} \quad .$$

The spectrum of a train of Gaussian pulses of length $2(L + \Delta L)$ recurring every T seconds will be found from the spectrum of a single pulse of the train. For the single pulse at any frequency $\omega_o/2\pi$,

$$g(\omega_o) = \frac{\text{erf}\sqrt{a}\,(L + \Delta L)}{\pi\sqrt{a}}\; e^{-\frac{(\omega - \omega_o)^2}{4a}} \quad .$$

For a period of such pulses recurring with a spacing $T = 1/C$, the sum of spectra of the individual pulses form a Fourier series of harmonics of C; therefore

$$f(t) = A_o + \sum_{n=1}^{a} A_n \cos 2\pi nCT \quad ,$$

where A_n is the sum of an infinite number (one from each pulse) of infinitesimal terms $g(2\pi nC)$ and $g(-2\pi nC)$, giving

$$A_n = \sum \frac{\text{erf}\sqrt{a}\,(L + \Delta L)}{\pi\sqrt{a}}\; e^{-\frac{(\omega' - 2\pi nC)^2}{4a}} \quad .$$

To put an absolute value on the amplitudes $g(\omega_o)$, it is necessary to average them over the recurrence period of the single pulse, making them infinitesimals. However, in the train of pulses recurring every $T = 1/C$ seconds, the amplitude of A_n can be determined by averaging the terms in $g(\omega_o)$ over an interval T; then

$$A_n = \frac{\text{erf}\sqrt{a}\,(L + \Delta L)}{\pi\sqrt{a}\;T}\; e^{-\frac{(\omega - 2\pi nC)^2}{4a}} \quad ,$$

and when $T = 4L \mp \frac{1}{C}$,

$$A_n = \frac{C \operatorname{erf}\sqrt{a}\, L \left(1 + \frac{\Delta L}{L}\right)}{\pi\sqrt{a}\,(4LC \mp 1)}\, e^{-\frac{(\omega - 2\pi nC)^2}{4a}} \quad ;$$

thus,

$$f(t) = A_o + A_1 \cos 2\pi Ct + A_2 \cos 2\pi\, 2Ct + \ldots \quad .$$

where A_n is known.

APPENDIX B. FOURIER COEFFICIENTS

The Fourier coefficients a_r and b_r, as obtained in Equation (2.9) are simplified here:

$$a_r = \frac{1}{\pi} \int_{-\pi}^{\pi} I_o \cos r \left[y - k_1' \sin\left(my + \frac{\phi_1'}{2}\right) - k_1'' \sin\left(ny + \frac{\phi_1''}{2}\right) \right] dy \quad .$$

It is sufficient to obtain the solutions to the following coefficients, as they are related to the ones in Equation (2.9):

$$a_r' = \int_{-\pi}^{\pi} \cos r \left[y + c_1 \sin(my + \alpha_1) + c_2 \sin(ny + \alpha_2) \right] dy \quad ,$$

$$b_r' = \int_{-\pi}^{\pi} \sin r \left[y + c_1 \sin(my + \alpha_1) + c_2 \sin(ny + \alpha_2) \right] dy \quad ,$$

$$a_r' + j b_r' = \int_{-\pi}^{\pi} e^{jr} \left[y + c_1 \sin(my + \alpha_1) + c_2 \sin(ny + \alpha_2) \right] dy \quad ,$$

$$a_r' - j b_r' = \int_{-\pi}^{\pi} e^{-jr} \left[y + c_1 \sin(my + \alpha_1) + c_2 \sin(ny + \alpha_2) \right] dy \quad .$$

Now, according to the property of Bessel Functions,

$$\begin{aligned} e^{jz \sin\theta} &= J_o(z) + 2 \left[J_2(z) \cos 2\theta + J_4(z) \cos 4\theta + \ldots \right. \\ &\quad + 2j \left[J_1(z) \sin\theta + J_3(z) \sin 3\theta + \ldots \right. \\ &= \sum_{p=-a}^{a} Jp(z) \, e^{jp\theta} \quad , \end{aligned} \tag{B.1}$$

since $J_{-p}(z) = (1)^{P} J_p(z)$; therefore, using the property in Equation (B. 1) gives

$$a'_r + j b'_r = \int_{-\pi}^{\pi} e^{jry} \sum_{p=-a}^{a} J_p(rc_1) \; e^{jp(my + a_1)} \sum_{q=-a}^{a} J_q(rc_2) \; e^{jq(ny + a_2)} \, dy$$

$$= \int_{-\pi}^{\pi} e^{jry} \sum_{p=-a}^{a} \sum_{q=-a}^{a} J_p(rc_1) \, Jq(rc_2) \; e^{j(pm + qn)\, y \, + \, j(pa_1 + qa_2)} \, dy \quad .$$

Because of the nature of the integrand, the order of integration and summation can be interchanged; therefore

$$a'_r + jb'_r = 2j \sum_{p=-a}^{a} \sum_{q=-a}^{a} J_p(rc_1) \; J_q(rc_2) \; e^{j(pa_1 + qa_2)} \; \frac{\sin(pm + qn + r)}{pm + qn + r} \; \pi \quad .$$

Now, noting that

$$J_v(-z) = J_v(ze^{j\pi}) = \frac{\sum_{m=o}^{a} (-1)^m \left(\frac{1}{2} \; z \, e^{j\pi}\right)^{v+2m}}{m! \; \Gamma(v + m + 1)} = e^{jv\pi} \sum_{m=o}^{a} \frac{(-1)^m \left(\frac{1}{2} z\right)^{v+2m}}{m! \; \Gamma(v + m + 1)} \quad ,$$

since $e^{j\,2\pi m} = 1$, therefore

$$J_v(-z) = e^{jv\pi} \; J_v(z) \quad .$$

Using the same procedure as before, we obtain

$$a'_r - jb'_r = 2j \sum_{p=-a}^{a} \sum_{q=-a}^{a} J_p(rc_1) \, J_q(rc_2) \; e^{jp(\pi + a_1) \, + \, jq(\pi + a_2)} \; \frac{\sin(pm+qn-r)\pi}{(pm+qn-r)}$$

$$= 2j \sum_{p=-a}^{a} \sum_{q=-a}^{a} (-1)^{p+q} J_p(rc_1) J_q(rc_2) e^{j(pa_1 + qa_2)} \frac{\sin(pm + qn - r)\pi}{pm + qn - r} ,$$

from which

$$a'_r = 2j \sum_{p=-a}^{a} \sum_{q=-a}^{a} J_p(rc_1) J_q(rc_2) e^{j(pa_1 + qa_2)} \cdot$$

$$\frac{(pm + qn - r) \sin(pm + qn + r)\pi + (-1)^{p+q} (pm + qn + r) \sin(pm + q - r)\pi}{(pm + qn)^2 - r^2} ,$$

$$b'_r = 2 \sum_{p=-a}^{a} \sum_{q=-a}^{a} J_p(rc_1) J_q(rc_2) e^{j(pa_1 + qa_2)}$$

$$\frac{(pm + qn - r) \sin(pm + qn + r)\pi - (-1)^{p+q} (pm + qn + r) \sin(pm + qn - r)\pi}{(pm + qn)^2 - r^2} .$$

As r, p, and q are integers, a'_r, and b'_r will not be zero when m and n do not have integral values. It must be noted that for large values of p and q, the quantity $1/\left[(pm + qn)^2 - r^2\right]$ becomes small, and therefore the double infinite series can be replaced by a finite series to permit computation.

APPENDIX C. EVALUATION OF erf(a - jb)

In the analysis of klystron response to Gaussian wave excitation, complex error functions of the type erf(a - jb), where a and b are real numbers, have often been encountered. Here, a method will be indicated to express the complex error function in terms of real integrals. Consider the expression,

$$\operatorname{erf}(a - jb) = \frac{2}{\sqrt{\pi}} \int_0^{a-jb} e^{-z^2}\, dz \quad ,$$

in the complex plane with $z = x + jy$.

As e^{-z^2} is an analytic function, $\oint f(z)\, dz = 0$ around a closed path of integration. Hence, integrating along the path shown by the arrows in Figure 13 gives

$$\int_0^a e^{-x^2}\, dx - j \int_0^b e^{-(a - jy)^2}\, dy = \int_0^{a-jb} e^{-z^2}\, dz \quad ;$$

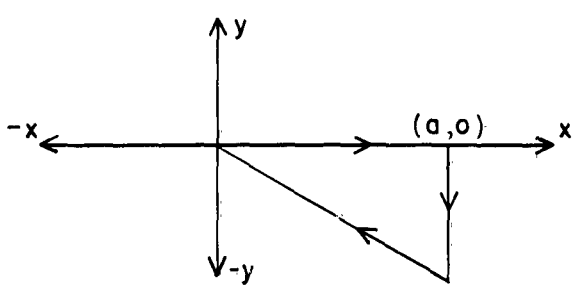

Figure 13. Path of Integration for the Function e^{-z^2}.

from which

$$\operatorname{erf}(a - jb) = \frac{2}{\sqrt{\pi}} \int_0^a e^{-x^2}\, dx - \frac{2}{\sqrt{\pi}} \int_0^b e^{-(a^2 - y^2) + 2jay}\, dy$$

$$= \operatorname{erf}(a) + \frac{2}{\sqrt{\pi}} \int_0^b e^{-(a^2 - y^2)} \sin 2ay\, dy - j \frac{2}{\sqrt{\pi}} \int_0^b e^{-(a^2 - y^2)} \cos 2ay\, dy .$$

This representation of a complex error function in terms of real integrals has been used frequently.

Some other important results follow:

$$\operatorname{erf}(-a - jb) = \operatorname{erf}(-a) - \frac{2}{\sqrt{\pi}} \int_0^b e^{-(a^2 - y^2)} \sin 2ay\, dy - \frac{j2}{\sqrt{\pi}} \int_0^b e^{-(a^2 - y^2)} \cos 2ay\, dy ,$$

as

$$\operatorname{erf}(a) = -\operatorname{erf}(-a)$$

$$\operatorname{erf}(a-jb) - \operatorname{erf}(-a - jb) = \frac{2}{\sqrt{\pi}} \int_{-a-jb}^{a-jb} e^{-z^2}\, dz$$

$$= 2 \operatorname{erf}(a) + \frac{4}{\sqrt{\pi}} \int_0^b e^{-(a^2 - y^2)} \sin 2ay\, dy ,$$

which is a real quantity. This same result can be obtained by contour integration around a suitable rectangle in the z-plane. Again

$$\operatorname{erf}(a - jb) - \operatorname{erf}(c - jb) = \operatorname{erf}(a) - \operatorname{erf}(c) + \frac{2}{\sqrt{\pi}} \int_0^b \left[e^{-(a^2 - y^2)} \sin 2ay \right.$$

$$\left. - e^{-(c^2 - y^2)} \sin 2cy \right] dy + j \frac{2}{\sqrt{\pi}} \int_0^b \left[e^{-(c^2 - y^2)} \cos 2cy \right.$$

$$\left. - e^{-(a^2 - y^2)} \cos 2ay \right] dy \quad .$$

These results show that a complex error function can be easily computed, and its real and imaginary parts separated. Considerable simplification in computation can result in specific problems. The asymptotic expansion, for example,

$$\operatorname{erf}(a) = 1 - \frac{e^{-a^2}}{a\sqrt{\pi}} \left[1 - \frac{1}{(2a^2)} + \frac{1 \cdot 3}{(2a^2)^2} - \frac{1 \cdot 3 \cdot 5}{(2a^2)^3} + \cdots \right] \quad ,$$

is convenient for computation when a is large.

REFERENCES

1. K. Spangenberg, Vacuum Tube, New York: McGraw-Hill, 1948.

2. A. H. W. Beck, Thermionic Valves, Cambridge: Cambridge, Univ. Press, (1958), pp. 198, 353.

3. J. R. Klauder, A. C. Price, S. Darlington, and W. J. Albersheim, "The Theory and Design of Chirp Radars," Bell Sys. Tel. Jour., 39 (1960), p. 745.

4. J. R. Klauder, "The Design of Radar Signals Having Both High Range Resolution and High Velocity Resolution," Bell Sys. Tel. Jour., 39 (1960), p. 809.

5. P. R. McIsaac, "Nonlinear Space-Charge-Wave Analysis," Research Report EE 513, Cornell University, (September 1961).

NANOSECOND STUDY

P. R. McIsaac

School of Electrical Engineering
CORNELL UNIVERSITY
Ithaca, New York

RESEARCH REPORT EE 541

NANOSECOND STUDY

P. R. McIsaac

LINEAR BEAM MICROWAVE TUBES

Technical Report No. 20 30 September 1962

Published under Contract No. AF30(602)-2573
Rome Air Development Center, Griffiss Air Force Base, New York

There are two elements that together determine the response of a microwave tube to short pulses. One of these is the electron beam (with the nonlinear characteristic being the most important factor), and the second is the interaction circuit. For a klystron, the interaction circuit is usually a resonant cavity; therefore the response of a resonant cavity to short pulses is of interest in estimating the short-pulse capability of klystrons. This section summarizes the results of a study of the response of a resonant cavity to a pulse with a Gaussian envelope.

It is assumed that the klystron cavity can be approximated by the equivalent circuit shown in Figure 1, that is, by a parallel resonant circuit. This circuit is driven by a current generator, i(t), which produces a r-f signal at frequency ω_o, with a Gaussian envelope:

$$i(t) = R_e\left[I_o\ e^{-\nu t^2}\ e^{j\omega_o t} \right] . \qquad (1)$$

The voltage across this circuit, v(t), is the signal whose characteristics are sought. The departure of the envelope of v(t) from a Gaussian shape is a measure of the distortion introduced by the finite bandwidth associated with the resonant cavity. The voltage, v(t), can be determined in a straightforward manner using Fourier transform techniques.

The admittance of the parallel resonant circuit; $Y(\omega)$ is given by

$$Y(\omega) = G + j\omega C \left(1 - \frac{1}{\omega^2 LC} \right) . \qquad (2)$$

Define,

$$Y_o = \sqrt{\frac{C}{L}} \quad ,$$

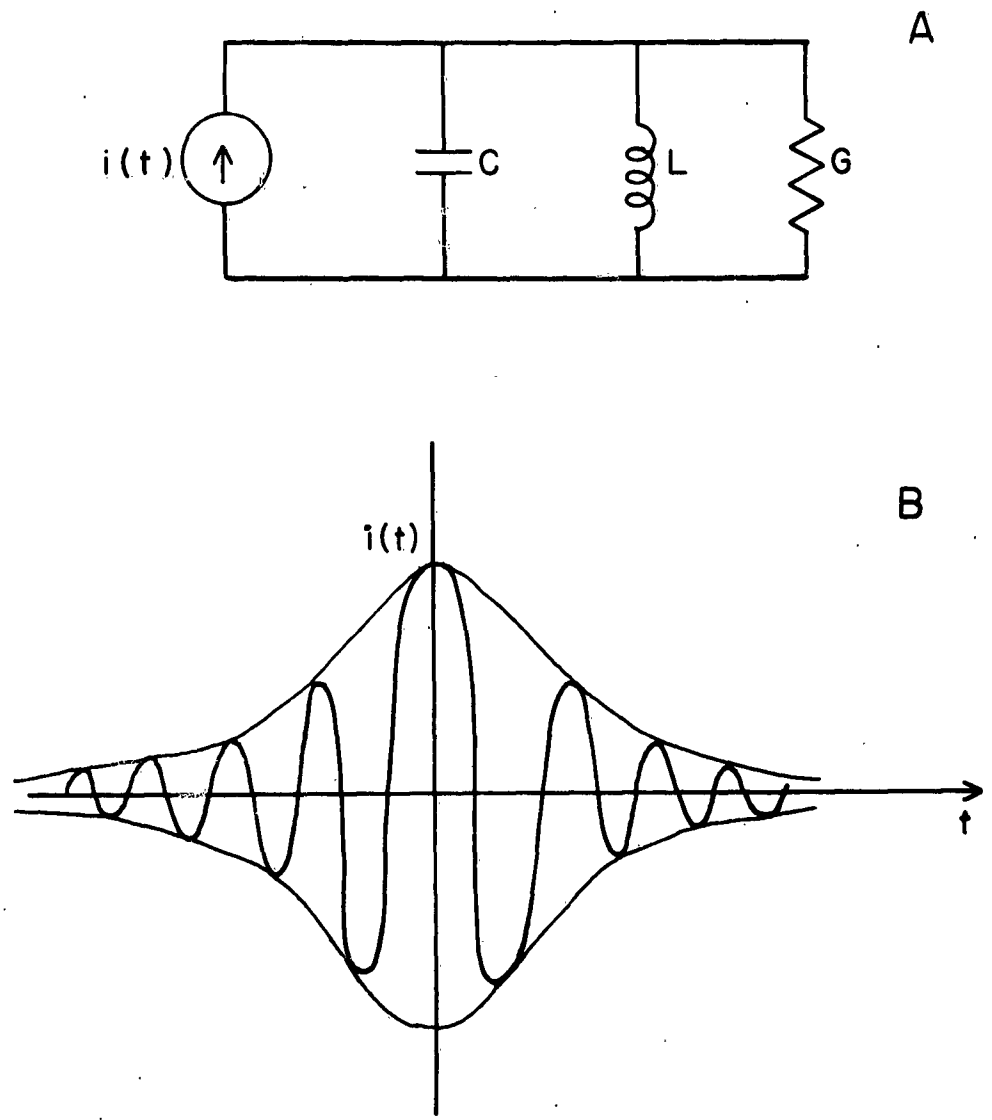

Figure 1. (a) Equivalent Circuit for Resonant Cavity Driven by a Current Pulse. (b) Current Pulse with Gaussian Envelope.

$$\omega_r^2 = \frac{1}{LC} \quad ,$$

$$Q = \frac{\omega_r C}{G} \quad ; \tag{3}$$

then

$$\frac{Y(\omega)}{Y_o} = \frac{1}{Q} + j\left(\frac{\omega}{\omega_r} - \frac{\omega_r}{\omega}\right) . \tag{4}$$

For simplicity, the resonant frequency of the cavity, ω_r, is taken equal to the carrier frequency of the input signal, ω_o. This will almost always be at least approximately true in practice.

Using the Fourier transform of the input current pulse, the Fourier transform of the output voltage pulse is

$$\frac{V(\omega)}{V_o} = \sqrt{\frac{\pi}{\nu}} \; \frac{e^{-\frac{(\omega - \omega_o)^2}{4\nu}}}{\frac{1}{Q} + j\left(\frac{\omega}{\omega_o} - \frac{\omega_o}{\omega}\right)} \quad , \tag{5}$$

where

$$V_o = \frac{I_o}{Y_o} = \sqrt{\frac{L}{C}}\, I_o \quad . \tag{6}$$

The output voltage as a function of time is

$$v(t) = \frac{R_e \omega_o}{4} \sqrt{\frac{\pi}{\nu}} \; V_o \left\{ \left(1 - \frac{j}{2Q\sqrt{1 - \frac{1}{4Q^2}}} \right) \right.$$

$$\left. \left[1 + \operatorname{erf}\left\{ \sqrt{\nu}\, t - \frac{\omega_o}{4Q\sqrt{\nu}} - j\,\frac{\omega_o}{2\sqrt{\nu}} \left(1 \mp 1 - \frac{1}{4Q^2} \right) \right\} \right] \right\}$$

$$e^{-\frac{\omega_o t}{2Q} - \frac{\omega_o^2}{2Q\nu}\left(1+\sqrt{1-\frac{1}{4Q^2}}\right) - j\sqrt{1-\frac{1}{4Q^2}}\,\omega_o t + j\frac{\omega_o^2}{4Q\nu}\left(1+\sqrt{1-\frac{1}{4Q^2}}\right)}$$

$$+\left(1+\frac{j}{2Q\sqrt{1-\frac{1}{4Q^2}}}\right)\left[1+\operatorname{erf}\ \nu t-\frac{\omega_o}{4Q\ \nu}\left(\sqrt{1-\frac{1}{4Q^2}}-1\right)\right]$$

$$e^{-\frac{\omega_o t}{2Q} + \frac{\omega_o^2}{2\nu}\left(\sqrt{1-\frac{1}{4Q^2}}+\frac{1}{4Q^2}-1\right) + j\sqrt{1-\frac{1}{4Q^2}}\,\omega_o t - j\frac{\omega_o^2}{4Q\nu}\left(\sqrt{1-\frac{1}{4Q^2}}-1\right)} . \qquad (7)$$

Figures 2 and 3 present the output voltage envelope as a function of time for two different pulse lengths and with Q as a parameter. In Figure 2, the length of the input current pulse is 100 r-f cycles between the -10 db points. For a Q of 10, the output voltage pulse envelope is nearly identical with the current pulse envelope. For a Q of 100, the voltage pulse is delayed in time by approximately 25 cycles, but its shape is still approximately Gaussian. Thus the amount of distortion of the envelope introduced is not large for $Q \lesssim 100$ in this case.

Figure 3 presents the results for a pulse length of 10 r-f cycles between the -10 db points. In this case, the increase in the pulse delay as the Q is increased is clearly evident. Further, although the $Q = 10$ curve appears to be nearly Gaussian, at $Q = 50$ or 100, the curves are far from Gaussian, having long tails. At $Q = 20$, the asymmetry of the curve is becoming evident; therefore $Q = 20$ may be taken as a rough dividing line between acceptable and excessive distortion.

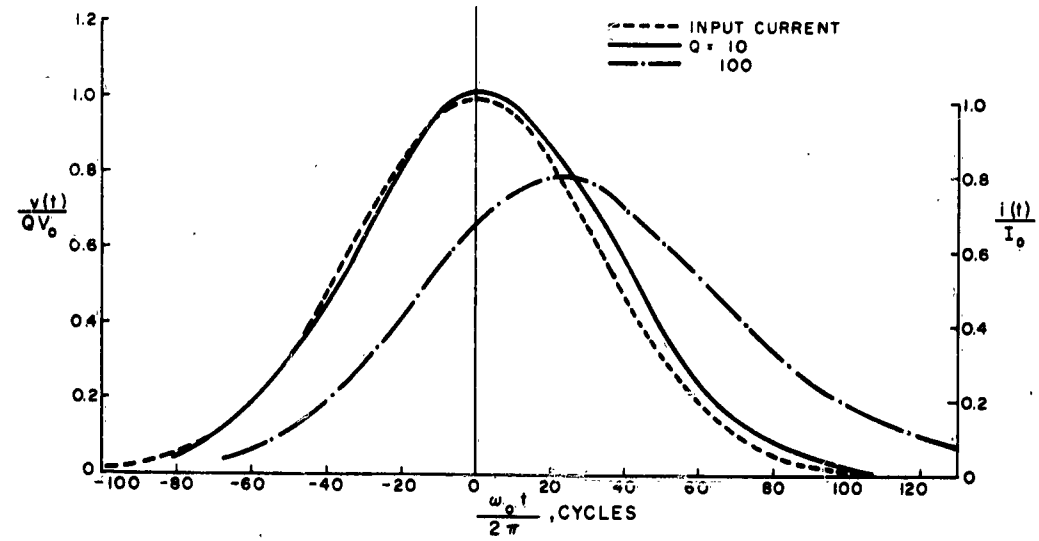

Figure 2. Response of Single Tuned Circuit to a Gaussian Current Pulse. (100 cycles between -10-db points.)

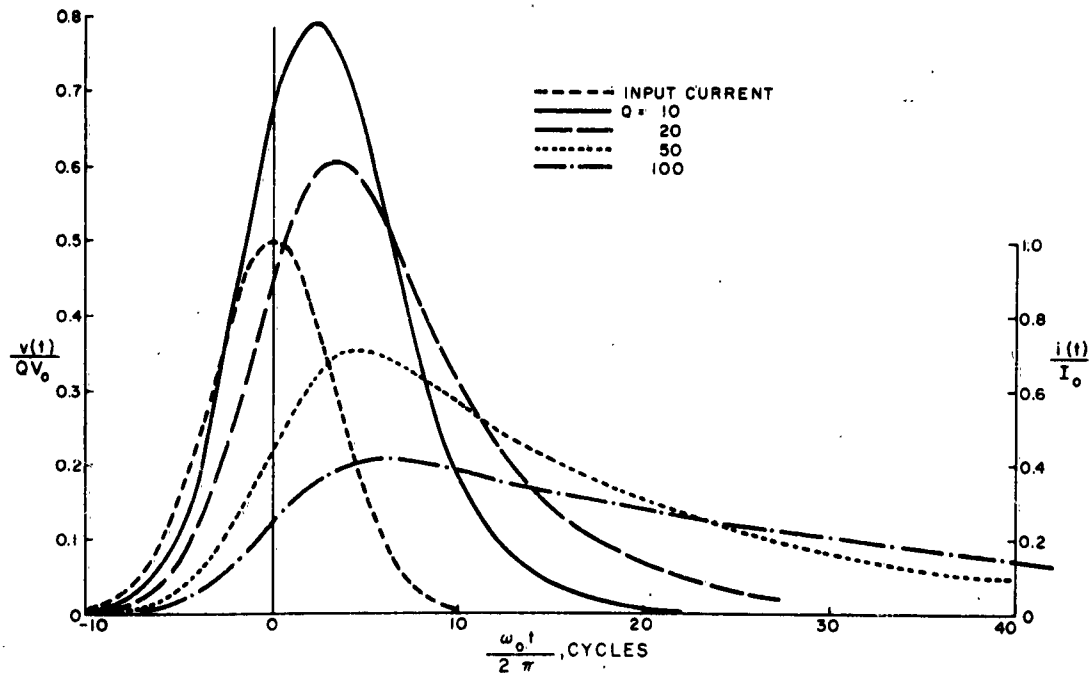

Figure 3. Response of Single Tuned Circuit to a Gaussian Current Pulse. (10 cycles between -10-db points.)

One measure of the distortion of the output voltage pulse is the extent to which the magnitude of its Fourier frequency spectrum departs from that of a Gaussian envelope pulse. The Fourier spectrum of the output voltage can be written from Equation (5) as

$$\sqrt{\frac{\nu}{\pi}}\ \frac{|V(\omega)|}{QV_o} = \frac{e^{-\frac{(\omega - \omega_o)^2}{4\nu}}}{\sqrt{1 + Q^2\left(\frac{\omega}{\omega_o} - \frac{\omega_o}{\omega}\right)^2}} \quad . \tag{8}$$

The ideal response is

$$\sqrt{\frac{\nu}{\pi}}\ \frac{|V(\omega)|\ \text{ideal}}{QV_o} = e^{-\frac{(\omega - \omega_o)^2}{4\nu}} \quad . \tag{9}$$

A measure of the distortion as a function of frequency can be defined as

$$D\left(\frac{\omega}{\omega_o}\right) = \frac{\nu}{\pi}\ \frac{-1}{QV_o}\left[\,|V(\omega)|_{\text{ideal}} - |V(\omega)|\,\right] \quad ,$$

$$D\left(\frac{\omega}{\omega_o}\right) = e^{-\frac{(\omega - \omega_o)^2}{4\nu}}\left[1 - \frac{1}{1 + Q^2\left(\frac{\omega}{\omega_o} - \frac{\omega_o}{\omega}\right)^2}\right] \quad . \tag{10}$$

Figures 4 and 5 show $D(\omega/\omega_o)$ versus ω/ω_o for 100 and 10 r-f cycles between -10 db points, respectively, with Q as a parameter. From Figure 4 for the 100-cycle case, $D(\omega/\omega_o)$ is negligible for $Q = 10$, and not too large for $Q = 100$. However, for the 10-cycle case of Figure 5, $D(\omega/\omega_o)$ has peaks of appreciable height at $Q = 20$, and these are very large for $Q = 100$. These curves, of course, corroborate the conclusions based on

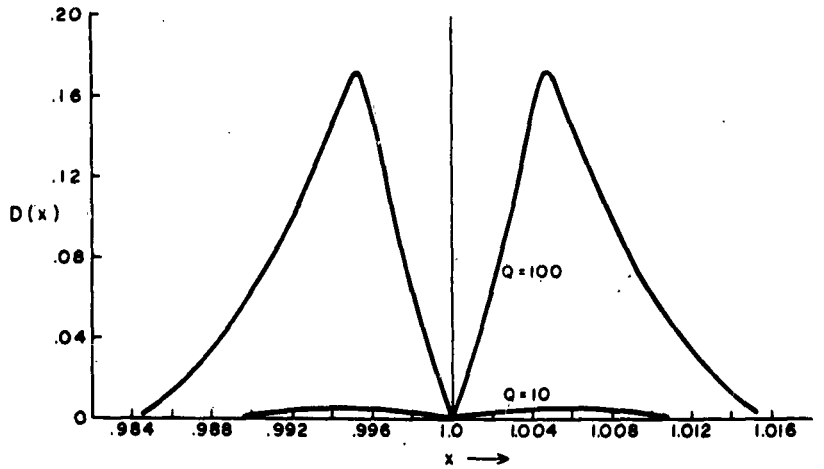

Figure 4. D(x) versus x. (N = 100 r-f cycles to -10-db points.)

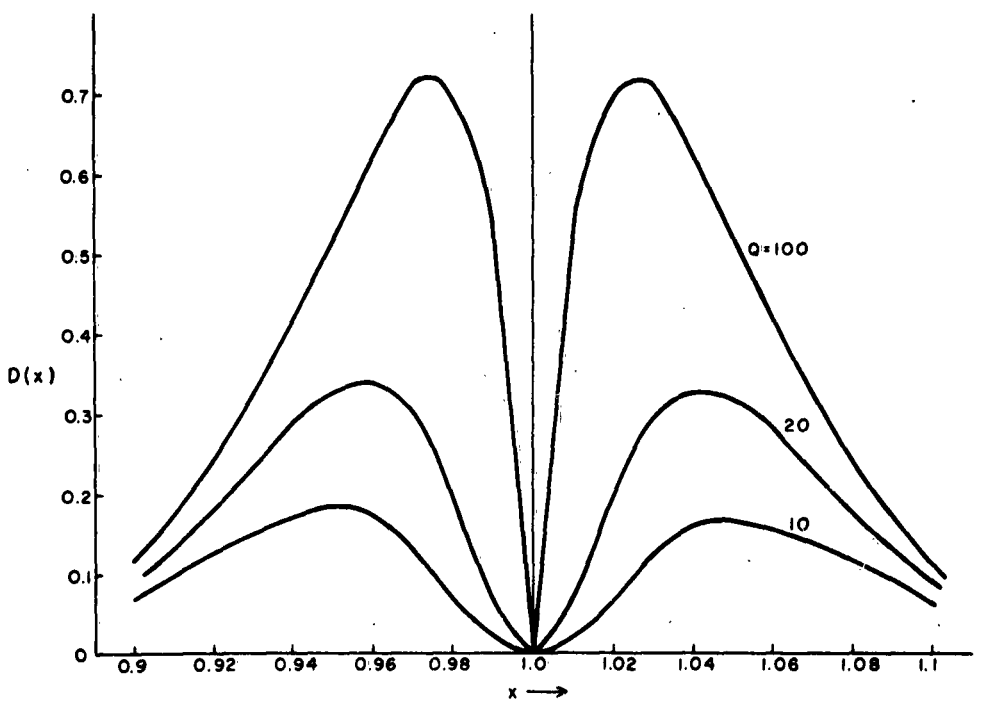

Figure 5. D(x) versus x. (N = 10 r-f cycles to -10-db points.)

the time response curves of Figures 2 and 3 since they are an alternative method of discussing the resonant circuit characteristics.

Two additional observations can be made concerning the $D(\omega/\omega_o)$ curves. The curves are slightly asymmetric about $\omega/\omega_o = 1.0$, the peaks being higher for $\omega < \omega_o$ than for $\omega > \omega_o$. This asymmetry decreases as Q increases, and is negligible for Q values where the distortion is large. Second, the location of the peaks of $D(\omega/\omega_o)$ tend toward $\omega/\omega_o = 1.0$ as Q is increased. A positive value of $D(\omega/\omega_o)$ corresponds, in a sense, to a deficiency in the Fourier spectrum of the output voltage pulse. As the Q is increased, the maximum "deficiency" occurs at a frequency closer to the resonant (and r-f carrier) frequency.

BALLISTIC ANALYSIS OF MODULATED ELECTRON BEAMS

I. Turkekul

School of Electrical Engineering
CORNELL UNIVERSITY
Ithaca, New York

RESEARCH REPORT EE 547

BALLISTIC ANALYSIS OF MODULATED ELECTRON BEAMS

I. Turkekul

LINEAR BEAM MICROWAVE TUBES

Technical Report No. 24 30 October 1962

Published under Contract No. AF30(602)-2573
Rome Air Development Center, Griffiss Air Force Base, New York

ACKNOWLEDGMENTS

The author wishes to express his gratitude to the following individuals and organizations for their assistance during the course of the investigation: to Professor G. C. Dalman, Chairman of his Special Committee, for his constant guidance and many helpful suggestions; to Professors L. F. Eastman, R. P. Agnew, and P. R. McIsaac for their advice on a course of study; to the Rome Air Development Center of the Air Research and Development Command, USAF for its support of the investigation; and to the Turkish navy for its scholarship and extended leave.

TABLE OF CONTENTS

	Page
LIST OF ILLUSTRATIONS	vii
LIST OF SYMBOLS	xii
ABSTRACT	xv
I. INTRODUCTION	1
II. ANALYSIS OF THE FIRST GAP	4
A. GRAPHIC ANALYSIS (Computer Problem)	4
B. FIRST-ORDER ANALYSIS	8
1. Velocity Modulation	8
2. Density Modulation	10
C. SECOND-ORDER ANALYSIS	12
1. Velocity Modulation	13
2. Density Modulation	15
III. ANALYSIS OF THE FIRST DRIFT SPACE	23
A. DENSITY	24
B. VELOCITY	26
IV. ANALYSIS OF THE SECOND GAP	34
A. COMPUTER PROBLEM	34
B. CALCULATION OF KINETIC ENERGY AND DISCUSSION	38
1. Two-Cavity Klystron and Velocity-Filter Gap	40
2. Loading Conditions of a Two-Cavity Klystron	61

Page

V. ANALYSIS OF SECOND DRIFT SPACE AND LAST CAVITY 64

A. COMPUTER PROBLEM 64

B. VELOCITY FILTERING 68

VI. CONCLUSIONS AND RECOMMENDATIONS 79

A. CONCLUSIONS 79

1. Exact Graphic Analysis and Its Approximation 79

2. Computer Solutions 80

B. RECOMMENDATIONS 82

APPENDIX A. INITIAL CONDITIONS AT ENTRANCE TO SECOND GAP (PLANE C) 84

REFERENCES 85

LIST OF ILLUSTRATIONS

Figure		Page
1	Schematic Diagram of Two-Cavity Klystron with Parallel Gridded Gaps.	5
2	Normalized Exit Velocity v_b/v_o versus Exit Time ωt_b, and Normalized Exit Current i_b/I_o versus Exit Time ωt_b, for Different D-C Gap Transit Angles, obtained by Graphic Analysis.	7
3	Transit-Time Correction Factor $(\omega t_b - \omega t_a - \theta_g)$ versus Entrance Time ωt_a Comparing Graphic and Analytical Methods.	11
4	Normalized Exit Velocity v_b/v_o versus Exit Time ωt_b, Comparing Graphic and Second-Order Methods.	15
5	Normalized Exit Velocity v_b/v_o versus Exit Time ωt_b for Different D-C Gap Transit Angles and Depths of Modulation.	16
6	Normalized Exit Velocity v_b/v_o versus Exit Time ωt_b for Different D-C Gap Transit Angles and Depths of Modulation.	17
7	Normalized Exit Current i_b/I_o versus Exit Time ωt_b Comparing Graphic and Second-Order Methods.	19
8	Normalized Exit Current i_b/I_o versus Exit Time ωt_b for Different D-C Gap Transit Angles and Depths of Modulation.	20

Figure		Page
9	Normalized Exit Current i_b/I_o versus Exit Time ωt_b for Different D-C Gap Transit Angles and Depths of Modulation.	21
10	(a) Absolute Value of Normalized Fundamental Current $\|i_1\|/I_o$ versus Bunching Parameter X , (b) Phase Angle, β_1, versus Bunching Parameter X .	27
11	(a) Absolute Value of Normalized Second-Harmonic Current $\|i_2\|/I_o$ versus Bunching Parameter X , (b) Phase Angle β_2 versus Bunching Parameter X ; in Drift Space.	28
12	(a) Absolute Value of Normalized Third-Harmonic Current $\|i_3\|/I_o$ versus Bunching Parameter X , (b) Phase Angle β_3 versus Bunching Parameter X in the Drift Space.	29
13	Absolute Value of Normalized Components of Current versus Drift Angle for Different Depths of Modulation.	30
14	Normalized Fundamental Current i_1/I_o versus Normalized Drift Distance $\beta_p z$ for Different D-C Gap Transit Angles. (The curves shown are those calculated by Solymar. The solid dots are the points calculated from Equation (3.9) of this study.)	31
15	Arrival Phase, $\omega t_c - L(1 - \Delta)$, versus Departure Phase ωt_b for the Drift Space for Different Bunching Parameters.	33
16	Normalized Exit Velocity v_c/v_o versus Exit Time ωt_c at End of Drift Space for Different Depths of Modulation.	33

Figure		Page
17	Absolute Value of Normalized Fundamental Current $\|i_{c_1}\|/I_o$ versus Drift Angle θ_o at entrance to Second Gap for Different Depths of Modulation.	41
18	Normalized Entrance Current i_c/I_o versus Entrance Time ωt_c (solid line) and Normalized Entrance Velocity v_c/v_o versus Entrance Time ωt_c (broken line) for Different Depths of Modulation and $\theta_{g_1} = 1.75$ Radians, $\theta_o = 2\pi$ Radians.	42
19	Normalized Exit Current i_d/I_o versus Exit Time ωt_d (solid line) and Normalized Exit Velocity v_d/v_o versus Exit Time ωt_d (broken line) for Different Phase Angles and $\alpha_1 = 0.8$, $\alpha_2 = 1.0$, and $\theta_{g_2} = \pi$.	45
20	Normalized Exit Current i_d/I_o versus Exit Time ωt_d (solid line) and Normalized Exit Velocity v_d/v_o versus Exit Time ωt_d (broken line) for Different Gap Lengths and $\alpha_1 = 0.8$, $\alpha_2 = 1.0$, and $\Gamma_2 = -\pi/2$.	47
21	Normalized Exit Current i_d/I_o versus Exit Time ωt_d (solid line) and Normalized Exit Velocity v_d/v_o versus Exit Time ωt_d (broken line) for Different Depths of Modulation and $\alpha_1 = 0.8$, $\theta_{g_2} = \pi/2$, and $\Gamma_2 = -\pi/4$.	48
22	Normalized Exit Current i_d/I_o versus Exit Time ωt_d (solid line) and Normalized Exit Velocity v_d/v_o versus Exit Time ωt_d (broken line) for Different Depths of Modulation and $\alpha_1 = 0.8$, $\theta_{g_2} = \frac{7\pi}{4}$, and $\Gamma_2 = -\pi/2$.	50
23	(a) Percentage of Incremental Charge Δq versus Velocity-Class v_d/v_o ; (b) Percentage Incremental Kinetic Energy ΔW versus Velocity-Class v_d/v_o at Entrance to Second Gap for $\alpha_1 = 0.8$.	52

Figure		Page
24	Percentage of Incremental Charge Δq versus Velocity-Class v_d/v_o for Different Depths of Modulation and $\alpha_1 = 0.8$, $\theta_{g_2} = \pi/2$, and $\Gamma_2 = -\pi/4$.	53
25	Percentage of Incremental Kinetic Energy ΔW versus Velocity-Class v_d/v_o for Different Depths of Modulation and $\alpha_1 = 0.8$, $\theta_{g_2} = \pi/2$, and $\Gamma_2 = -\pi/4$.	55
26	Percentage of Incremental Charge Δq versus Velocity-Class v_d/v_o for Different Depths of Modulation and $\alpha_1 = 0.8$, $\theta_{g_2} = \frac{7\pi}{4}$, and $\Gamma_2 = -\pi/2$.	56
27	Percentage of Incremental Kinetic Energy ΔW versus Velocity-Class v_d/v_o for Different Depths of Modulation and $\alpha_1 = 0.8$, $\theta_{g_2} = \frac{7\pi}{4}$, and $\Gamma_2 = -\pi/2$.	58
28	(a) Normalized Exit Velocity v_d/v_o versus Exit Time ωt_d; (b) Normalized Exit Current i_d/I_o versus Exit Time ωt_d for the Selected Catcher Gap (solid line) and for the Selected Velocity-Filter Gap (broken line).	59
29	(a) Equivalent Admittance Circuit for Second Gap, (b) Vector Diagram for Fundamental Component of Entrance Current i_{c_1}, and Voltage V_2 across Second Gap.	62
30	Schematic Diagram of a Two-Cavity Klystron and a Velocity-Filter Gap Combined.	65
31	(a) Normalized Exit Velocity v_f/v_o versus Exit Time ωt_f; (b) Normalized Exit Current i_f/I_o versus Exit Time ωt_f for $L_2 = \frac{9\pi}{4}$, $\theta_{g_3} = \frac{7\pi}{4}$, $\Gamma_3 = -\frac{\pi}{2}$, and $\alpha_3 = 1.0$.	70

Figure		Page
32	(a) Percentage of Incremental Charge Δq versus Velocity-Class v_f/v_o ; (b) Percentage of Incremental Kinetic Energy ΔW versus Velocity-Class v_f/v_o for $L_2 = \frac{9\pi}{4}$, $\theta_{g_3} = \frac{7\pi}{4}$, $\Gamma_3 = -\frac{\pi}{2}$, and $a_3 = 1.0$.	71
33	Relative Intensity versus Wavelength in Angstroms for a Tungsten Target at Various Voltages. (After measurements of Ulrey given by Richtmyer, Kennard, and Lauretsen.[9])	73
34	Mass Absorption Coefficient μ/ρ versus Wavelength in Angstroms for Lead Shield.	77

LIST OF SYMBOLS

d	modulating cavity gap separation
d_n	gap separation of n^{th} cavity
i	a-c current
I_o	d-c current
J_λ	intensity of X-ray radiation of wavelength λ
l_n	length of n^{th} drift space
P_k	kinetic power
t	time
v	a-c velocity
v_o	d-c velocity
V_o	d-c beam voltage
V_n	voltage across the gap of n^{th} cavity
W	normalized total kinetic energy per cycle
W_k	total kinetic energy per cycle
X	bunching parameter in the first drift space
z	axial co-ordinate

Z	normalized axial co-ordinate
a_n	depth of modulation for n^{th} cavity
β_1	phase angle of the fundamental current at plane c
β_p	ω_p/u_o
Γ_n	phase angle of the voltage across the n^{th} cavity
δ	transit angle correction factor
η	efficiency (defined as the ratio of total kinetic energy taken out of n^{th} cavity to the total kinetic energy of the electron beam at the entrance to the second gap).
θ	total transit angle of the modulating cavity
θ_{o_n}	n^{th} drift-space angle
θ_{g_n}	d-c transit angle of the n^{th} cavity
λ	wavelength of the X-ray radiation
ξ	total phase angle of the voltage across the first cavity
ϕ	total phase angle of the fundamental current at plane c
ω	frequency of input signal to modulating cavity

ABSTRACT

This report describes a ballistic analysis made of an electron beam in a two-cavity klystron, which was assumed to have infinite cross section, negligible space charge, nonrelativistic velocities, and gridded finite gaps. The operating parameters of a catcher gap for maximum efficiency and the velocity-filtering capabilities of a r-f gap interacting with a spent beam, at large signals were investigated. The term "velocity-filtering" means a reduction in the velocity of bunched electrons of a certain velocity-class. All the characteristics in this study were computed by a Burroughs Datatron 220 digital computer, when necessary.

The behavior of an electron beam in a buncher gap was investigated using a graphic analysis based on the results given by the digital computer. The velocity and current distributions emerging from this gap were formulated. The graphic results were approached by successively approximating the transit-time correction factor.

The results obtained by successive approximation were then used as initial conditions in analyzing the behavior of the electron beam in the first drift space. A Fourier series was derived which describes the various harmonics of the beam current as functions of the operating parameters of the buncher gap and the drift space, for large signals. The results are found to be in agreement with those in the literature.

The exit current and the exit velocity from the second gap were formulated as implicit functions of entrance and exit times in forms applicable to a digital computer, and the operating conditions of the second gap were taken as parameters. The computer data were sorted for both a

catcher gap and a velocity-filter gap by kinetic energy calculations. The catcher gap selected had an efficiency of 23.995 per cent.

The same procedure was applied to a second drift space and then to a third gap, so that the solutions corresponded to a combination consisting of a two-cavity klystron and a velocity-filter cavity. With the known operating parameters of the catcher gap and the velocity-filter gap, the value of the second drift angle for best filtering was determined. The velocity-filter gap selected had an efficiency of 5.368 per cent. The addition of the velocity-filter gap was shown to decrease the intensities of X-ray radiation through a given shield.

I. INTRODUCTION

The ballistic approach for analyzing an electron beam in a velocity-modulated tube was first introduced by Webster.[1] Although his theory lacks validity at or after crossover because of space-charge forces and does not apply to electron beams of finite radius because of fringing of the space-charge fields, it has two advantages: (1) It is simple and provides an insight into the physical phenomena and thus serves as a guide for more complicated theories, and (2) it is fairly accurate at large-signal levels for low-perveance beams.

The current tendency to demand higher power levels from klystrons increases the importance of ballistic theory. In an experiment, Mihran[2] showed that for large signals, the electron beam showed ballistic behavior; i.e., the debunching effect of the space-charge forces became less important. At the same time, in finite beams, the space-charge forces acted to enhance bunching at large signals by debunching inner and outer electrons differently.

In a high-power klystron, the velocity spread of the electrons in the beam increases considerably at large signals. Hard X-rays emanate from the collector of such a tube since the fast electrons reach velocities that are capable of producing these X-rays. This is a serious disadvantage of high-power klystrons, but it can, however, be overcome by devising some means of obtaining electronic interaction with the spent beam, the beam after the catcher gap. The well-known method of the d-c retarding field alone, i.e., application of a negative voltage to the collector, would not suffice, since the d-c retarding field may turn back some of the

slow electrons while decelerating the fast electrons. A r-f circuit, such as a r-f gap or a helix, on the other hand, can be designed to interact with the beam in such a way that only the fast electrons are decelerated. Such a r-f gap is analyzed in this study, and it is called the velocity-filter gap. A proper combination of the d-c and the r-f methods, then, may prevent radiation of X-rays.

The purpose of this study is to analyze the electron beam in a two-cavity klystron, using a ballistic approach, to determine the characteristics of the spent beam and to investigate the velocity-filtering capabilities of a r-f gap. To simplify this analysis a model is chosen with the following assumptions: (1) beam of infinite cross section, (2) negligible space charge, (3) gridded finite gaps, and (4) nonrelativistic velocities. All the characteristics in this study are computed by a Burroughs Datatron 220 digital computer when necessary.

The analysis of the first gap is given in Chapter II. First a graphic analysis is made by setting up exact equations for the gap and solving them with the computer; then analytical formulas are derived for the exit velocity and the exit current. These derivations are based on successive approximations to the transit time and are compared with the graphic analysis to determine the range of validity.

The results of Chapter II are used as initial conditions in Chapter III for the analysis of the drift space. Fourier analysis of the current at the end of the drift space results in a series which describes the various harmonics of the current as functions of the operating parameters of the first gap and the drift space for large signals. At this point, however, multivalued functions resulting from the occurrence of overtaking come into play, and explicit

analytical formulas no longer approximate exact formulas. In the rest of the analysis, therefore, one is restricted to dealing with exact implicit formulas.

In Chapter IV, the second gap is treated in the same way as the first gap. A r-f voltage is assumed across the second gap with variable amplitude and phase. The characteristics of the spent beam are determined by the computer and the results are sorted out for both a catcher gap and a velocity-filter gap by kinetic energy calculations.

Chapter V describes the effects of the second drift space and the velocity-filter gap on the characteristics of the spent beam. The analysis is similar to work in the previous chapters, the operating parameters for the catcher gap and the velocity-filter gap found in Chapter IV being used as initial conditions.

II. ANALYSIS OF THE FIRST GAP

The first or buncher gap modulates the velocity of an electron beam. This, in turn, causes density modulation in the drift space. In a finite gap, however, density modulation also takes place. This factor has been neglected in previous analyses, and including it here extends Webster's analysis.

Exact equations for the first gap will be derived from the equation of motion, and the characteristics of the beam will be calculated by the computer. Analytical expressions of functional relationships will be based on the exact graphic method with the assumptions mentioned. Thus in this chapter, a graphic analysis is first made, and then analytical formulas are obtained by successive approximations.

A. GRAPHIC ANALYSIS (Computer Problem)[3]

The equation of motion of electrons in the buncher gap, with a sinusoidal input voltage and no space charge, is a simple second-order differential equation,

$$\ddot{z} = \frac{eV_1}{md} \sin\omega t \quad . \tag{2.1}$$

Using the notation of Figure 1, integrating Equation (2.1) twice, and substituting boundary conditions at $t = t_a$ and at $t = t_b$, one obtains

$$\dot{z} = v_o + \frac{eV_1}{m\omega d} (\cos\omega t_a - \cos\omega t) \quad , \tag{2.2}$$

$$d = \left(v_o + \frac{eV_1}{m\omega d} \cos\omega t_a\right) (t_b - t_a) + \frac{eV_1}{m\omega^2 d} (\sin\omega t_a - \sin\omega t_b) \quad . \tag{2.3}$$

Defining the d-c transit angle and depth of modulation gives

$$\theta_g = \frac{\omega d}{v_o} \quad , \tag{2.4}$$

$$a = \frac{V_1}{V_o} \quad ; \tag{2.5}$$

and normalizing with respect to d-c velocity gives

$$\dot{Z} = \frac{\dot{z}}{v_o} = 1 + \frac{a}{2\theta_g} (\cos\omega t_a - \cos\omega t_b) \quad , \tag{2.6}$$

$$\theta_g = \left(1 + \frac{a}{2\theta_g} \cos\omega t_a\right)(\omega t_b - \omega t_a) + \frac{a}{2\theta_g} (\sin\omega t_a - \sin\omega t_b) \quad . \tag{2.7}$$

Equations (2.6) and (2.7) completely define the motion of electrons during the passage through the gap and give the implicit relation between entrance time and exit time with the gap transit angle and depth of modulation as parameters.

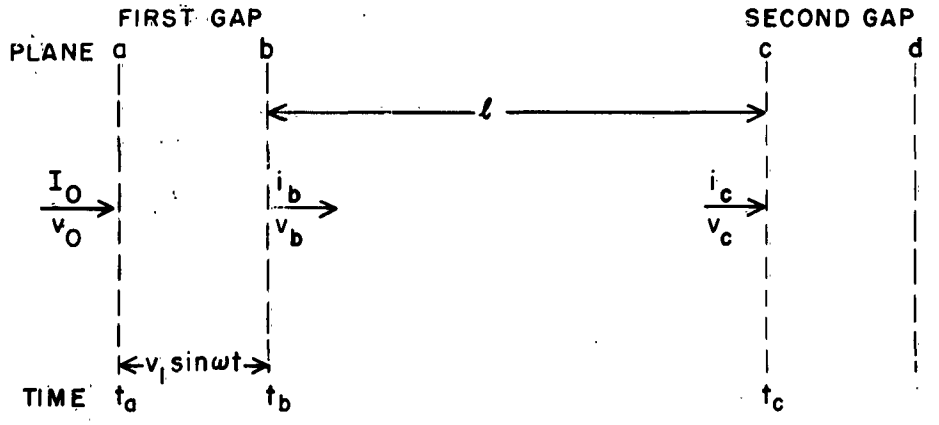

Figure 1. Schematic Diagram of Two-Cavity Klystron with Parallel Gridded Gaps.

The numerical computations of Equation (2.6) and (2.7) have been carried out on the digital computer and are presented in a series of graphs of normalized exit velocity, v_b/v_o, versus exit time, ωt_b; normalized exit current, i_b/I_o, versus exit time, ωt_b; and the transit-time correction factor, $\omega t_b - \omega t_a - \theta_g$, versus entrance time, ωt_a.

Exit current is obtained by applying the principle of conservation of charge through the gap; it can be determined from

$$\frac{i_b}{I_o} = \left| \frac{d\omega t_a}{d\omega t_b} \right| \quad . \tag{2.8}$$

Numerical values of the normalized current are found by measuring the slope of the curves of the transit-time correction factor versus entrance time at each point. Figures 2a, b, c show the results of this method for three different gap transit angles with depth of modulation as a parameter. Other results obtained by this method are presented in subsequent sections of this chapter.

It can be seen from Figures 2a, b, and c that the normalized exit current gradually becomes peaked as the d-c gap transit angle (θ_g) is increased, and that there is a phase difference between the normalized exit current and the normalized exit velocity. Since deceleration and acceleration of electrons during the corresponding half cycles of the input voltage counteract each other, there is a limit to this peaking of the exit current as the d-c gap transit angle is further increased; $\theta_g = \pi$ is a practical gap transit angle, and it is used in the computations throughout the rest of this chapter and in the next chapter.

The wave forms of the exit velocity and the exit current show that

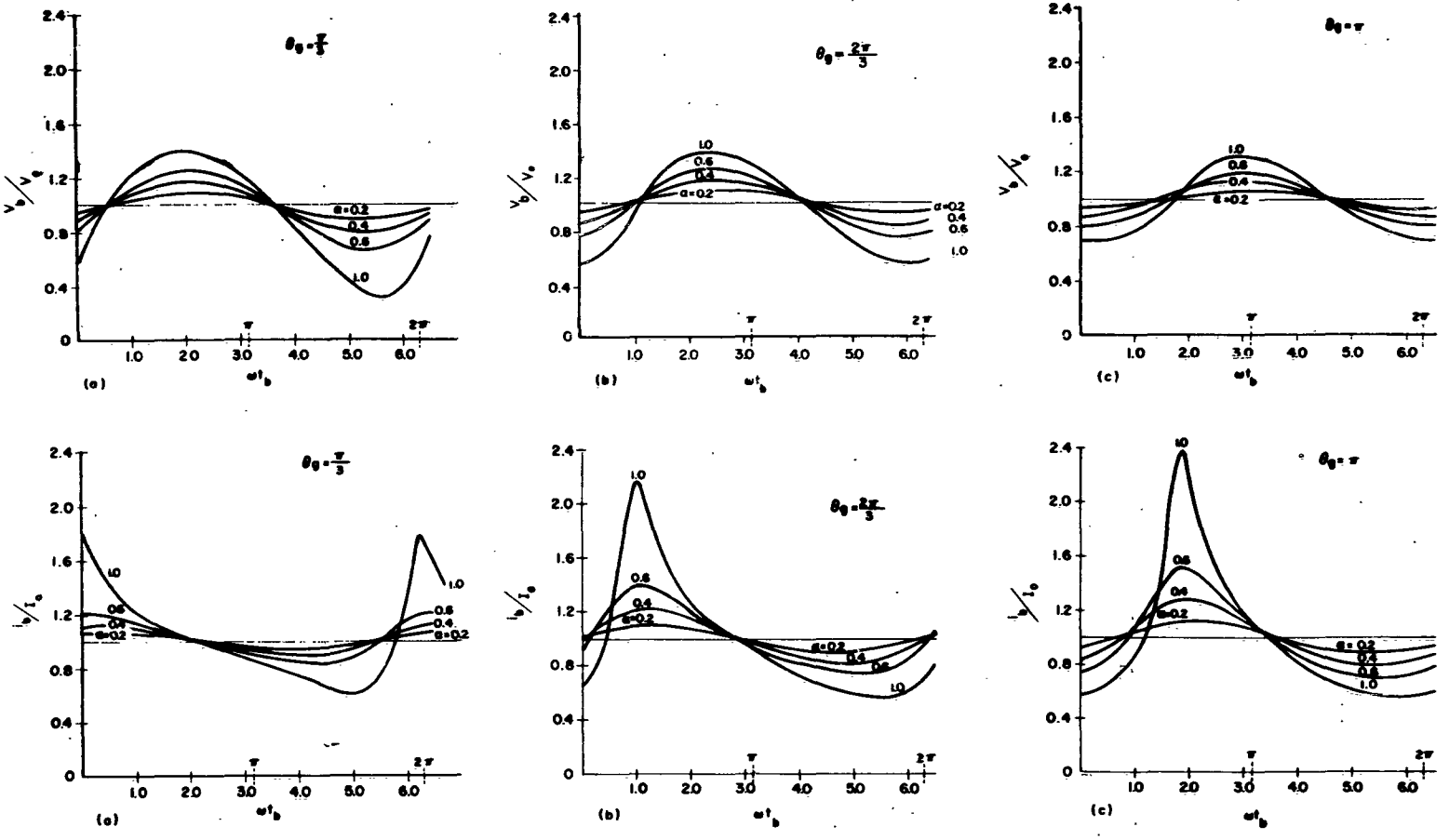

Figure 2. Normalized Exit Velocity v_b/v_o versus Exit Time ωt_b, and Normalized Exit Current i_b/I_o versus Exit Time ωt_b, for Different D-C Gap Transit Angles, Obtained by Graphic Analysis.

they both have harmonics and that transit-time effects are nonlinear in the buncher gap.

B. FIRST-ORDER ANALYSIS

When the results of graphic analysis are known, one can proceed with the analytical study by making approximations in the derivations, and comparing the results thus obtained with those of the exact graphic method. The discrepancies will show the validity and the range of the analytical forms.

1. Velocity Modulation

One must approximate the transit time, since it plays an important role in the physical phenomena within the buncher gap. Assuming a correction term,

$$\omega t_b = \omega t_a + \theta \quad , \tag{2.9}$$

where

$$\theta \doteq \theta_g(1 + \delta) \qquad \theta_g \delta = \omega t_b - \omega t_a - \theta_g \quad , \tag{2.10}$$

and substituting Equation (2.9) into Equation (2.2), one obtains for $t = t_b$,

$$v_b = v_o + \frac{e}{m} \frac{V_1}{\omega d} \; 2 \sin\frac{\theta}{2} \; \sin\left(\omega t_b - \frac{\theta}{2}\right)$$

$$= v_o + \frac{1}{2} v_o a \frac{\sin\frac{\theta}{2}}{\frac{\theta_g}{2}} \; \sin\left(\omega t_b - \frac{\theta}{2}\right) \quad . \tag{2.11}$$

Expanding $\sin(\omega t_b - \frac{\theta}{2})$ by trigonometric identities and neglecting δ terms of higher order than the linear term, one can write Equation (2.11) as

$$\frac{v_b}{v_o} = 1 + \frac{1}{2}\mu a \sin\left(\omega t_b - \frac{\theta_g}{2}\right) + \frac{1}{2}\alpha\delta \cos\frac{\theta_g}{2} \sin\left(\omega t_b - \frac{\theta_g}{2}\right) - \frac{1}{4}\mu a\theta_g \cos\left(\omega t_b - \frac{\theta_g}{2}\right) , \tag{2.12}$$

where

$$\mu \equiv \sin\frac{\theta_g}{2} \Big/ \frac{\theta_g}{2} \quad . \tag{2.13}$$

Integrating Equation (2.2) and substituting in it the boundary conditions at $t = t_a$ and at $t = t_b$, and Equation (2.9), one obtains

$$d = \frac{v_o\theta}{\omega} + \frac{a\theta v_o}{2\omega\theta_g} \cos(\omega t_b - \theta) + \frac{a v_o}{2\omega\theta_g} \left[\sin(\omega t_b - \theta) - \sin\omega t_b\right] \quad . \tag{2.14}$$

Assuming

$$\cos\left[\omega t_b - \theta_g (1 + \delta)\right] \approx \cos(\omega t_b - \theta_g) \quad ,$$

$$\sin\left[\omega t_b - \theta_g (1 + \delta)\right] \approx \sin(\omega t_b - \theta_g) \quad ,$$

$$\therefore \sin\left[\omega t_b - \theta_g\delta\right] \approx \sin\omega t_b \quad ,$$

and neglecting the $a\delta$ term gives

$$\delta = \frac{a}{2\theta_g^2} \left[A \sin\omega t_b + B \cos\omega t_b\right] \quad , \tag{2.15}$$

where

$$A \equiv 1 - \cos\theta_g - \theta_g \sin\theta_g \quad , \tag{2.16a}$$

$$B \equiv \sin\theta_g - \theta_g \cos\theta_g \quad . \tag{2.16b}$$

Substitution of Equation (2.15) into Equation (2.12) leads to

$$\frac{v_b}{v_o} = 1 + \Delta + \frac{1}{2}\mu a \sin\left(\omega t_b - \frac{\theta_g}{2}\right) + M \sin 2\ (\omega t_b + \varphi) \quad , \qquad (2.17)$$

where

$$\Delta \equiv \frac{1}{2}\left(\frac{a}{2\theta_g}\right)^2 (\cos\theta_g - 1) \quad , \qquad (2.18a)$$

$$M \equiv \sqrt{P^2 + Q^2} \quad , \qquad (2.18b)$$

$$P \equiv \frac{1}{2}\left(\frac{a}{2\theta_g}\right)^2 (\sin 2\theta_g - \sin\theta_g - \theta_g + 2\theta_g \sin^2\theta_g) \quad , \qquad (2.18c)$$

$$Q \equiv -\frac{1}{2}\left(\frac{a}{2\theta_g}\right)^2 \left(1 + \cos\theta_g - 2\cos^2\theta_g - \theta_g \sin 2\theta_g\right) \quad , \qquad (2.18d)$$

$$2\varphi \equiv \tan^{-1}\frac{Q}{P} \quad . \qquad (2.18e)$$

Equation (2.15) is plotted in Figure 3 for $\theta_g = \pi$. It can be seen that while Equation (2.15) is a good approximation for small signals, it is a less satisfactory approximation for large signals.

2. Density Modulation

Substituting Equation (2.15) into Equation (2.10) and rewriting it, one obtains

$$\omega t_a = \omega t_b - \theta_g - \frac{a}{2\theta_g}\left[A \sin\omega t_b + B\cos\omega t_b\right] \quad . \qquad (2.19)$$

As in the graphic method, one can, by using Equation (2.8), express the normalized exit current as

$$\frac{i_b}{I_o} = 1 + \frac{a}{2\theta_g}\ (B \sin\omega t_b - A\cos\omega t_b) \quad . \qquad (2.20)$$

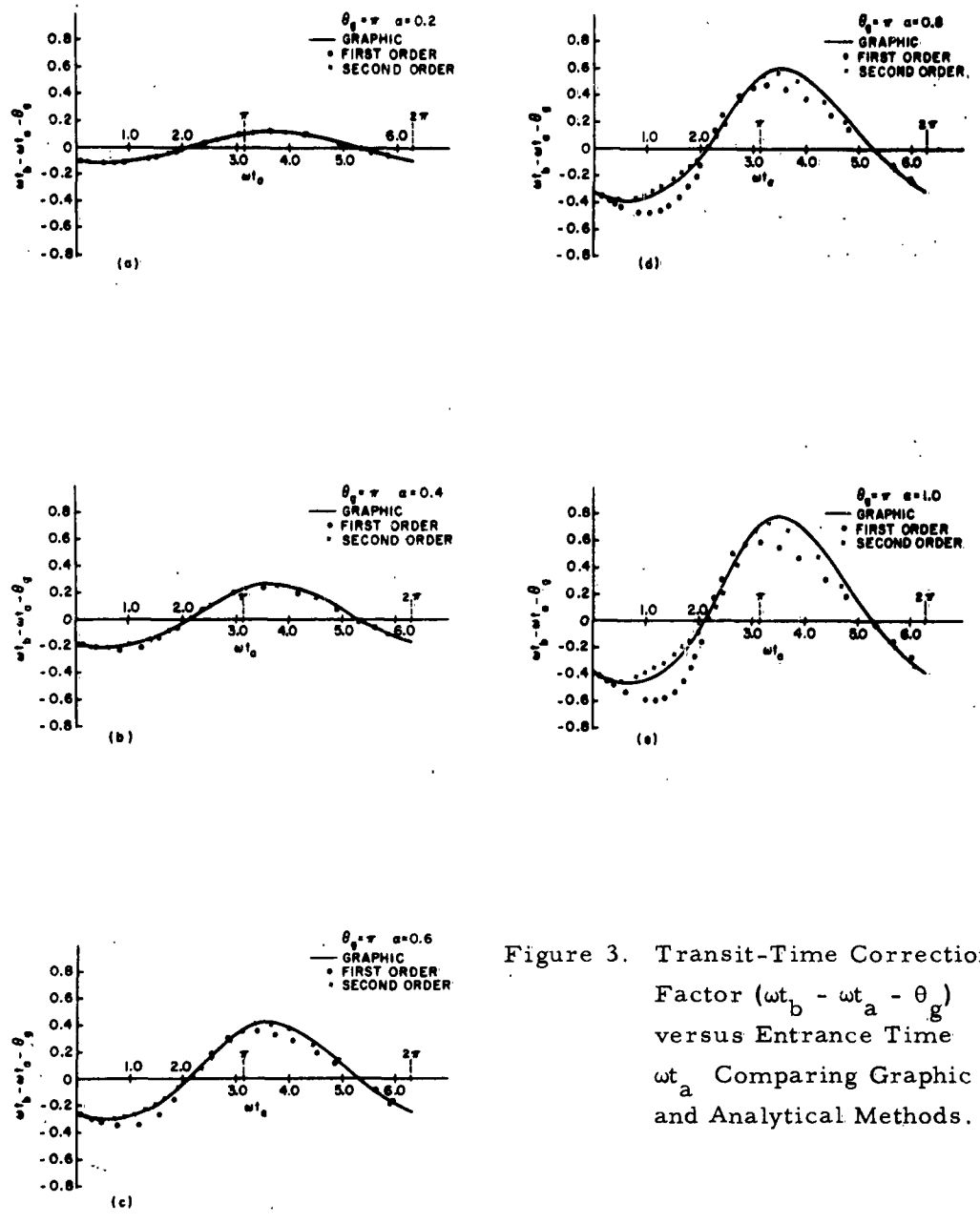

Figure 3. Transit-Time Correction Factor ($\omega t_b - \omega t_a - \theta_g$) versus Entrance Time ωt_a Comparing Graphic and Analytical Methods.

$$\theta \equiv \theta_g(1 + \delta_1 + \delta_2) \quad , \tag{2.23}$$

where δ_1 is given by Equation (2.15). Substituting Equation (2.23) into Equation (2.14), assuming

$$\cos(\omega t_b - \theta) \approx \cos(\omega t_b - \theta_g - \theta_g\delta_1) + \theta_g\delta_2 \sin(\omega t_b - \theta_g - \theta_g\delta_1) \quad ,$$

$$\sin(\omega t_b - \theta) \approx \sin(\omega t_b - \theta_g - \theta_g\delta_1) - \theta_g\delta_2 \cos(\omega t_b - \theta_g - \theta_g\delta_1) \quad ,$$

and neglecting $a\delta_2$ and δ_2^2 terms, one obtains

$$\delta_2 = -\delta_1 + \frac{a}{2\theta_g^2}\left[\sin\omega t_b - \sin(\omega t_b - \theta_g - \theta_g\delta_1) - \theta_g(1+\delta_1)\cos(\omega t_b - \theta_g - \theta_g\delta_1)\right] \quad , \tag{2.24a}$$

and

$$\omega t_b - \omega t_a - \theta_g = \frac{a}{2\theta_g}\left[\sin\omega t_b - \sin(\omega t_b - \theta_g - \theta_g\delta_1) - \theta_g(1+\delta_1)\cos(\omega t_b - \theta_g - \theta_g\delta_1)\right] \quad . \tag{2.24b}$$

Equation (2.24b) is plotted in Figure 3 for $\theta_g = \pi$. It can be seen from this figure that Equation (2.24b) gives a fair approximation to the graphic results for larger signal values.

1. Velocity Modulation

Substitution of Equation (2.24a) into Equation (2.13) leads, after some rearrangement, to

$$\frac{v_b}{v_o} = 1 + \frac{1}{2}\left(\frac{a}{2\theta_g}\right)^2(\cos\theta_g - 1) - \frac{1}{4}\left(\frac{a}{2\theta_g}\right)^4\left[A^2 + B^2 - AB\sin 2\theta_g - \frac{B^2 - A^2}{2}\cos 2\theta_g\right]$$

$$+\left(\frac{a}{2\theta_g}\right)\left[\sin\theta_g - \frac{\theta_g}{4}\left(\frac{a}{2\theta_g}\right)^2 (2A + A\cos 2\theta_g - B\sin 2\theta_g)\right] \sin\omega t_b$$

$$-\left(\frac{a}{2\theta_g}\right)\left[1 - \cos\theta_g + \frac{\theta_g}{4}\left(\frac{a}{2\theta_g}\right)^2 (2B - A\sin 2\theta_g - B\cos 2\theta_g)\right] \cos\omega t_b$$

$$+\frac{1}{2}\left(\frac{a}{2\theta_g}\right)^2 B\left\{\cos\theta_g - A\sin\theta_g + \frac{1}{2}\left(\frac{a}{2\theta_g}\right)^2 \left[(A^2+B^2)\sin 2\theta_g - 2AB\right]\right\} \sin 2\omega t_b$$

$$-\frac{1}{2}\left(\frac{a}{2\theta_g}\right)^2 \left\{A\cos\theta_g + B\sin\theta_g - \frac{1}{2}\left(\frac{a}{2\theta_g}\right)^2 \left[(A^2+B^2)\cos 2\theta_g + A^2 - B^2\right]\right\} \cos 2\omega t_b$$

$$+\frac{\theta_g}{4}\left(\frac{a}{2\theta_g}\right)^3 (A\cos 2\theta_g + B\sin 2\theta_g) \sin 3\omega t_b$$

$$-\frac{\theta_g}{4}\left(\frac{a}{2\theta_g}\right)^3 (A\sin 2\theta_g - B\cos 2\theta_g) \cos 3\omega t_b + \frac{1}{8}\left(\frac{a}{2\theta_g}\right)^4 \left[(B^2 - A^2)\sin 2\theta_g\right.$$

$$\left. + 2AB\cos 2\theta_g\right] \sin 4\omega t_b + \frac{1}{8}\left(\frac{a}{2\theta_g}\right)^4 \left[(B^2 - A^2)\cos 2\theta_g - 2AB\sin 2\theta_g\right] \cos 4\omega t_b \ . \tag{2.25}$$

Equation (2.25) is plotted in Figure 4 for $\theta_g = \pi$ for comparison with the graphic method, and in Figures 5 and 6 with the d-c gap transit angle as a parameter. It can be seen from Figure 4 that Equation (2.25) approximates the graphic method fairly well up to large signals. Figures 5 and 6 show the effect of the d-c gap transit angle on the velocity modulation. As expected, it can be seen that the modulation effect decreases, because of partial cancellation, as the d-c gap transit angle is increased.

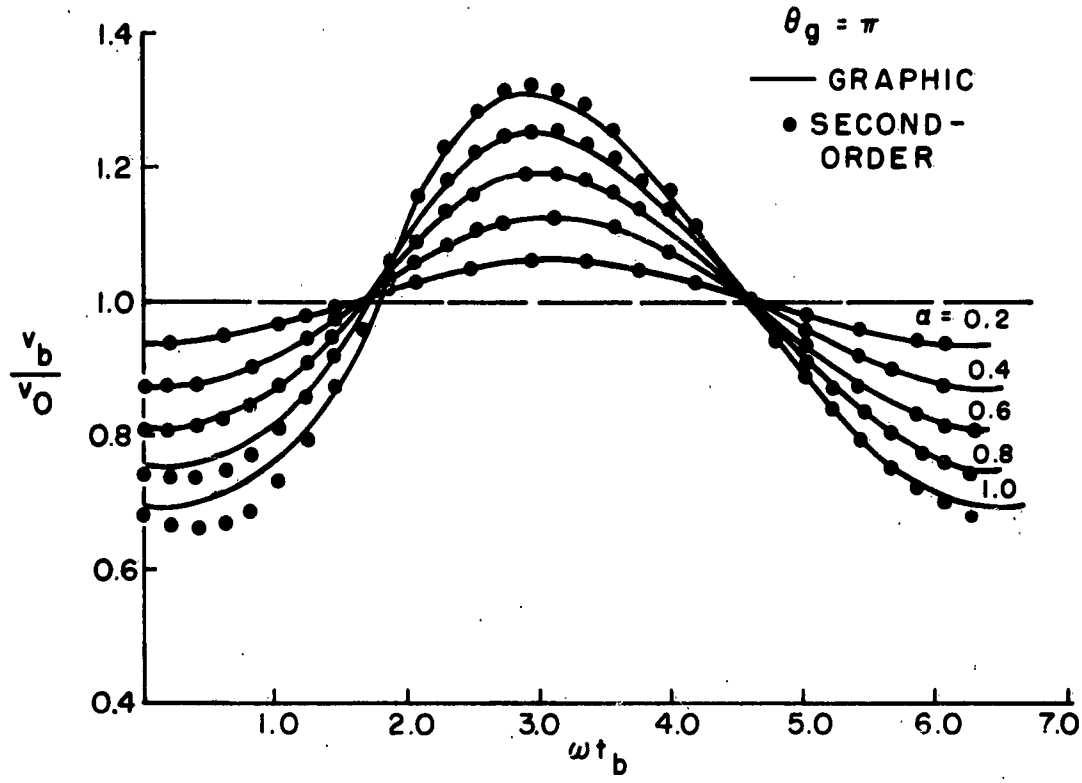

Figure 4. Normalized Exit Velocity v_b/v_o versus Exit Time ωt_b, Comparing Graphic and Second-Order Methods.

2. Density Modulation

Differentiating Equation (2.24b) and neglecting third-order terms, one obtains

$$\frac{i_b}{I_o} = \frac{d\omega t_a}{d\omega t_b} = 1 - \frac{a}{2\theta_g}\left[\cos\omega t_b - \cos(\omega t_b - \theta_g) + \theta_g\left(1 - \theta_g\frac{d\delta_1}{d\omega t_b}\right.\right.$$

$$\left.\left. - \theta_g\delta_1\frac{d\delta_1}{d\omega t_b}\right)\sin(\omega t_b - \theta_g) - \theta_g^2\left(\delta_1 + \delta_1^2 - \theta_g\delta_1\frac{d\delta_1}{d\omega t_b}\right)\cos(\omega t_b - \theta_g)\right] \quad (2.26)$$

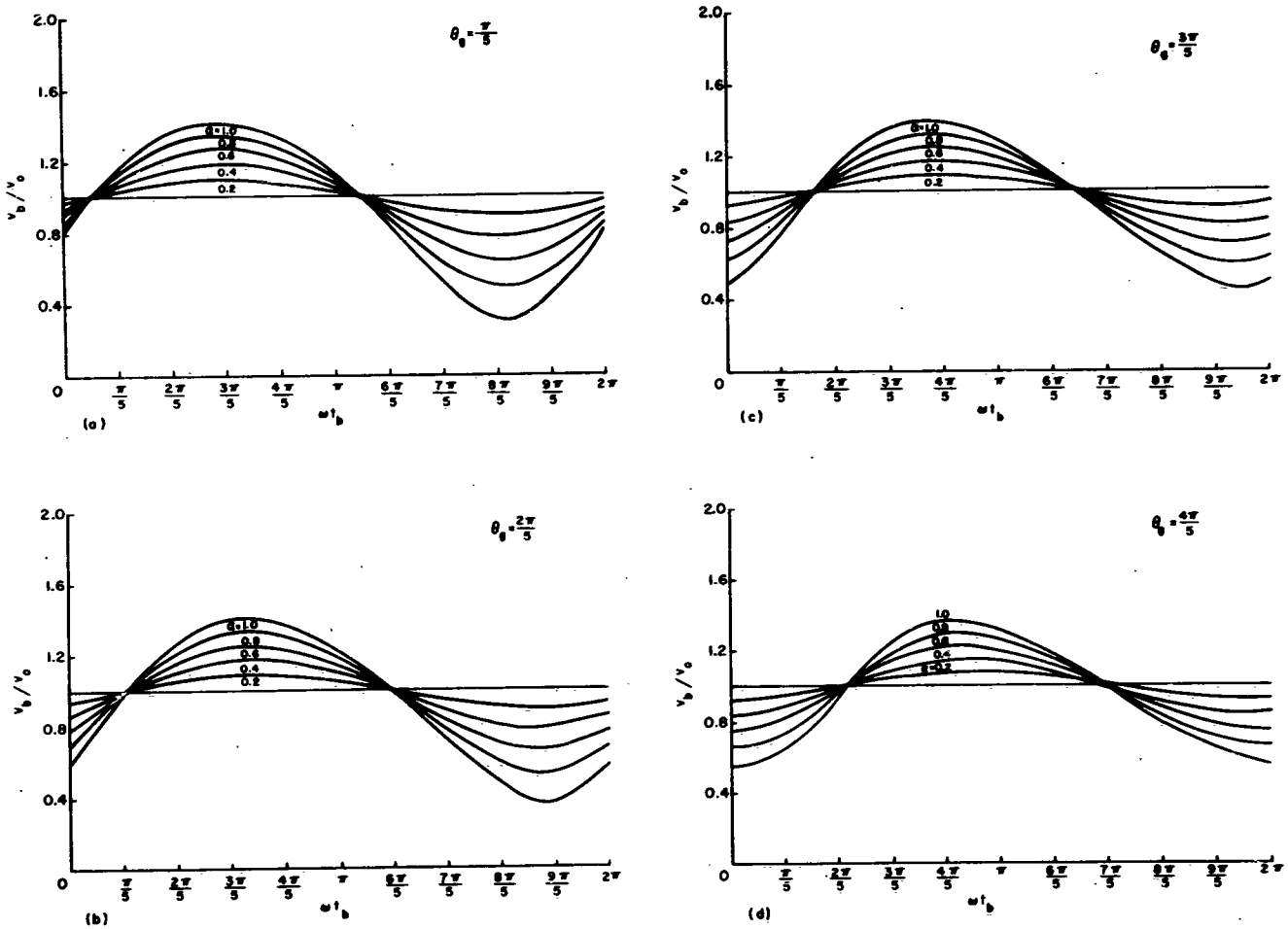

Figure 5. Normalized Exit Velocity v_b/v_o versus Exit Time ωt_b for Different D-C Gap Transit Angles and Depths of Modulation.

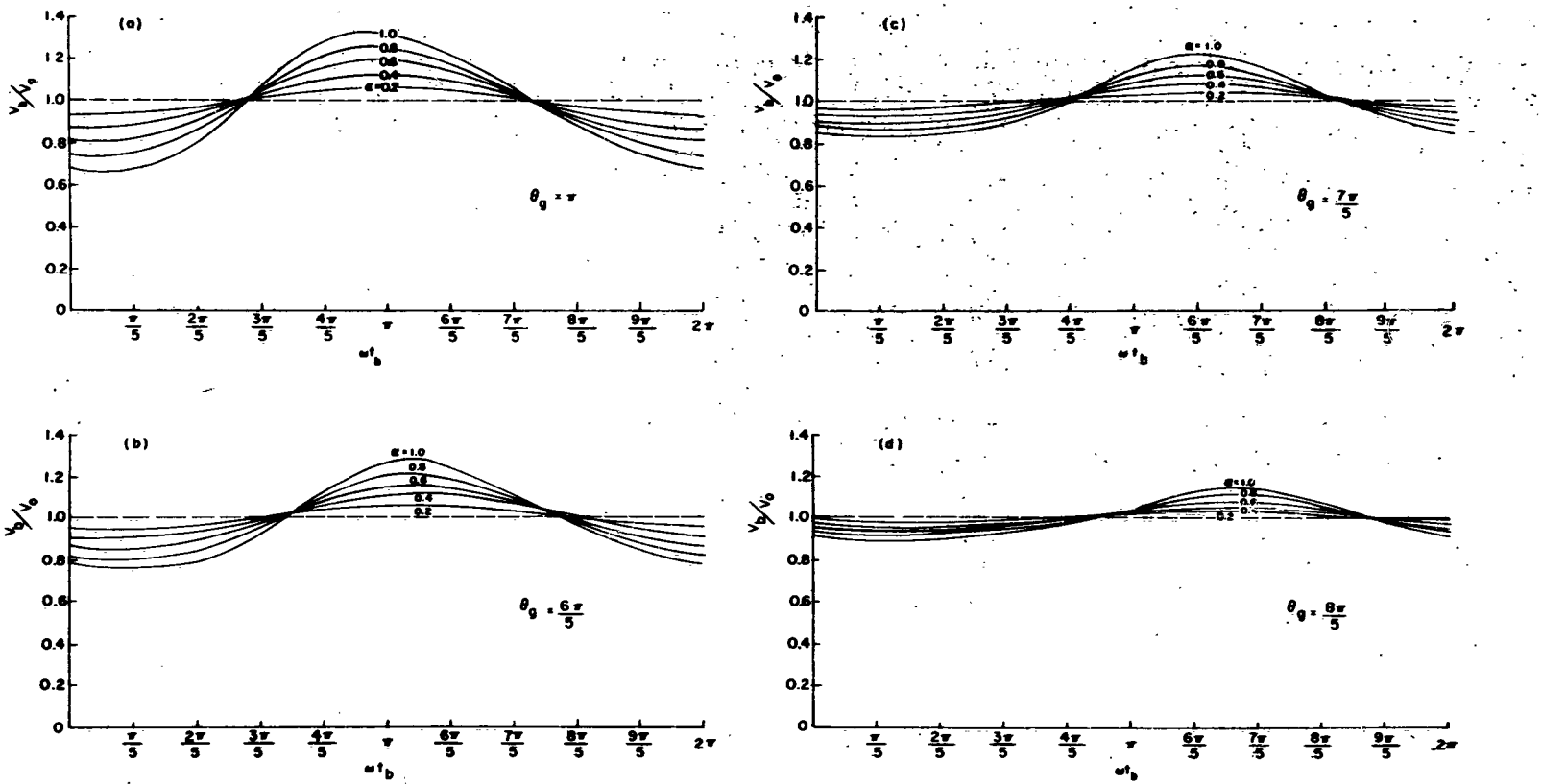

Figure 6. Normalized Exit Velocity v_b/v_o versus Exit Time ωt_b for Different D-C Gap Transit Angles and Depths of Modulation.

Substituting Equation (2.15) and its derivative with respect to ωt_b and rearranging terms gives

$$\frac{i_b}{I_o} = 1 + \left(\frac{a}{2\theta_g}\right)\left\{B + \frac{1}{2}\left(\frac{a}{2\theta_g}\right)^2\left[(A^2 + B^2 + \theta_g AB)\sin\theta_g - \frac{(A^2 - B^2)\theta_g}{2}\cos\theta_g\right]\right\}\sin\omega t_b$$

$$-\left(\frac{a}{2\theta_g}\right)\left\{A - \frac{1}{2}\left(\frac{a}{2\theta_g}\right)^2\left[(A^2 + B^2 - \theta_g AB)\cos\theta_g - \frac{(A^2 - B^2)}{2}\theta_g\sin\theta_g\right]\right\}\cos\omega t_b$$

$$+\left(\frac{a}{2\theta_g}\right)^2\theta_g(A\cos\theta_g + B\sin\theta_g)\sin 2\omega t_b - \left(\frac{a}{2\theta_g}\right)^2\theta_g(A\sin\theta_g - B\cos\theta_g)\cos 2\omega t_b$$

$$+\left(\frac{a}{2\theta_g}\right)^3\left[AB\cos\theta_g - \frac{(A^2 - B^2)}{4}\theta_g\cos\theta_g + \frac{(B^2 - A^2 - \theta_g AB)}{2}\sin\theta_g\right]\sin 3\omega t_b$$

$$-\left(\frac{a}{2\theta_g}\right)^3\left[AB\sin\theta_g - \frac{(A^2 - B^2)}{4}\theta_g\sin\theta_g - \frac{(B^2 - A^2 - \theta_g AB)}{2}\cos\theta_g\right]\cos 3\omega t_b \quad . \tag{2.27}$$

Equation (2.27) is plotted in Figure 7 for $\theta_g = \pi$ for comparison with the graphic method, and in Figures 8 and 9 with the d-c gap transit angle as a parameter. Again it can be seen from Figure 7 that Equation (2.27) approximates the graphic method fairly well up to large signals. Figures 8 and 9 show the effect of the d-c gap transit angle on density modulation. As in the graphic method, it can be seen that density modulation first increases with the d-c gap transit angle and then decreases.

It should be observed that the second-order analysis introduces harmonics up to the third harmonic in the current expression, and up to

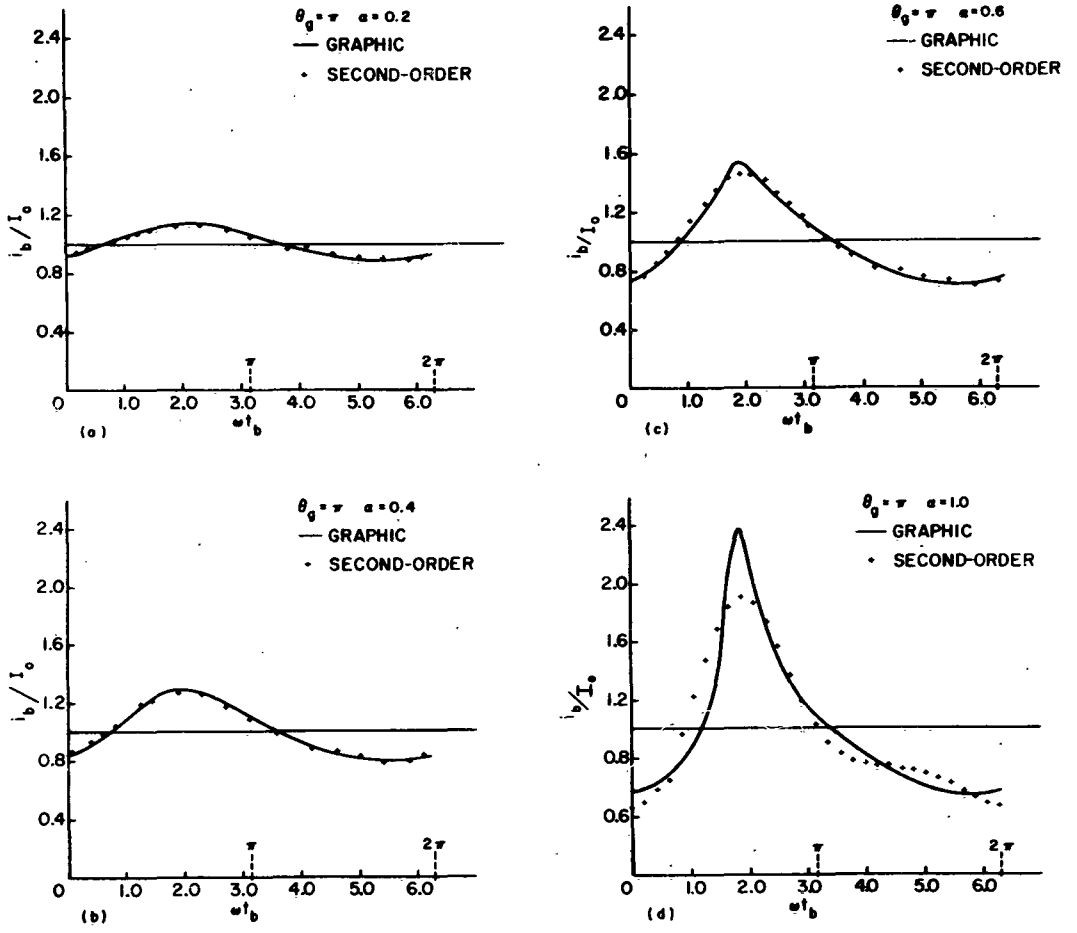

Figure 7. Normalized Exit Current i_b/I_o versus Exit Time ωt_b Comparing Graphic and Second-Order Methods.

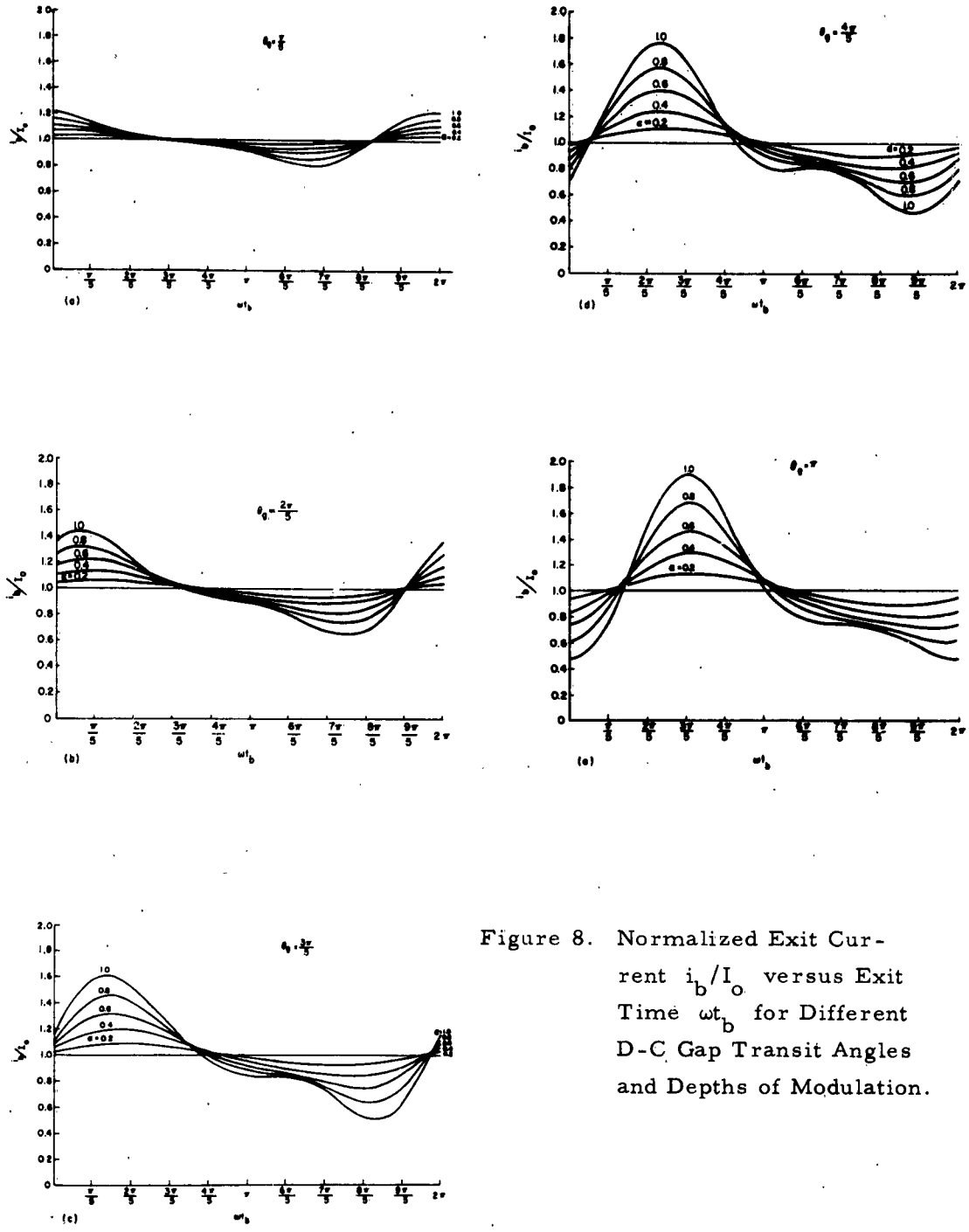

Figure 8. Normalized Exit Current i_b/I_o versus Exit Time ωt_b for Different D-C Gap Transit Angles and Depths of Modulation.

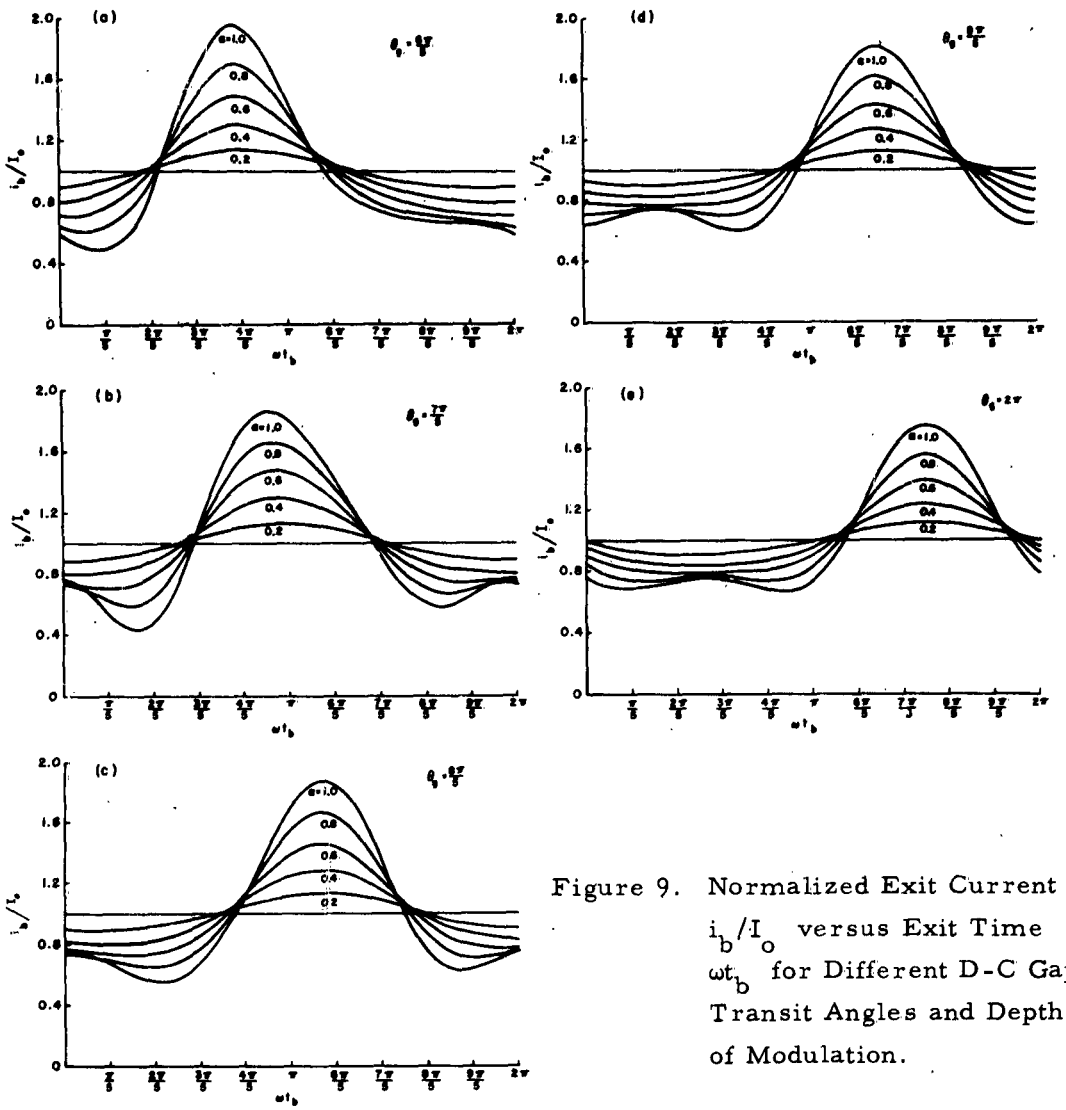

Figure 9. Normalized Exit Current i_b/I_o versus Exit Time ωt_b for Different D-C Gap Transit Angles and Depths of Modulation.

the fourth harmonic in the velocity expression, and that it extends the approximation to larger signals.

III. ANALYSIS OF THE FIRST DRIFT SPACE

The electron beam enters the drift space both velocity-modulated and density-modulated, and it drifts in a field-free space. This drift action produces further bunching of electrons, thereby increasing the harmonic content of the beam current. In his analysis, Webster neglects the density modulation produced in the gap, since his analysis deals with small signals. It was shown in the previous chapter that for large signals, the density modulation in the first gap was considerable, therefore the present analysis will consider the density modulation in the gap. It will include only first-order terms, however, and will not consider space-charge debunching. Although the present analysis is not valid after crossover, it will be extended beyond crossover; for qualitatively, it anticipates important trends.

The time at plane c (see Figure 1) can be expressed as

$$\omega t_c = \omega t_b + \frac{\omega l}{v_b} \quad . \tag{3.1}$$

Shifting the reference of time gives

$$\omega t_b' = \omega t_b - \frac{\theta_g}{2} \quad . \tag{3.2}$$

Dropping the prime, and neglecting the second-harmonic term in Equation (2.17), one obtains from Equation (3.1),

$$\omega t_c - \phi = \omega t_b - X \sin \omega t_b \quad , \tag{3.3}$$

where

$$\phi \equiv \theta_o (1 - \Delta) + \frac{\theta_g}{2} \quad , \tag{3.4a}$$

$$\theta_o \equiv \frac{\omega l}{v_o} \quad , \tag{3.4b}$$

$$X \equiv \frac{1}{2} \mu a \theta_o \quad . \tag{3.4c}$$

Equation (3.3) shows the functional relationship between the entrance and exit times of the drift space.

A. DENSITY

The principle of conservation of charge for the drift space states that

$$i_b \, d\omega t_b = i_c \, d\omega t_c \quad . \tag{3.5}$$

One can express the current at plane c as a Fourier series given by

$$i_c = A_o + \sum_{n=1}^{\infty} A_n \cos n(\omega t_c - \phi) + B_n \sin n(\omega t_c - \phi) \quad , \tag{3.6}$$

where

$$A_o = I_o \quad , \tag{3.7a}$$

$$A_n = \frac{1}{\pi} \int_o^{2\pi} i_c \cos n(\omega t_c - \phi) \, d\omega t_c \quad , \tag{3.7b}$$

$$B_n = \frac{1}{\pi} \int_o^{2\pi} i_c \sin n(\omega t_c - \phi) \, d\omega t_c \quad . \tag{3.7c}$$

If one uses Equations (2.20), (3.2), (3.3) and (3.5), then Equations (3.7b and c) become

$$A_n = \frac{I_o}{\pi} \int_o^{2\pi} \left[1 + N \sin\left(\omega t_b + \psi + \frac{\theta_g}{2}\right)\right] \cos n\left[\omega t_b - X \sin \omega t_b\right] d\omega t_b \quad , \quad (3.8a)$$

$$B_n = \frac{I_o}{\pi} \int_o^{2\pi} \left[1 + N \sin\left(\omega t_b + \psi + \frac{\theta_g}{2}\right)\right] \sin n\left[\omega t_b - X \sin \omega t_b\right] d\omega t_b \quad . \quad (3.8b)$$

Using Bessel function expressions[4] for trigonometric functions, integrating, and using recursion formulas for Bessel functions, one obtains

$$\frac{i_c}{I_o} = 1 + 2\left[1 + \frac{N}{X} \sin\left(\psi + \frac{\theta_g}{2}\right)\right] \sum_{n=1}^{\infty} J_n(nX) \cos n\,(\omega t_c - \phi) \quad ,$$

$$+ 2N \cos\left(\psi + \frac{\theta_g}{2}\right) \sum_{n=1}^{\infty} \frac{J_n'(nX)}{n} \sin n(\omega t_c - \phi) \quad . \quad (3.9)$$

It can be seen from Equation (3.9) that the beam current at plane c is rich in harmonics and that each harmonic can be calculated for any specified condition from the equation. Equation (3.9) reduces to that of Webster for small signals. It should also be noted that an additional phase angle, β_n, is introduced by the two independent components of each harmonic, given by

$$\tan \beta_n = \frac{\left[1 + \frac{N}{X} \sin\left(\psi + \frac{\theta_g}{2}\right)\right] n J_n(nX)}{N \cos\left(\psi + \frac{\theta_g}{2}\right) J_n'(nX)} \quad . \quad (3.10)$$

Figures 10a, 11a, and 12a show the first three harmonics, and Figures 10b, 11b, and 12b show the phase angles of these harmonics as a function of the bunching parameter (X), with the depth of modulation as a parameter, for $\theta_g = \pi$. The maximum amplitudes of the fundamental current for different depths of modulation (see Figure 10a) are seen to be greater than the usual value of 1.16, which was also predicted in a ballistic analysis by Webber[5] that included space-charge effects.

The first three harmonics are also plotted in Figure 13 as functions of the drift angle θ_o for $\theta_g = \pi$. Qualitatively Figure 13a resembles the experimental curves of Mihran, who also observed a saturation of the maxima of the fundamental current, although he did not explain the resaon for this.

Although space-charge effects were neglected in this study, the results obtained parallel those of others within the range of validity. A comparison with Solymar's[6] results is shown in Figure 14, where it was assumed that

$$\beta_p Z = \frac{\theta_o}{k} \quad . \tag{3.11}$$

B. VELOCITY

The transit time through the drift space can be assumed to be

$$\omega t_b - (\omega t_c - \phi) = \sum_{l=1}^{\infty} b_l \sin l(\omega t_c - \phi) \quad , \tag{3.12}$$

where

$$b_l = \frac{1}{\pi} \int_{-\pi}^{\pi} \left[\omega t_b - (\omega t_c - \phi)\right] \sin l(\omega t_c - \phi)\, d(\omega t_c - \phi) \quad . \tag{3.13}$$

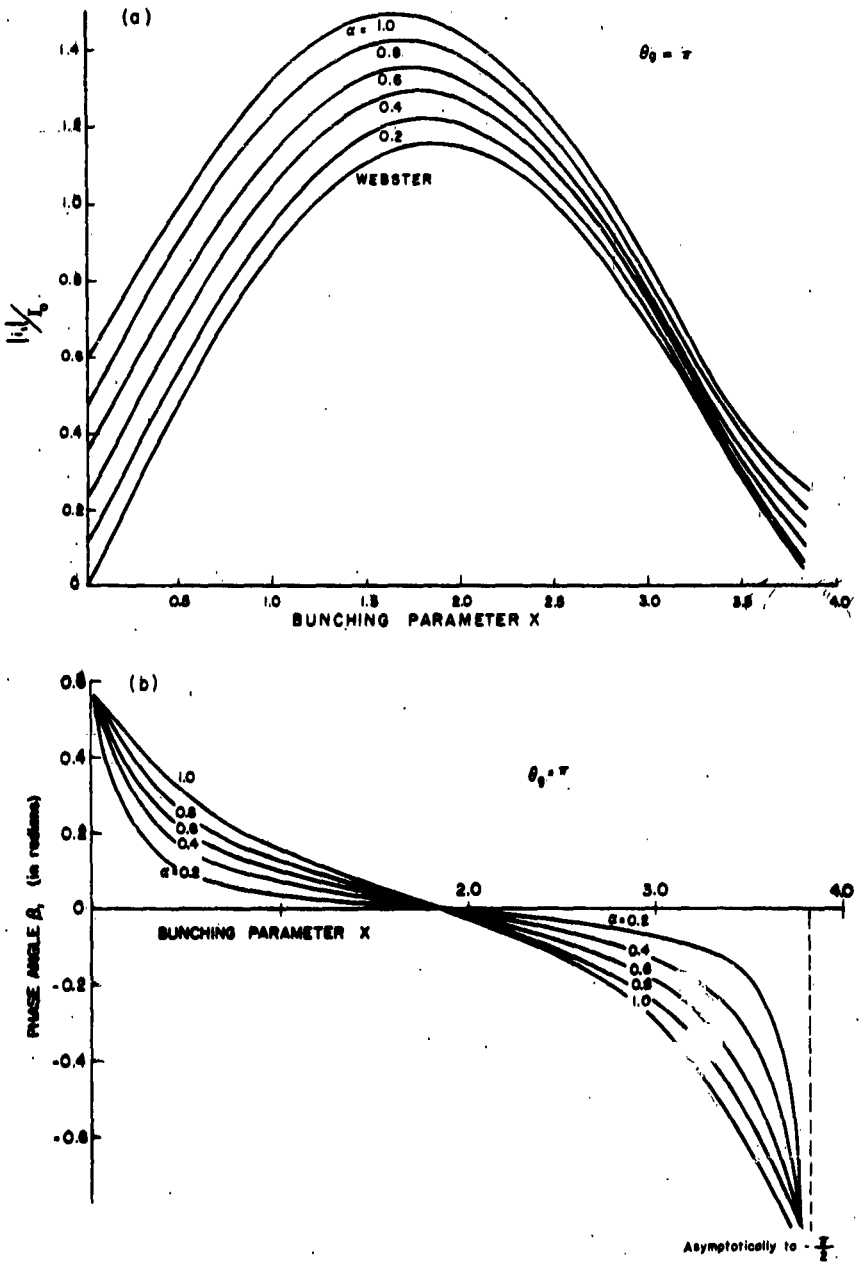

Figure 10. (a) Absolute Value of Normalized Fundamental Current $|i_1|/I_o$ versus Bunching Parameter X , (b) Phase Angle, β , versus Bunching Parameter X .

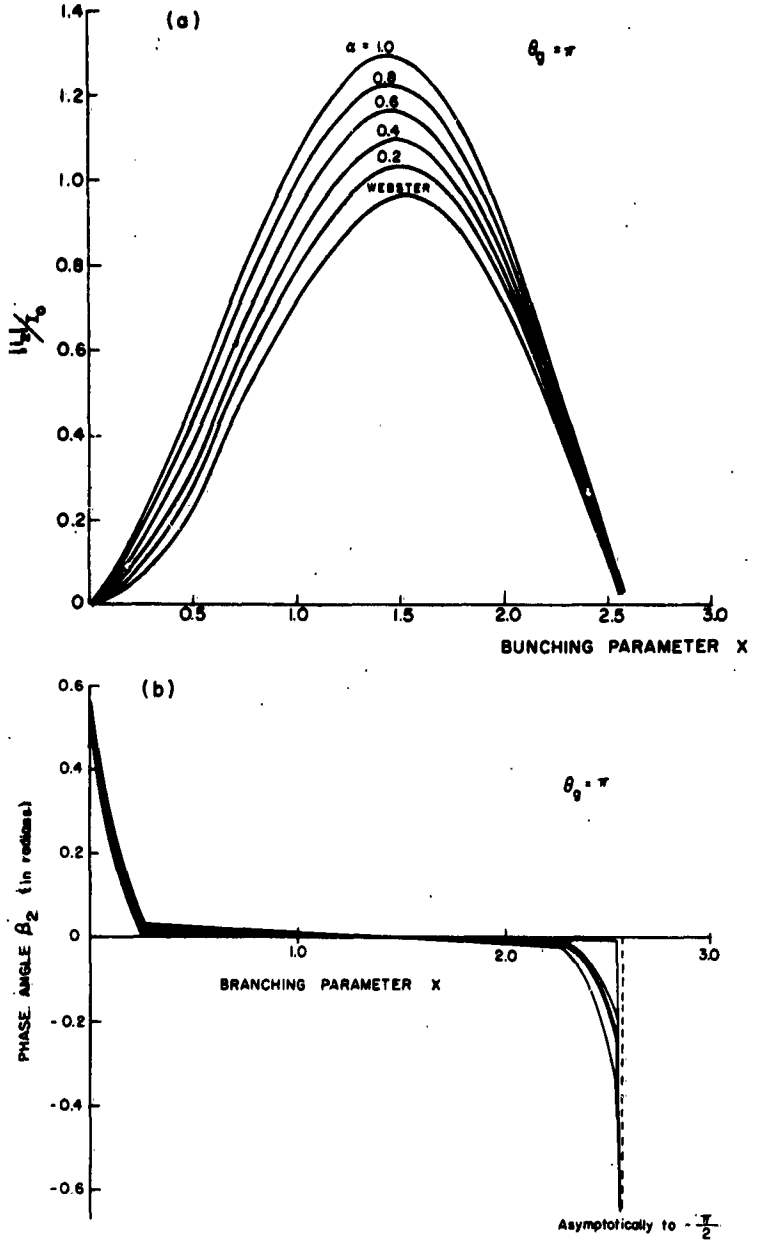

Figure 11. (a) Absolute Value of Normalized Second-Harmonic Current $|i_2|/I_o$ versus Bunching Parameter X , (b) Phase Angle β_2 versus Bunching Parameter X , in Drift Space.

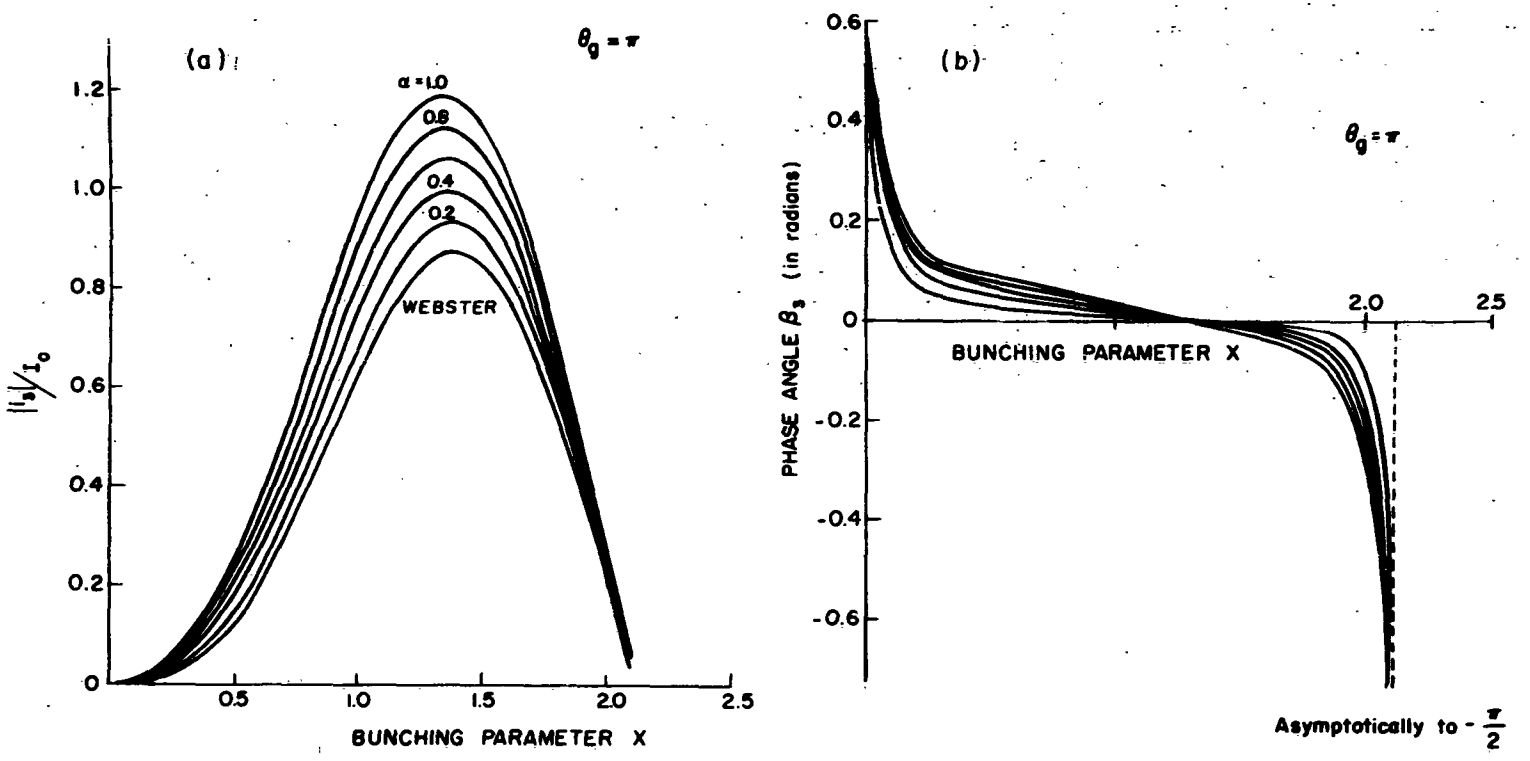

Figure 12. (a) Absolute Value of Normalized Third-Harmonic Current $|i_3|/I_o$ versus Bunching Parameter X, (b) Phase Angle β_3 versus Bunching Parameter X in the Drift Space.

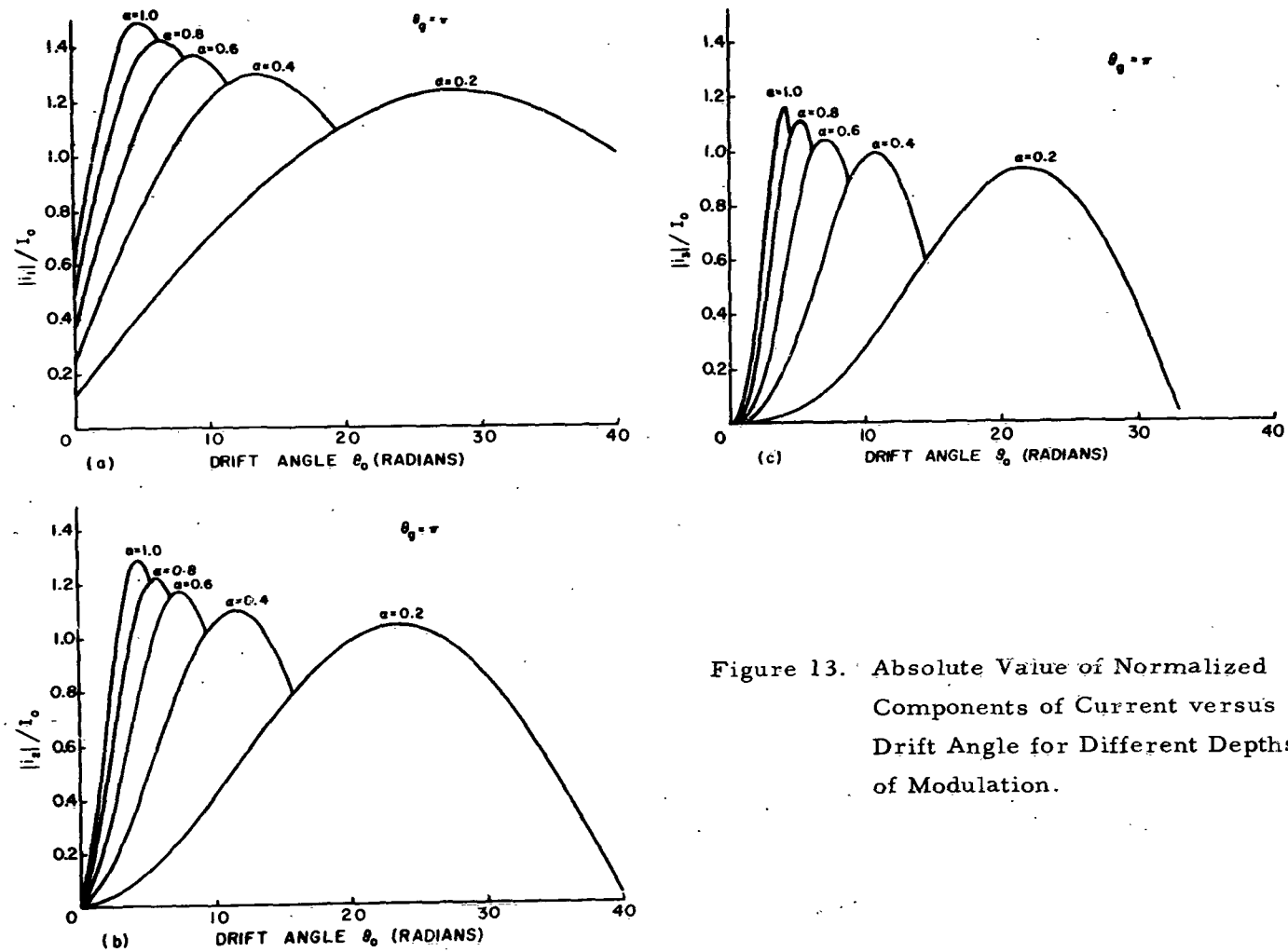

Figure 13. Absolute Value of Normalized Components of Current versus Drift Angle for Different Depths of Modulation.

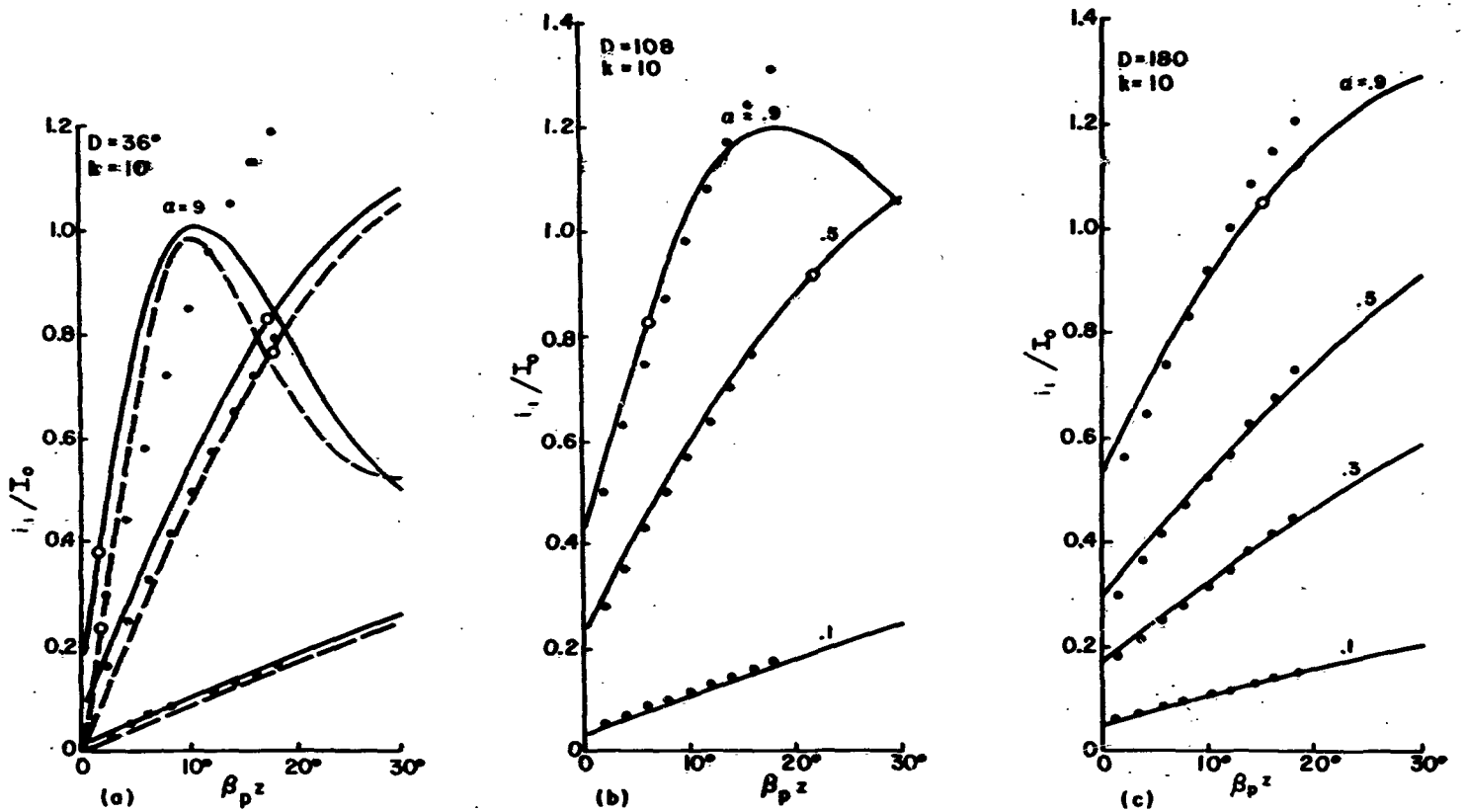

Figure 14. Normalized Fundamental Current i_1/I_o versus Normalized Drift Distance $\beta_p z$ for Different D-C Gap Transit Angles. (The curves shown are those calculated by Solymar. The solid dots are the points calculated from Equation (3.9) of this study.)

Integrating Equation (3.13) by parts and substituting Equation (3.3), one obtains

$$\omega t_b = \omega t_c - \phi + \sum_{l=1}^{\infty} \frac{2}{l} J_l(lX) \sin l(\omega t_c - \phi) \quad . \qquad (3.14)$$

Equation (3.14) shows the functional relationship between the entrance time and the exit time of the drift space. Figure 15 shows a comparison of Equation (3.3) and (3.14), where only the first three harmonics are included in Equation (3.14).

Since the drift space is assumed to be field-free, the equation of motion becomes

$$\ddot{z} = 0 \quad . \qquad (3.15)$$

Integrating Equation (3.15) and applying the boundary conditions at $t = t_b$, substituting Equation (2.17) with second harmonic terms neglected and Equations (3.2) and (3.14), one obtains

$$\frac{v_c}{v_o} = 1 + \Delta + \frac{1}{2} \mu a \sin \left[(\omega t_c - \phi) + \sum_{l=1}^{\infty} \frac{2J_l(lX)}{l} \sin l(\omega t_c - \phi) \right] \quad . \qquad (3.16)$$

Equation (3.16) is plotted in Figure 16 with depth of modulation as a parameter for $\theta_g = \pi$ and $\theta_o = \pi/2$.

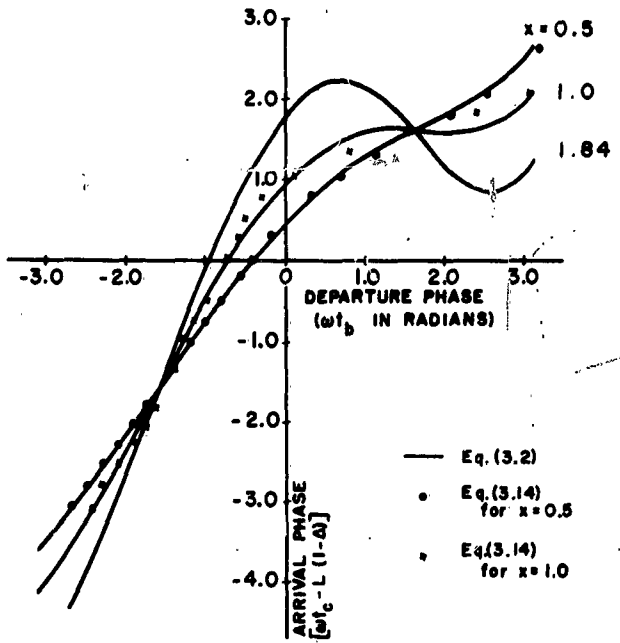

Figure 15. Arrival Phase, $\omega t_c - L(1 - \Delta)$, versus Departure Phase ωt_b for the Drift Space for Different Bunching Parameters.

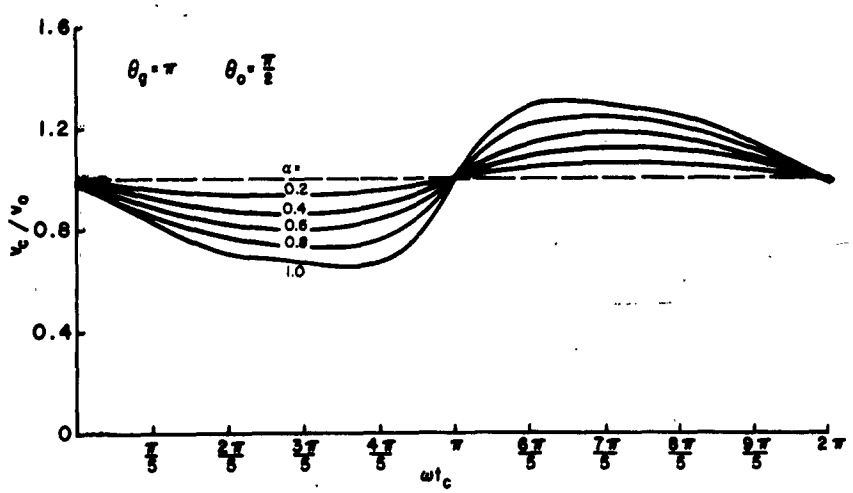

Figure 16. Normalized Exit Velocity v_c/v_o versus Exit Time ωt_c at End of Drift Space for Different Depths of Modulation.

IV. ANALYSIS OF THE SECOND GAP

It is well known that an electron beam has nonlinear characteristics and is rich in harmonics at the end of a klystron drift space. Analysis of the beam through a second gap, therefore, becomes complicated, because of overtaking and the multivalued nature of transit times. Analytical formulas, which can be derived from such an analysis by making approximations similar to those made in Chapter II, become implicit expressions of entrance and exit times as well as of various operating parameters.

For these reasons, only computer solutions are obtained in the remaining parts of this study. Thus the main effort will be directed to computing velocities and currents of a spent beam as functions of time rather than formulating them analytically. This will permit realization of the purpose of this study: (1) to investigate the characteristics of a spent beam in a two-cavity klystron and (2) to investigate the velocity-filtering capabilities of a r-f gap, using these characteristics as initial conditions. Additional information will be obtained about power output and tuning conditions of the catcher gap of a two-cavity klystron for optimum operation, since both velocities and currents will be known at the entrance to and at the exit of the second gap. Numerical calculations of kinetic energy will suffice for this purpose.

A. COMPUTER PROBLEM

Fundamental current at the entrance to the second gap can be expressed, by combining its two components, (see Equations 3.9 and 3.10), as

$$i_{c_1} = k \sin(\omega t - \phi + \beta_1) \quad , \tag{4.1}$$

where k is the amplitude of the fundamental. Assuming a voltage V_2 across the second gap with a phase angle Γ_2 with respect to fundamental current, one can write the equation of motion for this gap as

$$\ddot{z} = -\frac{e}{m} \frac{V_2}{d} \sin(\omega t + \xi) \quad , \tag{4.2}$$

where

$$\xi = -\phi + \beta_1 + \Gamma_2 \tag{4.3}$$

Integrating Equation (4.2) twice, substituting initial conditions at $t = t_c$, and normalizing with respect to d-c velocity, one obtains

$$\dot{Z} = \frac{v_c}{v_o} + \frac{a_2}{2\theta_{g_2}} \left[\cos(\omega t + \xi) - \cos(\omega t_c + \xi)\right] \quad , \tag{4.4}$$

$$Z = \left[\frac{v_c}{v_o} - \frac{a_2}{2\theta_{g_2}} \cos(\omega t_c + \xi)\right] (t - t_c) + \frac{a_2}{2\omega\theta_{g_2}} \left[\sin(\omega t + \xi) - \sin(\omega t_c + \xi)\right] \quad , \tag{4.5}$$

where a_2 is the ratio of the assumed voltage V_2 to the d-c beam voltage V_o, and where the d-c gap transit angle, θ_{g_2}, is defined by

$$\theta_{g_2} \equiv \frac{\omega d_2}{v_o} \quad . \tag{4.6}$$

Applying boundary conditions at $t = t_d$ to Equations (4.4) and (4.5) and multiplying Equation (4.5) by ω gives the following equations:

$$\theta_{g_2} = \left[\frac{v_c}{v_o} - \frac{a_2}{2\theta_{g_2}} \cos(\omega t_c + \xi)\right] (\omega t_d - \omega t_c) + \frac{a_2}{2\theta_{g_2}} \left[\sin(\omega t + \xi) - \sin(\omega t_c + \xi)\right] , \tag{4.7}$$

$$\frac{v_d}{v_o} = \frac{v_c}{v_o} + \frac{a_2}{2\theta_{g_2}} \left[\cos(\omega t_d + \xi) - \cos(\omega t_c + \xi)\right] . \tag{4.8}$$

Equation (4.7) is used to compute the exit time ωt_d, and Equation (4.8) to compute the normalized exit velocity v_d/v_o for a given entrance time ωt_c and for different gap parameters of a_2, θ_{g_2}, and Γ_2.

The normalized exit current is found by using the principle of conservation of charge, and is expressed as,

$$\frac{i_d}{I_o} = \frac{\frac{i_c}{I_o}}{\left|\frac{d\omega t_d}{d\omega t_c}\right|} . \tag{4.9}$$

The denominator of Equation (4.9) is derived by differentiating Equation (4.7) with respect to ωt_c, and it is given by

$$\frac{d\omega t_d}{d\omega t_c} = \frac{\frac{v_c}{v_o} - \frac{a_2}{2\theta_{g_2}} (\omega t_d - \omega t_c) \sin(\omega t_c + \xi) - (\omega t_d - \omega t_c) \frac{d}{d\omega t_c}\left(\frac{v_c}{v_o}\right)}{\frac{v_c}{v_o} + \frac{a_2}{2\theta_{g_2}} \left[\cos(\omega t_d + \xi) - \cos(\omega t_c + \xi)\right]} . \tag{4.10}$$

It should be noted that the normalized entrance velocity v_c/v_o given by Equation (3.16) is a single-valued function of ωt_c and cannot be used for

large signals. On the other hand, the normalized entrance current i_c/I_o, given in series form by Equation (3.9), is not suitable for a computer.

In the first drift space one has

$$i_b\, d\omega t_b = i_c\, d\omega t_c \quad , \tag{3.5}$$

$$\ddot{z} = 0 \quad , \tag{3.15}$$

$$\frac{i_b}{I_o} = 1 + N \sin(\omega t_b + \psi) \quad , \tag{2.21}$$

$$\frac{v_b}{v_o} = 1 + \Delta + \frac{1}{2}\mu a \sin\left(\omega t_b - \frac{\theta_g}{2}\right) + M \sin 2(\omega t_b + \psi) \quad . \tag{2.17}$$

Defining

$$x_k = \omega t_b - \frac{\theta_g}{2} \tag{4.11}$$

and neglecting the second-harmonic term in Equation (2.17), one can derive the following formulas, which take the multivaluedness into account, and which can be used in a computer:

$$\omega t_c = x_k + \frac{\theta_{o1}}{1 + \Delta + \frac{1}{2}\mu a \sin x_k} \quad , \tag{4.12}$$

$$\Delta t_k = \frac{d\omega t_c}{dx_k} = 1 - \frac{\frac{1}{2}\theta_{o1}\mu a \cos x_k}{\left(1 + \Delta + \frac{1}{2}\mu a \sin x_k\right)^2} \quad , \tag{4.13}$$

$$\frac{i_c}{I_o} = \sum_k \frac{1 + N \sin(x_k + \psi + \theta_g/2)}{|\Delta t_k|} \quad , \tag{4.14}$$

$$\frac{v_c}{v_o} = 1 + \Delta + \frac{1}{2} \mu a \sin x_k \quad , \tag{4.15}$$

$$\frac{d}{d\omega t_c}\left(\frac{v_c}{v_o}\right) = \frac{\frac{1}{2} \mu a \cos x_k}{\Delta t_k} \quad . \tag{4.16}$$

Equation (4.14) gives the sum of the series in Equation (3.9) and is easily applicable to computer programming. Equation (4.15) is likewise multi-valued and can therefore also be used for large signals.

It should be noted that Equation (4.9) does not contain the summation sign; therefore it gives the component of the normalized exit current i_d/I_o which corresponds to an increment of a specific entrance time ωt_c. The intention here is to follow the separate current contributions from the increments of different entrance time ωt_c in future computations. This point will be discussed again in later sections.

B. CALCULATION OF KINETIC ENERGY AND DISCUSSION

Equations (4.7) – (4.9) with the auxiliary Equations, (4.10) and (4.12) – (4.16) were computed by the digital computer. In order to allow experimental verification of the results obtained from the computer, the physical magnitudes of the input parameters were selected to be applicable to the dynamic beam analyzer,[7] which is an experimental tool available in this laboratory. Therefore a value of 1.75 radians for the d-c transit angle of the first gap θ_g and a value of 2π radians for the normalized drift distance θ_o were chosen. This value of θ_o places the second gap at about one-eighth of a space-charge wavelength of the dynamic beam tester.

The depths of modulation in the first gap α_1 and the second gap α_2 are taken from 0.2 to 1.0 in 0.2 steps; the d-c gap transit angle of the second gap θ_{g_2} was taken from $\pi/4$ to 2π radians in $\pi/4$-radian steps; and finally the phase angle Γ_2 of the assumed voltage V_2 across the second gap with respect to the fundamental current at the entrance was taken from $-\pi$ to π radians in $\pi/4$-radian steps. For all cases mentioned above, the entrance time ωt_c was changed from 0 to 2π radians with different increments chosen from the curves of the normalized entrance current i_c/I_o versus entrance time ωt_c as needed. Thus, it can be seen that the computer calculations cover a wide range of operating conditions.

It should be pointed out here that the assumed voltage V_2 across the second gap may either be induced by the electron beam or be applied externally. Separation of these states is possible by kinetic energy calculations at the entrance to the second gap and at the exit from it. Obviously, a decrease in kinetic energy through the second gap indicates that power is taken out and that the voltage V_2 is induced by the electron beam. An increase in kinetic energy, on the other hand, signifies that power is fed into the second gap and hence that voltage V_2 is applied externally. The argument for the existence of such a gap voltage depends upon the physical realizability of the circuit parameters associated with its phase angle Γ_2, i.e., actual total admittance and resonant frequency of a specific cavity used as the second gap. This point will be discussed further in the next section.

The computer data are so arranged that, for a given set of operating parameters, the normalized exit current i_d/I_o, the normalized exit velocity v_d/v_o, and the exit time ωt_d are given, together with their corre-

sponding counterparts at the entrance; i.e., the normalized entrance current i_c/I_o, the normalized entrance velocity v_c/v_o, and the entrance time ωt_c.

Normalized kinetic energy per cycle of the electron beam can be computed from

$$2\pi W = \frac{W_k}{I_o V_o} = \int_o^{2\pi} \left(\frac{i}{I_o}\right)\left(\frac{v}{v_o}\right)^2 \, d\omega t \quad , \tag{4.17}$$

where W_k is the kinetic energy per cycle, i/I_o is the normalized current, and v/v_o is the normalized velocity at time ωt.

1. Two-Cavity Klystron and Velocity-Filter Gap

Figure 17 shows the fundamental component of beam current at the entrance to the second gap for different depths of modulation a_1 at the first gap with a value of 1.75 radians for the d-c transit angle of the first gap θ_g as a function of the first drift angle θ_o. The drift angle of 2π radians used in the computer run is shown by a vertical dashed line. It is seen from the figure that the maximum value of the fundamental current occurs between $a_1 = 0.6$ and $a_1 = 0.8$.

Figure 18 shows the normalized current i_c/I_o and the normalized velocity v_c/v_o at the entrance to the second gap for different depths of modulation a_1 at the first gap. Velocity curves in Figure 18 indicate that there are two stationary points on all curves. These points correspond to those electrons that pass through the first gap at times when the r-f field at the first gap changes from decelerating to accelerating and vice versa. With respect to the stationary points, therefore, electrons in the beam at

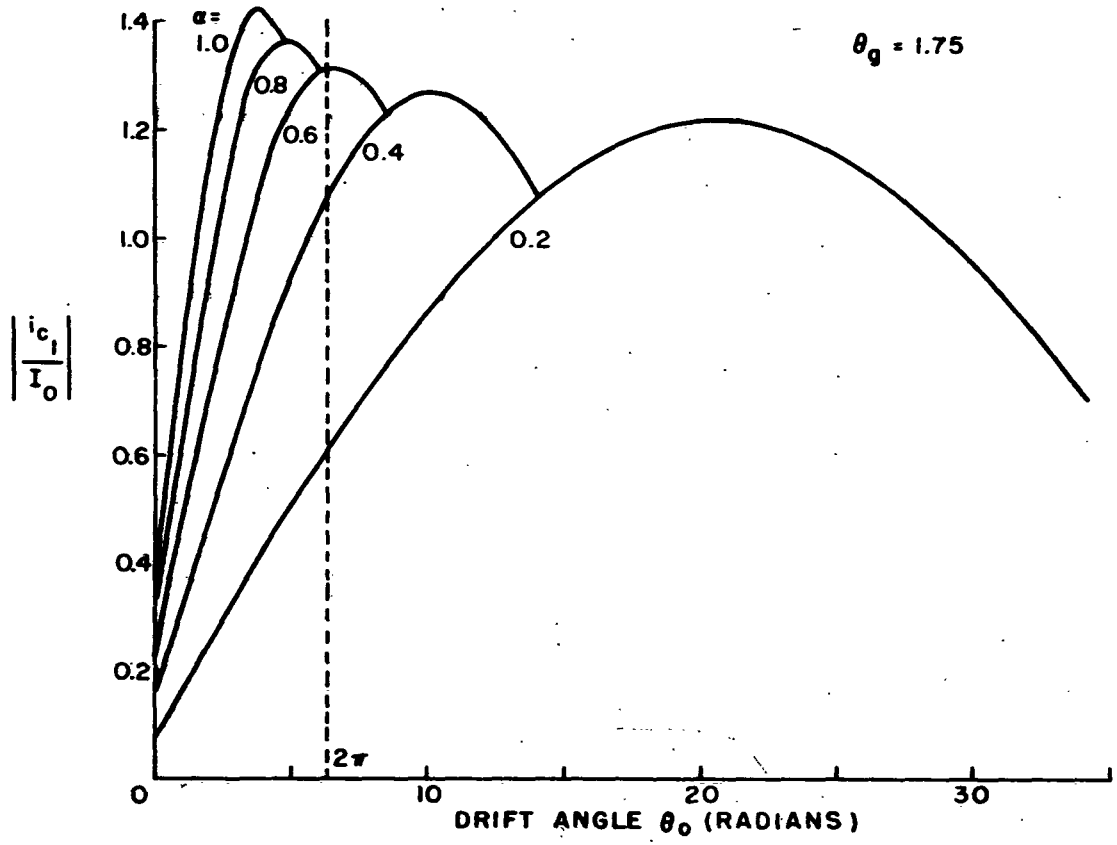

Figure 17. Absolute Value of Normalized Fundamental Current $|i_{c_1}/I_o|$ versus Drift Angle θ_o at Entrance to Second Gap for Different Depths of Modulation.

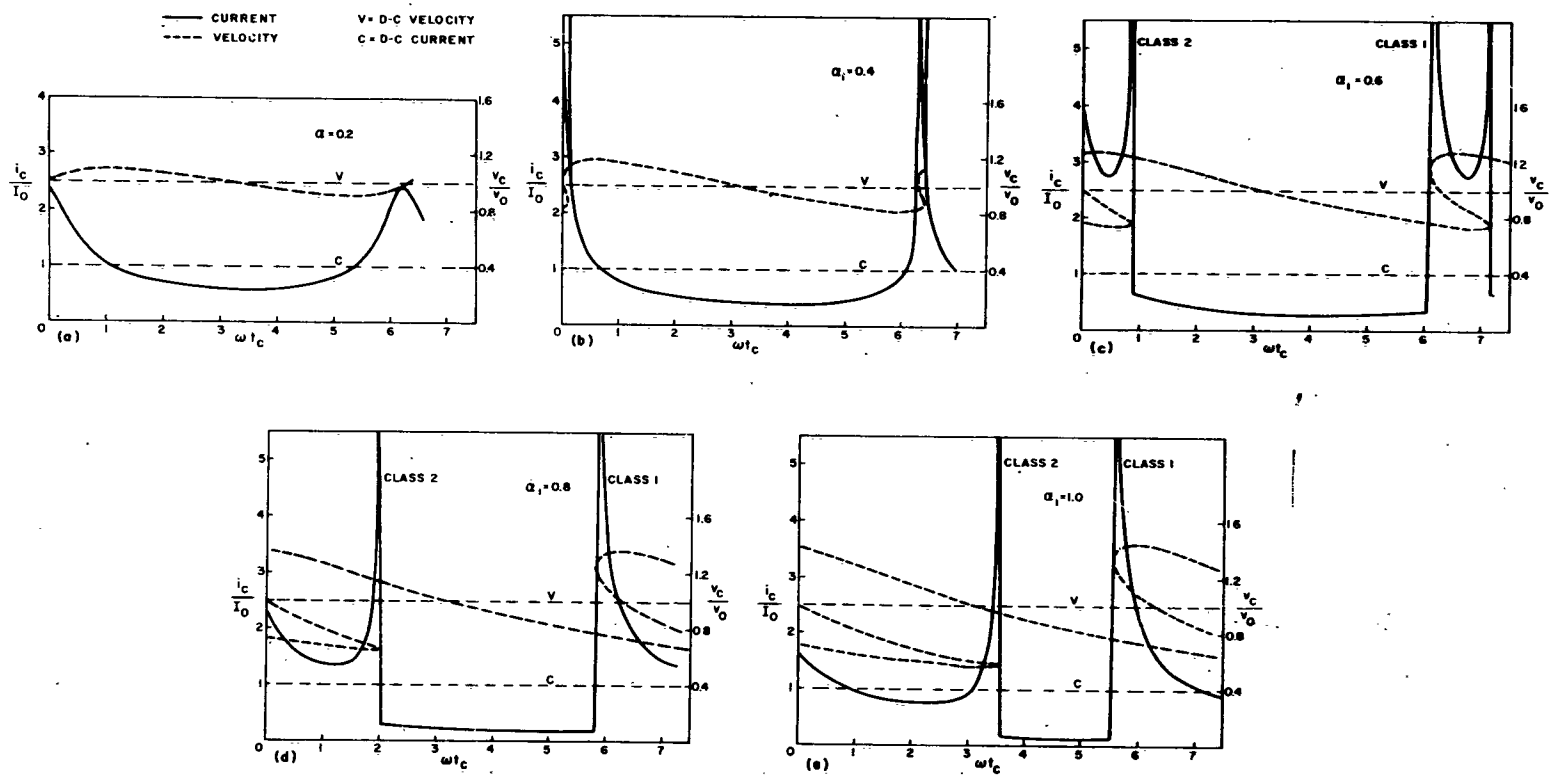

Figure 18. Normalized Entrance Current i_c/I_o versus Entrance Time ωt_c (solid line) and Normalized Entrance Velocity v_c/v_o versus Entrance Time ωt_c (broken line) for Different Depths of Modulation and $\theta_{g_1} = 1.75$ radians, $\theta_o = 2\pi$ radians.

the entrance to the second gap gan be divided into the following classes:

Class 1 - bunched fast electrons (near the first stationary point),
Class 2 - bunched slow electrons (near the first stationary point),
Class 3 - electrons near the second stationary point.

It is obvious from Figure 18 that as the depth of modulation α_1 is increased, two bunches of electrons occur, one of fast electrons (Class 1) and the other of slow electrons (Class 2). Since the drift angle θ_o is constant, Class 1 and Class 2 electrons begin to debunch at about $\alpha_1 = 0.8$. The optimum bunching occurs between $\alpha_1 = 0.6$ and $\alpha_1 = 0.8$, which can also be easily predicted from Figure 17. The deviation of velocity from the d-c value increases as the depth of modulation α_1 is increased.

The operating parameters of this analysis are the depths of modulation at the first gap α_1, and at the second gap α_2, the d-c transit angle of the second gap θ_{g_2}, and the phase angle Γ_2 of the voltage V_2 across the second gap with respect to the fundamental component of the beam current at the entrance to the second gap. In the following analysis, therefore, one of these parameters will be varied while the other three parameters are held constant. Numerical calculations of Equation (4.17) using the computer data show the types of operation shown in Table I.

TABLE I.

Types of Operation Indicated by Computer Data

Type	Kinetic energy w (normalized)	Maximum value of exit velocity v_d/v_o (normalized)
Type 1	decrease	decrease
Type 2	decrease	increase
Type 3	increase	increase

Cases of Type 3 are automatically excluded, since they are not included in the present study, but they might be used to represent the middle cavity in an analysis of a three-cavity klystron. The amount of the decrease in the normalized kinetic energy is, in general, greater in Type 1 than in Type 2. Further computations for Type 1 show that the greatest decrease in maximum velocity does not necessarily accompany the maximum output power, and the operating parameters are different for each of these cases.

In Figures 19 - 28 and in Figure 31, each class of electrons will be designated so that the reader can refer to Figure 18 to get a clear picture of the behavior of the electron beam. Figure 19 shows, for $a_1 = 0.8$, $a_2 = 1.0$, and $\theta_{g_2} = \pi$, the normalized exit current i_d/I_o, and the normalized exit velocity v_d/v_o, as functions of the exit time ωt_d when Γ_2 is varied from 0 to $-\pi$ radians in $\pi/4$-radian steps. Since the gap width and the voltage across the gap are constant, this series of graphs corresponds to the cases where the magnitude of the r-f field is held constant and the phase of it with respect to the beam is shifted. It is seen that under these operating conditions Class 1 and Class 2 electrons undergo changes while Class 3 electrons (of which there are only a few) are affected very little. As Γ_2 is increased in the negative direction, the two bunches already existing come closer and form a single bunch. This bunching seems to be related to the velocity in such a manner that the maximum velocity of Class 1 electrons increases as the negativeness of Γ_2 is increased and as power is fed into the gap. The case for $\Gamma_2 = -\pi/4$ is the optimum operation for this series for output power, but the efficiency is very small since the bunch of Class 2 electrons is accelerated while the bunch of Class 1 electrons are decelerated in passing through the gap. Overtaking occurs within the

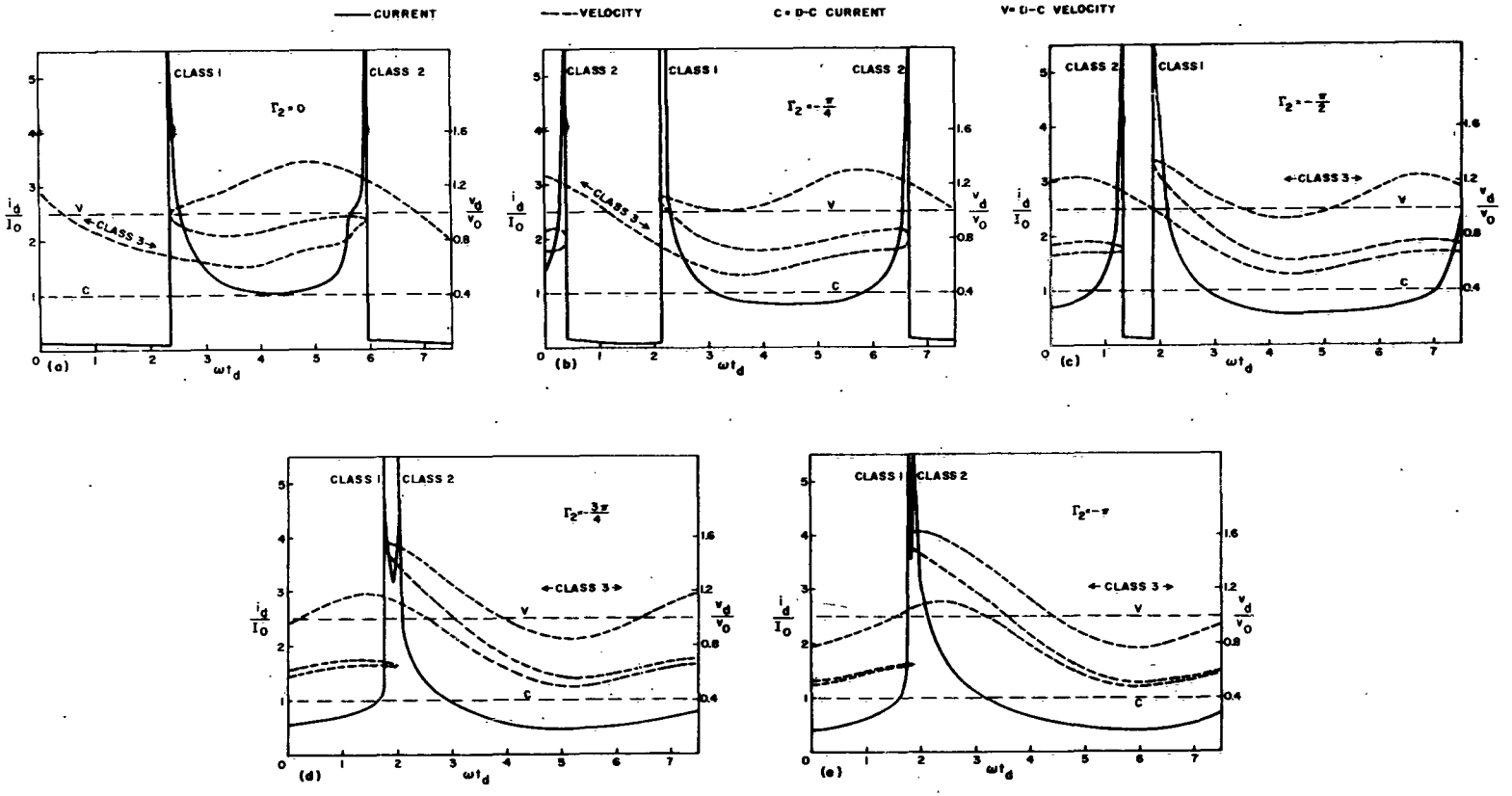

Figure 19. Normalized Exit Current i_d/I_o versus Exit Time ωt_d (solid line) and Normalized Exit Velocity v_d/v_o versus Exit Time ωt_d (broken line) for Different Phase Angles and $a_1 = 0.8$, $a_2 = 1.0$, and $\theta_{g_2} = \pi$.

gap between $\Gamma_2 = -\pi/2$ and $\Gamma_2 = -3\pi/2$.

Figure 20 shows, for $\alpha_1 = 0.8$, $\alpha_2 = 1.0$, and $\Gamma_2 = -\pi/2$, the normalized exit current, i_d/I_o, and the normalized exit velocity, v_d/v_o, as functions of the exit time ωt_d, when θ_{g_2} is varied from $3\pi/4$ to $7\pi/4$ radians in $\pi/4$-radian steps. As θ_{g_2} is increased, Class 1 and Class 2 electrons first bunch together, overtaking occurs within the gap, and then these two classes of electrons begin to debunch. It should be noticed that the magnitude of the r-f field decreases continuously in this series of graphs. The phase angle Γ_2 is such that both the bunch of Class 1 electrons and the bunch of Class 2 electrons are decelerated continuously from one case to the other. At the beginning of the series; power is fed into the gap for $\theta_{g_2} = 3\pi/4$ and $\theta_{g_2} = \pi$ cases, but it is taken out for the remaining cases. The case for $\theta_{g_2} = 7\pi/4$ represents the velocity-filter gap, in which there is a 10.3 per cent decrease in the maximum velocity, and the efficiency is 13.5 per cent.

Figure 21 shows, for $\alpha_1 = 0.8$, $\theta_{g_2} = \pi/2$, and $\Gamma_2 = -\pi/4$, the normalized exit current, i_d/I_o, and the normalized exit velocity, v_d/v_o, as functions of the exit time, ωt_d, when α_2 is varied from 0.2 to 1.0 in 0.2 steps. This series of graphs represents the catcher gap of a two-cavity klystron. In these cases, the debunching of the beam during one cycle and the phase angle Γ_2 are optimum for energy extraction from the beam. Velocity spread and efficiency increase as α_2 (and therefore the magnitude of the r-f field) is increased. Velocities of Class 1 electrons change little, but the amount of charge of this class of electrons decreases continuously. Velocities and the amount of charge of Class 2 electrons change drastically, and a split occurs in the bunch of Class 2 electrons.

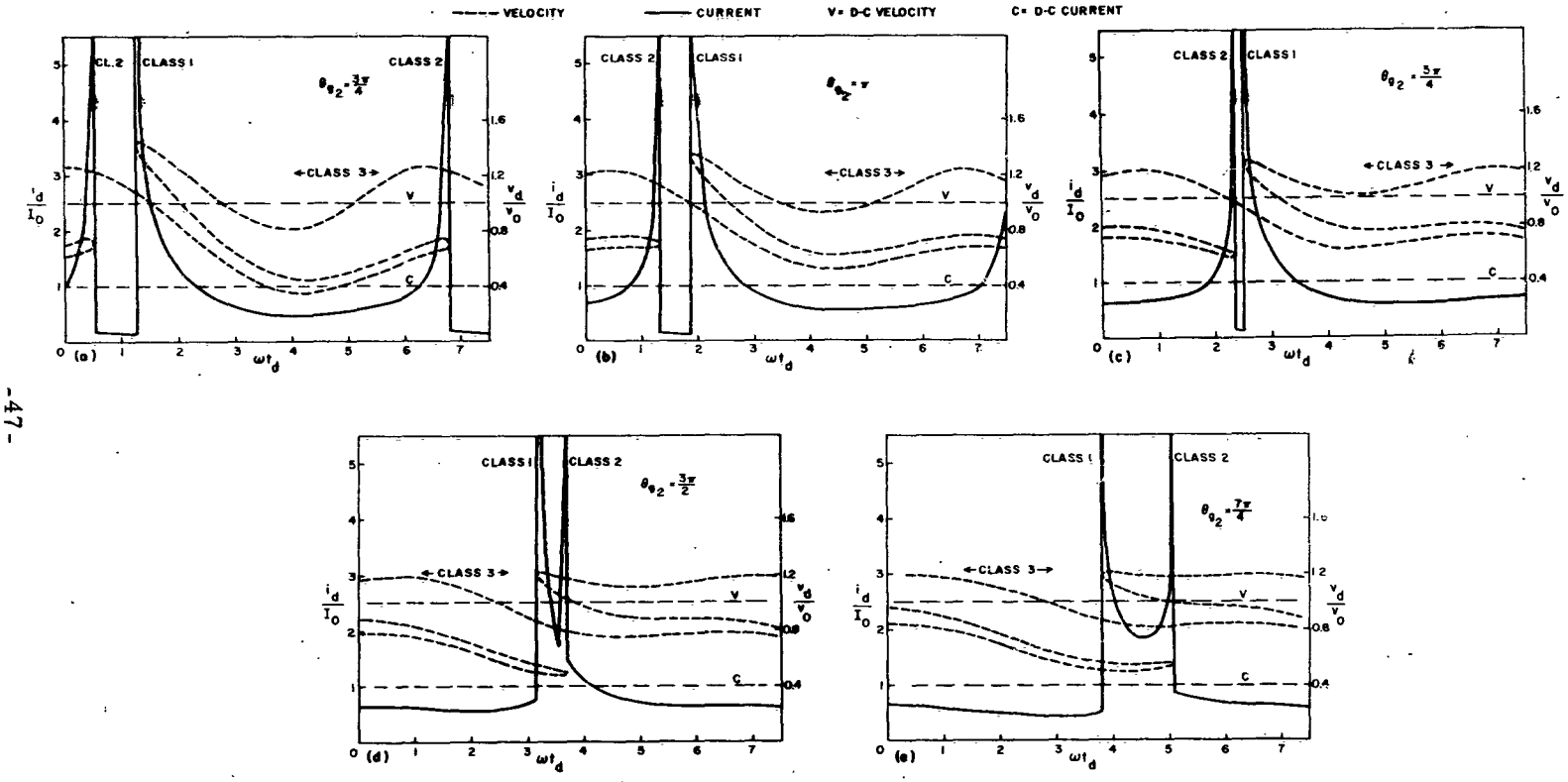

Figure 20. Normalized Exit Current i_d/I_o versus Exit Time ωt_d (solid line) and Normalized Exit Velocity v_d/v_o versus Exit Time ωt_d (broken line) for Different Gap Lengths and $a_1 = 0.8$, $a_2 = 1.0$, and $\Gamma_2 = -\pi/2$.

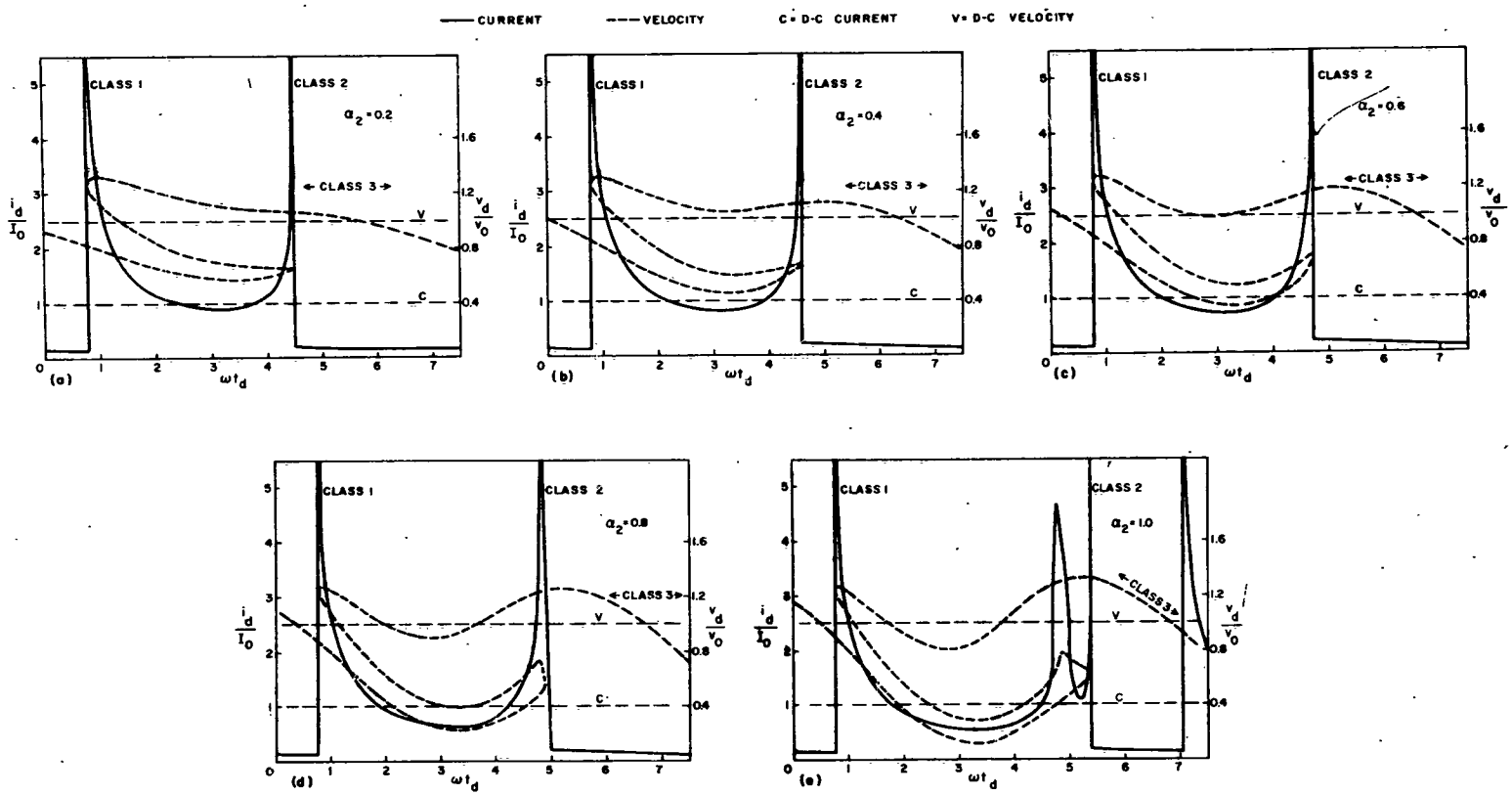

Figure 21. Normalized Exit Current i_d/I_o versus Exit Time ωt_d (solid line) and Normalized Exit Velocity v_d/v_o versus Exit Time ωt_d (broken line) for Different Depths of Modulation and $\alpha_1 = 0.8$, $\theta_{g_2} = \pi/2$, and $\Gamma_2 = -\pi/4$.

Class 3 electrons, on the other hand, fall out of phase and take energy from the r-f field; consequently their velocities (and hence their kinetic energies) increase.

Figure 22 shows, for $\alpha_1 = 0.8$, $\theta_{g_2} = 7\pi/4$, and $\Gamma_2 = -\pi/2$, the normalized exit current i_d/I_o, and the normalized exit velocity v_d/v_o, as functions of the exit time ωt_d, when α_2 is varied from 0.2 to 1.0 in 0.2 steps. This series of graphs represents the velocity-filter gap when the electron beam at the entrance is assumed to be a spent beam. Since the gap is long, overtaking within the gap has already occurred between Class 1 electrons and Class 2 electrons. They appear as a single split bunch. The debunching between the two classes of electrons increases as α_2 increases (therefore the magnitude of the r-f field increases), whereas Class 3 electrons pass through the gap almost unaffected. The interesting feature of this series of graphs is that whereas Class 1 electrons are being decelerated and are giving their energies to the r-f field, Class 2 electrons are accelerated and take energy from the r-f field. Velocity spreads, output powers, and efficiencies are smaller than those of the cases shown in Figure 21, but the extent of the decrease in the maximum normalized velocity is greater.

The behavior of the electron beam when it passes through the catcher gap of a two-cavity klystron and through the velocity-filter gap is shown in Figures 21 and 22 respectively. A better understanding can be obtained if, in addition, one examines the changes in the incremental charge Δq and in the incremental kinetic energy ΔW of electrons in a specific range of velocities. For this purpose bar graphs representing percentages of Δq and ΔW for ranges of velocities spanning ten per cent of the d-c velo-

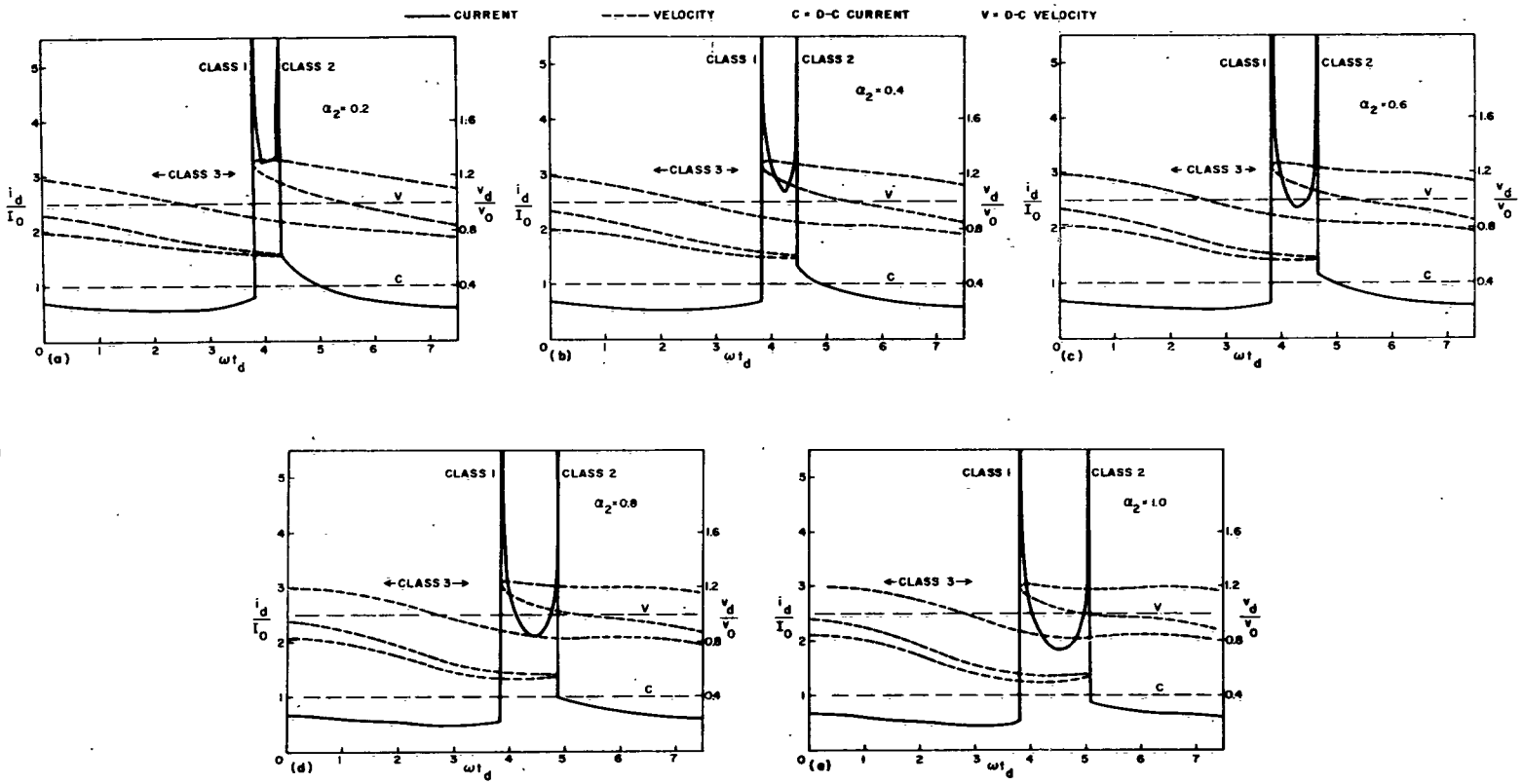

Figure 22. Normalized Exit Current i_d/I_o versus Exit Time ωt_d (solid line) and Normalized Exit Velocity v_d/v_o versus Exit Time ωt_d (broken line) for Different Depths of Modulation and $\alpha_1 = 0.8$, $\theta_{g_2} = 7\pi/4$, and $\Gamma_2 = -\pi/2$.

city are used. Each ten-per-cent span will be termed a velocity-class in this report. Electrons will be designated either by their velocity-class or as: (1) slow electrons – those having velocities less than the d-c velocity, (2) fast electrons – those having velocities more than the d-c velocity.

Figure 23 shows the percentage of incremental charge Δq, and the percentage of full incremental kinetic energy ΔW versus velocity-class at the entrance to the second gap for the case of $a_1 = 0.8$. It is seen that the total incremental charge is 49.264 per cent, the total incremental kinetic energy is 28.303 per cent for slow electrons; and the total incremental charge is 50.736 per cent, the total incremental kinetic energy is 71.697 per cent for fast electrons. It is also apparent that the charge is accumulated mostly at the extremes, and that this accumulation of charge corresponds to the existence of bunches in the beam at the entrance to the second gap. On the other hand, since the kinetic energy is proportional to the square of the velocity, the total kinetic energy of the fast electrons is about 2.5 times the total kinetic energy of the slow electrons, whereas the ratio of total charges is almost equal to one.

Figure 24 shows, for $a_1 = 0.8$, the percentage of incremental charge Δq versus the normalized velocity-class v_d/v_o, with a_2 as a parameter, at the exit of the catcher-gap selected (i.e., $\theta_{g_2} = \pi/2$ and $\Gamma_2 = -\pi/4$). In each case of this series of graphs except in Figure 24b, it is seen that the total percentage of Δq is decreased for fast electrons, and that the velocity spread is wider than that at the entrance, although the maximum velocity-class does not exceed 1.4. This obviously means that, on the average, the electrons are decelerated and power is taken out from the

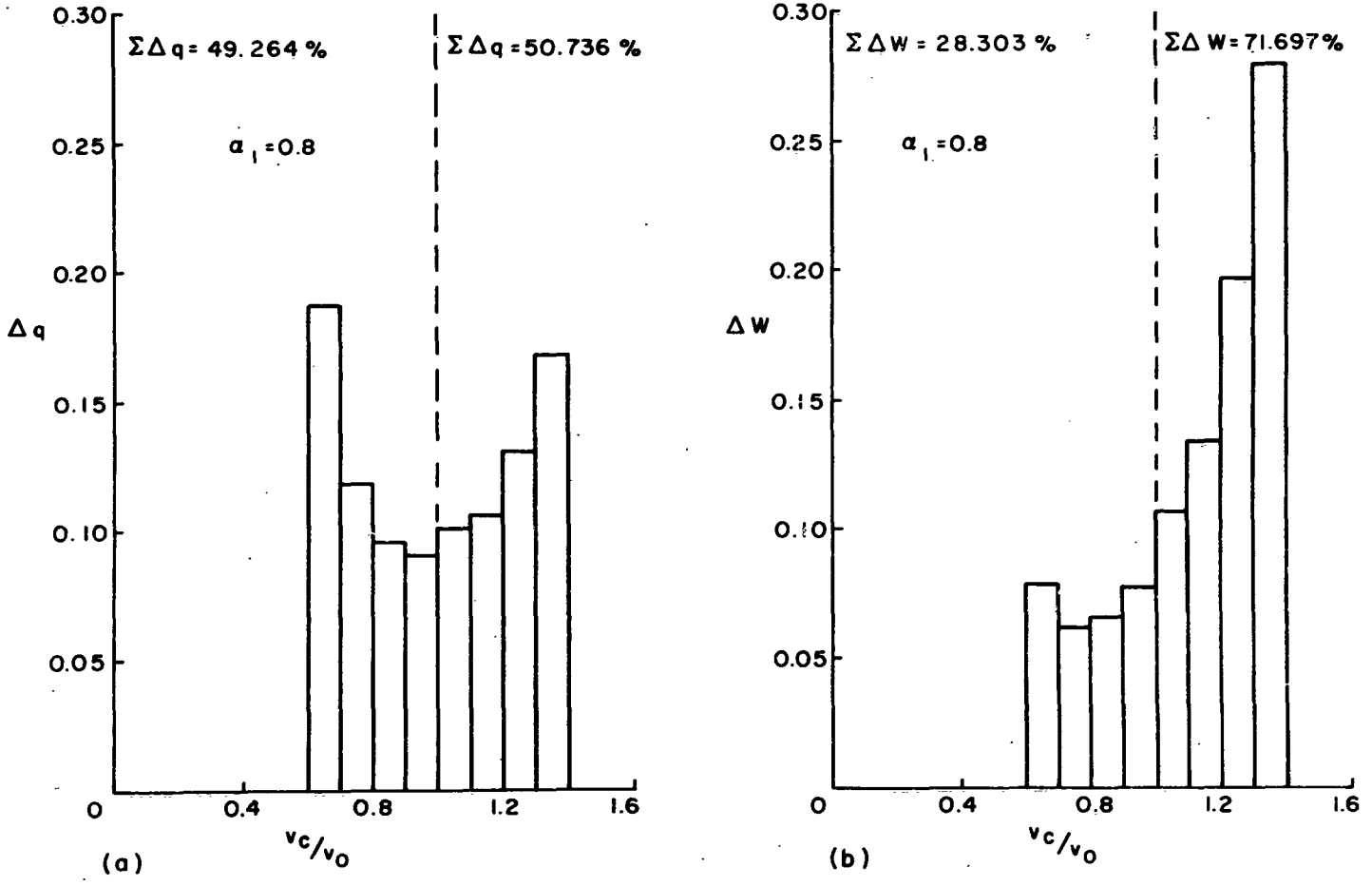

Figure 23. (a) Percentage of Incremental Charge Δq versus Velocity-Class v_d/v_o ; (b) Percentage of Incremental Kinetic Energy ΔW versus Velocity-Class v_d/v_o at Entrance to Second Gap for $\alpha_1 = 0.8$.

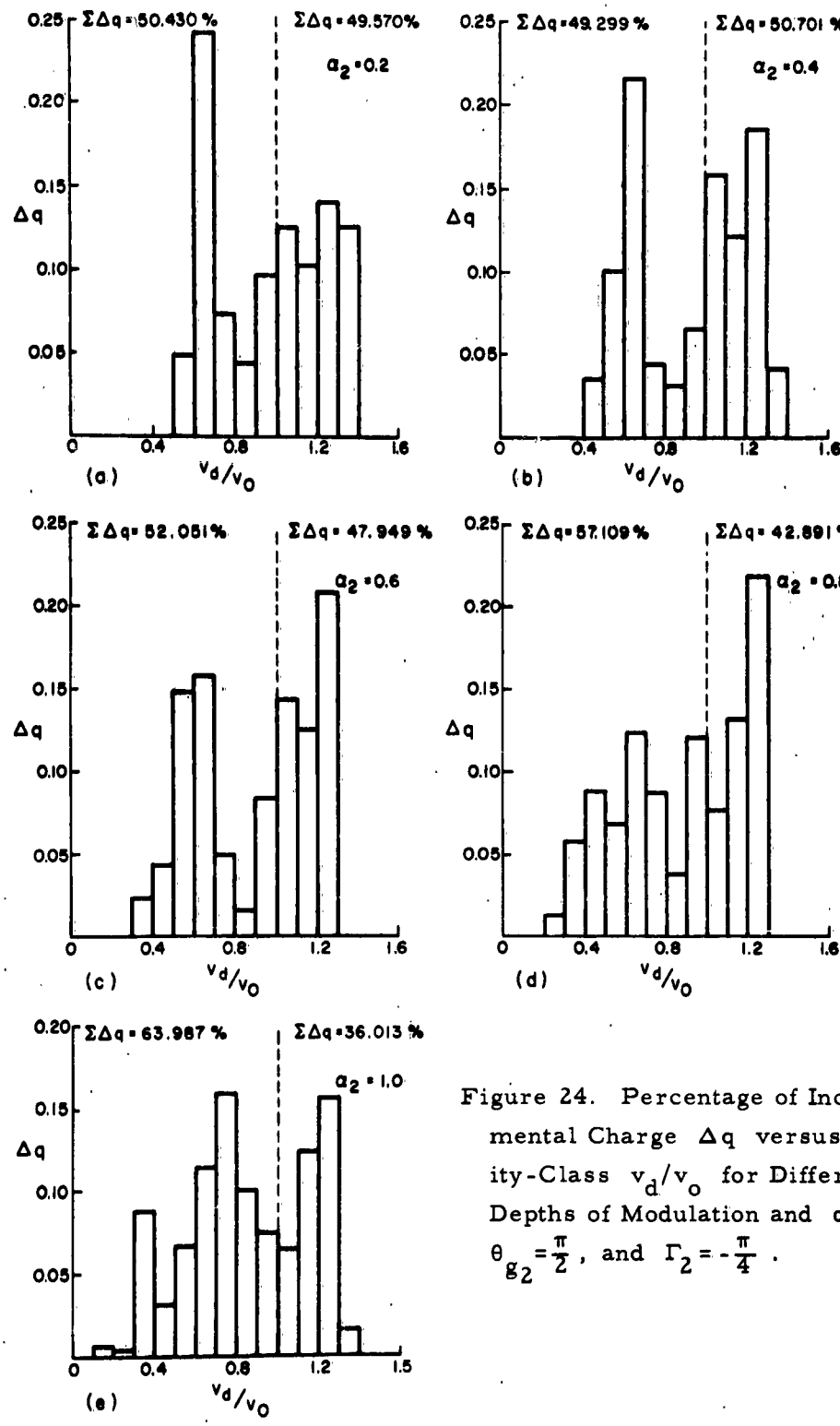

Figure 24. Percentage of Incremental Charge Δq versus Velocity-Class v_d/v_o for Different Depths of Modulation and $a_1 = 0.8$, $\theta_{g_2} = \frac{\pi}{2}$, and $\Gamma_2 = -\frac{\pi}{4}$.

electron beam. The main effect of increasing the r-f field (i.e., increasing a_2) in this gap is to decelerate the electrons. In some velocity-classes, there is an increase in the percentage of Δq when a_2 is increased. This increase occurs because at the entrance to the gap, the electrons in a velocity-class have different phases with respect to the r-f voltage across the gap. Some of these electrons are accelerated while others are decelerated. To visualize this phenomenon, one should examine the adjacent velocity-classes. In Figure 24(d), for example, both the percentages of Δq for the velocity classes 1.1 and 1.2 show slight increases from the previous case. Examining the velocity-class 1.0 (i.e., 1.0 – 1.1), one can see that the decrease in this class of electrons is greater than the increase in the higher velocity-classes. In other words, a few of the electrons of velocity-class 1.0 are accelerated while a greater number of them are decelerated.

Bar graphs representing the percentage of incremental kinetic energy ΔW versus the normalized velocity-class, v_d/v_o, with a_2 as a parameter, are depicted in Figure 25 for the catcher gap selected. It is seen that as a_2 is increased, the total kinetic energy for the electron beam, as well as for the fast electrons, decreases continuously. The total kinetic energy for the slow electrons first decreases and then increases as a_2 is increased. This increase is not due to the acceleration of slow electrons, but is due mainly to the increase in their total charge. The changes in the total kinetic energy of the slow electrons are, however, only a few per cent. Observing the same phenomenon as in Figure 24(d), one can see that the percentages of ΔW for the two velocity-classes 1.1 and 1.2 show slight increases, but the decrease in the percentage of ΔW for the velocity-class 1.0 is greater

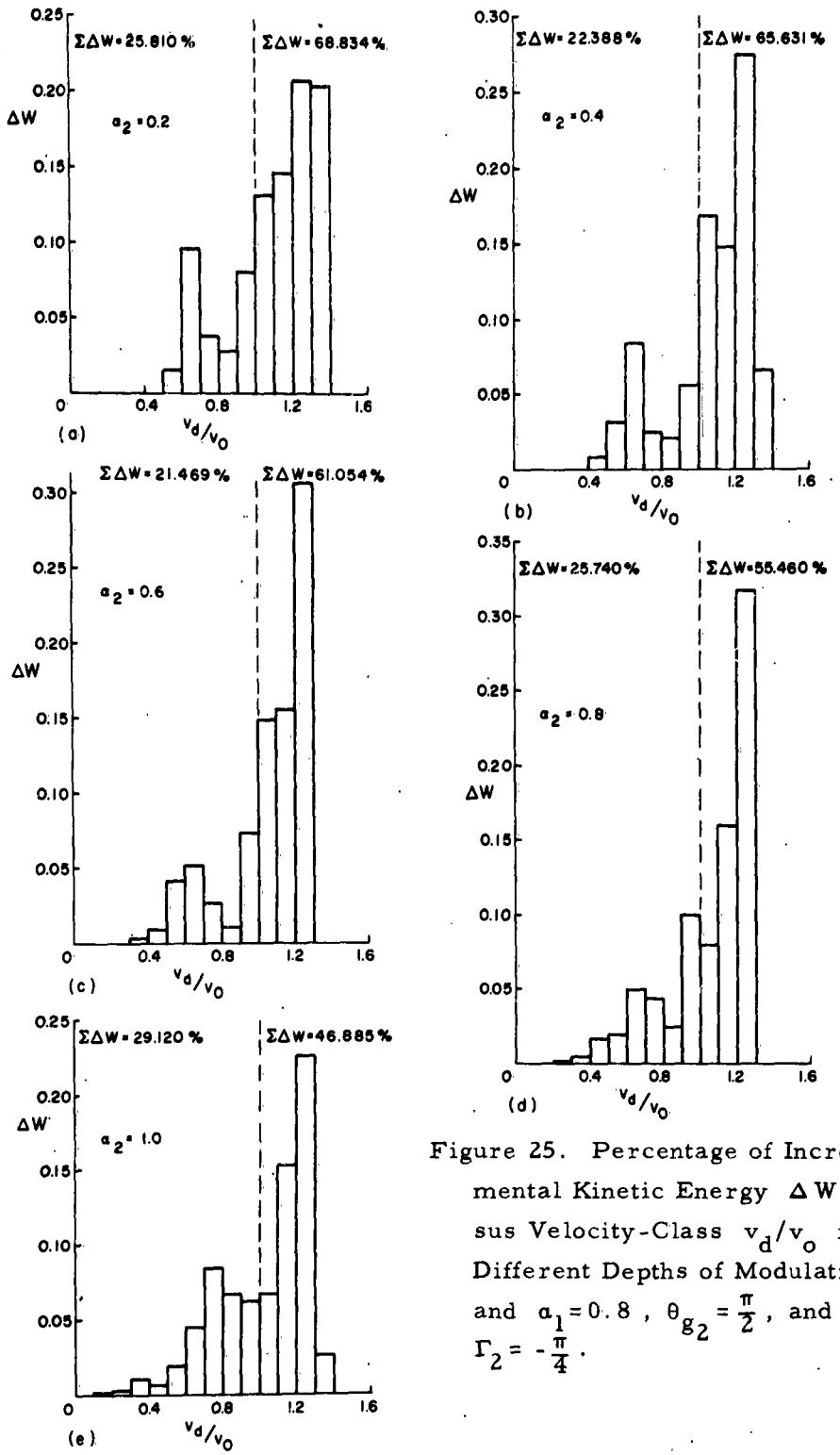

Figure 25. Percentage of Incremental Kinetic Energy ΔW versus Velocity-Class v_d/v_o for Different Depths of Modulation and $a_1 = 0.8$, $\theta_{g_2} = \frac{\pi}{2}$, and $\Gamma_2 = -\frac{\pi}{4}$.

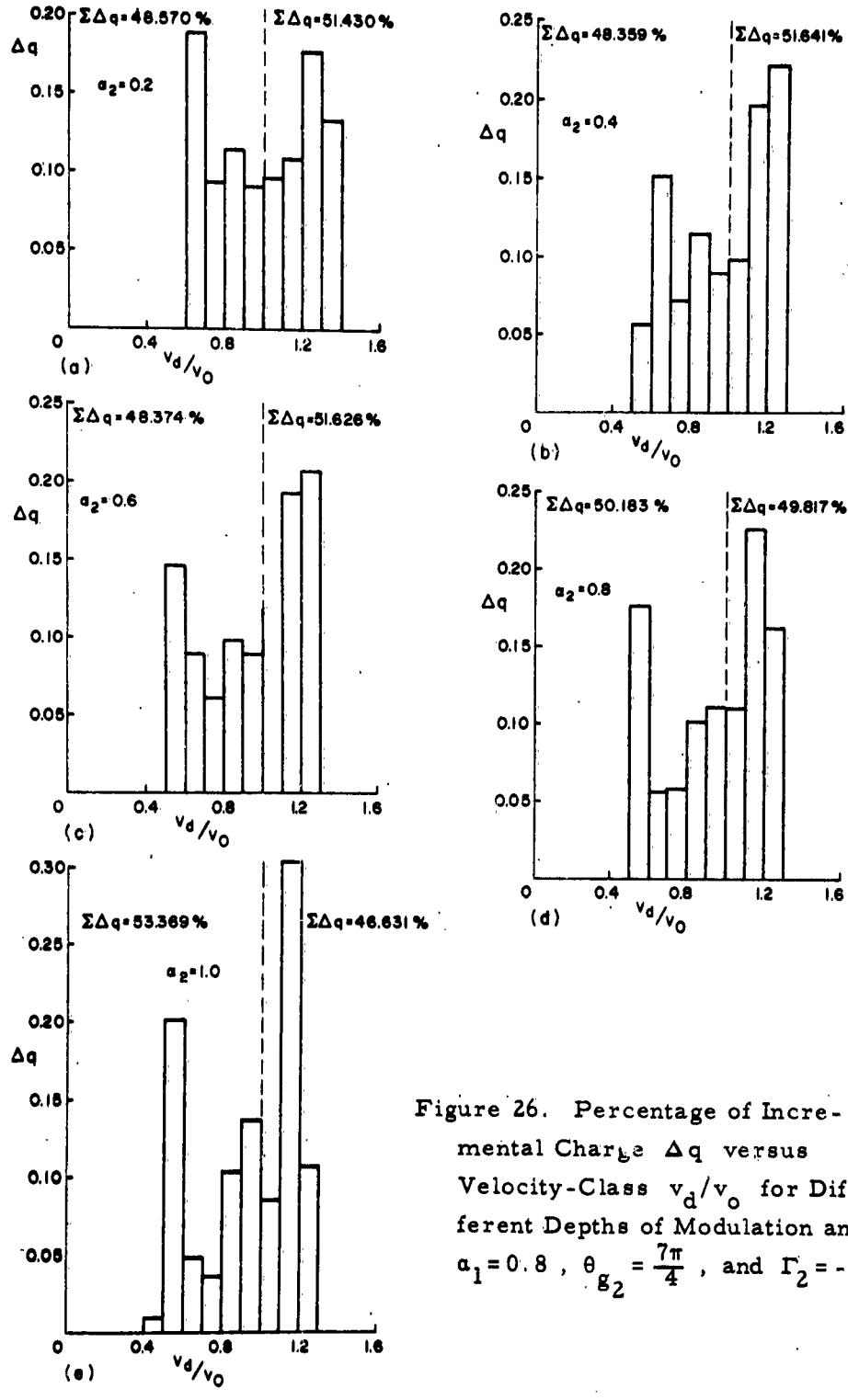

Figure 26. Percentage of Incremental Charge Δq versus Velocity-Class v_d/v_o for Different Depths of Modulation and $a_1 = 0.8$, $\theta_{g_2} = \frac{7\pi}{4}$, and $\Gamma_2 = -\frac{\pi}{2}$.

than the increase in the higher velocity-classes.

Figure 26, which is similar to Figure 24, is for the velocity-filter gap selected (i.e., $\theta_{g_2} = 7\pi/4$, $\Gamma_2 = -\pi/2$), and for $\alpha_1 = 0.8$. The total percentages of Δq for both the slow electrons and the fast electrons change a few per cent as α_2 increases. The percentages of Δq of the velocity-classes higher than 1.2, however, decrease appreciably, from 30 per cent to 7.80 per cent. In contrast to this, the percentages of Δq of the velocity-classes lower than 0.7 increase from 18.75 per cent to 25.80 per cent.

Figure 27 shows the percentage of incremental kinetic energy ΔW versus the normalized velocity-class v_d/v_o, with α_2 as a parameter, for the selected velocity-filter gap. The total percentages of ΔW both for the electron beam and for the fast electrons decrease continuously, as expected from Figure 26, but as α_2 is increased the total percentages for the slow electrons first decrease and then increase. This increase is comparable to the increase in the total percentage of Δq, since most of the change occurs near the velocity-class 1.0.

An illustrative comparison between the catcher gap and the velocity-filter gap is shown in Figure 28. One salient point is the occurrence of over-taking within the gap in the case of the velocity-filter gap. The beam is also bunched more in the velocity-filter gap than in the catcher gap. On the other hand, the velocity spread of the electrons and hence the output power is larger in the catcher gap.

A numerical comparison between the catcher gap and the velocity-filter gap, selected as indicated, is given in Table II. In the table there are two columns for each case; the left column represents the percentage of decrease in maximum velocity, and the right column the percentage of power

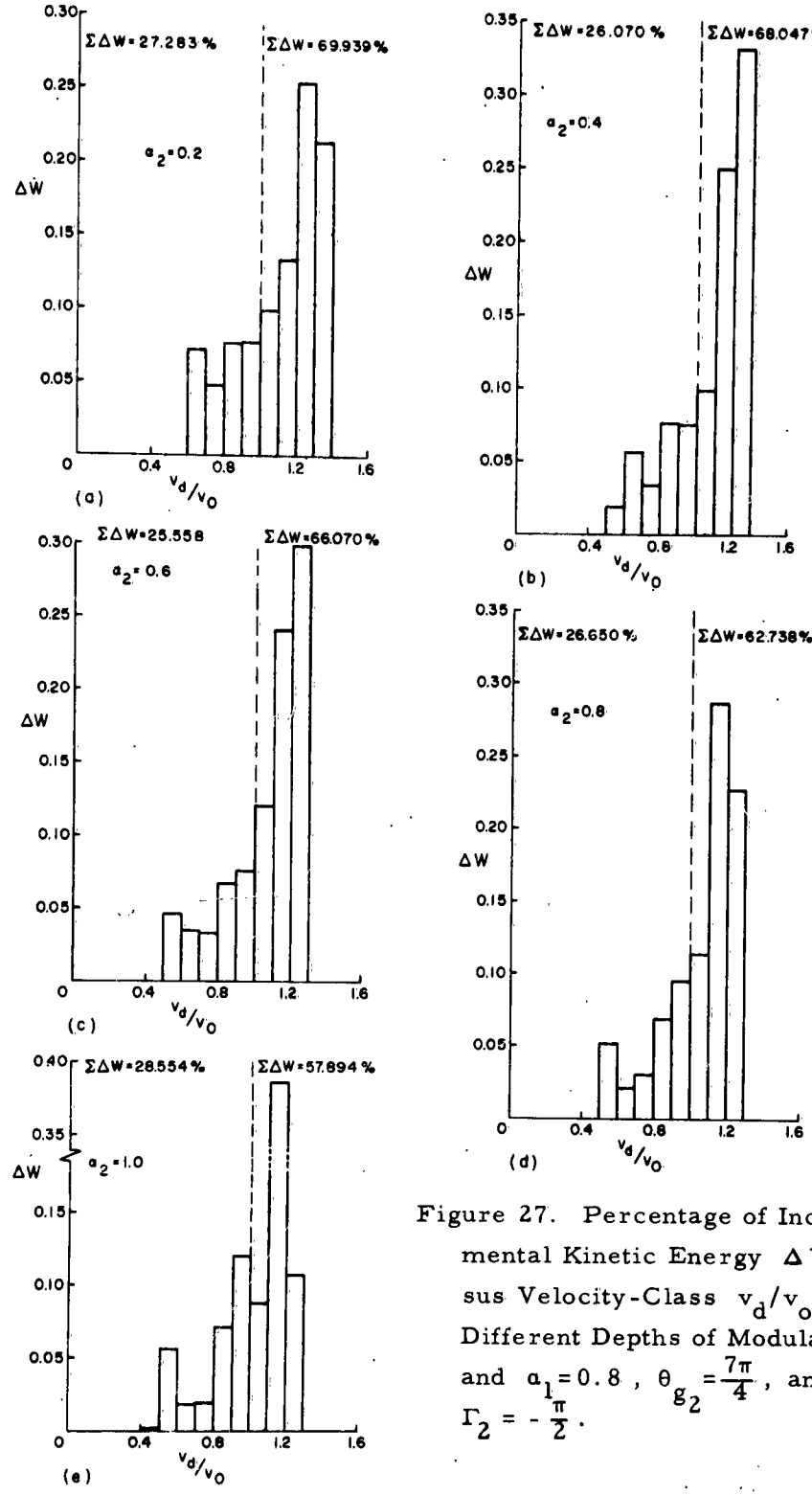

Figure 27. Percentage of Incremental Kinetic Energy ΔW versus Velocity-Class v_d/v_o for Different Depths of Modulation and $a_1 = 0.8$, $\theta_{g_2} = \frac{7\pi}{4}$, and $\Gamma_2 = -\frac{\pi}{2}$.

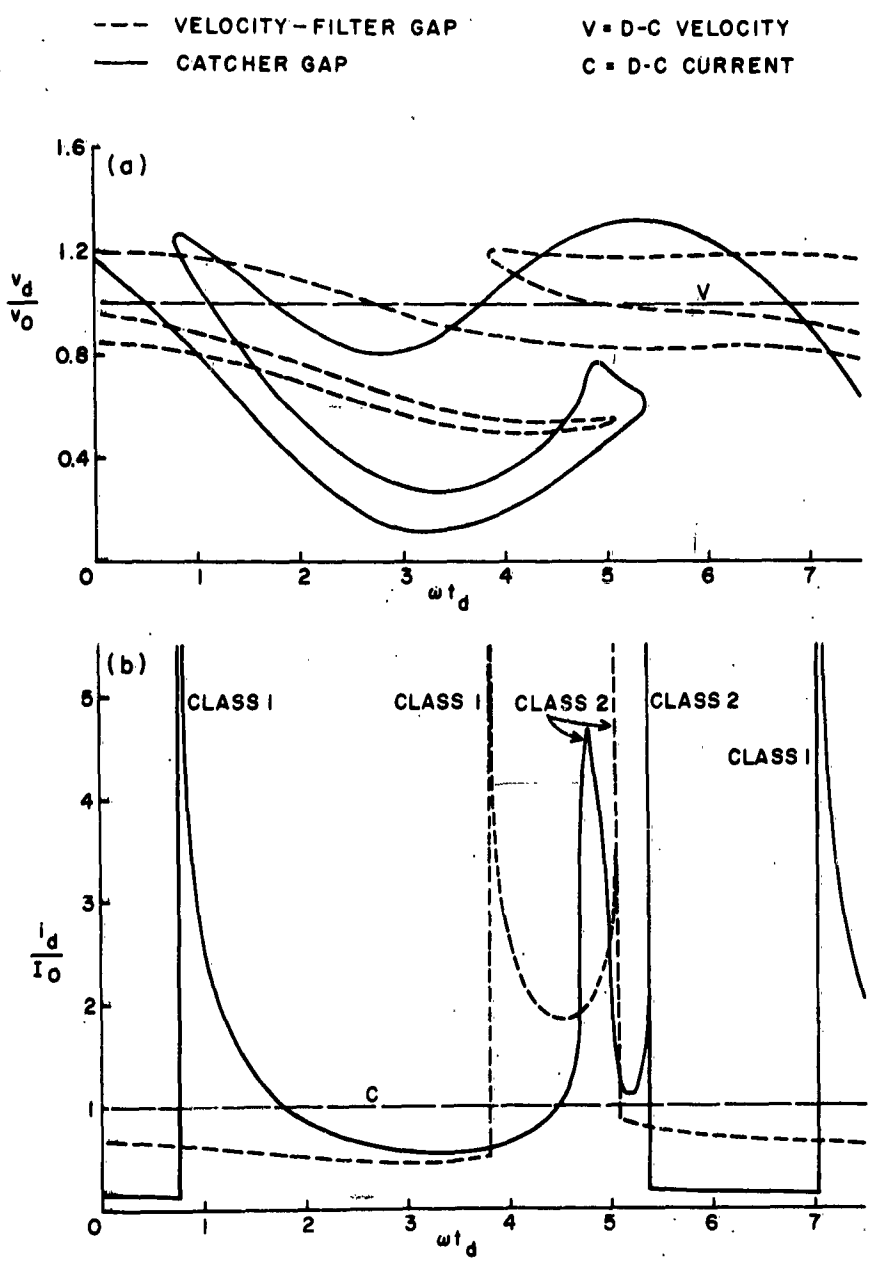

Figure 28. (a) Normalized Exit Velocity v_d/v_o versus Exit Time ωt_d; (b) Normalized Exit Current i_d/I_o versus Exit Time ωt_d for the Selected Catcher Gap (solid line) and for the Selected Velocity-Filter Gap (broken line).

TABLE II.

Velocity Decreases and Efficiencies
for Catcher Gap and for Velocity-Filter Gap

	$\theta_{g_2} = \pi/2$ $\Gamma_2 = -\pi/4$		$\theta_{g_2} = 7\pi/4$ $\Gamma_2 = -\pi/2$	
a_2	Velocity decrease (%)	Efficiency (%)	Velocity decrease (%)	Efficiency (%)
0.2	1.881	5.356	2.128	2.778
0.4	3.278	11.981	4.255	5.883
0.6	4.363	17.477	6.294	8.372
0.8	5.247	18.571	8.310	10.612
1.0	2.370	23.995	10.327	13.552

exchange. It is apparent that the decrease in maximum velocity is not proportional to output power in the case of the catcher gap, as it appears to be in the velocity-filter gap.

It can be concluded from the analysis of this chapter that at large signal levels one cannot easily predict the operating parameters for a catcher gap without calculating the kinetic energies at the entrance of the gap and at the exit from it. In contrast to this, the operating parameters for a velocity-filter gap can easily be predicted by the decrease in the maximum velocity at the exit from the gap. Efficiency of a velocity-filter gap is usually lower than that of a catcher gap, since slow electrons, being out of phase, are accelerated and take energy from the r-f field. This suggests elimination of slow electrons in a spent beam by some means, pre-

ferably electrostatic, before the beam is allowed to pass through a velocity-filter gap.

2. Loading Conditions of a Two-Cavity Klystron

It was previously mentioned that the existence of the assumed voltage V_2 across the second gap depends upon the physical realizability of the circuit parameters. Once the operating parameters and the power exchange for the second gap are known from the preceding analysis, the circuit parameters can be determined.

The equivalent circuit for the second gap is shown in Figure 29, where G_T represents the total conductance, and B_T represents the total susceptance of the cavity proper; i.e.,

$$G_T = G_l + G_c + G_b \quad , \tag{4.18}$$

$$B_T = B_l + B_c + B_b \quad , \tag{4.19}$$

where

G_l = load conductance referred to the cavity,

G_c = conductance representing the circuit loss in the cavity,

G_b = beam-loading conductance,

B_l = load susceptance referred to the cavity,

B_c = susceptance representing the tuning of the cavity,

B_b = beam-loading susceptance,

I_i = induced current at the cavity.

Figure 29b shows the vector diagram for the fundamental component of the entrance current i_{c_1} and the voltage V_2 across the second gap.

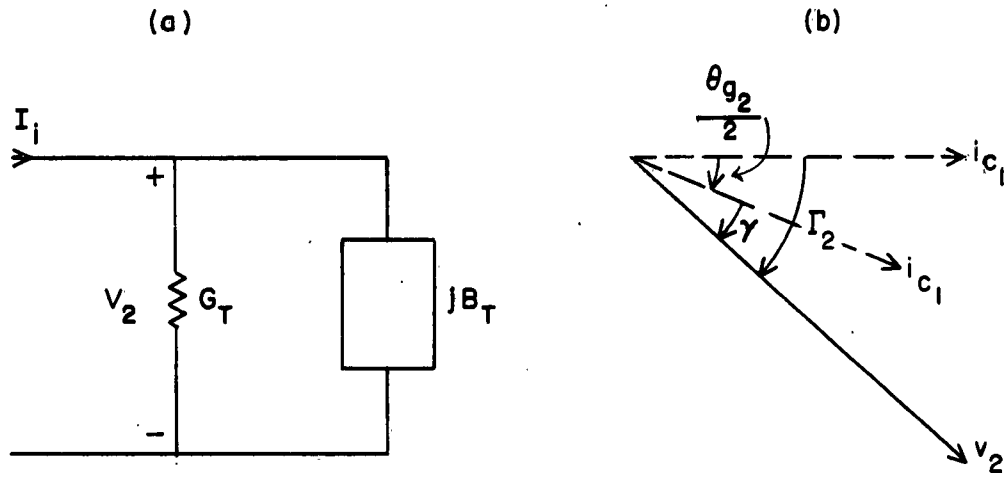

Figure 29. (a) Equivalent Admittance Circuit for Second Gap, (b) Vector Diagram for Fundamental Component of Entrance Current i_c, and Voltage V_2 across Second Gap.

When the reference is shifted to the center of the gap, the phase angle γ between i_{c_1} and V_2 represents the phase angle of the total admittance shown in Figure 29a if the cavity has a high Q; that is, if no harmonics are present in the induced current. The difference between the calculated kinetic energies at the entrance and exit of the second gap represents the power transferred to the load and the power dissipated in the cavity. One can then write

$$P_k = \frac{W_{k_{entrance}} - W_{k_{exit}}}{2\pi} \quad , \tag{4.20}$$

$$P_k = \frac{G' V_2^2}{2} \quad , \tag{4.21}$$

where

$$G' = G_l + G_c \quad . \tag{4.22}$$

One can thus determine the load conductance G_l referred to the cavity from Equations (4.20) - (4.22) and from measured values of Q_o and Q_x of the cavity.

V. ANALYSIS OF SECOND DRIFT SPACE AND LAST CAVITY

In this chapter it is assumed that the operating characteristics of the catcher gap and the velocity filter gap are as determined in the previous chapter, Because of the complexity of obtaining analytical formulas for the current and the velocity of the beam as functions of exit time, ωt_d, at the exit from the second gap, only computer solutions are sought for these characteristics. Also, in the formulation of the problem, which follows, the total current is not calculated; instead, current contributions from the increments of different ωt_c times are traced along the tube. Thus the physical phenomena taking place at any point along the tube are readily understood. The analysis here is similar to that of Chapter IV. The known characteristics of the catcher gap will provide the initial conditions at the entrance to the second drift space, and the known characteristics of the velocity-filter gap will be used as those of the third gap.

A. COMPUTER PROBLEM

Since the second drift space is again assumed to be a field-free space, the equation of motion is

$$\ddot{z} = o \quad . \tag{5.1}$$

The time at plane e (see Figure 30) can be expressed as

$$\omega t_e = \omega t_d + \frac{\theta_{o2}}{v_d/v_o} \quad , \tag{5.2a}$$

$$\theta_{o2} = \frac{\omega l_2}{v_o} \quad . \tag{5.2b}$$

Integrating Equation (5.1) once and applying the boundary conditions at $t = t_d$, one obtains

$$\frac{v_e}{v_o} = \frac{v_d}{v_o} \quad , \tag{5.3}$$

where v_d/v_o is given numerically by the computer. Differentiating Equation (5.2a) with respect to ωt_d, one obtains

$$\frac{d\omega t_e}{d\omega t_d} = 1 - \frac{\frac{\omega l_2}{v_o} \frac{d}{d\omega t_d}\left(\frac{v_d}{v_o}\right)}{\left(\frac{v_d}{v_o}\right)^2} \quad . \tag{5.4}$$

From Equation (4.8), one can derive

$$\frac{d}{d\omega t_d}\left(\frac{v_d}{v_o}\right) = \frac{\frac{d}{d\omega t_c}\left(\frac{v_c}{v_o}\right) + \frac{a_2}{2\theta_{g_2}} \sin(\omega t_c + \xi)}{\frac{d\omega t_d}{d\omega t_c}} - \frac{a_2}{2\theta_{g_2}} \sin(\omega t_d + \xi) \quad ; \tag{5.5}$$

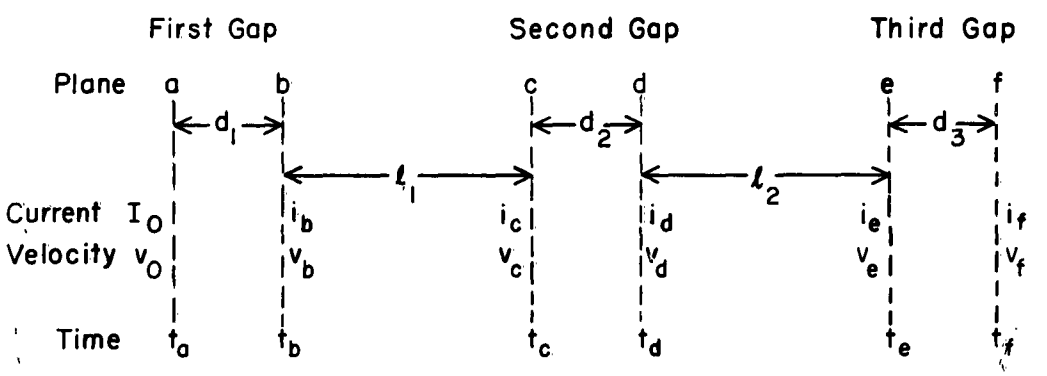

Figure 30. Schematic Diagram of the Combination of a Two-Cavity Klystron and a Velocity-Filter Gap.

$d\omega t_d/d\omega t_c$ is given in Equation (4.1) and $d(v_c/v_o)/d\omega t_c$ in Equation (4.16). Using the principle of conservation of charge for the second drift space, one obtains

$$\frac{i_e}{I_o} = \frac{\frac{i_d}{I_o}}{\left|\frac{d\omega t_e}{d\omega t_d}\right|} \quad . \tag{5.6}$$

Equations (5.2) – (5.6) define the normalized current, i_e/I_o, and the normalized velocity, v_e/v_o, as functions of time, ωt_e, corresponding to specific ωt_c times.

Assuming a voltage V_3 across the gap with a total phase Γ_3 with respect to the fundamental current at the entrance, one can write the equation of motion for the third gap as

$$\ddot{z} = -\frac{e}{m}\frac{V_3}{d}\sin(\omega t + \Gamma_3) \quad . \tag{5.7}$$

Integrating Equation (5.7) twice, substituting initial conditions at $t = t_e$, and normalizing with respect to d-c velocity, one obtains

$$\dot{Z} = \frac{v_e}{v_o} + \frac{a_3}{2\theta_{g_3}}\left[\cos(\omega t + \Gamma_3) - \cos(\omega t_e + \Gamma_3)\right] \quad , \tag{5.8}$$

and

$$Z = \left[\frac{v_e}{v_o} - \frac{a_3}{2\theta_{g_3}}\cos(\omega t_e + \Gamma_3)\right](t - t_e) + \frac{a_3}{2\omega\theta_{g_3}}\left[\sin(\omega t + \Gamma_3) - \sin(\omega t_e + \Gamma_3)\right] \quad , \tag{5.9}$$

where a_3 is the ratio of the assumed voltage, V_3, to the d-c beam voltage V_o, and the d-c gap transit angle, θ_{g_3}, is defined by

$$\theta_{g_3} \equiv \frac{\omega d_3}{v_o} \quad . \tag{5.10}$$

Applying boundary conditions at $t = t_f$ to Equations (5.8) and (5.9) and multiplying the latter by ω gives the following equations:

$$\theta_{g_3} = \left[\frac{v_e}{v_o} - \frac{a_3}{2\theta_{g_3}} \cos(\omega t_e + \Gamma_3)\right] (\omega t_f - \omega t_e)$$

$$+ \frac{a_3}{2\theta_{g_3}} \left[\sin(\omega t_f + \Gamma_3) - \sin(\omega t_e + \Gamma_3)\right] \quad , \tag{5.11}$$

$$\frac{v_f}{v_o} = \frac{v_e}{v_o} + \frac{a_3}{2\theta_{g_3}} \left[\cos(\omega t_f + \Gamma_3) - \cos(\omega t_e + \Gamma_3)\right] \quad . \tag{5.12}$$

Equation (5.11) is used to compute the exit time, ωt_f, and Equation (5.12) to compute the normalized exit velocity, v_f/v_o.

The principle of conservation of charge for the third gap results in

$$\frac{i_f}{I_o} = \frac{\frac{i_e}{I_o}}{\left|\frac{d\omega t_f}{d\omega t_e}\right|} \quad . \tag{5.13}$$

The denominator of Equation (5.13) is found by differentiating Equation (5.11) with respect to ωt_e; therefore

$$\frac{d\omega t_f}{d\omega t_e} = \frac{\frac{v_e}{v_o} - \frac{a_3}{2\theta_{g_3}} (\omega t_f - \omega t_e) \sin(\omega t_e + \Gamma_3) - (\omega t_f - \omega t_e) \frac{d}{d\omega t_e} \frac{v_e}{v_o}}{\frac{v_e}{v_o} + \frac{a_3}{2\theta_{g_3}} \left[\cos(\omega t_f + \Gamma_3) - \cos(\omega t_e + \Gamma_3)\right]} \quad , \tag{5.14}$$

where

$$\frac{d}{d\omega t_e}\left(\frac{v_e}{v_o}\right) = \frac{d\omega t_d}{d\omega t_e}\ \frac{d}{d\omega t_d}\left(\frac{v_d}{v_o}\right) = \frac{\dfrac{d}{d\omega t_d}\left(\dfrac{v_d}{v_o}\right)}{\dfrac{d\omega t_e}{d\omega t_d}} \quad . \qquad (5.15)$$

It should be noted that since all the derivatives are single-valued, the reversal of the derivatives at various stages of this analysis is valid. This is a result of considering the components only, rather than the total contributions of current from the increments of ωt_c time. Total currents and corresponding velocities can be plotted from computer data at any major point along the tube.

B. VELOCITY FILTERING

Equations (5.2) – (5.6) for the second drift space and Equations (5.11) – (5.15) for the third gap were computed by the digital computer. Since the operating parameters of the catcher gap and the velocity-filter gap were known, they were used as constants of the problem, with the normalized second drift angle θ_{o2} as a variable.

One can see from Figure 28a that Class 1 electrons and Class 3 electrons have almost the same velocity, and they are almost π radians apart. The drifting of the electron beam in the second drift space, therefore, will not alter their relative positions with respect to each other. Consequently, in the third gap, with the known operating parameters for the velocity-filter gap, Class 3 electrons will be accelerated while Class 1 electrons are decelerated. This will result in a greater maximum normalized velocity in the electron beam at the exit from the third gap than

that at the exit from the second gap, which can be shown to be an improvement so far as the intensities of the X-ray radiation are concerned, since the amount of charge of Class 1 electrons is very much larger than that of Class 3 electrons. These intensities are calculated and discussed in the latter part of this chapter.

The computer data have shown that for the velocity-filter gap to be most effective on Class 1 electrons, the optimum drift angle θ_{o2} must be $9\pi/4$. The normalized exit current, i_f/I_o, and the normalized exit velocity, v_f/v_o, as functions of the exit time, ωt_f, are shown for the optimum case in Figure 31 where $\theta_{o2} = 9\pi/4$, $\theta_{g3} = 7\pi/4$, $\Gamma_3 = -\pi/2$, and $\alpha_3 = 1.0$. Each number on the curve shown in Figure 31a is the number assigned to an electron at plane c (Figure 30), which is chosen as an initial condition for the computer problem of Chapter IV. (The initial conditions at plane c for $\alpha_1 = 0.8$ are given in Appendix I.) It is apparent from Figure 31a that several overtakings occur, some in the second drift space and some in the third gap. These are due mainly to the large velocity spread in the electron beam at the exit from the catcher gap. The important groups of electrons are the decelerated Class 1 electrons and the accelerated Class 3 electrons. The rest are used only to compute the total kinetic energy of the electron beam. Bar graphs similar to those previously used are shown in Figure 32. If Figure 32a is compared to Figure 24e, it is apparent that, following the velocity-filter gap, the two bunches existing in the electron beam shift to lower velocities, but a small percentage of electrons (of Class 3) shift to higher velocities. The velocity spread, therefore, is somewhat the same as it was at the exit from the second gap. Both these shifts can again be seen if Figure 32b is compared to Figure 25e. It should be noted that

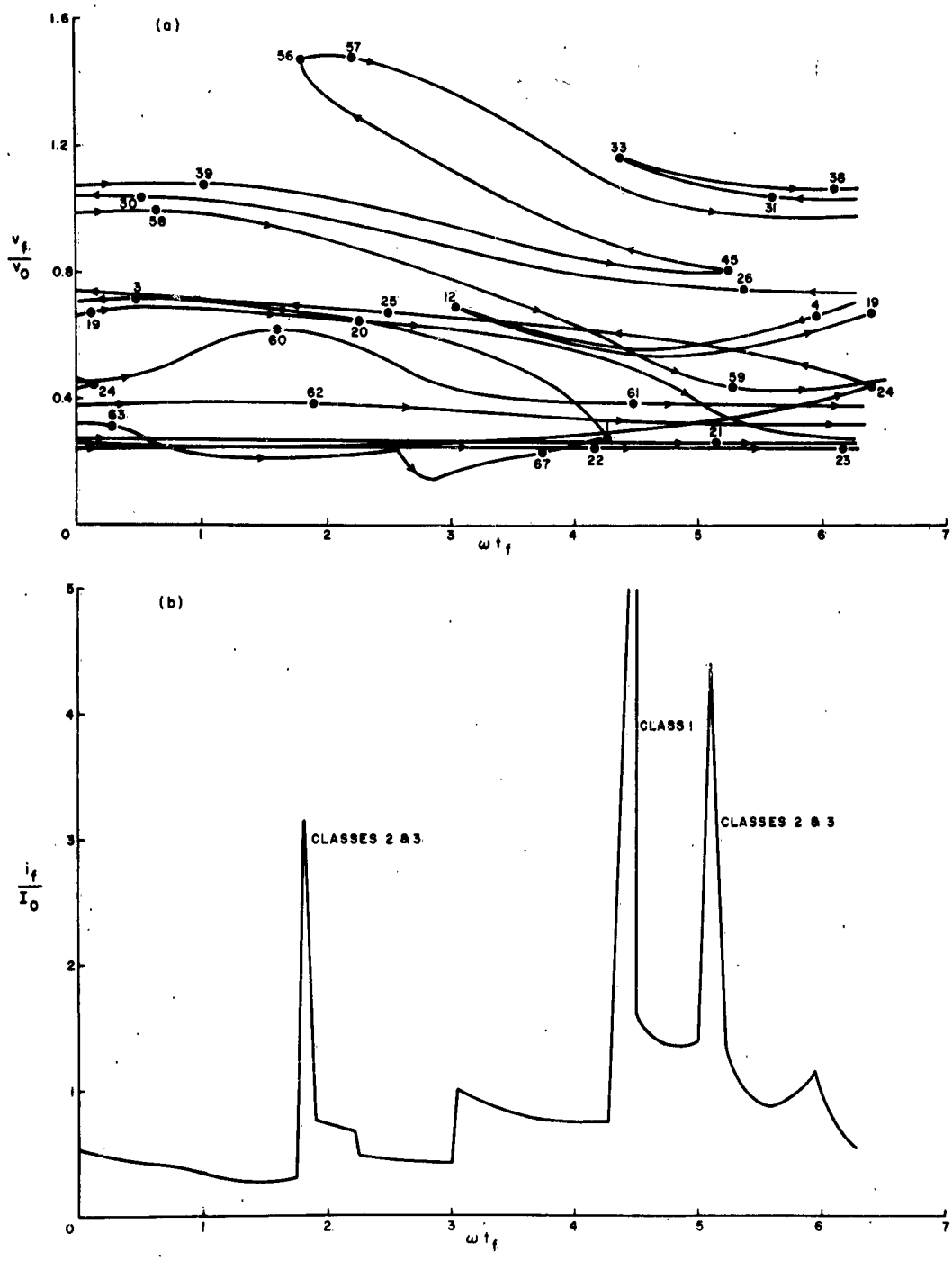

Figure 31. (a) Normalized Exit Velocity v_f/v_o versus Exit Time ωt_f; (b) Normalized Exit Current i_f/I_o versus Exit Time ωt_f for $L_2 = 9\pi/4$, $\theta_{g_3} = 7\pi/4$, $\Gamma_3 = -\pi/2$, and $\alpha_3 = 1.0$.

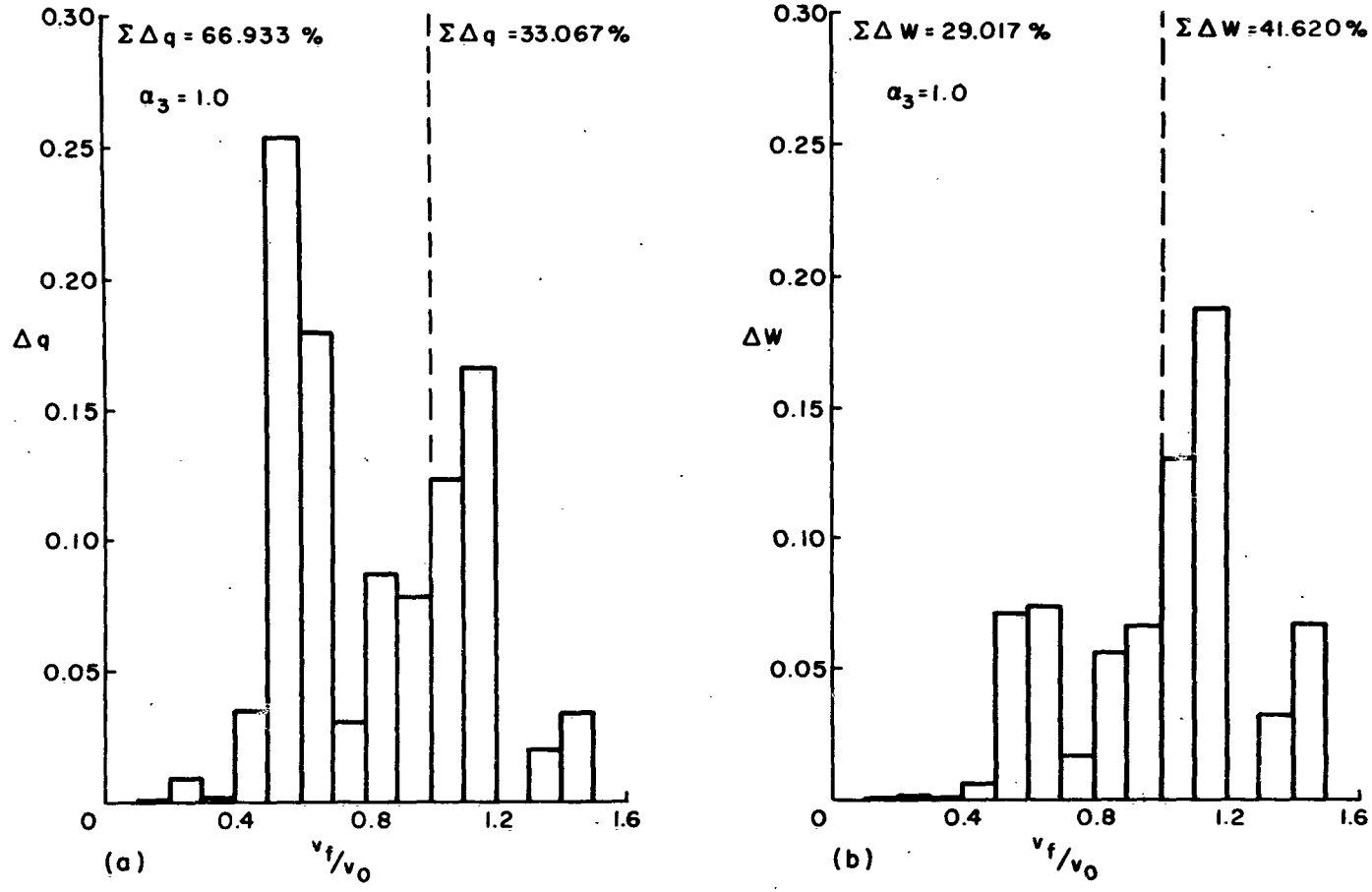

Figure 32. (a) Percentage of Incremental Charge Δq versus Velocity-Class v_f/v_o ; (b) Percentage of Incremental Kinetic Energy ΔW versus Velocity-Class v_f/v_o for $L_2 = \frac{9\pi}{4}$, $\theta_{g_3} = \frac{7\pi}{4}$, $\Gamma_3 = -\frac{\pi}{2}$, and $\alpha_3 = 1.0$.

for slow electrons the total incremental kinetic energy, $\Sigma\Delta W$, does not show an increase, but for fast electrons it shows a definite decrease. This is as expected, since the velocity-filter gap selected interacts primarily with the fast electrons. The calculations of the total kinetic energy show that the power is taken out and that the efficiency of the selected velocity-filter gap is 5.368 per cent.

The power taken out from the velocity-filter gap represents a further decrease in the total kinetic energy of the spent beam and hence a decrease in the total X-ray radiation from the collector (the target). Because of unavoidable phases and velocities of Class 3 electrons, the hardness of this radiation increases. In spite of this, the introduction of the velocity-filter gap produces an improvement in X-ray radiation simply by decelerating the highly bunched Class 1 electrons. In the following discussion the transmission of the continuous X-ray spectrum (Bremsstrahlung) through a given shield will be considered, and the transmitted intensities of various wavelengths, with and without the velocity-filter gap, will be compared.

The continuous X-ray spectrum has some interesting features. The wavelength characteristics of the continuous spectrum are independent of the material of the target, but are determined by the voltage applied to the tube (see Figure 33). It is seen from Figure 33 that for a definite voltage, no radiation occurs up to a certain wavelength, (λ_{min}). "Having passed this wavelength, the intensity rises sharply to a maximum, and then gradually falls to a relatively low value. The intensity of the continuous spectrum is dependent on the target material, the tube current and the applied voltage as well as on the thickness of the target."[8, 9] It was shown that the con-

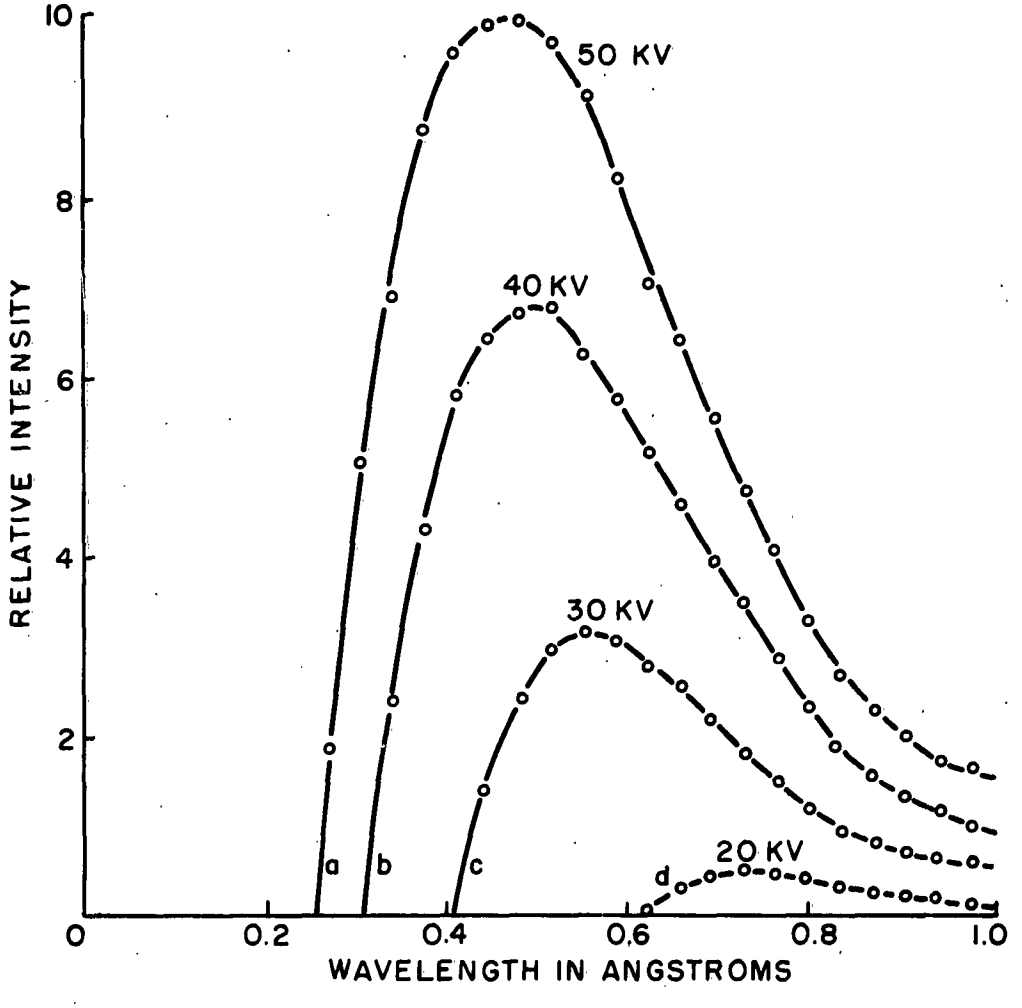

Figure 33. Relative Intensity versus Wavelength in Angstroms for a Tungsten Target at Various Voltages. (After measurements of Ulrey given by Richtmyer, Kennard, and Lauretsen.[9])

tinuous spectrum emitted by a thick target can be approximated by the continuous spectrum emitted by a thin target. The usual assumption is that the total emission from a thick target is obtained by considering a summation over each of the emissions from a series of thin targets one behind the other, with the energy of the incident electrons decreasing for each succeeding thin target.[10] In this discussion, however, we are not interested in the absolute value of the intensity of the continuous spectrum at a specific wavelength, but in the relative intensity transmitted through a given shield. Qualitative relations of the various parameters will therefore suffice.

The equations for the minimum wavelength and the intensity of radiation at a given wavelength in terms of the voltage and the current of the electron beam are:

$$\lambda_{min} = \frac{k}{V} \quad , \tag{5.16}$$

and[11]

$$J_\lambda = K \frac{1}{\lambda^2} \, i_1 \quad . \tag{5.17}$$

From Equations (5.16) and (5.17), one can write for two different wavelengths:

$$\frac{J_{\lambda 1}}{J_{\lambda 2}} = \left(\frac{V_1}{V_2}\right)^2 \left(\frac{i_1}{i_2}\right) \quad , \tag{5.18}$$

which can be transformed into

$$\frac{J_{\lambda 1}}{J_{\lambda 2}} = \left(\frac{v_1}{v_2}\right)^2 \frac{W_1}{W_2} \quad , \tag{5.19}$$

since

$$V = \frac{1}{2} \frac{m}{e} v^2 \quad , \tag{5.20}$$

where W_1 represents the kinetic energy corresponding to i_1 and v_1.

The transmission intensity varies exponentially with the mass absorption coefficient, μ/ρ,, the density, ρ,, and the thickness, x,, of the shield material, as,

$$\frac{J}{J_o} = e^{-\left(\frac{\mu}{\rho}\right)_{\lambda_o} \rho x} \quad . \tag{5.21}$$

The mass absorption coefficient depends on the shield material and the wavelength λ, and is usually directly proportional to the density and inversely proportional to the wavelength. Mass absorption coefficients are determined experimentally and are given in the literature.

If a reference intensity at a given wavelength is chosen, then from Equations (5.19) and (5.21), one has

$$\frac{J}{J_{ref}} = e^{-\left(\frac{\mu}{\rho}\right)_{\lambda_n} \rho x} \cdot \left(\frac{v_n}{v_{ref}}\right)^2 \frac{W_n}{W_{ref}} \quad . \tag{5.22}$$

Since the present work is intended to apply to high-power klystrons, a d-c beam voltage of 250 kv is chosen for the two-cavity klystron for the following computations. It is seen from Figures (24e) and (25e) that the maximum percentage of Δq and the maximum percentage of ΔW are those of velocity-class 1.2. The intensity of radiation from this velocity-class of electrons, therefore, is taken as the reference intensity. The

material of the shield is lead ($\rho = 11.005$ gr/cm^3) and the thickness of it is assumed to be such as to drop the reference intensity to $1/e$ of its incident magnitude. The mass absorption coefficients for lead are plotted in Figure (34), in the wavelength range of interest.[12] Equation (5.21), then, gives

$$\frac{J}{J_{ref}} = e^{-.4 \times 11.005\, x} = \frac{1}{e}$$

$$x = .22717 \text{ cm.}$$

This thickness of .22717 cm and Equation (5.22) are used in the rest of the computations. The results are tabulated in Table III.

It is seen from Table III that the maximum transmitted intensity with the velocity-filter gap is less than the maximum transmitted intensity (the reference) without it.

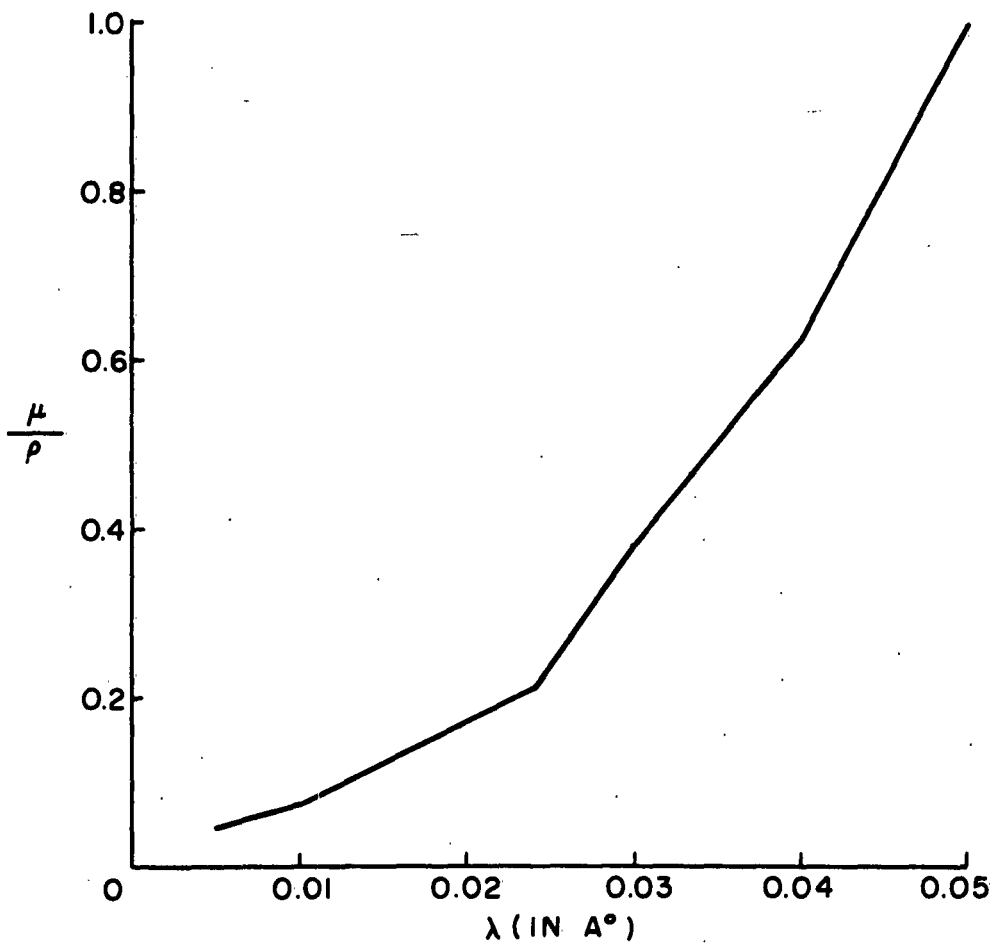

Figure 34. Mass Absorption Coefficient μ/ρ versus Wavelength in Angstroms for Lead Shield.

TABLE III.

Ratios of the Transmitted Intensity to the Reference Intensity with and without the Velocity-Filter Gap.

	Velocity-class	Equivalent voltage in kv	Minimum Wavelength λ_{min} in A°	Mass absorption coefficient (μ/ρ)	Kinetic energy	Transmitted intensity J/J_{ref}
Without velocity-filter gap	1.0 – 1.1	275.6	.0435	.7520	.315004	.022377
	1.1 – 1.2	330.6	.0363	.5300	1.021034	.151560
	1.2 – 1.3	390.6	.0307	.4000	1.515621	.367879*
	1.3 – 1.4	455.6	.0263	.2555	.168071	.068294
With velocity-filter gap	1.0 – 1.1	275.6	.0435	.7520	.872499	.061981
	1.1 – 1.2	330.6	.0363	.5300	1.257900	.186720
	1.3 – 1.4	455.6	.0263	.2555	.217011	.088181
	1.4 – 1.5	525.6	.0228	.1810	.448031	.252997†

*Reference

† Accelerated Class 3 electrons

VI. CONCLUSIONS AND RECOMMENDATIONS

A. CONCLUSIONS

Although this study was based on a very simple model, many interesting and important results were obtained, which may serve as guides for future investigations. Conclusions from this ballistic analysis can be grouped under: (1) exact graphic analysis and its approximation, which includes the first gap and the first drift space, and (2) computer solutions, which includes the second gap, the second drift space, and the third gap.

1. Exact Graphic Analysis and Its Approximation

Exact graphic analysis reveals the physical relationships in the first gap and in the drift space, but it is tedious and time consuming and does not give the functional relationships between the various parameters. Approximating the graphic method analytically, on the other hand, is demonstrated to be valid, the second-order method both approximating the large-signal cases well and also giving analytical formulas that reveal information about the harmonics.

In the first gap both velocity and current modulations are produced during the passage of the electron beam through the gap, and the transit time plays an important role in these phenomena. The velocity modulation is proportional to the depth of modulation a_1, but is inversely proportional to the d-c gap transit angle θ_{g_1}. The difference between the minimum velocity and d-c velocity is greater than the corresponding difference between the maximum velocity and the d-c velocity. Like the velocity modulation, the current modulation is also proportional to the depth of modulation,

but it varies with the d-c gap transit angle, first increasing and then decreasing. Both velocity and current expressions contain harmonics at the exit from the first gap, but this effect is more pronounced in the expression for the current.

In the first drift space, density modulation is produced in a velocity-modulated electron beam through drift action. The beam current develops harmonics, and the amplitudes of harmonics are proportional to the depth of modulation. The maximum value of the fundamental current is seen to be greater than the value of 1.16 predicted by Webber.[5] The point in the drift space at which the maximum value of a harmonic occurs is inversely proportional to the depth of modulation. As the depth of modulation is increased, two bunches of electrons occur, one of fast electrons (Class 1) and the other of slow electrons (Class 2). These results have been shown, at least qualitatively, in the works of others. An additional phase angle β_n is introduced into the current by the two independent components of each harmonic. The velocity becomes more nonlinear at the end of the drift space (overtaking occurs), but its extreme values do not change.

2. Computer Solutions

The multivalued nature of transit times and the occurrence of overtaking make it impossible to derive explicit analytical formulas for the velocity and the current of the electron beam at the second gap and beyond; thus one is limited to graphic analysis, i.e., the digital computer solutions. One salient point in the formulation of the computer problems is consideration of the components instead of the total contributions of current from the increments of ωt_c time. This causes all the time derivatives to be single-valued.

The graphic analysis revealed that one cannot easily predict the operating parameters for a catcher-gap without calculating the kinetic energies at the entrance of the gap and at the exit from it. It was seen that the electron beam debunches as the operating parameters are adjusted for maximum energy extraction. This is also shown by Webber.[13] Optimum operating parameters for the catcher-gap of a two-cavity klystron were found to be $\theta_{g_2} = \pi/2$ radians, $\Gamma_2 = -\pi/4$ radian. The maximum efficiency was 23.995 per cent for $\alpha_1 = 0.8$ and $\alpha_2 = 1.0$ with the selected initial conditions of $\theta_{g_1} = 1.75$ radians and $\theta_{o1} = 2\pi$ radians.

The operating parameters for a velocity-filter gap used as the second gap were easily predicted by the decrease in the maximum velocity at the exit from the gap. The optimum values were found to be $\theta_{g_2} = 7\pi/4$ radians and $\Gamma_2 = -\pi/2$ radians. This gap, which is a rather long gap, showed interaction with the fast electrons (Class 1). The electron beam became more bunched in passing through the gap.

Even with the velocity-filter gap as a third gap in combination with the two-cavity klystron, Class 3 electrons showed undesirable behavior. This was a result of their being at the same velocity as Class 1 electrons and almost half a cycle apart from them. The drifting of the electron beam in the second drift space, therefore, did not alter their relative positions with respect to each other. Consequently, in the third gap, with the known operating parameters for the velocity-filter gap, Class 3 electrons were accelerated while Class 1 electrons were decelerated. This resulted in a greater maximum velocity at the exit from the third gap than that at the exit from the catcher-gap. It was shown, however, that the inclusion of the velocity-filter gap was an improvement so far as the intensities of the X-ray

radiation transmitted through a given shield were concerned (see Table II), since the amount of charge of Class 1 electrons was very much larger than that of Class 3 electrons. To obtain the greatest decrease in the velocity of Class 1 electrons, the optimum second drift length was found to be $\theta_{o2} = 9\pi/4$ radians. Under these operating conditions, an efficiency of 5.368 per cent was obtained for $\alpha_3 = 1.0$. Thus it was demonstrated that the idea of interaction of a r-f gap with a group of bunched electrons having a specific velocity-class is feasible.

B. RECOMMENDATIONS

The combination of the two-cavity klystron and the velocity-filter gap partly solves the problem of X-ray radiation resulting from the acceleration of Class 3 electrons. Since their velocities are greater than those of Class 1 electrons at the exit from the third gap, the relative positions of these classes will alter in a third drift space. In fact, an additional optimum drift space can be introduced such that Class 1 electrons and Class 3 electrons come to the same phase. Inclusion of an additional velocity-filter gap at the end of this optimum drift space obviously will further decrease the velocity of this new group of electrons and hence the X-ray radiation. A number of alternating drift spaces and velocity-filter gaps may completely reduce the radiation to safe levels.

The acceleration of Class 3 electrons can be avoided by tuning the velocity-filter gap to the second harmonic of the beam current. The phase of the induced voltage across the gap can be adjusted such that the r-f field interacts with both Class 1 electrons and Class 3 electrons in the decelerating half cycle.

Experimental verification of the results obtained in the analysis of this report can be made on a device such as the dynamic beam tester.[7] Although there will be discrepancies between experimental and analytical results because of the limitations of the model, qualitative agreement between the two is expected.

The model used in the above analysis was a simple one. The same kind of analysis can be applied to a model that has gridless gaps, finite size, and that is modified for space charge.

APPENDIX A.
INITIAL CONDITIONS AT ENTRANCE TO SECOND GAP (PLANE C)

(θ_{g_1} = 1.75 radians, α_1 = 0.8, θ_{o_1} = 2π radians)

Electron no.	Time	Normalized velocity	Normalized component current	Electron no.	Time	Normalized velocity	Normalized component current	Electron no.	Time	Normalized velocity	Normalized component current
n	ωt_c	v_c/v_o	i_c/I_o	n	ωt_c	v_c/v_o	i_c/I_o	n	ωt_c	v_c/v_o	i_c/I_o
1	.200	.720648	.203387	24	.200	.949176	.905942	47	1.800	1.158969	.313954
2	.400	.708945	.212843	25	6.283185	1.002564	1.095834	48	1.850	1.152639	.308198
3	.600	.697773	.225171	26	6.200	1.028247	1.219381	49	1.900	1.146321	.302669
4	.800	.687152	.241524	27	6.100	1.063077	1.439242	50	1.950	1.140026	.297364
5	1.000	.677133	.263860	28	6.000	1.104585	1.833450	51	2.000	1.133753	.292266
6	1.200	.667783	.295909	29	5.950	1.129547	2.197772	52	2.050	1.127498	.287364
7	1.400	.659251	.345734	30	5.900	1.159782	2.907187	53	2.100	1.121268	.282651
8	1.600	.651865	.435440	31	5.850	1.203425	5.629951	54	2.600	1.060626	.244266
9	1.800	.646592	.664387	32	5.850	1.283080	5.602494	55	3.100	1.003609	.217866
10	1.850	.645978	.802519	33	5.900	1.310843	2.871670	56	3.600	.950649	.199819
11	1.900	.646026	1.073562	34	5.950	1.325186	2.157251	57	4.100	.901822	.188030
12	1.950	.647827	2.093169	35	6.000	1.334324	1.786587	58	5.100	.815991	.179293
13	1.950	.660110	2.336703	36	6.100	1.344292	1.381072	59	5.700	.771490	.183311
14	1.900	.669454	1.323102	37	6.200	1.347779	1.150158	60	5.800	.764551	.184778
15	1.850	.677165	1.056814	38	6.283185	1.347535	1.017763	61	5.850	.761131	.185612
16	1.800	.684316	.923765	39	.200	1.339406	.806984	62	5.900	.757744	.186515
17	1.600	.711270	.718130	40	.400	1.324428	.672960	63	5.950	.754390	.187489
18	1.400	.738150	.655712	41	.600	1.305240	.578237	64	6.000	.751069	.188539
19	1.200	.766213	.638434	42	.800	1.283352	.507024	65	6.100	.744524	.190877
20	1.000	.796131	.645942	43	1.000	1.259747	.451353	66	6.200	.738109	.193561
21	.800	.828537	.672874	44	1.200	1.235092	.406631	67	6.283185	.732873	.196082
22	.600	.864128	.719896	45	1.400	1.209862	.369996				
23	.400	.903861	.792801	46	1.600	1.184403	.339546				

REFERENCES

1. D. L. Webster, "Cathode Ray Bunching," Jour. Appl. Phys., 10 (July 1939), pp. 501-508.

2. T. G. Mihran, "The Effect of Space Charge on Bunching in a Two-Cavity Klystron," I.R.E. Trans., ED-6 (January 1959).

3. G. C. Dalman, Unpublished work.

4. H. B. Dwight, Tables of Integrals and Other Mathematical Data, New York: Macmillan (1953), pp. 174-191.

5. S. E. Webber, "Ballistic Analysis of a Two-Cavity Finite Beam Klystron," I.R.E. Trans., ED-5 (April 1958), pp. 98-108.

6. L. Solymar, "Exact Solutions of the One-Dimensional Bunching Problem," Jour. Elect. Control, 10 (March 1961).

7. A. S. Gilmour, Jr., "A Beam Tester for Studying the Characteristics of D-C and Velocity-modulated Electron Beams," Research Report EE 495, Cornell University (May 1961).

8. A. H. Compton, X-Rays and Electrons, New York: D. Van Nostrand (1928), pp. 27-28.

9. F. K. Richtmyer, E. H. Kennard, and T. Lauritsen, Introduction to Modern Physics, New York: McGraw-Hill (1955), pp. 374-377.

10. S. Flugge, Handbuch der Physik, Vol. 30, Berlin: Springer (1957), p. 349.

11. "High-Power Tube Program," Semiannual Technical Summary Report to ARPA(U), Lincoln Laboratory, M.I.T. (30 June 1962), p. 19.

12. C. D. Hodgman, Handbook of Chemistry and Physics, Cleveland; Clemical Rubber (1952), p. 2240.

13. S. E. Webber, "Some Calculations on the Large Signal Energy Exchange Mechanisms in Linear Beam Tubes," I.R.E. Trans., ED-7 (July 1960), pp. 154-162.

REDUCTION OF SPURIOUS-OUTPUT SIGNALS IN HIGH-POWER KLYSTRONS

A. R. Howland, Jr.

School of Electrical Engineering
CORNELL UNIVERSITY
Ithaca, New York

RESEARCH REPORT EE 540

REDUCTION OF SPURIOUS-OUTPUT SIGNALS IN HIGH-POWER KLYSTRONS

A. R. Howland, Jr.

LINEAR BEAM MICROWAVE TUBES

Interim Report 20 September 1962

Published under Contract No. AF30(602)-2573
Rome Air Development Center, Griffiss Air Force Base, New York

CONTENTS

	Page
ABSTRACT	v
I. INTRODUCTION	1
A. Description of the Radio-Frequency Compatibility Problem	1
B. Need for Solution to R-F Interference Problem	2
II. APPROACH FOR A SOLUTION TO A R-F COMPATIBILITY PROBLEM	2
III. TEST SYSTEM	12
A. Requirements for Test System	12
B. Test System for High-Power Klystron	13
IV. MEASUREMENTS OF SPURIOUS-OUTPUT SIGNALS PLANNED	17

ABSTRACT

This report describes the study of a particular radio-frequency interference problem. The objective of this work is to develop and verify by experiment a design technique for a high-power klystron with reduced harmonic output.

The work has three aspects: (1) an approach for a solution to a r-f compatibility problem, (2) the test system, and (3) measurements of spurious-output signals. The approach followed to develop the design information is obtained by considering the higher-order modes present in the output cavity and placing these mode resonances systematically at optimum frequencies. The test system is constructed from a high-power radar transmitter transmission line and includes a sampling system with a higher-order mode. Measurements will be made on the second, third, and fourth harmonics of an unmodified and a modified klystron to determine the effectiveness of reducing the harmonically related spurious-output signals experimentally.

I. INTRODUCTION

The problems arising from radio-frequency interference in a microwave electromagnetic environment are manifold. These problems may render entire systems inoperative, produce erroneous system results, and reduce the number of systems that can be used, since each system occupies so much of the electromagnetic spectrum.

A. Description of the Radio-Frequency Compatibility Problem

Radio-frequency compatibility arises from a characteristic of electromagnetic signals; that is, each time a wanted signal is generated, an infinite set of unwanted or spurious signals is also generated. This interference is compounded, since each signal (desired or spurious) can mix with every other signal (desired or spurious) in any nonlinear device to produce other sets of spurious energy, etc. Obviously, if most of the signals in these infinite sets of spurious outputs did not have zero amplitude, the useful electromagnetic spectrum would be even more limited than it is today. The resultant of all of these signals, termed "noise," is observed as part of the ambient noise level of the electromagnetic environment. The products, which are referred to as spurious output signals, are those signals whose amplitude is well above the "noise floor." These are the signals which cause most of the problems, because they are the strongest, and they are often overlooked during the design stage of any system.

A classic example of radio-frequency compatibility is reported by Campbell.[1] He describes interference in a radar-to-communication system. In this type of system it is entirely possible that a spurious signal from the radar will be much greater than the transmitted fundamental or carrier-

frequency signal of the communication system. Radar systems have spurious output signals that will interfere not only with communications systems but also with other radar systems. Considerable effort has gone into programs designed to predict the level and type of radio-frequency compatibility that may be expected in a given electromagnetic environment.[2]

B. Need for Solution to R-F Interference Problem

As higher-power emitters of radio-frequency energy are developed and as receivers are designed to be more sensitive, the problems of radio-frequency compatibility become more pronounced. If these problems were solved, there would be room within the electromagnetic spectrum for larger numbers of operational systems.

As the higher powers desired in output signals are achieved, the level of the unwanted signals increases. There is, therefore, a greater need to solve problems of radio-frequency interference in order to protect the lower-power systems of today. The solution of such problems requires both extensive and high-level engineering effort.

II. APPROACH FOR A SOLUTION TO A R-F COMPATIBILITY PROBLEM

Progress toward solving an environmental problem such as radio frequency compatibility is made only by pursuing realistic parts of the over-all problem. There are high-power multicavity pulsed klystrons operating today within the microwave region of the electromagnetic spectrum which generate spurious output signals. The major spurious signals emitted from such klys-

trons are harmonically related to the fundamental or desired output signal of the klystron. It has been found that the variations in the level of the spurious output signals from klystrons which differ only in serial number* are approximately equal to the variations in spurious signal level found between tubes which differ in model number.[2]

The specific problem chosen, then, is the reduction of harmonically related spurious output signals in high-power klystrons. Harmonics of the fundamental signal are generated by velocity modulation, by which the klystron operates. There are harmonic signals present on the klystron's electron beam as it interacts with the output cavity of the klystron, regardless of whether the total input signal includes harmonics of the desired input frequency.[3] (Klystrons have been used as frequency multipliers.)

There are two approaches to the problems caused by spurious outputs. One method is to suppress the spurious outputs after they have been generated in a nonlinear device and then coupled into the system's transmission line. Theoretically this can be done by filters. From the system engineer's viewpoint, this is a very inefficient method of solving the problem, since the addition of filters gives no new information about the operating mechanism of a klystron. Therefore this method does not make for progress in klystron development. The other method is to improve the design procedure for the devices that generate or amplify microwave signals. In doing this, the design procedure must be improved to treat the generation of spurious outputs as well as the fundamental output in a high-power microwave tube that would

*They are of the same type and model number.

normally be used as the final or power-amplifier stage of a high-power microwave radar transmitter. The work reported here deals with this design procedure and is essentially a continuation of the work started by L. A. MacKenzie.[4]

In approaching the spurious output problem for microwave tubes one can study either the active portion, or electron beam; or the passive portion, or tube circuitry. This work approaches the problem from the passive standpoint, although it is recognized that the active portion of the klystron under study cannot be ignored. It is possible to design a model of the cavity with its associated coupling mechanism mathematically. Thus, it is possible to design control of the spurious output signals in the cavity, even though it is heavily loaded. This can be done because the impedance developed across the interaction gap of the doubly re-entrant cavity can be considered as a function of frequency. The cavity analysis technique used in this study is the normal mode expansion of the given boundary-value problem, where both the wave equation and Maxwell's equations are to be satisfied.

The design of klystron output cavities by the procedure that permits analysis of effects removed from the fundamental must be done by a method that does not make so many approximations that higher-order effects are eliminated from the equations for cavity design. Boundary conditions will be expressed as infinite series, where necessary in the solution of this boundary value problem.

The structure to be considered for this initial study (Figure 1) is a typical re-entrant, gridless-gap klystron cavity with an axially symmetric, output-coupling iris that feeds a coaxial line. The structure will be considered to be lossless.

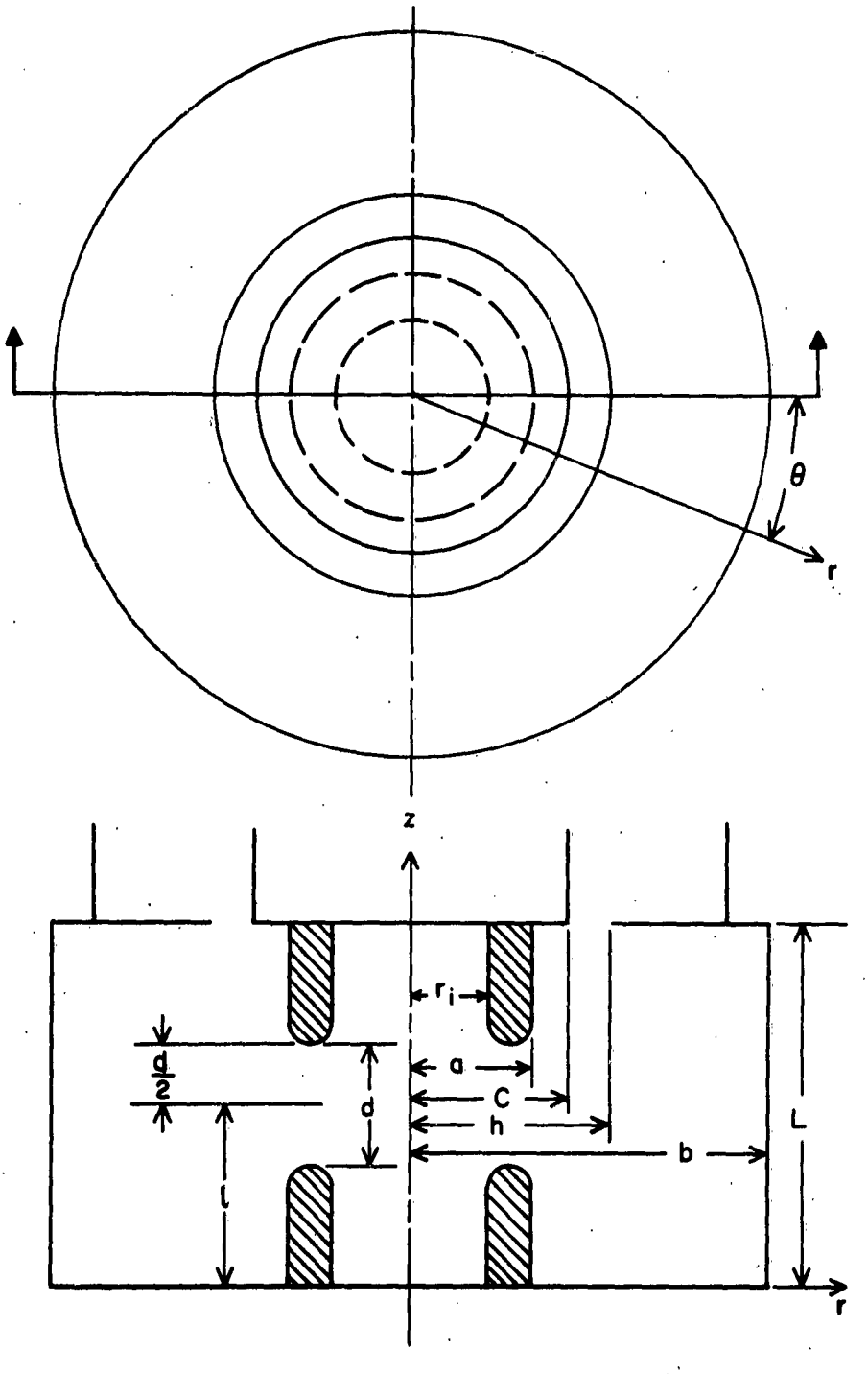

Figure 1. Co-ordinate System of Cavity with Symmetrical Coupling Iris.

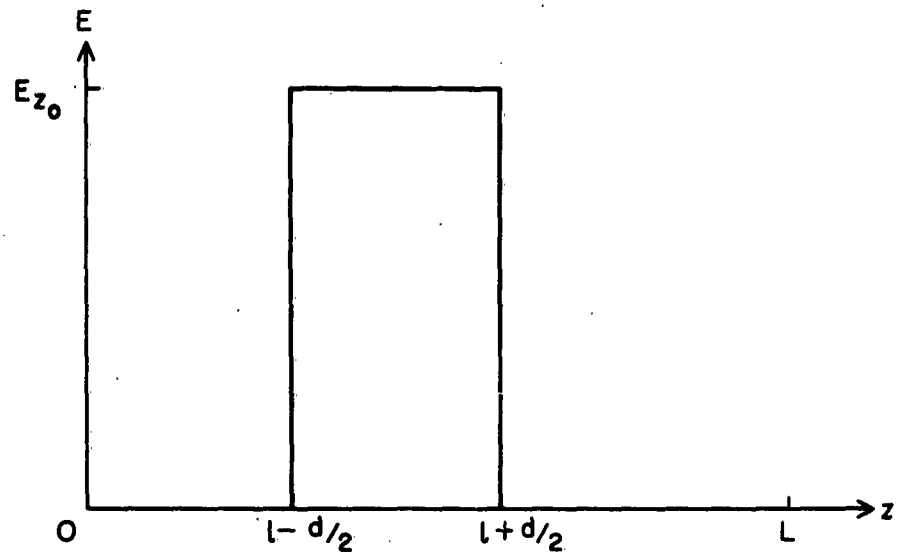

Figure 2. Assumed Interaction Gap Field (r = a).

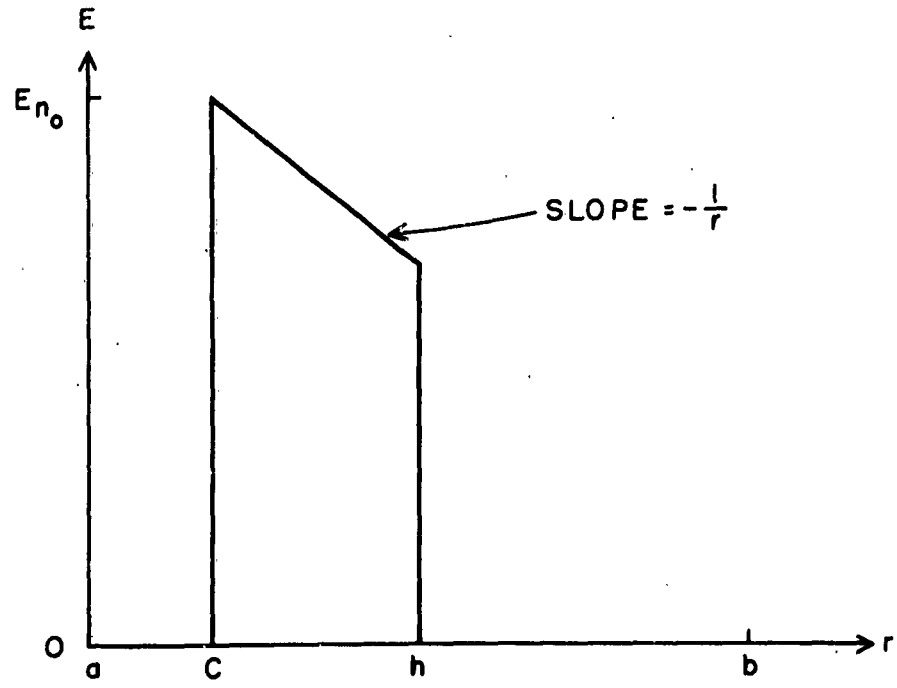

Figure 3. Assumed Coupling Iris Field (z = L).

The modal solution of the structure shown in Figure 1 for symmetrical modes may be expressed by TM_{onm} field components, where the "o" subscript indicates symmetry in the θ direction. As a first step in the solution of this boundary value problem, a field will be assumed at the interaction gap (Figure 2) and also at the coupling iris (Figure 3) of the cavity:

$$E_z\Big|_{r=a} = \begin{cases} 0 & 0 \leq Z < 1 - \frac{d}{2} \\ E_{z_o} e^{j\omega t} & 1 - \frac{d}{2} < Z < 1 + \frac{d}{2} \\ 0 & 1 + \frac{d}{2} < Z \leq L \end{cases} \tag{1}$$

$$E_r\Big|_{z=L} = \begin{cases} 0 & a < r \leq c \\ \frac{E_{r_o}}{r} e^{j\omega t} & c < r < h \\ 0 & h < r \leq b \end{cases} \tag{2}$$

where E_{z_o} and E_{r_o} are shown graphically in Figures 2 and 3 respectively.

In order that the desired signal produced by the interaction of the active (electron beam) portion and the passive (tube circuitry) portion of the microwave tube be capable of reaching the system load (antenna), neither E_z nor E_r can be identically zero. Thus for a symmetrical mode to be capable of transferring a useful signal from the electron beam of the klystron to the system load, the mode must be of the TM type not of the TE type.

If a mode of the TM_{onm} type is considered, where it is known that neither E_z nor E_r are zero for the TM_{onm} modes, then the field component equations are:

$$E_r = \frac{\beta_z}{k} \left[A_m J_1 (kr) + B_m N_1 (kr) \right] \sin \beta_z z \, e^{j\omega t} \quad , \tag{3}$$

$$E_\theta = 0 \quad , \tag{4}$$

$$E_z = \left[A_m J_o (kr) + B_m N_o (kr) \right] \cos \beta_z z \, e^{j\omega t} \quad , \tag{5}$$

$$H_r = 0 \quad , \tag{6}$$

$$H_\theta = j \frac{\omega e}{k} \left[A_m J_1 (kr) + B_m N_1 (kr) \right] \cos \beta_z z \, e^{j\omega t} \quad , \tag{7}$$

$$H_z = 0 \quad , \tag{8}$$

where

$$\left.\begin{aligned} k^2 &= \beta_{z_1}^2 - \gamma_o^2 \quad , \\ \beta_{z_1} &= j \beta_z \quad , \\ \gamma_o &= j\omega(\mu e)^{1/2} \quad . \end{aligned}\right\} \tag{9}$$

The E-field boundary conditions that must be met by this structure are

$$E_r\Big|_{z=o} = 0 \quad , \tag{10}$$

$$E_r\Big|_z = L = \begin{cases} 0 & a \leqslant r < c \\ \dfrac{E_{r_o}}{r} e^{j\omega t} & c < r < h \\ 0 & h < r \leqslant b \end{cases} \quad , \tag{2}$$

$$E_z\Big|_{r = b} = 0 \quad , \tag{11}$$

$$E_z\Big|_{r=a} = \begin{cases} 0 & 0 \leq z < l - \frac{d}{2} \\ E_{z_o} e^{j\omega t} & l - \frac{d}{2} < z < l + \frac{d}{2} \\ 0 & l + \frac{d}{2} < z \leq L \end{cases} \quad . \qquad (1)$$

For convenience in matching these boundary conditions, the structure as shown in Figure 1 will be divided into two cavities. The resultant field component equations for each of the cavities will then be added to give the field solution of the original cavity. Since the principle of superposition is valid for Maxwell's equations, it is possible (but certainly not necessary), to follow this convenient procedure. The two cavities to be studied in this manner are shown in Figures 4 and 5.

The admittance functions of the interaction gap and the coupling gap can be combined to form a set of two equations with two unknowns. Solutions to this set of equations will yield the mode resonance frequency for the axially symmetric modes. The first zero or solution to this set of equations will be the desired fundamental mode resonance.

It should be pointed out that this analysis has assumed that the drift tube of the interaction gap is of zero thickness and that the top plate of the cavity, which contains the coupling gap, is also of zero thickness. The transmission line effects of a finitely thick drift tube and a top plate of the cavity have not been considered. They have been omitted because the amount of phase shift introduced by them is very small at the mode resonances of immediate interest. The usual normal mode expansion of the field components of the cavity leads to a determination of the cavity admittances at the interaction gap (electron beam to cavity) and the coupling gap (cavity to output transmission line).

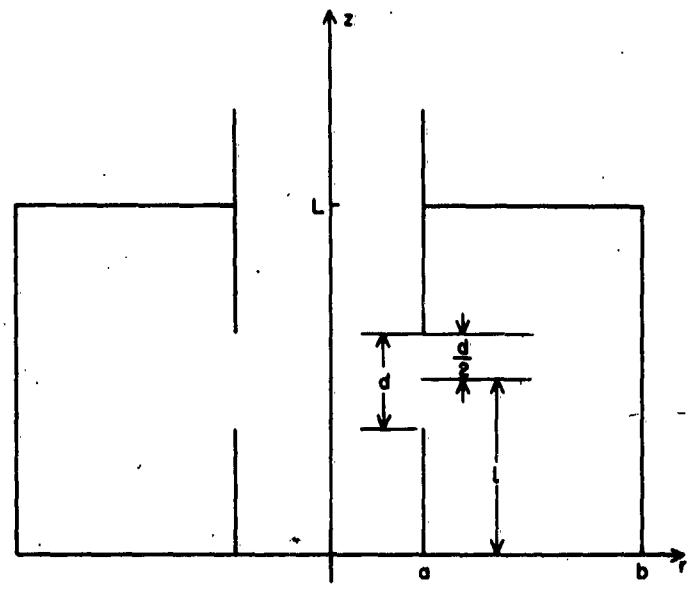

Figure 4. Interaction Cavity.

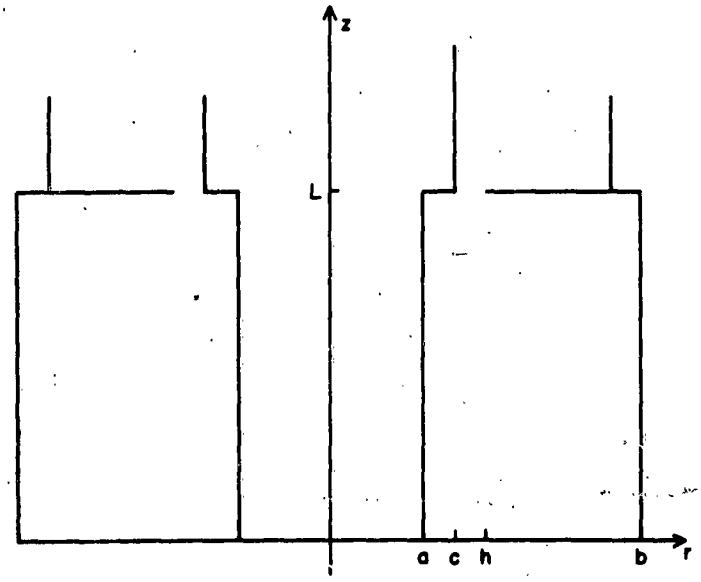

Figure 5. Coupling Cavity.

The total admittance function is:

$$Y_g + Y_{g_1} =$$

$$-j\omega\epsilon\left\{\frac{2\pi a\, D_1(k_4 a)}{k_4 L\, D_o(k_4 a)} + \sum_{m=1}^{\infty} \frac{16\, La\, D_1(k_4 a)\cos\frac{2m\pi l}{L}\sin\frac{2m\pi}{2L}}{d^2 m^2 \pi k_4 D_o(k_4 a)}\right.$$

$$+\left[\frac{4\pi \ln\frac{h}{c}\cos\beta_{Z_5} l \sin\beta_{Z_5}\frac{d}{2}}{d^2\beta_{Z_5}\ln\frac{b}{a}\sin\beta_{Z_5} L}\right.$$

$$\left.\left.+\sum_{m=1}^{\infty}\frac{2\pi^3 a\lambda_m N_o(\lambda_m a)\left[D_o(\lambda_m c) - D_o(\lambda_m h)\right]\cos\beta_{Z_5} l \sin\frac{\beta_{Z_5}}{2}}{d^2\beta_{Z_5}^2\left[N_o(\lambda_m a) - N_o(\lambda_m b)\right]\sin\beta_{Z_5} L} D_1(\lambda_m a)\right]\frac{E_{r_o}}{E_{Z_o}}\right\}$$

$$+ j\frac{2\pi a}{d}\sqrt{\frac{\epsilon}{\mu}}\left\{\frac{J_1(k_o a)}{J_o(k_o a)} - \frac{2a}{d}\sum_{m=1}^{\infty}\frac{k_o a}{\xi^3}\left[1 - e^{-\frac{d\xi}{a}}\right]\right\} \qquad (12)$$

$$Y_c + Y_{c_1} =$$

$$-\frac{j\omega\epsilon}{h-c}\left(\left\{\frac{2\pi\cos\beta_{Z_5} L(h-c)}{\beta_{Z_5}\ln\frac{b}{a}\sin\beta_{Z_5} L}\right.\right.$$

$$+\sum_{m=1}^{\infty}\frac{\pi^3\lambda_m\left[D_o(\lambda_m c) - D_o(\lambda_m h)\right]\cos\beta_{Z_5} L}{\ln\frac{h}{c}\,\beta_{Z_5}\left[N_o(\lambda_m a) - N_o(\lambda_m b)\right]\sin\beta_{Z_5} L}\left[h(h-l)\, D_1(\lambda_m h)\right.$$

$$\left.\left.\left.- c(c-l)\, D_1(\lambda_m c) - \frac{1}{\lambda_m} D_o(\lambda_m h) + \frac{1}{\lambda_m} D_o(\lambda_m c)\right]\right\}\right.$$

$$+\left\{\frac{d\pi\left[h(h-l)\, D_1(k_4 h) - c(c-l)\, D_1(k_4 c) - \frac{1}{k_4} D_o(k_4 h) + \frac{1}{k_4} D_o(k_4 c)\right]}{k_4 L\, D_o(k_4 a)\ln\frac{h}{c}}\right.$$

$$+\sum_{m=1}^{\infty}\frac{r(-1)^m\cos\frac{m\pi l}{L}\sin\frac{m\pi d}{2L}}{m k_4 D_o(k_4 a)\ln\frac{h}{c}}\Big[h(h-l)\,D_1(k_4 h)-c(c-l)D_1(k_4 c)-\frac{1}{k_4}D_o(k_4 h)$$

$$+\frac{1}{k_4}D_o(k_4 c)\Big]\Bigg\}\frac{E_{r_o}}{E_{Z_o}}\Bigg)-\frac{2\pi}{(h-c)\ln\frac{h}{c}}\Bigg\{(h-c)\frac{\ln\frac{h}{c}}{\ln\frac{p}{c}}$$

$$+\frac{j\omega\epsilon\pi^2}{4\beta_6}\sum_{m=1}^{\infty}\frac{a_{m_6}N_o(a_{m_6}c)\left[D_o(a_{m_6}c)-D_o(a_{m_6}h)\right]}{N_o(a_{m_6}c)-N_o(a_{m_6}p)}\Big[h(h-l)D_1(a_{m_6}h)$$

$$-c(c-l)D_1(a_{m_6}c)-\frac{1}{a_{m_6}}D_o(a_{m_6}h)\Big]\Bigg\} \qquad (13)$$

III. TEST SYSTEM

The test of any analytical solution lies in experimental verification of the method or technique used. Experimental verification of a solution to the problem discussed here consists of a test set for measuring spurious-output signals and the support system required to drive the device under test.

A. Requirements for Test System

The measurement test set must permit measurements to be made under actual operating conditions, specifically at full power, for extrapola-

tions from reduced power may be of no value. The support system includes a high-power modulator, a r-f signal source, a r-f driver, the necessary protective circuits, and so forth. The entire support system must be designed so that the results obtained may be traced to the device under test.

B. Test System for High-Power Klystron

The construction of the new output structure has been centered around the four-cavity Varian VA-87 klystron. This klystron operates between 2.8 – 2.9 Gc/s with a peak power output at the fundamental of 2 Mw, at a beam voltage of 115 kv and 1.3 Mw at 90 kv.

The new output structure, shown in Figure 6, consists of a new output cavity, coaxial output transmission line, and a transition from the coaxial line to the normal S-band waveguide. A high-vacuum ball valve has been placed in the drift space between the output cavity and the third cavity. This valve permits the change of the output structure without letting the electron gun down to atmospheric pressure. This tube does have an oxide-coated cathode.

Thus, the test instrument consists of the electron gun, the input cavity, the second cavity, and the third cavity, which form a hot-test system. This test instrument is capable of being used to test the performance of any output structure under the meaningful conditions of full-rated power. In addition to the modifications made to the VA-87 at the output end of the tube, it was also necessary to remove the electron gun and add a flange in the gun region in order that the cathode could be recoated as required. Also a vacuum pump connection has been made to the electron gun. The test tube is continuously pumped from both the electron gun and output structure while

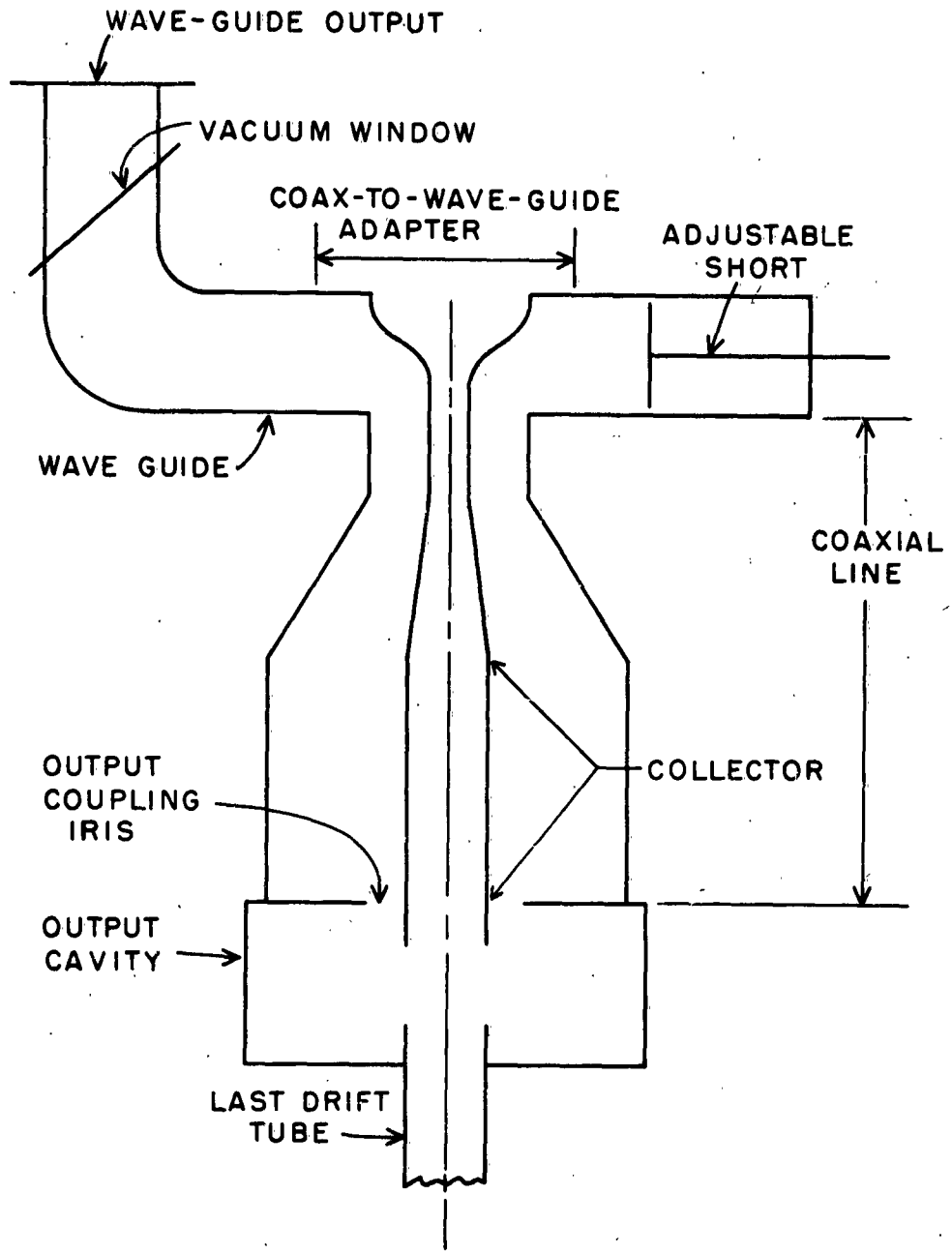

Figure 6. New Output Structure for VA-87.

tests are performed. The photograph of the test instrument portion of the tube shown in Figure 7 was taken during construction.

The high-voltage power supply required to supply the beam voltage to the VA-87 is assembled from an AN/FPS-6 power supply and modulator. This unit with the pulse transformer supplies a 2-microsecond pulse to the VA-87. The beam voltage is continuously variable from 0 – 115 kv. The pulse repetition rate is continuously variable from 200 – 500 pps.

The r-f oscillator and driver are respectively a lighthouse tube in a cavity (part of the AN/TS-155E/UP signal generator) and a small three-cavity c-w space-charge-focused klystron (Sperry SAS-60). The r-f input drive level to the VA-87 is continuously variable from 0 w to 6 w peak. Optimum drive level is approximately 2.5 w peak. The signal generator unit contains the system trigger. In this system it is possible to have (1) the r-f signal pulse centered inside the beam voltage pulse, (2) the r-f signal pulse and beam voltage pulse the same, and (3) the beam voltage pulse centered inside the r-f signal pulse.

Even after the design and fabrication of the output structure and the construction of support system required for the VA-87, this test system for spurious-output signals is by no means complete. The signal sampling system remains to be considered.

The signal sampling system must be capable of measuring signals that are 20 or more decibels below the fundamental signal and far removed from the fundamental. These signals are at two, three, and four times the fundamental signal (f_o), and are therefore propagated in the S-band wave guide outside of the usual frequency range. This means that these signals will propagate in more than one mode and that problems of the various coupling coefficients to the various mode must be solved.

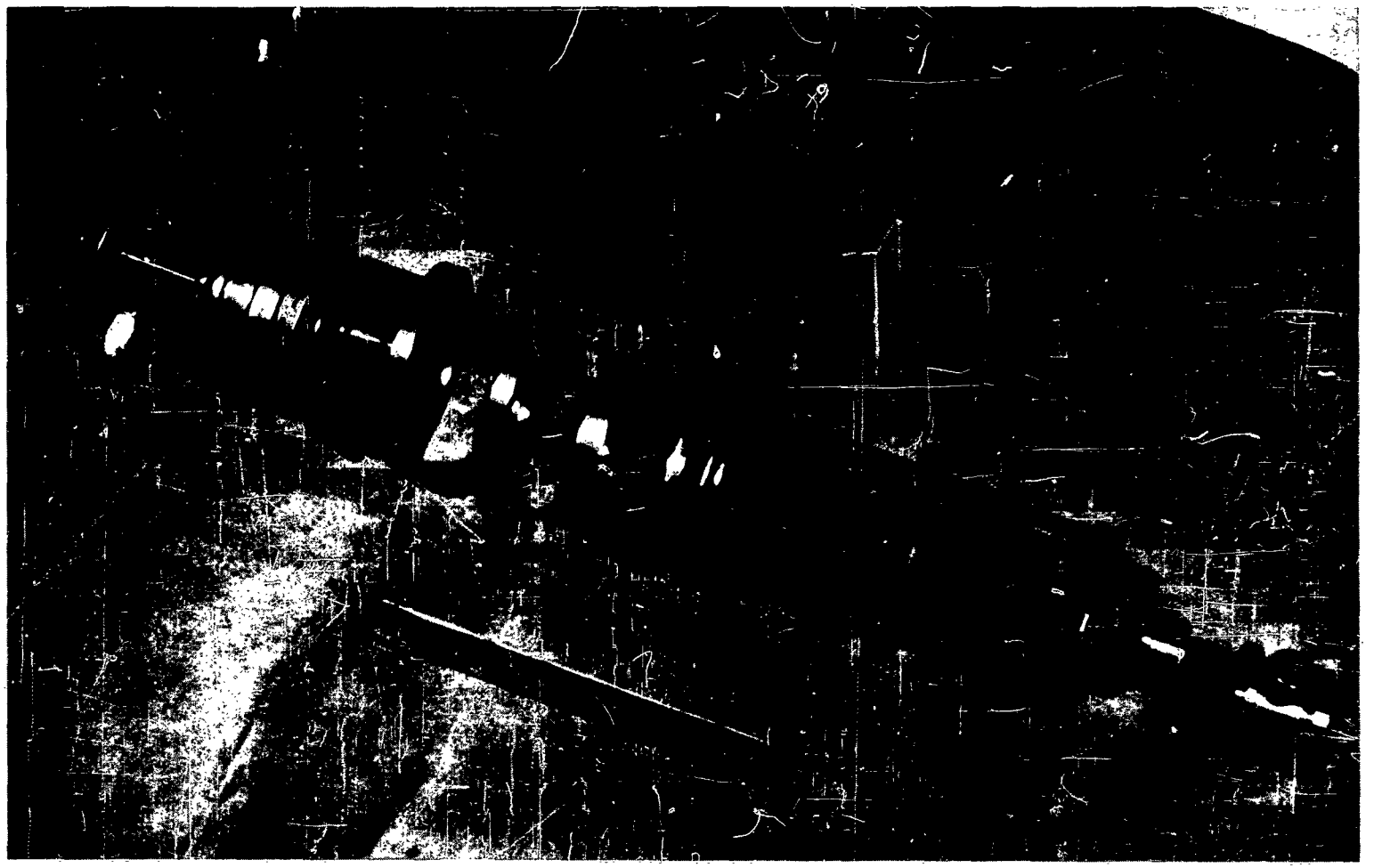

Figure 7. VA-87, Test Instrument.

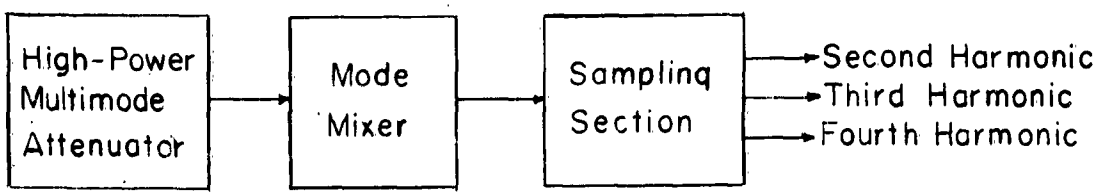

Figure 8. Signal-sampling Device.

The resulting spurious-output test facility is an unusually versatile system and certainly capable of measuring the entire output of any high-power S-band output structure placed on the VA-87 test vehicle. A block diagram of the test facility is shown in Figure 9.

IV. MEASUREMENTS OF SPURIOUS-OUTPUT SIGNALS PLANNED

The second, third, and fourth harmonics of the fundamental signal will be measured on two different VA-87 tubes. The first or "before" tube is just as it comes from the manufacturer, i.e., no modifications. The second or "after" tube is the VA-87 modified to serve as test instrument. Only one output structure will be built and tested during this study. Future programs could use this test facility to study other output structures. The comparison of the spurious-output signals measured on the "before" and "after" tubes of this study will present a direct measure of the improvement in the reduction of spurious-output signal levels that results from the use of this cavity design technique.

Measurements are now in progress. This program will give specific results obtained for the second, third, and fourth harmonics for the unmodified or "before" VA-87 and the modified or "after" VA-87. These signals will be measured as a function of r-f input signal power level, r-f input signal frequency, and beam voltage of the VA-87. A report of these results will be published at the conclusion of the measurements. The report will also include details of cavity design.

V. REFERENCES

1. R. D. Campbell, "Radar Interference to Microwave Communication Services," Electrical Engineering, October 1958.

2. Delmar C. Ports, et al. Interference Prediction Study, Jansky and Bailey, Washington, D. C., Reports prepared under Air Force Contract Number AF 30(602)-1934.

3. Edward L. Ginzton, Microwave Measurements, McGraw-Hill: New York, p. 16.

4. L. A. MacKenzie, "Klystron Cavities for Minimum Spurious Output Power," Research Report EE 418, Cornell University (January 1959).

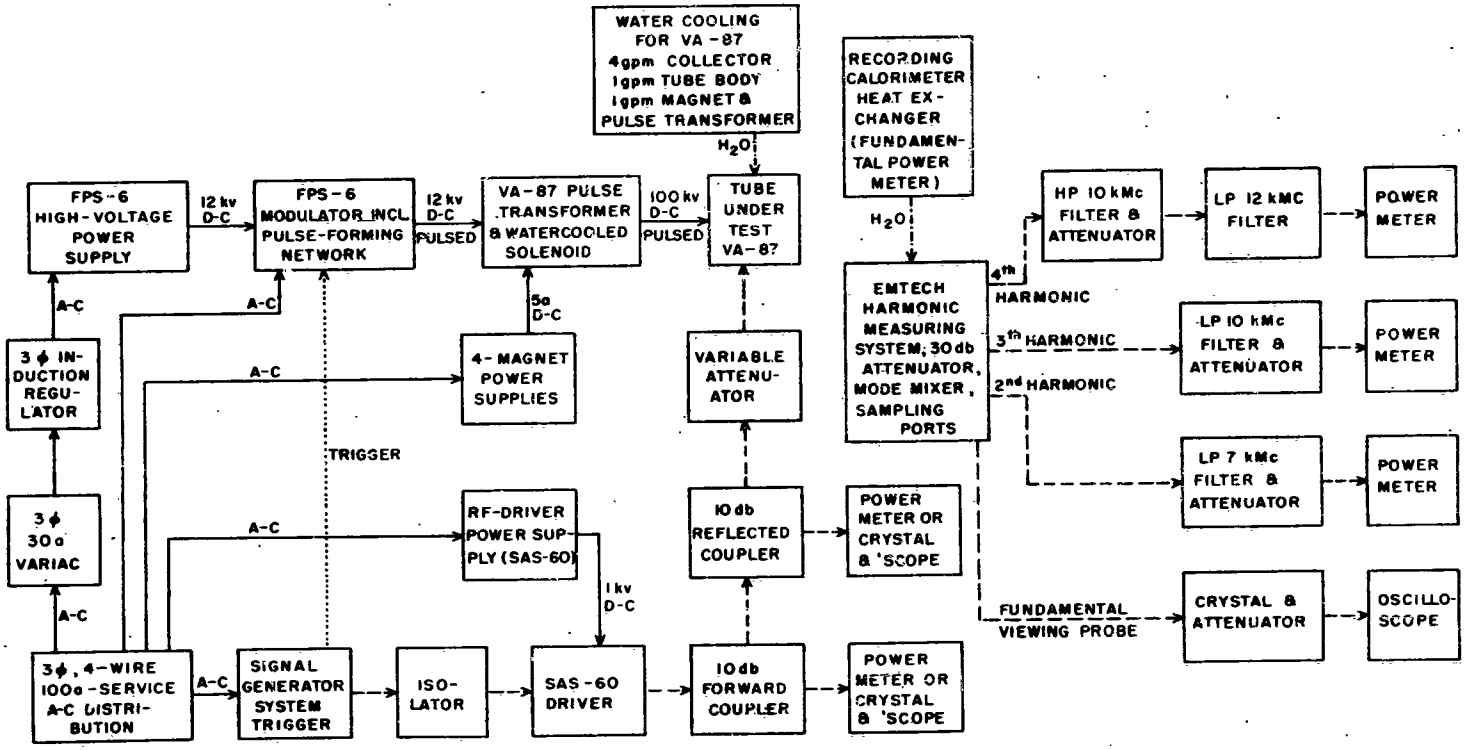

Figure 9. VA-87 System.

DISTRIBUTION LIST FOR CONTRACT REPORTS

	No. of Copies
RADC (RALTP), ATTN: R. H. Chilton Griffiss AFB NY	4
RADC (RAAPT) Griffiss AFB NY	1
RADC (RAALD) Griffiss AFB NY	1
GEEIA (ROZMCAT) Griffiss AFB NY	1
RADC (RAIS, ATTN: Mr. Malloy) Griffiss AFB NY	1
U. S. Army Electronic Research and Development Labs Liaison Office RADC Griffiss AFB, N. Y.	1
AUL (3T) Maxwell AFB Ala	
ASD (ASAPRD) Wright-Patterson AFB Ohio	1
Chief, Naval Research Lab ATTN: Code 2027 Washington 25, DC	1
Air Force Field Representative Naval Research Lab ATTN: Code 1010 Washington 25, D. C.	1
Commanding Officer U. S. Army Electronics Research and Development Labs ATTN: SELRA/SL-ADT Ft Monmouth, N. J.	1
National Aeronautics and Space Administration Langley Research Center Langley Station Hampton Virginia ATTN: Librarian	1

	No. of Copies
Central Intelligence Agency ATTN: OCR Mail Room 2430 E. Street NW Washington 25, D.C.	1
U. S. Strike Command ATTN: STRJ5-OR Mac Dill AFB Fla	1
AFSC (SCSE) Andrews AFB Washington 25, D. C.	1
Commanding General U S Army Electronic Proving Ground ATTN: Technical Documents Library Ft Huachuca, Arizona	1
ASTIA (TISIA-2) Arlington Hall Station Arlington 12, Va.	10
AFSC (SCFRE) Andrews AFB Washington 25, D. C.	1
Hq USAF (AFCOA) Washington 25 DC	1
AFOSR(SRAS/Dr. G. R. Eber) Holloman AFB New Mexico	1
Office of Chief of Naval Operations (Op-724) Navy Dept Washington 25 DC	1
Commander US Naval Air Dev Cen (NADC Lib) Johnsville, Pa.	1
Commander Naval Missile Center Tech Library (Code NO 3022) Pt Mugu, California	1
Bureau of Naval Weapons Main Navy Bldg Wash 25 DC ATTN: Technical Librarian, DLI-3	1

	No. of Copies
Redstone Scientific Information Center US Army Missile Command Redstone Arsenal, Alabama ATTN: Technical Library	1
Commandant Armed Forces Staff College (library) Norfolk 11 Va.	1
ADC (ADOAC-DL) Ent AFB Colorado	1
AFFTC (FTOOT) Edwards AFB California	1
Commander US Naval Ordnance Lab (Tech Lib) White Oak, Silver Springs, Md.	1
Commanding General White Sands Missile Range New Mexico ATTN: Technical Library	1
Director US Army Engineer R and D Labs Technical Documents Center Ft Belvoir, Va.	1
ESD (ESRL) L G Hanscom Field Bedford, Mass	1
Commandant US Army War College (Library) Carlisle Barracks, Pa.	1
APGC (PGAPI) Eglin AFB, Florida	1
AFSWC (SWOI) Kirtland AFB, New Mexico	1
AFMTC (Tech Library MU-135) (MTBAT) Patrick AFB, Florida	1
RTD (RTGS) Bolling AFB Washington 25, D. C.	1

	No. of Copies
European GEEIA Rgn (ZEM) APO 332 New York, N. Y.	1
Hq. Pacific GEEIA Rgn (ZPM) APO 915 San Francisco, California	1
Western GEEIA Rgn (ZSM) McClellan AFB California	1
Eastern GEEIA Rgn (ZMMRS) Brookley AFB Alabama	1
Inspection Office (Tech Lib) Central GEEIA Rgn (AFLC) Tinker AFB Oklahoma	1
Sylvania Electric Products, Inc. Physics Laboratory Bayside, N. Y.	1
Bell Telephone Laboratories, Inc. Murray Hill Laboratory Murray Hill, N. J. Attn: Dr. J. Pierce	1
Univ. of Washington Dept. of Electrical Engineering Seattle 5, Wash. Attn: A. E. Harrison	1
University of Minnesota Dept. of Electrical Engineering Minneapolis, Minn. Attn: Dr. W. Shepherd	1
Watkins-Johnson Co. Palo Alto, California Attn: Dr. L. Roberts	1
ESD (ESAT) L. G. Hanscom Field Bedford, Mass.	1
Physical Electronic Labs 2493 Pulgas Ave. E. Palo Alto, California	1

	No. of Copies
RCA Power Tubes Div. Lancaster, Pa Attn: Mr. Merrill Hoover	1
Office of Technical Services Dept. of Commerce Washington 25, D. C.	5
Liafield Research Institute McMinnville, Oregon Attn: Dr. W. Dyke, Director Attn: Dr. Charbonier	1
Director of Research and Technology HQS, USAF Washington 25, D. C. Attn: AFDT-ER	1
Phillips Research Laboratories Irvington on the Hudson, N.Y. Attn: Dr. George Esperson	1
Columbia Radiation Laboratory Columbia Univ. 538 W. 120th St. N.Y. 17, N.Y. Attn: Technical Library	1
Univ. of Illinois Dept. of Electrical Engineering Electron Tube Section Urbana, Illinois	1
University of Florida Dept. of Electrical Engineering Gainsville, Fla.	1
Carlyle Barton Laboratory The Johns Hopkins University Charles and 34th St. Baltimore 18, Md.	1
Stanford University Microwave Laboratory Stanford, California Attn: Dr. M. Choderow	1
Watkins-Johnson 3333 Hillview, Palo Alto, California Attn: Mr. D. Watkins	1

	No. of Copies
Massachusetts Institute of Technology Research Laboratory of Electronics Cambridge 39, Mass. Attn: Documents Library	1
Polytechnic Institute of Brooklyn Microwave Research Institute Brooklyn, N. Y. Attn: Morris Ettenberg	1
Harvard Univ. Cruft Laboratory Cambridge, Mass. Attn: Technical Library	1
Sylvania Microwave Tube Lab 500 Evelyn Ave. Mt. View, California Attn: Mr. D. Gordman	1
Varian Associates 611 Hansen Way Palo Alto, California Attn: T. Moreno	1
Sperry Gyroscope Company Electronics Tube Division Great Neck, N. Y. Attn: Dr. C. Wang	1
Raytheon Co. Spencer Lab Microwave and Power Tube Division Burlington, Mass Attn: Mr. J. Lind Attn: Library	2
Secretariat Advisory Group on Electron Tubes 346 Broadway New York 13, N. Y.	1
Chief, European Office Air Research and Development Command Shell Bldg. 60 Rue Cantersteen Brussels, Belgium	2

	No. of Copies
California Inst. of Technology Dept. of Electrical Engineering Pasadena, California Attn: Prof. L. M. Field	1
University of Colorado Dept. of Electrical Engineering Boulder, Colorado Attn: Prof. W. Worcester	1
General Electric Co. Electron Tube Div. of Research Lab The Knolls Schenectady, N. Y. Attn: Mr. E. D. McArthur	1
Huggins Laboratories 999 East Arques Ave. Sunnyvale, California Attn: R. Huggins	1
Hughes Aircraft Co. Electron Tube Laboratory Culver City, California Attn: J. T. Milek	1
Chief, Bureau of Ships Attn: Code 312 Main Navy Bldg. Washington 25, D. C	1
Office of the Chief Signal Officer Dept. of the Army Attn: SIGRD Washington 25, D. C.	1
AFPR General Electric Co. P. O. Box 91 Lockland Br. Cincinnati 15, Ohio	1
Chief, AF Section MAAG Germany Box 810 APO 80 New York, N. Y.	1
Mr. Norman Moore Litton Industries 960 Industrial Rd. San Carlos, California	1

	No. of Copies
M.I.T. Lincoln Labs P. O. Box 73 Lexington 73, Mass Attn: Mr. R. Butman	1
University of Michigan Electron Physics Labs 3503 East Engineering Bldg Ann Arbor, Mich. Attn: Dr J. Rowe	1
General Electric Co. Microwave Lab 601 California Ave. Palo Alto, California Attn: S. Webber	1
I.T.T. Laboratories 500 Washington Avenue Nutley 10, New Jersey Attn: Mr. A. K. Wing	1
RCA Laboratories Electronics Research Lab Princeton, New Jersey Attn: W. Webster, Director	1
Eitel-McCullough, Inc. San Bruno, California Attn: J. Hall	1
Chalmers Institute of Technology Research Lab of Electronics Gibraltargarten 5G Gothenburg Sweden Attn: Prof. O. E. H. Rydbeck	1
Royal Institute of Technology Microwave Dept. Stockholm 70, Sweden Attn: Prof. Bertil Agdur	1
Norwegian Defense Research Establishment Kjeller pr Lillestrom, Norway Attn: Mr. Finn Lied	1
NERA A/S Bergen Bergen, Norway Attn: Mr. Erling Illokken	1

Dentre De Physique Electronique
Domaine de Corbeville par Orsay
(Seine-et-Oise)
Attn: Dr. Wendt

Research Library
Eitel-McCullough, Inc.
301 Industrial Way
San Carlos, California
Attn: D. Dunn

Commanding Officer and Director
U S Navy Electronics Lab (LIB)
San Diego 52 California